Monte Carlo Study of Confined Liquid Crystals: Films, Droplets and Biaxial Nematics

A Thesis Submitted for the Award of the Degree of

Doctor of Philosopy in Physics

By

G. Sai Preeti

School of Physics

University of Hyderabad

Hyderabad,500046,India

April 2009

To

My Beloved

Bhagawan Sri Sathya Sai Baba

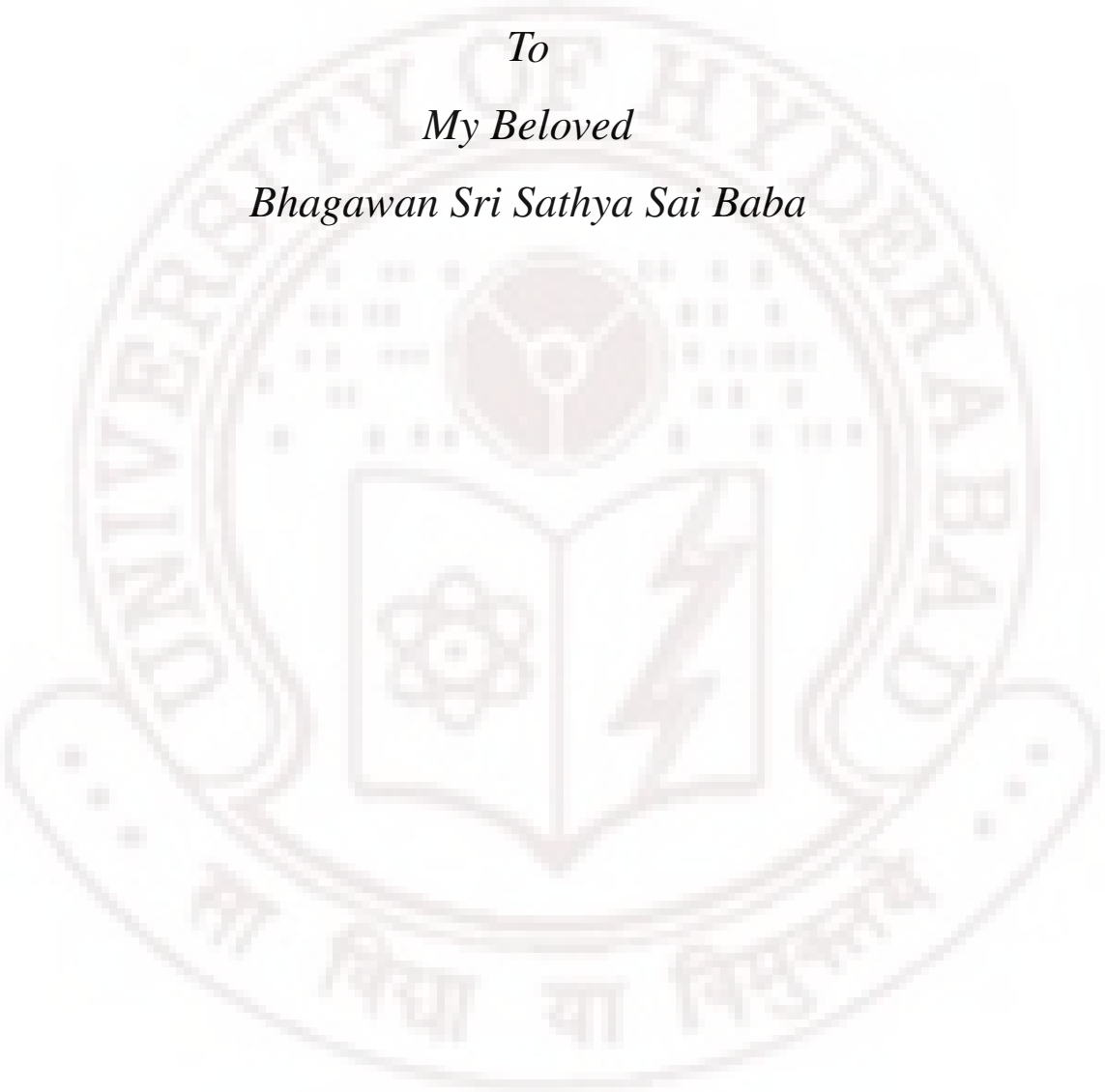

Table of Contents

List of Tables

List of Figures

Declaration

I hereby declare that the work presented in this thesis titled 'Monte Carlo Study of Confined Liquid Crystals: Films, Droplets and Biaxial Nematics' has been carried out by me under the supervision of Prof. V.S.S.Sastry, School of physics, University of Hyderabad, Hyderabad, India, as per the Ph.D ordinances of the University. I declare, to the best of my knowledge, that no part of this thesis has been submitted for the award of a research degree of any other University.

G. Sai Preeti,

Registration No: 03PHPH06.

Certificate

This is to certify that the thesis work entitled "**Monte Carlo Study of Confined Liquid Crystals: Films, Droplets and Biaxial Nematics**" being submitted to the University of Hyderabad by **G. Sai Preeti** (Reg. No. 03PHPH06), for the award of the degree of Doctor of Philosophy in Physics, is a record of *bona fide* work carried out by him under my supervision.

The matter embodied in this report has not been submitted to any other University or Institution for the award of any degree or diploma.

Prof. Vipin Srivatsava
Dean,
School of Physics,
University of Hyderabad,
Hyderabad–500046

Prof. V.S.S.Sastry
Supervisor,
School of Physics,
University of Hyderabad,
Hyderabad–500046

Acknowledgements

On the completion of this thesis, I reflect upon to remember all the help I got over the course of my PhD. A great number of people have contributed by helping me in assorted ways in this journey of research and the making of the thesis and deserve special mention here. It is a pleasure to express my gratitude to all of them in my humble acknowledgment.

Words would not suffice to express my heartfelt gratitude to my supervisor, guide and mentor Prof. V. S. S. Sastry, who has supported me throughout my thesis patiently supporting me with his knowledge and experience, whilst allowing me the room to explore on my own way. In addition to teaching me Physics, he has taught to solve a few equations in life.

I would also like to express my gratitude to Prof. K. P. N. Murthy who always had the time to teach me physics and always remind me that life always treats you good. When it's not treating you good, it just means you are not treating it good. Thank you, Sir.

I would like to thank Prof. Claudio Zannoni for his encouragement and the opportunity given to me to work with him during and after my PhD. My thesis would not be what it is now without the collaboration with him and his group at the University of Bologna.

I would like to thank Prof. Paolo Pasini, INFN, Bologna, for the timely help he has always extended. I also thank him for the opportunity he has given me to work with him in future. In a similar context I would like to thank Prof. C. Chiccoli, INFN, Bologna.

I would like to thank the Dean of School of Physics, Prof. Vipin Srivatsava for providing me the facilities of the school.

I would like to thank The Director, Center for Modeling, Simulation and Design, University of Hyderabad, for providing me with the facilities of the Center and the financial assistances to attend various conferences. In this context I would like to thank the CMSD for the facilities and the staff of CMSD for their timely help.

I would like to acknowledge the staff of School of Physics for providing me the help and the environment to pursue my research here.

I am grateful to the DST (HPC)/IBM for the assistance provided to me with a research fellowship during my PhD. I would also like to thank the DST which approved of Indo-Italian collaboration project due to which I could leverage upon the expertise of the Italian members. I would also like to that the Department of Atomic Energy, India, for providing me with a research fellowship in the initial year of my PhD.

I would like to express my deepest gratitude to all my teachers who taught me at school

and college levels.

I would like to express my gratitude to my lab mates Mr. M Trivikram Rao, Ms. D. Jayasri, Ms. M. Rajeswari, Ms. Regina Jose and Ms. Kamala Lath for enlivening the long hours in the lab and being there as co-travelers in this journey through the ups and down of research. In this context, I would like to also thank my other group members. I need to acknowledge Vikram, Raji and Regina for helping me with my thesis at the critical time.

It would be really unfair of me if I do not mention those people who have played a important role for my stay at the university and supported me during these days - Santa, Jaggu, Rajib, Gayatri, Manju, Prem, Ramya, Saravana, Gnanavel, Bari, Rizwan, Satish, Iswari, Shalini, Sridevi, Raji, Kj, Lakshmi, Madhurima. I would also like to mention here my friends from school and my favorite group 'ptp98', and my friends in college. Dearest friends, I am sorry if I have missed your names here but I am always grateful to you all. Once again thank you so much.

I spent some part of my life here during these years with my relative and my cousins in Hyderabad. Thanks for being there when I need you all. I have to mention a special note to my all time favorite pinni, Ms. J. Nirmala, thanks pinni for every week end.

I would like to thank my father Prof. G. V. Prabhakara Rao and my mother Mrs. G. Lalitha for standing by me always and encouraging me. My brothers, Dr. G. Ramkiran and my little brother Mr. G. Prasanth Sai, this would not be a success with you both. Thank you.

Last but the least, I would like to thank my sole inspiration Bhagawan Sri Sathya Sai Baba giving me the strength to accomplish this endeavor.

G. Sai Preeti,

Preface

Liquid crystals are interesting soft materials which develop variable degree of both orientational and positive ordering with the variation of suitable control parameters, usual the ambient temperature. The simplest of these phases is the nematic phase, with an appreciable orientational order, but otherwise liquid like in its mechanical behavior. The symmetry of the nematic phases could be uniaxial or biaxial, depending on the interactions between the different components of a molecular tensor. Being soft materials, the structure of liquid crystals can be relatively easily influenced by their interaction with the surfaces, and hence the physical properties of anisotropic medium can be readily manipulated by bounding surfaces and applied fields. This feature of liquid crystals has made them eminently suitable to many optical applications, the striking feature being display devices are an important step to look for novel applications. The confining geometries share a common feature: the competing boundary conditions imposed in the geometrical structures or through bounding conditions that induce new features in the free energy profiles leading to a sequence of novel phases with interesting the equilibrium structures, the control variable being either temperature, or the size of the system, or the anchoring influence at the surface. The different aspect of such behavior can be simulated by modeling these scenarios using simple lattice – based Hamiltonian models. The most known and widely used pair-wise additive lattice Hamiltonian is the Lebwohl - Lasher model, $U = -\varepsilon_{ij} P_2(\cos(\varepsilon_{ij}))$, based on Maier – Saupe theory. An extension of the LL model is used to describe a liquid crystal with biaxial molecules. Prediction of expected behavior of liquid crystals through Monte Carlo simulations modeled on such Hamiltonians, under the influence of differing geometrical confinements and as a function of temperature, is the primary objective of this thesis. With this objective Chapter - 1 sketches a brief review of liquid crystal physics relevant to the work reported.

A brief review of Metropolis algorithm and extension to non - Boltzmann methods is presented in chapter 2 to indicate the methodology adopted in the present work. The efficiency and applicability of such canonical sampling methods is put to severe test in certain physical conditions where the free energy profiles of the system under considerations either develop very shallow minima, or even barriers between two such minima. In such cases, the guided random walk (with simple Metropolis method with 'simple flip') become very inefficient, or is restricted to a single, then more efficient algorithms like non - Boltzmann

sampling methods are used. Finally, different physical properties relevant to the present study and details of the computation from the knowledge of canonical ensembles are presented.

The results of Monte Carlo simulations carried out on different liquid crystal systems are presented in the subsequent chapters. Chapter 3 presents the effect of confinement on thin films of liquid crystals comprising of uniaxial molecules. In this context, the extensive Monte Carlo simulations (based on canonical sampling methods) carried out on planar hybrid films using Lebwohl-Lasher model are supplemented by investigating this film with entropic sampling techniques. This permits a relatively error-free estimation of different properties of the medium with very fine variation of temperature. These simulations have supplemented the earlier conclusions, in helping to look for additional features of the director configurations in this film as a function of temperature. While confirming the presence of an intermediate biaxial phase over a small temperature range, this study specifically reported on the fluctuations in these order parameters particularly in different layers (in terms of their variance), to serve as possible signatures of the onset of the biaxial phase. It may be noted that the onset of the intermediate phase leaves only a weak signature Cv profile, as a shoulder. The low temperature phase with a bent director structure was further investigated by varying the thickness of the film.

Motivated by the role of hybrid boundary conditions to induce phase biaxiality in a confined system of uniaxial molecules, a thin cylindrical film embedded between two concentric cylindrical substrates was investigated with the two bounding surfaces inducing axial (along the axis of the cylinder) or radial (within each plane perpendicular to the axis of the cylinder). The interest here is that, unlike the case of the planar films, the two bounding surfaces have unequal surface area and have different curvatures, thus leading to different energy costs per unit area at the two surfaces. Under these conditions looking for possible creation of intermediate cylindrical layers of molecules which experience a competing and balanced effect of the hybrid anchoring influences from the two cylindrical surfaces required initial experimentation with different anchoring regimes assigned to the surfaces. It is found that this cylindrical film also has, under appropriately chosen anchoring conditions with specific geometry, an intermediate stable phase over a small temperature. There are striking similarities between the behavior of this specifically tailored cylindrical film and the hybrid planar film as far as phase biaxial symmetry is concerned. The thesis reports simulational results on this film based on canonical sampling methods.

The next two chapters focus on the macroscopic behavior of canonical ensembles of biaxial molecules, as reported by Markov Chain Monte Carlo simulations. The lattice Hamiltonian chosen for this purpose incorporates the interactions of both uniaxial as well as biaxial components of (second rank) tensorial attributes of neighboring molecules. This imparts to the system, the principle possibility of inducing biaxial symmetry, arising both from the phase biaxiality (from the biaxial organization of uniaxial components of the molecules) and molecular biaxiality (non-zero average contributions from the molecular

biaxial components directly). In addition such a model also generates a small contribution to order in the direction of the primary director arising from the self organization of the biaxial components of the molecules. Thus there are four order parameters which characterize the medium, and a study of these parameters and their fluctuations, along with the average energy and its fluctuations (specific heat) as function of temperature is the objective of these studies. In this context, Chapter 4 reports MC studies on a general Hamiltonian incorporating the above interactions with two variable parameters. These two in effect control the ability of the biaxial properties at the molecular level to influence the otherwise uniaxial phase obtained by the self organization of the essentially long rod like molecules. While the mutual interactions of two interacting molecules through their pure biaxial components (Term-A) create a macroscopic biaxial symmetry referred to as molecular biaxiality, the interactions involving mixed terms (Term-B) lead to the other two order parameters mentioned above. The earlier MC simulations showed that interaction between pure biaxial components (i.e. Term-A) only is responsible for the onset of a biaxial phase. Subsequent studies, based on bifurcation analysis of the general model taking into account both the above terms (i.e. Term-A and Term-B), led to an appreciation of the role Term-B in influencing the sequence and nature of thermally induced phases in such systems. In this context, the present work focuses on carrying out systematic study of the phase diagrams obtainable while spanning the two-parameter space of the interaction. Essentially one tries to change the relative importance of the above two Terms, and see it has a qualitative effect on the phase sequence that can be generated by varying the temperature of the system (control parameter). This work presents detailed phase diagrams, which one hand readily agree with the results reported earlier in certain limiting cases of choice of these parameters, and on the other indicate the progressive development of an intervening stable uniaxial nematic phase over a wide parameter space. Further study of these phase diagrams with interest on the molecular aspects of these choices could prove to be very interesting.

Chapter-5 describes the effect of confining such biaxial systems in planar geometries with hybrid anchoring conditions, much like the known case of hybrid planar film of uniaxial molecules. The major difference in this case however is that the geometric confinement applies to two axes of molecules, and is qualitatively different from uniaxial case, - it is more restrictive. This leads to two possibilities: 1. one can study the effect of such anchoring (employing equal, but variable, anchoring strengths at both the surfaces) on the thermally induced phase sequences and director configurations within each such phase through layer-wise computations; and 2. for a given choice of intermolecular interaction strengths, one can fine tune the relative importance of boundary conditions by varying the anchoring strength with a view to looking for a possible surface induced structural transition. This Chapter presents the results of MC simulations on such a film based on the biaxial Hamiltonian (satisfying the London dispersion approximation), and reports the existence of two interesting low temperature biaxial phases, as well as a structural transition within the lower temperature biaxial phase with changes in anchoring strength. These aspects

have been illustrated by computing the four different order parameters and their fluctuations (with spatial resolution), and specific heat under different experimental conditions.

The LL Hamiltonian implies that the three elastic constants for the splay, bend and twist distortions are set equal to one another $(K_1 = K_2 = K_3 = K)$, and corresponds to the so-called spherical approximation. However in real nematics they are never equal, and their relative values do play an important role in determining the visco-elastic properties of the nematic medium. An interesting attempt has been made some time back to derive a lattice based Hamiltonian (with nearest neighbor coupling), starting with continuum elastic energy expression. The result is that there is now such a model lattice Hamiltonian whose interaction parameters have functional dependence on the three elastic constants (called elastic Hamiltonian, for convenience). This in turn permits tuning of the Hamiltonian to a specific liquid crystal system. However there is an important caveat in applying this Hamiltonian reliably, and originates from the fact that the space discretization of the energy to allow for the convenience of the lattice model demands that the spatial resolution so imposed should be consistent with the implicit assumption of the ability of the model to account for observed distortions through the variations of director fields only. Making use of the flexibility allowed by this model to investigate the influence of the elastic properties on the observable properties, the polymer dispersed liquid crystal (PDLC) droplets are revisited. There were earlier studied with different boundary conditions, based on LL model Hamiltonian. In the present case, the droplets were considered with radial boundary conditions, and this leads to the simplification that the relevant distortion which matters is restricted to splay only. These droplets are investigated with the elastic Hamiltonian as a function of the anchoring strength at the polymer interface. The results indicate that there is a sharp anchoring induced transition from a uniaxially ordered droplet to an essentially radially ordered droplet, and the anchoring characteristics are, as expected, influenced by the value of the splay elastic constant (K_1). The behavior is studied by computing the radial as well as axial order parameters (including layer-wise variation in different concentric spherical shells making up the droplet), and their fluctuations. The transition shows a very strong hysteresis. The validity of the model is checked by changing the spatial resolution in the model (which in effect translates to simulations at different reduced temperatures). The results show that this is a wetting transition, and is dependent only on the relative importance of the effects of splay distortion versus radial anchoring at the surface.

In conclusion, the thesis attempts to investigate liquid crystals under different conditions. These include study of assembly of interacting uniaxial (cylindrically symmetric) molecules under different confining conditions of geometry and anchoring, of assembly of interacting biaxial molecules under different conditions of mutual interactions of such molecules. These latter studies are also extended to confined biaxial systems to look for novel features, as were observed earlier in confined uniaxial systems. Finally, PDLC systems were studied with a relatively new Hamiltonian which incorporates the elastic properties as parameters of the model. It appears that confined liquid crystals are emerging as

very useful soft materials capable of exhibiting novel structures, on one hand conveniently tunable by the Hamiltonian parameters (properties inherent to the LC system) and external boundary conditions, and on the other suitably prepared to have the necessary free energy profiles by choice of the temperature of the medium.

Chapter 1

A Brief Introduction to Liquid crystal Physics

A liquid that is interesting due to the order present in it. - A liquid crystal, an oxymoron.

The term *liquid crystal* signifies a state of aggregation that is intermediate between the crystalline solid and amorphous liquid. Liquid crystalline phases appear in the so - called mesogens which are composed of molecules having an anisotropic shape and interacting with each other. In the most disordered condensed phase - the isotropic phase - each molecule uniformly explores positions and orientations throughout the whole available space by diffusion mechanisms. In contrast, in the most ordered crystalline phase, the positions of the molecules are fixed in a lattice as are their orientations with respect to this lattice. The simplest example of a mesophase is the nematic phase which appears in systems of elongated molecules tending to orient parallel to each other while showing no positional order, which gives this phase its liquid character.

The first subsection of this chapter contains a brief introduction to liquid crystal (LC) physics, which includes an introduction to different types of ordering and their quantification. Also introduced are the possible interaction among molecules with biaxial symmetry, and their consequences leading to a new (biaxial) phase. The next subsection gives a brief introduction to surface physics and confinement. The last subsection describes the different models used in the Monte Carlo studies which have been elaborated upon in the later chapters of the thesis.

1.1 Phases of Liquid crystal

It was only in the end of the year 1888 that the word 'liquid crystal' was coined, although for many generations people used them without knowing that as such. In daily life, liquid crystals come across in many forms viz. soap, lubricants, TV displays and more recently, calculator and computer displays. The study of liquid crystals has drawn considerable attention from all branches of science and technology [1]. While the technological applications of liquid crystals is of significant interest, liquid crystal physics continues to provide excitement and challenges to condensed matter and soft material scientists due to the wide variety of physical phenomenon that it encompasses [2] [3] [4] [5].

Liquid crystals are mesophases - a state in-between solids and liquids. They flow like a liquid but have properties like birefringence as in crystalline solids. These anisotropic properties arise due to the anisotropic molecular structures. These could be rods, discs or even combinations. This thesis is concerned with rod like molecules. Structurally, liquid crystals are long organic molecules of the size of 10-15 A^o in length, and about $5A^o$ in breadth. The characteristic feature of a medium comprised of such molecules is the presence of long range orientational order - they align along the long axis of the molecules. The order in these liquid crystals is mainly controlled by temperature - *thermotropic liquid crystals*, or by the concentration of the liquid-crystalline material in the solution - *lyotropic liquid crystal*. All the studies discussed in this thesis are concerned with thermotropic liquid crystals.

With variation of temperature, thermotropic liquid crystals can be characterized into different phases depending on the order developed in them [6]. At high temperatures the liquid crystal is in an isotropic phase, which is the most symmetrical phase and the orientational order in this phase is expected to be zero due to the inherent spherical symmetry of the molecules. With decrease in temperature a (weak first order) transition occurs signalling the onset of orientational order and breaking the spherical symmetry. The nematic liquid crystal can have a high degree of long - range orientational order of molecules, but no

translational order. The molecules are spontaneously oriented with their long axes approximately parallel to each other. The preferred direction usually varies across a macroscopic medium, but a homogenous aligned specimen is optically uniaxial and strongly birefringent. The mesophase owes its fluidity to the ease with which the molecules slide past one another while still retaining their parallelism. The average preferred direction of a nematic liquid crystal is called a director, $\hat{n}$.

The cholesteric mesophase is a nematic type of liquid crystal except that it is composed of optically active molecules. These molecules form a helical structure. The molecules are aligned perpendicular to the axis of the spiral. Optically inactive molecules or racemic mixtures result in a helix of infinite pitch which corresponds to a true nematic. Thermodynamically, the cholesteric is very similar to the nematic as the energy of the twist forms only a minute part of the total energy associated with the parallel alignment of the molecules.

With further decrease in temperature more ordered mesophases are formed - the Smectic phases. In the smectic phase translational order is present in addition to the orientational order. Smectic phases can be differentiated from one another depending on the orientation of the molecules in every layer. In smectic A, the molecules are upright with respect to the layer planes, whereas in smectic C the molecules are tilted at an angle. These liquid crystals typically crystallize with further cooling.

A liquid crystal is said to be biaxial when the three axis are distinct unlike a uniaxial liquid crystal which has a preferred axis, around which the system is rotationally symmetric(figure 1.1). When such molecules constitute the medium the nematic phase can in principle show up which is no longer cylindrically symmetric(uniaxial) and can exhibit a biaxial order. The characteristic physical parameter that differentiates the above various phases in a liquid crystal is the order parameter.

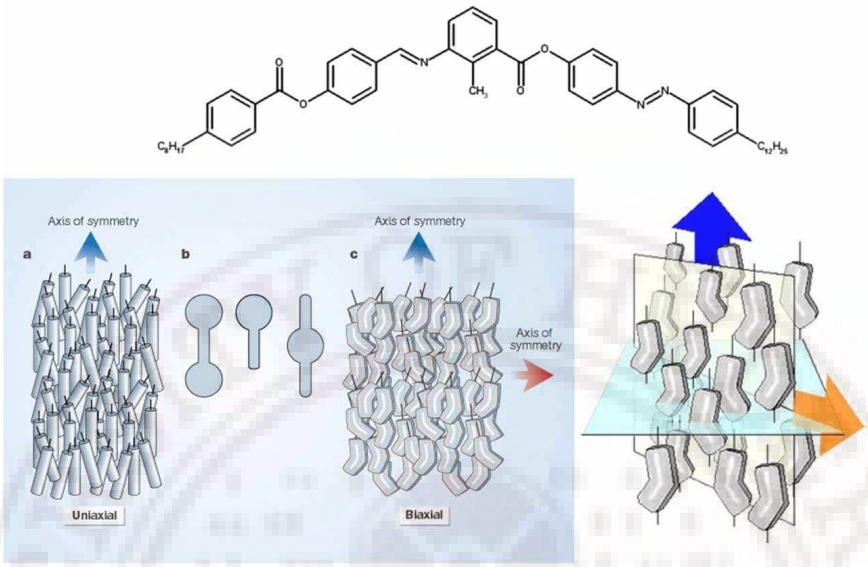

Figure 1.1: An illustrative picture of a biaxial molecules and biaxial nematic phase.

1.2 Order Parameter

The order parameter is a normalized parameter that indicates the amount of order present in the system. It is normally defined for convenience in such a way that it is zero in one phase, say above the transition temperature and non-zero below. Proven to be very convenient to define an appropriate order parameter to facilitate unambiguous quantification of the symmetry of the medium for its experimental observation and subsequent interpretation through suitable theoretical formulations.

In order to identify appropriate order parameters of the nematic LC system, it is important to note that it is the probability distribution of the orientations of the constituent molecules that undergoes qualitative changes due to changes in the symmetry of the system, and therefore any measure of such loss of symmetry should be derivable from the features of the distribution function. Formation of layered structures (like in smectic phases)decreases the symmetry of the medium further with respect to the homogeneities

of the density, and such order parameter hence should be obtained from probability distribution of the molecular positions. The order parameters in liquid crystals are very transparently formulated starting with appropriate distributions, as indicated below [7].

Consider a system with 'N' molecules in a certain state of aggregation [8]. Assuming that these particles are classical and fixed at a position specified by the vector $\mathbf{r}$, and are specific in their orientation Ω with respect to a laboratory frame. The orientation of the molecule Ω is given in terms of the Euler angles (α, β, γ). Now, let us assume that a molecule is formed of a collection of connected rigid rotors, if $\mathbf{r}$ gives its position and Ω the orientation of one rigid fragment and another set of variables, Φ specifies the orientation of the other fragments with respect to the first (conformational variable). With only one rotor, $\Phi = \phi$ specifies the conformational state. $P(r, \Omega, \Phi)$ gives the probability of a particle to have a position $(r + dr)$, orientation $(\Omega + d\Omega)$, and internal state $(\Phi + d\Phi)$. The average of any quantity $< A(r, \Omega, \Phi) >$ is given as

$$\begin{aligned} < A > &= < A(r, \Omega, \Phi) > \\ &= \int dr d\Omega d\Phi A(r, \Omega, \Phi) P(r, \Omega, \Phi). \end{aligned} \tag{1.2.1}$$

Here the volume elements dr, $d\Omega$ are $dxdydz$ and $d\alpha sin\beta d\beta d\gamma$ respectively, and for one rotor $d\Phi = d\phi$. The normalization of the distribution $f(r, \Omega, \Phi)$, is

$$\int dr d\Omega d\Phi P(r, \Omega, \Phi) = 1. \tag{1.2.2}$$

This singlet distribution f contains all the information necessary to calculate one particle properties.

$$f(r, \Omega, \Phi) =< \delta(r - r')\delta(\Omega - \Omega')\delta(\Phi - \Phi') > \tag{1.2.3}$$

where $\delta(a - a')$ is the dirac delta function, a counting device since it is different from zero only when the primed value equals the desired. The distribution function is obtained by counting all of the particles that have the position-orientation-internal variables equal to the desired value in the given configuration and then averaging over the equilibrium configurations. Generalization of the distribution for n variables is a general multiplet

distributions. The singlet distribution function can be written in terms of Fourier integral representation of the positional delta function

$$\delta(r - r') = (2\pi)^{-3} \int dk exp(i\mathbf{k}.(\mathbf{r} - \mathbf{r}')). \tag{1.2.4}$$

The expansion of angular delta function is either in generalized spherical harmonics or Wigner rotation matrices $D^L_{m,n}$

$$\delta(\Omega - \Omega') = \sum_{L=0}^{\infty} \sum_{m=-L}^{L} \sum_{n=-L}^{L} \{(2L+1)/8\Pi^2\} D^L_{m,n}(\Omega) D^{L*}_{m,n}(\Omega'). \tag{1.2.5}$$

The functions $D^L_{m,n}$ with the integers L, m, n $(L \geq 0, -L \leq m \leq L, -L \leq n \leq -L)$ constitute a convenient set in the space of variables, and indeed represent physically the presence of different types of symmetries with respect to the angular variables. Let $\Psi_\lambda(\Phi)$ be a basis set for the internal variables and representing as delta function gives

$$\int d\Phi \Psi_\lambda(\Phi) \Psi^*_{\lambda'}(\Phi) = k_\lambda \delta(\lambda - \lambda'). \tag{1.2.6}$$

1.2.1 Orientational Order

For a nematic medium, it is sufficient to consider a distribution function independent of translation, i.e, this particle is independent of the position vector $\mathbf{r}$. In a nematic liquid crystal the position of the molecules does not play an important role. A isotropic-nematic transition is distinguished by the building up of a orientational order. This thesis deals mainly with nematic-isotropic transition although positional ordering is important to study a nematic-smectic transitions. If the molecules are considered to be rigid and the system is uniform, only the orientational degrees of freedom are relevant so $f(\mathbf{r}, \Omega, \Phi)$ reduces to $f(\Omega)$

$$f(\Omega) = \sum_{L,m,n} p_{L,m,n} D^L_{m,n}(\Omega). \tag{1.2.7}$$

Assuming the axis of cylindrical symmetry, the director is along the laboratory Z axis. Thus rotating the sample about Z no observable property will change. The probability of a molecule in the sample having a orientation (α, β, γ) should be the same whatever be the angle α, m must be zero in $D^L_{m,n}$ and $f(\Omega) = f(\beta, \gamma)$.

In addition, if a uniaxial mesophase has a plane perpendicular to the director $(D_{\infty h})$, i.e. $\hat{n}$ and $-\hat{n}$ are not distinguishable then only terms with even L can appear. Considering molecules are cylindrically symmetric, the rotation about the molecular axis will not modify the distribution $f(\Omega)$. The value of γ does not change the distribution function $f(\Omega)$, then $n = 0$ in $D^L_{m,n}$. Accordingly, we have $f(\beta) = f(\Omega)/4\Pi$.

Consider a cylindrical particle with the director parallel to the laboratory Z axis.

$$f(\Omega) = f(\beta) = \sum f_L D^L_{0,0} \tag{1.2.8}$$

$$D^L_{0,0} = P_L(cos\beta) \tag{1.2.9}$$

$$f(\beta) = \sum_{i=1}^{\infty} f_L P_L(cos\beta) \tag{1.2.10}$$

where $P_L(x)$ are the Legendre polynomials and $f_L = (2L+1)\Omega^{-1}\int d\Omega f(\beta)P_L(cos\beta)$. $f_L \equiv 0$ for odd parameters of L as $\hat{n} = -\hat{n}$, so $f_L s$ are non-zero for even L. The first nonzero order parameter is

$$f_0 = 1 \tag{1.2.11}$$

$$\begin{aligned} f_2 &= \frac{5}{\Omega}\int d\Omega f(\beta)P_2(cos\beta) = 5\left\langle P_2(cos\beta)\right\rangle \\ &= 5\left\langle \frac{1}{2}(3cos^2\beta - 1)\right\rangle \equiv 5S \end{aligned} \tag{1.2.12}$$

where S is a scalar order parameter which describes the degree of uniaxial orientational order of the molecules about the director. The value of S is in the interval $[-\frac{1}{2}, 1]$: in a perfect nematic phase $\beta = 0$ for all molecules, so $S = 1$. When the orientations of the molecules are perfectly random $< cos^2\beta >= \frac{1}{3}$ and $S = 0$. The minimum value of order parameter corresponds to when all the molecules align perpendicular to the director. The first non-trivial term of the distribution function is

$$\begin{aligned} f(\beta) &= 1 + 5SP_2(\cos\beta) = 1 + 5S\frac{1}{2}(3\cos^2\beta - 1) \\ &= 1 + 5S\frac{1}{2}(3(\hat{n}.\hat{a})^2 - 1) = 1 + 5S\frac{1}{2}[3(n_i a_i)(n_i a_i) - 1] \\ &= 1 + 5S\frac{1}{2}[3(n_i a_i)(n_i a_i) - \delta_{ij}a_i a_j] = 1 + 5S\frac{1}{2}[3(n_i n_j) - \delta_{ij}]a_i a_j \\ &= 1 + 5S\frac{1}{2}[3(\hat{n}\otimes\hat{n}) - I_{ij}]a_i a_j = 1 + 5(Q)_{ij}a_i a_j \end{aligned} \tag{1.2.13}$$

and

$$Q = \frac{1}{2}S(3\hat{n} \otimes \hat{n} - 1) \tag{1.2.14}$$

is the tensorial order parameter of the nematic liquid crystal, which represents the quadrupole moment of the distribution i.e. the deviation from the prefect sphere. Here, I is the second rank unit tensor.

The order parameter is a second order tensor that has 9 degrees of freedom. Due to symmetry $Q_{ij} = Q_{ji}$, the degrees of freedom are reduced by 3. Also, $tr(Q) = 0$ reduces the degrees of freedom further by one. Hence, there are only 5 degrees of freedom. The symmetric traceless tensor order parameter has five independent components degrees of freedom. The five degrees of freedom considered here are the two angles that determine the direction of the director, the scalar order parameter, the angle specifying the secondary director and the biaxiality parameter. With respect to the 5 base tensors of the symmetrical traceless tensor the parametrization of the order parameter can be given as

$$\begin{aligned}
T_0 &= \frac{3\hat{n} \otimes \hat{n} - I}{\sqrt{6}} \\
T_1 &= \frac{\hat{e_1} \otimes \hat{e_1} - \hat{e_2} \otimes \hat{e_2}}{\sqrt{2}} \\
T_{-1} &= \frac{\hat{e_1} \otimes \hat{e_2} - \hat{e_2} \otimes \hat{e_1}}{\sqrt{2}} \\
T_2 &= \frac{\hat{e_1} \otimes \hat{n} + \hat{n} \otimes \hat{e_1}}{\sqrt{2}} \\
T_{-2} &= \frac{\hat{e_2} \otimes \hat{n} - \hat{n} \otimes \hat{e_2}}{\sqrt{2}}.
\end{aligned} \tag{1.2.15}$$

The above tensors are traceless and they are orthogonal with respect to the metric T_n : $T_m = tr(T_n T_m) = \delta_{nm}$. The order parameter can be given as

$$Q = \sum_{m=-2}^{2} q_m T_m \tag{1.2.16}$$

where $q_m = tr(QT_m)$. The multiplicative constants are set so that the amplitude q_0 represents the scalar order parameter. The parameters $q_{\pm 1}$ are non-zeros if the order is biaxial and parameters $q_{\pm 2}$ represent the deviations in the orientations of the director with respect to the assumed director $\hat{n}$.

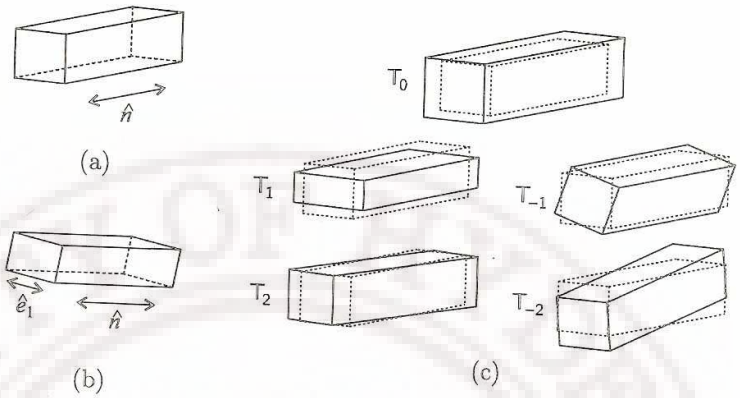

Figure 1.2: A visualization of the basis vector of order parameter (courtesy [9])

When the molecules are non-cylindrical then an extra angle γ is needed to define their orientation with respect to the laboratory frame. γ gives the extra angle of rotation needed around the molecular z-axis, and hence integer n has a non-zero value in $D^L_{m,n}$, thus making $f(\Omega) = f(\beta, \gamma)$

$$f(\Omega) = f(\beta, \gamma) = \sum_{L,n} f_{L,n} D^L_{0,n}(\beta, \gamma). \tag{1.2.17}$$

Orthogonality of the basis set immediately permits identifying the coefficient $f_{L,n}$

$$f(\beta, \gamma) = \frac{1}{4\Pi} \sum_{L=0}^{\infty} \sum_{n=-L}^{L} (2L+1) < D^{L,*}_{0,n} >< D^L_{0n} > (\beta, \gamma). \tag{1.2.18}$$

Biaxial molecules have molecular frame axis along the C_2 axes [10]. For such molecules with C_{2h} group, the symmetry operation gives the restriction

$$< D^L_{m,n} >= (-)^m < D^L_{m,n} >= (-)^{L+m} < D^L_{m,n} > . \tag{1.2.19}$$

This implies L and m have to be even. The relevant order parameters are

$$< D^2_{0,n} >; \tag{1.2.20}$$

$$< D^2_{2,n} >= (-)^n < D^{2,*}_{-2,n} > \tag{1.2.21}$$

If the particles constituting the phase are cylindrically symmetric, then there are two independent orders, which include phase biaxiality also. If the constituent molecules of the

biaxial phase are themselves biaxial, then the different order parameters are

$$\begin{aligned}
&< D^2_{0,0} > \\
&< D^2_{0,2} >=< D^2_{0,-2} > \\
&< D^2_{2,0} >=< D^2_{-2,0} > \\
&< D^2_{2,2} >=< D^2_{-2,2} >=< D^2_{2,-2} >=< D^2_{-2,-2} > .
\end{aligned} \tag{1.2.22}$$

Another approach considers how to extract these same order parameters from tensors, or dyadics, constructed from the vectors $\mathbf{e_z^{(i)}}$, $\mathbf{e_x^{(i)}}$ and $\mathbf{e_y^{(i)}}$. A vector $\mathbf{u}$ can be represented as a column matrix $U = [\mathbf{u_x}, \mathbf{u_y}, \mathbf{u_z}]^T$ in the basis E_x, E_y, E_z. The vector $\mathbf{u}$ can be represented as

$$\mathbf{u} = \mathbf{u_x}E_x + \mathbf{u_y}E_y + \mathbf{u_z}E_z. \tag{1.2.23}$$

The dyadic $\mathbf{u} \otimes \mathbf{u}$ is then represented by the matrix UU^T. The dyadic Q^{zz} can be given in two stages: initially P^{zz}, constructed from the vectors $\mathbf{e_z^{(i)}}$.

$$P^{zz} = \frac{1}{N}\left(\sum_{i=1}^{N} e_z^{(i)} \otimes e_z^{(i)}\right) \equiv < e_z^{(i)} \otimes e_z^{(i)} > . \tag{1.2.24}$$

Secondly, the Saupe order tensor is defined as

$$Q^{zz} = (3P^{zz} - I)/2 \tag{1.2.25}$$

Similarly, P^{xx} and P^{yy} and hence the corresponding Q^{xx} and Q^{yy} are obtained by replacing z by x or y in 1.2.25.

P and Q dyadics have the same eigenvectors, though their eigen vectors differ: if v is an eigenvector of P with eigenvalue λ, then it is an eigenvector of Q with eigenvalue $(3\lambda - 1)/2$. It may be noted that the sum of eigen values of a Q dyadics is zero by construction.

The eigenvector associated with the dominant eigenvalue of Q^{zz} is the system director by convention, and the corresponding eigenvalue gives a measure (S) of the orientational order along the major director. The size and sign of S give how well the molecular long axes are organized (aligned), and the orientation of their average ordering direction with respect to the reference direction chosen. If the system's properties are invariant with respect to

arbitrary rotation about the director, the system is said to be uniaxial. Otherwise, the system is said to be biaxial. To quantify this, the axes of the molecules are projected on to the plane orthogonal to the major director. If the axes of the molecules are equally likely to point in any one of those directions, then the system has no biaxiality; on the other hand, if projections show a preferred direction, then the system does display biaxiality called phase biaxiality. To give some measure of this, diagonalize the matrix Q_{zz}; in other words, we find its components in a basis built out of its eigenvectors. This gives a matrix of the form

$$\begin{pmatrix} q_x & 0 & 0 \\ 0 & q_y & 0 \\ 0 & 0 & q_z \end{pmatrix}.$$

where $|q_z| \geq |q_y| \geq |q_x|$ by choice. Since S is related to q_z as $S = 1.5q_z$ and $q_x+q_y+q_z = 0$, one has for the ordering matrix of the major axis of the molecules in its principle system:

$$\begin{pmatrix} -S/2 - \xi & 0 & 0 \\ 0 & -S/2 + \xi & 0 \\ 0 & 0 & S \end{pmatrix}.$$

So ξ, which is given by half the difference between the smaller eigenvalues of Q_{zz} measures the extent to which it is possible to distinguish a direction in the plane orthogonal to the director. If ξ = 0, then the system is unchanged by a rotation about the director; if ξ is non-zero, there is a preferred direction orthogonal to the director, and we have a phase biaxial system. We regard the density of molecular long axes as determining an ellipsoid in space. Then the major axis of this ellipsoid lies along the system director, and its magnitude determines the order parameter. The difference between the minor axes is a measure of the extent to which the molecule directors are not equally scattered in all directions perpendicular to the system director, and gives the phase biaxiality parameter.

1.3 Phenomenological free energy and Maier Saupe Theory

1.3.1 Landau's theory of Phase transition

A phenomenological description of a phase transition is possible using Landau theory, as has been treated in many well written books [11] [12]. An order parameter is defined to describe the change in symmetry, accompanying a phase transition. Typically the system is expected to undergo a transition from high temperature phase to a low temperature less symmetric phase. Taking the specific example of the transition from an isotropic to the nematic phase on cooling, the order parameter is defined as a tensor which becomes zero in the more symmetrical phase. The thermodynamic quantities of the less symmetric phase can be obtained by expanding the thermodynamic potential at the transition point. This procedure, originally was developed for continuous transitions, is extended to cover first order transition also suitably, and for weak first order $I-N$ transition. Landau description certainly provides a convenient basis to understand the qualitative characteristics of this phenomenon.

An extension to phase transitions in liquid crystal was suggested by De Gennes [13]. The nematic phase is described by a symmetric tensorial (second rank) order parameter $\tilde{Q}$ with zero trace. Expansion of the thermodynamic potential up to the 4^{th} order in the tensor order parameter $\tilde{Q}$ has been found sufficient to describe satisfactorily the nematic-isotropic phase transition. Following [11], Gibbs free energy per unit volume at constant pressure and temperature is:

$$G = G_{iso} + \frac{1}{2}A_{\alpha\beta\gamma\delta}Q_{\alpha\beta}Q_{\gamma\delta} - \frac{1}{3}B_{\alpha\beta\gamma\delta\mu\nu}Q_{\alpha\beta}Q_{\gamma\delta}Q_{\mu\nu} + \frac{1}{4}C_{\alpha\beta\gamma\delta\mu\nu\varrho\sigma}Q_{\alpha\beta}Q_{\gamma\delta}Q_{\mu\nu}Q_{\varrho\sigma} \tag{1.3.1}$$

$$Q_{\alpha\beta} = S(N_{\alpha\beta} - \frac{1}{3}\delta_{\alpha\beta}). \tag{1.3.2}$$

For capturing the essential features, it is more convenient to deal with the case of a uniaxial nematic phase requiring only one order parameter. Then the above potential can be written

in terms of scalar order parameter S as

$$G = G_{iso} + \frac{1}{2}A(T)S^2 - \frac{1}{3}BS^3 + \frac{1}{4}CS^4 \tag{1.3.3}$$

$$A(T) = A_0(T - T^*). \tag{1.3.4}$$

G and G_{iso} represent the Gibbs free energy in the nematic and the isotropic phases, respectively. A linear term in the order parameter is not considered since this would mean that the free energy per unit volume of the nematic phase would be less than the free energy of the isotropic phase at all temperatures. The negative sign before B is taken as per convention. A_0 and T^* are constants, T^* is a temperature slightly lower than the transition temperature T_C, A_0 is independent of temperature. Near the phase transition the temperature dependencies of B and C are neglected. C must be greater than zero, as a negative value of C would not allow G to have a minimum for a finite value of S. If there were to be a stable nematic phase at a certain value of S, then G must have a minimum at this value of S. The equilibrium value of S is obtained by minimizing the free energy density with respect to S. Taking the derivative of equation 1.3.3, the solutions are

$$S_{\pm} = \frac{B}{4C}\left\{1 \pm \left[1 - \frac{24aC(T - T*)}{B^2}\right]^{1/2}\right\} \tag{1.3.5}$$

$S = 0$ represents a phase with no order – an isotropic phase. The other two values of S represent the local maximum and the local minimum for the non – zero values of S. If S is the local minimum, then the solution containing the negative sign must be either the local maximum or the local minimum solution, and the positive sign being the other. At T_C both $S = 0$ and $S > 0$ must have local minima with the same value of free energy per unit volume G_{iso}. Setting the two values to zero and combining the requirements we get

$$\begin{aligned} S_c &= 0, \qquad T_c = T_c^* \\ S_c &= \frac{B}{3C} \qquad T_c = T_c^* + \frac{B^2}{27A_0C}. \end{aligned} \tag{1.3.6}$$

S_+ is a stable solution, as this gives a solution $S_c = B/(3C)$ at T^*. The solution (1.3.5)

determines a third temperature T_c^{**}

$$T_c^{**} = T_c + \frac{B^2}{24A_0C}. \tag{1.3.7}$$

If $T = T_c^{**}$ the solutions S_- and S_+ do not hold good because of their imaginary values.

Landau de-Gennes theory distinguishes four different temperature regions.

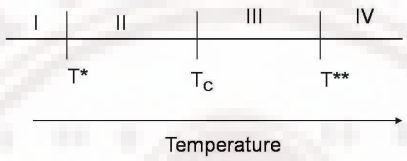

Figure 1.3: Schematic representation of the different temperature regions and the available phases.

- Phase IV (figure 1.3): $T > T_c^{**}$: Only solution $S = 0$, i.e. the isotropic phase exists and is stable.

- Phase III (figure 1.3): $T_c < T < T_c^{**}$: The minimum of the free energy still gives $S = 0$, i.e. the isotropic phase in the thermodynamic stable state. An energy density barrier of height $f_n(S_-) - f_n(S_+)$ exists between the two minima $S = 0$ and $S = S_+$. At T_c^{**} the height of the barrier becomes zero, for $S_+(T_c^{**}) = S_-(T_c^{**}) = B/4C$ and this corresponding point in free energy density curve is a point of inflection. The temperature $T_c^{\dagger}$ corresponds to super heating temperature.

- Phase II (figure 1.3): $T_c^* < T < T_c$: Here $S = S_+$ gives a lowest free energy and $S = 0$ is relative minimum. The nematic phase is a stable state in this range of temperature. The $S = S_-$ corresponds to a relative maximum of the free energy density. The free energy height barrier is $f_n(S_-) - f_i$. At T_c^* the height becomes zero, because $S_- = 0$. This implies that the isotropic phase, which can be obtained by super cooling, is metastable in the temperature region between T_c^* and the clearing point T_c.

- Phase I (figure 1.3): $T < T_c^*$: The nematic phase is the thermodynamically stable phase as S_+ gives the lowest free energy density, S_- a relative minimum and $S = 0$ a relative maximum. The S_- describes a phase where the molecules orient perpendicular to the uniaxial phase. T_C^* is the super cooling temperature.

Figure 1.4 shows the discontinuity in the free energy at the transition temperature with the variation in S for different temperatures.

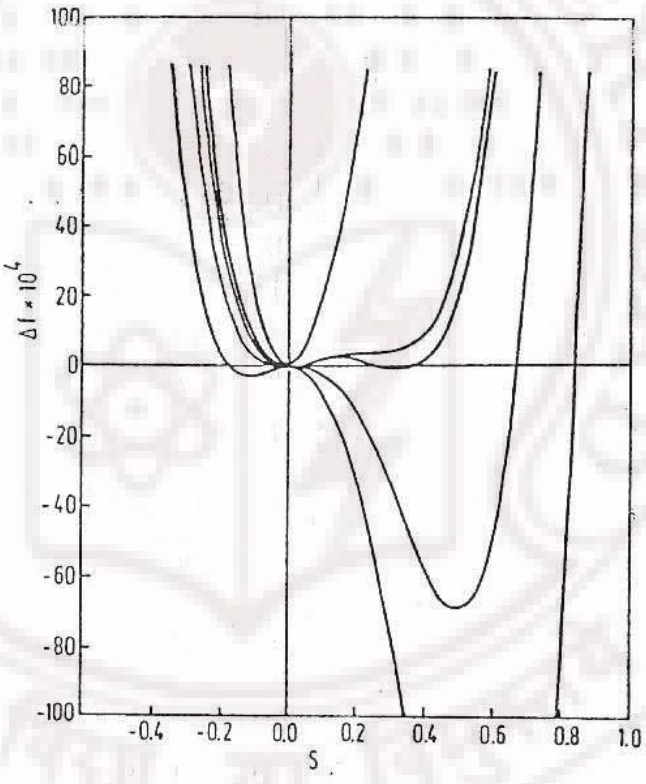

Figure 1.4: The free energy density plots for different temperatures with the change in order parameter [11]

1.3.2 Maier-Saupe Theory

Maier Saupe [14] [6] [11] [12] theory is a molecular theory that starts with the behavior of one molecule in the "field" of other molecules and determines the characteristics of a macroscopic phase. This approach that has proved to be extremely useful in developing a

theory of spontaneous long range orientational order and the related properties of the nematic phase, is a molecular field method. Each molecule is assumed to be in an average orienting field due to its environment, but otherwise uncorrelated with its neighbors. A macroscopic sample contains a huge number of molecules and it's not predictable to account for all possible interactions among all molecules. As a result approximations and simplifications are necessary, and result in a simplified treatment.

Maier-Saupe theory uses the concept of orientational order in the nematic phase. Each molecules is assumed to experience an average attractive potential $U(\theta)$ given by

$$U(\theta) = -\varepsilon \left\langle P_2 \left(\cos\theta\right)\right\rangle P_2\left(\cos\theta\right) \tag{1.3.8}$$

where ε is the strength of the potential. The distribution function is related to the potential by

$$f(\theta) = Z^{-1} \exp\left[\frac{-U\left(\theta\right)}{k_B T}\right] \tag{1.3.9}$$

where Z serves to normalize the $f(\theta)$. In its original form Maier and Saupe considered anisotropic Van de Waal forces between the molecules. Every molecule possesses an anisotropic polarizability determined by α_l (lateral component) and α_t (transverse component) or alternatively by $\bar{\alpha} = (\alpha_l + 2\alpha_t)/3$ and $\delta\alpha = \alpha_l - \alpha_t$. In a perturbation expansion this leads to three types of contributions, which are proportional to the quantities

$$\alpha.\alpha, \qquad \alpha.\delta\alpha \qquad \text{and} \qquad \delta\alpha.\delta\alpha \tag{1.3.10}$$

In spite of the anisotropy, a spherical average was assumed. In this consequence, only the last term contributes to the anisotropic part of the free energy and thus to ε, stabilizing under appropriate conditions the nematic phase. For such averages, any contributions from the first two terms is zero. The extreme point in the Maier-saupe theory is the existence of a nematic phase due to the presence of the anisotropic part of the dispersion interaction energy between the molecules. This interaction energy originates from the intermolecular electrostatic interactions, which is taken into account by means of perturbation theory, called the dispersion energy. The simple expression for interaction of a single molecule

in a sea of molecules under the above simplifying condition is given as

$$U_i(\theta_i) = -\frac{A}{V^2} S\Big(\frac{3}{2} cos^2\theta_i - \frac{1}{2}\Big) \tag{1.3.11}$$

where θ_i is the angle between the long axis of the molecule and the director. A is a constant that is independent of temperature, V is the volume of the sample. Few approximations were made in this context regarding the electrostatic interactions and the properties of the molecules.

1. As long as long range order is assumed the permanent dipoles can be neglected. This means that the interaction between the molecules is due to induced dipoles only. A momentary dipole moment of one molecule induces a dipole moment on other molecule resulting in attractive interaction.

2. Molecules are considered as rotationally symmetric with respect to the long axis of the molecule - molecules are perfect cylinders. The interaction between the molecules can depend only on the angle between them.

3. For a given molecule the distribution of the centers of mass of the remaining molecules may be assumed to be spherically symmetric.

4. The degree of orientational order of the molecules enters into the mean-field potential in a linear way.

The Maier – Saupe theory thus tends to ignore the short range forces and have contributions from the long range forces only. One of the major criticisms on Maire Saupe theory is the complete negligence of short range forces which should be important for elongated molecules forming nematogens [15]. The success of this theory however lies in the generalization of the Van de Waal interactions, and it does provide a qualitative insight into the factors that contribute to the orientational ordering [16].

1.4 Effect of Confinement

Liquid crystals are part of soft matter whose physical properties are fairly difficult to predict from their atomic or molecular constituents. Soft matter self-organizes into mesoscopic physical structures with length scales that are much larger than the microscopic scale, and yet could be much smaller than the macroscopic (overall) scale of the material. Another important feature of soft matter is that all predominant physical behavior occurs at an energy scale comparable to thermal energy at room temperature.

Liquid crystals find wide use in liquid crystal displays, which rely on the optical properties in the presence or otherwise of external (electric) fields. Liquid crystalline materials confined to different geometries attracted considerable attention due to their novel electro-optic properties and their rich physical phenomena. Surface effects on liquid crystal have thus become very important for both theoretical and experimental investigators, and play crucial role in technological applications like displays.

Experimentally it is known that there are different methods of aligning a liquid crystal on a substrate. Two of these methods that are commonly known and used widely are rubbing and photo alignment. Depending on the substrate used different alignments are achieved, but it is still not known as to why some substrates align whereas some do not. Different methods of alignment effective for different substrates are reviewed very comprehensively [17]. The commonly known liquid crystalline director alignments near a solid substrate are homeotropic, planar and titled orientations.

LC develops an order in the direction of the easy axis of the substrate on which it is confined [18] [19] [20]. The aligning action of the polymer layer proceeds to the 'first molecular layer' via the anisotropic Van der Waal interaction and the excluded volume effects due to the topology of the interface. The LC aligns through the nematic interactions at the shear plane; the LC's anchorage is fairly weak and defines a slippery surface. Further into the bulk, the orientational order is transmitted via intermolecular forces that are responsible for the orientational order in the LC. In the absence of any other orienting field

(electric or magnetic field, flow, other surface, etc) this orientation is imposed on the bulk molecules via the elastic forces which tend to orient all the molecules parallel to each other. This phenomenon of orientation of a liquid crystal by a surface, called anchoring, is very similar to the epitaxy of solids on substrates.

Both orientational and positional orders are induced into the LC due to the surface. There is a first layer of molecules that transmits the aligning action of the surface into the bulk. This aligning action is transmitted through the medium by the elastic properties of the LC. Liquid crystals are known to have very small elastic constants in the range of $\sim 10^{-7}$ units. The positional order that is unstable in bulk nematic decays within the smectic correlation length from the surface whereas the orientational order is relatively long ranged. In a macroscopic picture, a confining homogenous surface aligns a nematic liquid crystal because it represents a state of spontaneously broken continuous rotational symmetry and corresponds to the minimization of the free energy.

Under these conditions, theoretical calculations of the surface energy with the bulk LC energy showed that the liquid crystals tend to align along the direction of the groove more readily than perpendicular to the groove. Grooves are produced by rubbing, unidirectional polishing, tangential evaporation or by the formation of grating on the substrate. The resulting model is based on the elastic continuum theory of nematic liquid crystal and the liquid crystal alignment is a result of the minimum of free energy of the system. In this picture, the effect of confining surface can be considered as the coupling of a spatially homogenous potential to the excitation modes in the nematic. Those modes that are unstable, decay from the surface and give rise to different orders, LC layers near the surface with a thickness of correlation length.

1.4.1 Anchoring Energy and Extrapolation length

Deep in the nematic phase, the variation in scalar order parameter does not play an important role. The main contributions to the elasticity are due to the elastic deformation of the

director field which contributes to the free energy density.

$$F = \frac{1}{2}\{K_{11}(\nabla.\hat{n})^2 + K_{22}[\hat{n}.(\nabla \times \hat{n})]^2 + K_{33}[\hat{n} \times (\nabla \times \hat{n})]^2\}. \tag{1.4.1}$$

The first three terms correspond to the three deformations of the director field, *viz.* splay, twist and bend deformations, respectively. This free energy density is invariant with respect to rotations of the system as a whole, space inversions and the transformation $\hat{n} \rightarrow -\hat{n}$. The relative elastic anisotropy of a typical nematic is usually not more than 50%, so it is reasonable to assume, for simplification that $K_{11} = K_{22} = K_{33} = k$. Consider a twist deformed nematic place between two solid substrates. Let axes x (easy axis of lower substrate direction) and t (easy axis of substrate 2) be energetically preferable directions of the nematic orientations near the solid walls. Due to the twist deformation in the bulk of the sample, the director in the areas adjacent to the wall deviate from x and t by, say angles ϕ_1 and $\tau - \phi_2$, respectively. So extra terms are needed to be added to account for the free energy density due to the excess surface energy. In the coordinate representation of the director $\mathbf{n}(cos\phi, sin\phi, 0)$, these terms can be written as

$$\begin{aligned} F_{1S} &= F^a_{1s} + F^i_{1s} = \frac{1}{2}W_1\phi_1^2 + F^i_{1s} \\ F_{2S} &= F^a_{2s} + F^i_{2s} = \frac{1}{2}W_2(\tau - \phi_2)^2 + F^i_{2s}. \end{aligned} \tag{1.4.2}$$

Here F^i_{1s} and F^i_{2s} are the densities of the isotropic surface energy of the nematic, the functions F^a_{1s} and F^a_{2s} are the angle-dependent anisotropic parts of the surface energy and the coefficients W_1 and W_2 are the so-called anchoring energies of the nematic liquid crystal. The physical meaning of W_1 and W_2 is evident as they are the energies required for maximum deviation of the director in the wall-adjacent areas from the easy orientation. There are usually two types of anchoring, connected with the azimuthal angle θ, W_θ and the other connect to the polar angle ϕ, W_ϕ. Considering only W_ϕ, the total free energy of the nematic is:

$$F = F_0 + \frac{1}{2}k\int_0^d (\frac{d\phi}{dz})^2 dz + \frac{1}{2}W_1\phi_1^2 + \frac{1}{2}W_2(\tau - \phi_2)^2. \tag{1.4.3}$$

Here the isotropic energy F_0 includes both surface and bulk parts, d is the film thickness, and $k = K_{22}$ (twist deformed LC). In equilibrium state the free energy is minimal and its variation δF is zero:

$$\delta F = \big[k\frac{d\phi}{dz} - W_2(\tau-\phi)\big]\delta\phi|_{z=d} + \big[-k\frac{d\phi}{dz} + W_1\phi\big]\delta\phi|_{z=0} - k\int_0^d \frac{d^2\phi}{dz^2}\delta\phi dz = 0. \quad (1.4.4)$$

since $\delta\phi$ is arbitrary. The condition $\delta F = 0$ is satisfied by initializing

$$\begin{aligned} \frac{d^2\phi}{dz^2} &= 0 \\ -k\frac{d\phi}{dz} + W_1\phi = 0, &\quad z = 0, \\ k\frac{d\phi}{dz} - W_2(\tau-\phi) = 0 &\quad z = d. \end{aligned} \quad (1.4.5)$$

The first equation reflects the equilibrium distribution of the director in the bulk of a sample, while the rest are boundary conditions. Hence the solution of equation 1.4.5 is

$$\phi = az + b \quad (1.4.6)$$

using the boundary conditions

$$\phi = \frac{W_2\tau}{k(1 + W_2/W_1) + W_2 d}(z + k/W_1). \quad (1.4.7)$$

When the anchoring is the same at both the surfaces *i.e.* $W = W_1 = W_2$ then,

$$\phi = \frac{W\tau}{2k + Wd}(z + k/W). \quad (1.4.8)$$

Hence the director deviations at the substrates are

$$\begin{aligned} \phi_1 &= \tau\frac{k}{2k + Wd}, \\ \phi_2 &= \tau\frac{k + Wd}{2k + Wd}. \end{aligned} \quad (1.4.9)$$

When the nematic director is strongly fixed at the surfaces, $W \to \infty$, $\phi_1 \to 0$ and $\phi_2 \to \tau$, *i.e.* the director near the walls coincides with the easy axis of the substrates.

If W is finite, the angle ϕ is zero when $z = -k/W$. The parameter

$$b = |z| = \frac{k}{W}, \quad (1.4.10)$$

having the dimension of length, is usually called the extrapolation length. The anchoring strength is measured in terms of extrapolation length which denotes the length on which the director field would relax to the one preferred by the substrate. It is the measure for the relevance of the competing elastic distortion vs. violating substrate order.

1. When the interaction energy of the nematic molecules with the substrate F_s^a is of the same magnitude as the mesophase interaction F, $F_s^a \sim F$. Then $b \sim a$, the molecular length is comparable to molecular size, this case is so called strong anchoring.

2. When interaction of substrate with the liquid crystal is very much less than the mesophase interaction, $F_s^a << F$. The extrapolation length is much greater than the molecular lengths, $b >> a$. This condition is called weak anchoring.

Confined nematics exhibit peculiar physical phenomena connected to fundamental liquid crystal properties and lead to various important applications [21] [22]. The confining surfaces, for instance curved and/or possibly with antagonistic boundary conditions, can result in general in frustration of systems, leading possibly to observable transitions between a variety of thermally driven non- trivial equilibrium structures [22]. This is conveniently visualized as a resulting free energy profile in the appropriate parameter space exhibiting rugged features, manifesting as richness in the stable director space. The overall effect on the director field is difficult to predict, as in confined systems a competition exists between the effects due to the boundary conditions, the ordering interactions inside the LC system, and the disordering effects due to the temperature [23]. The study of confined liquid crystals thus is interesting from the point of observation of new stable structures that can be formed by appropriate external conditions and the transitions among these structures thereof [24] [25].

Consider the case of a second-order transition between an ordered and a disordered phase. When such a transition is approached from the disordered phase (in which the order parameter of the transition is zero) chosen to be, fluctuations of this order parameter appear in the bulk with a correlation length ξ which diverge at the transition. If the system is in

contact with an interface favoring the ordered phase, the correlation length at the surface will become infinite in a direction parallel to the surface plane. This creates an ordered layer at the surface in which the order parameter decreases exponentially from a non-zero value at the surface to zero in the bulk over a penetration length ξ_s; ξ_s is equal to the correlation length ξ and thus diverges at the transition. This phenomenon is called critical adsorption.

When the transition between two phases I and II is approached, say from phase I, a layer of phase II can form at the surface: phase II is said to wet the surface. If the thickness of the phase II layer becomes infinite at coexistence, wetting is complete; if the thickness remains finite at coexistence wetting is partial. Another useful parameter of the wetting transition is the contact angle θ, between the surface and the phase I – phase II interface (between phase – I and phase – II) taken in phase I. When $\theta = 0$, phase I completely wets the interface between phase II and the other phase. When $0 < \theta < \pi$, phase I partially wets the interface. With such a definition, partial wetting by phase I or by phase II are equivalent.

Studies of confinement of liquid crystals have been carried out by using experimental techniques, theoretical methods and computer simulations in the recent past. Experimental studies have been done, mainly on the preparations on substrates that align the LC in particular desired direction [17]. Theoretical studies focussed on mean field methods and phenomenological studies [26]. In the latter approach the free energy is considered by adding relevant surface energy terms. Minimization of this free energy yields the director configuration in the system consistent with the boundary conditions. Relatively, computer simulations methods of more recent origin, and both Monte Carlo and Molecular Dynamics simulations have been quite successful in investigating the confined LC systems in the perspective.

The simplest perturbation can arise from symmetry breaking induced by the surface: the nematic phase is characterized by a translation invariance which is broken by the presence of a surface. As a result the center of mass of the molecules nearest to the surface may have a tendency to be located in a plane parallel to the surface, *i.e.* a layer of molecules tends

to form at the surface. Due to the intermolecular forces present the existence of this layer favors the formation of a second one, and so on. The presence of a surface is thus likely to induce a positional order of the molecules at the interface between the nematic liquid crystal and the other phase.

Surface layering may be obtained at the interface due to solid substrates, arising from the molecule-substrate interactions. This type of ordering has been revealed by scanning tunneling microscopy used to obtain the images of the first monolayer of mesogenic molecules in contact with the substrate. Another method which has been used to investigate nematic-substrate interface and also monolayers of nematogens is optical second harmonic generation. This method yields detailed information about the orientation of the molecules: mean tilt with respect to the surface normal, distribution of azimuthal orientation in the plane of the surface and the existence of dipolar anchoring. Several methods have been used to measure the surface order parameter: pretransitional birefringence measurements in the isotropic phase, refractive index measurements, optical reflectivity measurements, ellipsometry, evanescent-wave ellipsometry, and electrically induced surface twist measurements.

The main issue concerning the anchoring of nematic liquid crystals is to relate the observed anchorings with the structure of the interfaces and to find the microscopic interactions responsible for the orientation of these phases by surfaces. It is thus impossible to predict from a microscopic basis which type of anchoring a given interface should induce. Phenomenological approaches based on a macroscopic point of view consider only the orientation of the nematic phase and the dependence of the interfacial energy on this orientation, without considering the detailed structure of the interface. Anchoring transitions also appear in the same way as phase transitions. Anchoring transition can be defined as change from one anchoring state to another, obtained by varying suitable control parameters determining the interface structure. Such a transition can be continuous or discontinuous, and can separate anchorings of the same type or of different types.

These confined systems can be studied using computer simulations which has certain

practical advantages for example, imposition of complex boundary conditions can be mimicked in simulation experiments more. There are situations where phenomenological calculations proceed to be too difficult to give interesting predictions, whereas computer simulations yielded with relative ease, some of the essential features in the systems due to confinement under such complex bounding conditions [9] [27]. To understand these systems, all the desired parameters can be computed and plotted with respect to the variable. This thesis in this context reports Monte Carlo simulations of confined liquid crystals, mainly hybridly confined liquid crystal films and droplets. The properties of confined systems are examined by computing different macroscopic physical observables as a formation of external variables, with a view to focussing on subtle changes in director structures. The next chapter provides a brief introduction to Monte Carlo technique, with the algorithms used for the study of these different systems.

1.5 Models studied

Computer simulation of liquid crystals has become a widely used tool to study the dynamics and the different structures in condensed matter systems [28] [29] [30] [31] [32] [33] [34] [35]. This is a tool that lies midway between experimental and theoretical (analytical) techniques. In simulations, the system is analyzed over long periods of time or a statistical average over a large ensemble is taken. In real sense simulation is a bridge between experiments and analytical theory. Structural and dynamical data can be obtained that can be compared to the available experimental data. Stability of different models to interpret the experimental observations can be explained using simulation techniques [36].

Different models have been proposed for liquid crystals using mean-field methods and phenomenological methods. One model widely used is due to Gay-Berne [37] model, and is not confined to a lattice. As a rule, such off – lattice models are on hand more realistic and offer flexibility in investigating complex phase diagrams involving layer structures. On the other hand, due to the more additional degrees of freedom introduced in this model, the

simulations are more computer intensive, requiring almost an order of magnitude more effort to obtain reliable predictions. To study the nematic – isotropic transition the lattice spin model is most convenient as it captures simply the physical nature of interaction leading to this transition. Thus, the present work relies exclusively on lattice models.

Computer simulations of lattice spin models for liquid crystal have been giving interesting opportunities to study anisotropic medium. In particular these models are easy to study the nematic-isotropic transition where the orientation of the spins gives rise to a transition. By adding different terms to the existing model new aspects of liquid crystals arising from subtle changes in the symmetry of the system can be studied. Three lattice models of liquid crystals that are used in this work are given in some detail below. Monte Carlo simulations were carried out by modeling droplets, hybrid films and different kind of substrates percolating various orders into the medium [38].

1.5.1 Lebwohl Lasher Model

A simple prototype lattice Hamiltonian which has the required symmetry of nematic liquid crystals was proposed by Lebwohl and Lasher (LL) [39]. Nematic liquid crystals are usually found with uniaxial symmetry, and this model captures this property when applied to bulk systems. Considering this symmetry, every molecule can be represented as a headless spin at every lattice point of an $L \times L \times L$ cubic lattice with periodic boundary conditions. Every spin is fixed in its position but has infinite degrees of freedom in its orientation. With respect to a three dimensional laboratory frame, every spin is represented by a unit vector having a specifical orientation. The interaction between any two such spins is represented by a pair potential of the form

$$E = -\epsilon_{ij}(\frac{3}{2}cos^2\theta_{ij} - \frac{1}{2}) \tag{1.5.1}$$

where ϵ_{ij} is a positive constant, ϵ, for nearest neighbor spins i and j and zero otherwise. P_2 is the second order Legendre polynomial and θ_{ij} is the angle between two molecules.

This interaction tends to bring molecules parallel to one another and embeds the symmetry $\hat{n} = -\hat{n}$. LL model is widely used to study the orientational dynamics and different physical properties at the nematic-isotropic transition. When the focus is exclusively on the orientational degree of freedom, uncoupled from the translational degrees. It represents the lattice version of Maier and Saupe theory. The above potential (equation 1.5.1) was investigated based on Monte Carlo techniques with the Metropolis algorithm. This lattice was found to undergo a transition at $kT/\epsilon = 1.1234 \pm 0.0006$ with a spontaneous order of $\langle P_2(\cos(\theta))\rangle = 0.33 \pm 0.04$ at the transition.

Utility of the LL model was well demonstrated by numerical simulations that were carried out, both on bulk and confined systems. This model provides the right kind of first order nature observed in real systems, and has been shown to be a very useful prototype model for the study of isotropic-nematic transition, much like the Ising and Heisenberg model for magnetics.

1.5.2 Biaxial Liquid Crystal Model

Most molecular theories of nematic liquid crystals assume that the constituent molecules are cylindrically symmetric. In real systems, the molecules are rarely cylindrically symmetric, and hence the molecular structures is in principle expected to play a very important role. Molecules that are not symmetric about their long axes, are known as biaxial liquid crystals. A general expansion of the pair–wise intermolecular potential together with the molecular field approximation, was developed for an ensemble of such particles [40].

The model used here is a pair-wise interaction lattice model [41] based on a mean field work . From this model equation

$$V = -U_o \left\{ q.q' + \gamma \left(q.b' + q'.b \right) + \lambda \left(b.b' \right) \right\} \tag{1.5.2}$$

a Hamiltonian was derived where the orientations of the molecules are used to compute the interaction energy between two particles. Consider classical, identical particles, possessing

D_{2h} symmetry, whose centers of mass are associated with a three-dimensional (simple-cubic) lattice N^3; let $x_\mu \in N^3$ denote the coordinate vectors of their centers of mass. The interaction potential will be isotropic in orientation space, and restricted to nearest neighbors, involving particles or sites labeled by μ and ν, respectively. The orientation of each particle can be specified via an orthonormal triplet of 3-component vectors (e.g. eigenvectors of its inertia tensor), say $\{w_{\mu,j}, j = 1, 2, 3\}$; in turn these are defined by an ordered triplet of Euler angles $\omega_\mu = \{\phi_\mu, \theta_\mu, \psi_\mu\}$; particle orientations are defined with respect to a common, but otherwise arbitrary, Cartesian frame. The two molecules can be represented as u_j for $w_{\mu,j}$ and v_k for $w_{\mu,k}$. Here, for j, u_j and v_j has the same functional dependence on ω_μ and ω_ν, respectively. Let $\tilde{\Omega}$= $\Omega_{\mu\nu}$ denote the set of Euler angles defining the rotation transforming u_i to v_j. Then,

$$f_{jk} = (u_j.v_k), \qquad G_{jk} = P_2(f_{jk}) \tag{1.5.3}$$

where P_2 denotes the second Legendre polynomial. The continuous interaction potentials used for this study are defined by appropriate linear combinations of terms G_{jk} , which can be cast in the form,

$$U = -\epsilon \left\{ G_{33} - \Gamma \left[G_{11} - G22 \right] + \Lambda \left[2(G_{11} + G_{22}) - G_{33} \right] \right\}. \tag{1.5.4}$$

Here ϵ denotes a positive constant setting the temperature and the energy scales, $T^* = k_B T/\epsilon$. $|\Gamma|$ and $|\Lambda|$ are often taken lesser than one; setting these two terms to zero makes equation 1.5.4 converges to Lebwohl-Laser model. It was shown using MC simulation that a biaxial phase does not result even with the above model as long as the third therm is neglected *i.e.* Λ=0 [42]. Many different approximations were proposed for equation 1.5.4 , one of the most known being the London-de Born-Heller approximation, where $\Lambda = \Gamma^2$.

In this approximation, the above experiments can be conveniently recast in terms of relative orientation of the neighboring spins as [43].

$$U(\omega_{ij}) = -\epsilon_{ij}\{P_2(cos\beta_\mu) + 2\lambda[R^2_{02}(\omega_\mu) + R^2_{20}(\omega_\mu)] + 4\lambda^2 R^2_{22}(\omega_\mu)\} \tag{1.5.5}$$

with the biaxial molecules or spins fixed to lattice sites of a three-dimensional lattice. ϵ_{ij} is the coupling parameter, taken as constant when nearest neighbors, λ the biaxiality parameter accounting for the deviation from cylindrical symmetry. The relative orientation of a molecular pair is considered in terms of ω_μ. This in a Cartesian frame can be expanded as

$$U_{ij} = -\epsilon(\frac{3}{2}V_{33} - \lambda\sqrt{6}(V_{11} - V_{22}) + \lambda^2(V_{11} + V_{22} - V_{12} - V_{21}) - \frac{1}{2}). \qquad (1.5.6)$$

where $V_{ij} = (u_i.v_j)^2$, and is related to direction cosines for the molecular pair. A phase diagram was proposed for this potential, where for a particular value of λ the so called Landau point is observed. A detailed Monte Carlo study at this point proved this to be a second order type of transition [44].

Based on mean-field considerations [41] a pair-wise lattice model was proposed which is more general and is not restricted to London's approximation. In this model two parameters (Γ and Λ) were considered as controlling the biaxiality of the medium and Monte Carlo simulations were done for a particular choice of these biaxiality parameters [45]. This model is a more generalized form of the equation 1.5.6. Latter chapters in this thesis deals with a detailed study on these models and interesting consequences of the variation of the parameters of the Hamiltonian.

1.5.3 Luckhurst Elastic Model

When studying confined systems where the elastic properties would play an important role due to the boundary conditions, a more information and relevant model can also be considered. A lattice based Hamiltonian which explicitly takes into account the elastic properties of the medium via the three elastic coefficients (splay (K_1), twist (K_2), and bend (K_3) elastic constants is discussed here with this objective. This interaction is derived within the approximation of confine it to nearest neighbor lattice elements. Its application to Schadt – Helfrich cell was demonstrated through detailed Monte Carlo simulations [46].

The director configuration of a system with a given geometry and boundary conditions is determined by minimizing the elastic free energy of the sample in the continuum limit.

The corresponding energy density in the nematic phase is expressed in terms of powers of the gradient of the director **n**, restricting to only the quadratic terms, as

$$\Psi = \frac{1}{2}\{K_1 \left(\nabla.\mathbf{n}\right)^2 + K_2 \left[\mathbf{n}.\left(\nabla \times \mathbf{n}\right)\right]^2 + K_3 \left[\mathbf{n} \times \left(\nabla \times \mathbf{n}\right)\right]^2\}. \tag{1.5.7}$$

Only very simple systems permit an analytical solution of the above equation, and very often, in practice, free energy is calculated through numerical procedures. An alternative method is to assume a lattice model of pair-wise interacting nearest neighbors elements stipulated by a model Hamiltonian, and construct an equilibrium ensemble at different reduced temperatures (measured in units of the interaction strength introduced in the Hamiltonian), employing the usual Markov chain Monte Carlo methods [47] based on Metropolis algorithm. Earlier work on these droplets based on this methodology using Lebwohl-Lasher model was limited by the fact that the interaction energy depends only on the relative orientation of the two particles but not their relative positions, and hence cannot distinguish between the different deformations. This potential thus corresponds to an assumption of equal elastic constants (spherical approximation).

An alternative approach, initiated by Gruhn and Hess [48], and later developed by Romano and Luckhurst [49], involves derivation of a model potential for a pair-wise additive interaction between local directors, which approximately reproduces the elastic free energy density of the system. This is achieved by mapping the above equation onto a suitable expansion of the interaction potential. In this scheme, the space is discretized to a cubic lattice, each site representing a director. The free energy of the system is defined as the sum of pairwise additive interactions between nearest neighboring sites. An expression, with appropriate multiplicative and additive constants chosen to scale the isotropic average of the energy to be zero, is then derived to be used as model potential for Monte Carlo simulations. These naturally are defined through specific combinations of the three elastic coefficients, thereby making the model rich and useful so as to make them applicable to real systems with differing elastic constants. Derivation of the potential used in this work is briefly outlined below, in order to introduce the notation.

The pair potential between two directors located at two neighboring sites, say j and k, is expanded in terms of a complete set of basis functions depending on the orientation of the two directors $\mathbf{n}_j$ and $\mathbf{n}_k$ and the orientation of the vector joining them $\mathbf{r}$. The $S-$functions [46] $S_{L_j,L_k,J}(\mathbf{n}_j, \mathbf{n}_k, \mathbf{r})$ were found to be suitable for this purpose. Here the index L_j refers to the j-th director, L_k to the k-th director and J corresponds to the inter-director vector taking the values from $(L_j + L_k)$ to $|L_j - L_k|$. In this particular application it was found that the $S-$functions depend only on the scalar invariants associated with the vectors in their argument, viz. $a_j = \mathbf{n}_j.\mathbf{r}$, $a_k = \mathbf{n}_k.\mathbf{r}$, $b_{jk} = \mathbf{n}_j.\mathbf{n}_k$ and $c_{jk} = \mathbf{n}_j.(\mathbf{n}_k \times \mathbf{r})$. The symmetry of the nematic phase requiring that $\mathbf{n} = -\mathbf{n}$ demands that the total rank, $(L_j + L_k + J)$, of the S-function be even, thereby eliminating the factors c_{jk}. Thus the pair potential between two neighboring sites j and k is expanded in terms of $S-$functions restricted to terms of even total rank, with suitable coefficients, as [50] [46]

$$\Phi_{jk} = \sum_{L_j,L_k,J} \varphi_{L_j,L_k,J} S_{L_j,L_k,J}\left(a_j, a_k, b_{jk}\right). \tag{1.5.8}$$

This pair potential is then mapped onto the expression for the free energy density, assuming small angular displacements of the director so as to replace the gradients by finite increments. Finally certain well-defined deformations are considered in both the pair potential and the initial free energy density (approximated for small deviations), so as to derive relation between the coefficients of expansion in the pair potential and the elastic constants. The final expression for the pair potential $\Phi_{L_j,L_k,J}$ is given by

$$\begin{aligned}\Phi_{jk} = \lambda\left[P_2\left(a_j\right) + P_2\left(a_k\right)\right] + \mu\left(a_j a_k b_{jk} - \frac{1}{9}\right) + \\ \nu P_2\left(b_{jk}\right) + \rho\left[P_2\left(a_j\right) + P_2\left(a_k\right)\right] P_2\left(b_{jk}\right).\end{aligned} \tag{1.5.9}$$

Here, P_2 is the second rank Legendre polynomial. The coefficients of expansion are related to the elastic constants through the following relations, involving the chosen linear

dimension Λ of the volume element in the cubic lattice to represent their local directors:

$$\begin{aligned}\lambda =& \frac{1}{3}\Lambda\left(2K_1 - 3K_2 + K_3\right)\\ \mu =& 3\Lambda\left(K_2 - K_1\right)\\ \nu =& \frac{1}{3}\Lambda\left(K_1 - 3K_2 + K_3\right)\\ \rho =& \frac{1}{3}\Lambda\left(K_1 - K_3\right).\end{aligned} \tag{1.5.10}$$

An interesting feature of this potential is that Λ, enters as a length scale over which the director gradient is discretized and defines the lattice parameter corresponding to the distance between the neighboring sites. By setting all the elastic constants equal to each other, say K, the above potential is reduced to the form of the Lebwohl-Lasher potential,

$$\Phi_{jk}^{LL} = -\epsilon P_2\left[\cos\left(\mathbf{n}_j.\mathbf{n}_k\right)\right]. \tag{1.5.11}$$

Under these special conditions, the energy scale parameter ϵ, is equal to ΛK for the present model. In general, the total free energy of the system is then given by

$$\Psi = \frac{1}{2}\sum_{j=1}^{N}\sum_{k=1}^{6}\Phi_{jk}, \tag{1.5.12}$$

where N is the number of sites. Following the procedure adopted earlier, the scaled potential for use in simulations is obtained by dividing equation 1.5.9 by $|\nu|$. This leads to a scaled temperature, to be used in the Monte Carlo scheme, given by

$$T^* = k_BT/|\nu| = 3k_BT/(\Lambda|K_1 - 3K_2 - K_3|). \tag{1.5.13}$$

With one elastic constant approximation $i.e.$ $K_1 = K_2 = K_3 = K$ this equation 1.5.9 reduces to the LL model (equation 1.5.1). A Monte Carlo simulation of this model was investigated by simulating the three Freedericksz transitions as well as that of the Schadt - Helfrich cell [46]. An extension of this model was proposed to mimic a chiral nematic liquid crystal [51]. This model is used in the later chapters of the thesis to model a polymer dispersed liquid crystal [23].

Bibliography

[1] G.Durand and J.D.Lister. Recent advances in liquid crystals. *Ann. Rev. Mate. Sci.*, 23:269, 1973.

[2] S.Chandrashekar and N.V.Madhusudana. Liquid crystals. *Ann. Rev. Mate. Sci.*, 10:133–135, 1980.

[3] Michael J. Stephen and J.P.Straley. Physics of liquid crystals. *Reviews of Modern Physics*, 64:617, 1974.

[4] M.Carme Calderer. Mathematical study of liquid crystal. 2004.

[5] Zhengping Zhang, Amitabha Chakrabarti, Ole G Mouritsen, and Martin J. Zuckermann. Substrate–induced bulk alignment of liquid crystals. *Phys. Rev. E*, 53:2461 – 2465, 1996.

[6] S.Chandrashekar. *Liquid crystals*. Cambridge University Press, 1977.

[7] C.Zannoni. *Molecular Physics of Liquid Crystals*. Academic Press, 1979.

[8] C. Zannoni. *Nuclear Magentic Resonance in Liquid Crystals*. D.Reidel Publishing Company, Dordrecht, 1983.

[9] Andreja sarlah. *Effect of the confining substrates on nematic order-fluctuations in liquid crystals*. PhD thesis, School of Mathematics and physics, University of Ljubljana, 2001.

[10] C. Zannoni. *The Molecular Dynamics of Liquid Crystals*. D.Reidel Publishing Company, Dordrecht, 1989.

[11] G.Vertogen and W.H.de Jeu. *Thermotropic Liquid crystals, Fundamentals*. Springer-Verlag, Berlin, 1988.

[12] Peter J.Collings and Michael Hird. *Introduction to Liquid Crystals Chemistry and Physics*. Taylot and Francis, 1998.

[13] P.D de Gennes and J. Prost. *The Physics of Liquid Crsytals*. Oxfords University Press, 1995.

[14] G.R.Luckhurst. *Molecular Phhysics of Liquid Crystals*. Academic Press, 1979.

[15] G. R. Luckhurst and C. Zannoni. Why is the maier-saupe theory of nematic liquid crystals so successful? *Nature*, 267:412, 1977.

[16] W. H. de Jeu. *Phase Transitions in Liquid Crystal*. Plenum Press; NATO Scientific Affairs Division, 1992.

[17] J.Cognard. Alignment of nematic liquid crystals and their mixtures. *Mol. Cryst. Liq. Cryst. Suppl. 1*, 1982.

[18] B.Jerome. Surface effects and anchoring in liquid crystals. *Rep. Prog. Phys.*, 54:391, 1991.

[19] B.Jerome. Interfacial structural transitions in nematic liquid crystals. *J.Phys:Condens. Matter*, 6:A269–A273, 1994.

[20] B.Jerome. Nematic liquid crystals at interfaces. *Mol. Cryst. Liq. Cryst.*, 212:21–32, 1992.

[21] G P Crawford and S Zumer, editors. *Liquid Crystals In Complex Geometries*. Routledge, UK.

[22] Theo Rasing. *Surfaces and Interfaces of Liquid Crystals*. Springer-Verlag New York, LLC, 2004.

[23] P. Pasini, C. Chiccoli, and C. Zannoni. *Advances in the Computer Simulations of Liquid Crystals*. Kluwer, Dordrecht, 2000.

[24] Eugene C Gartland. Structures and structural phase transitions in confined liquid crystal system.

[25] J.Evans. Fluids adsorbed in narrow pores: phase equilibria and structure. *J.Phys: Condens. Matter*, 2:8989–9007, 1990.

[26] A.Poniewierski and A.Samborski. Anchoring of nematic liquid crystals at a solid substrate. *Phys.Rev. E*, 53:2436, 1996.

[27] Gregor Skacej. *Modeling of strongly confined liquid crystalline systems*. PhD thesis, University of Ljubljana, 2002.

[28] Michael P. Allen. Liquid crystal systems. *Computational Soft Matter: From Synthetic Polymers to Proteins*, 23:289–320, 2004.

[29] Michael P. Allen. Introduction to molecular dynamics simulations. *Computational Soft Matter: From Synthetic Polymers to Proteins*, 23:1–28, 2004.

[30] C M Care and D J Cleaver. Computer simulation of liquid crystals. *Reports On Progress in Physics*, 68:2665, 2005.

[31] Greg D.Wall and Douglas J. Cleaver. Computer simulation studies of confined liquid-crystal films. *Phys. Rev. E*, 56:4306, 1997.

[32] N.V.Priezev, G.Skacej, R.A.Pelcovits, and S.Zumer. External and intrinsic anchoring in nematic liquid crystals: A monte carlo study. *Phys. Rev. E*, 68:041709, 2003.

[33] M.P.Allen. *Mol. Phys.*, 96:1391–1397, 1999.

[34] M.P.Allen. Molecular simulation and theory of the isotropicnematic interface. *Jour. of chem. Phys.*, 112:5447, 2000.

[35] M.P.Allen and Mark A.Wllen. Simulation of structure and dynamics near the isotropic-nematic transition. *Phys Rev. Lett.*, 78:1291, 1997.

[36] Martin A. Bates. Testing experimental analysis techniques for liquid crystal using computer simulations. *Liquid Crystal*, 32:1365–1377, 2005.

[37] J. G. Gay and B. J. Berne. Modification of the overlap potential to mimic a linear sitesite potential. *J. Chem. Phys.*, 74:3316, 1981.

[38] D.J.Cheung and F.Schmid. *arxiv:cond-mat*, 0522298v1.

[39] P.A. Lebwohl and G. Lasher. Nematic liquid crystal order - a monte carlo calculation. *Phys. Rev. A*, 6:426, 1972.

[40] G. R. Luckhurst, C. Zannoni, P. L. Nordio, and U. Segre. Molecular field theory for uniaxial nematic liquid crystals formed by noncylindrically symmetric molecules. *MP*, 30:1345, 1975.

[41] A.M.Sonnet, E.G.Virga, and G.E.Durand. Dielectric shape dispersion and biaxial transitions in nematic liquid crystals. *Phys. Rev. E*, 67:061701, 2003.

[42] G. R. Luckhurst and S. Romano. Computer simulation studies of anisotropic systems uniaxial and biaxial nematics formed by noncylindrically symmetric molecules. *Mol. Phys.*, 40:129, 1980.

[43] F. Biscarini, C. Chiccoli, P. Pasini, F. Semeria, and C. Zannoni. Phase diagram and orientational order in a biaxial lattice model. a monte carlo study. *Phys. Rev. Lett.*, 75:1803–1806, 1995.

[44] C. Chiccoli, P. Pasini, F. Semeria, and C. Zannoni. A detailed monte carlo investigation of the tricritical region of a biaxial liquid crystal systems. *Int. J. Mod. Phys. C*, 10:469–476, 1999.

[45] Silvano Romano. Computer simulation of a biaxial nematogenic model on a three-dimensional lattice and based on a recently proposed interaction potential. *Physica A*, 337:505 519, 2004.

[46] P.J. Le Masurier, G.R. Luckhurst, and G. Saielli. *Liq. Cryst.*, 28:769, 2001.

[47] K. P. N. Murthy. *Monte Carlo methods in Satistical Physics*. Universities Press, 2003.

[48] T. Gruhn and S. Hess. *Z. Naturforsch.*, A51:1, 1996.

[49] G.R. Luckhurst, , and S. Romano. *Liq. Cryst.*, 26:871, 1999.

[50] S. Romano. *Int. J. Mod. Phys. B*, 12:2305, 1998.

[51] G. R. Luckhurst and G. Saielli. A pairwise additive potential for the elastic interaction energy of a chiral nematic. *Mol. Cryst. Liq. Cryst.*, 395:183–192, 2003.

Chapter 2

Brief Introduction to Computer Simulations

A simple model can shed more light on Nature's workings than a series of ab-initio calculations of individual cases, which, even if correct, are so detailed that they hide reality instead of revealing it. ... A perfect computation simply reproduces Nature, it does not explain it. P.W. Anderson

2.1 Computer Simulation - An Integrating Tool

Computer simulation is a convenient technique to estimate, as accurately as possible different physical properties of a model system. It is one of the tools available for investigating mesogenic behavior. However, a relative newcomer compared to the many experimental and theoretical approaches available, and its role is often complementary. Computer simulation studies can yield unique insight into molecular ordering and phase behavior and so inform the development of new experiments or theories. Molecular simulations can provide systematic structure property information, through which links can be established between molecular properties and macroscopic behavior. Alternatively, simulation can be used to test the validity of various theoretical assumptions.

Computer simulations are a bridge between theory and experiment. Given a particular model based on a theoretical concept, it can be used to mimic a phenomenon. Different parameters that are acquired experimentally can be compared with those obtained through simulations. The exactness of a computer simulation – a computer experiment – depends on the model used. These models are mostly proposed based on a particular theory, that

tries to explain the system. A well-focused simulation helps one to understand what happens in a experiment and test the underlying postulates at the fundamental level. For a better understanding of experiments some of these results can also be simulated by imposing on the system the required conditions, one simple example being the simulated NMR spectrum in LC system to appreciate different director configurations [1]. A study aimed at examining the role of a simulation as a research aid that has the potential if bridge the gap between theory and reality in the case of electric circuits was undertaken [2]. It was seen that simulations can provide unique advantages for enhancing understanding of the theoretical principles, by bridging the gap between the theoretically idealized models and their formal representations of reality.

In their application to problems of statical physics, computer Simulations serve as a bridge between microscopic and macroscopic properties. The microscopic models proposed are based on molecular interactions, and it is required that of the macroscopic properties of the system be predicted. Simulations provide the hidden truths behind macroscopic properties. The importance of computer simulation 1. measure of extreme condition that are experimentally prohibitive or difficult. 2. Details of molecular motion and structure impossible or difficult to study experimentally. 3. Molecular motions that are too fast or slow to be captured using experimental methods. In general, a computer simulation approach requires, the setting up of appropriate models of the molecules of interest and the determination of the equilibrium state of a sufficiently large system of these particles at the chosen external (thermodynamic), like conditions of temperature, pressure etc. by numerical simulation methods.

Computer simulation is a convenient technique to obtain different parameters and to study the relevant phase transitions. The study of the correlation between molecular interactions and the macroscopic properties obtained is of primary of interest in computational statistical physics. The molecular complexity in liquid crystals makes computer simulations a convenient tool to study them. They are anisotropic materials, experimental techniques like NMR, polarization techniques liquid crystals have been used to study their

properties and their transitions. Continuum models based on phenomenological elastic constants and hydrodynamic transport coefficients are of great success in modeling. Molecular Modeling and Computer Simulation techniques have recently seen major progresses, due to the continuous impressive increase in the availability of high performance computing resources at affordable resources.

Confined liquid crystal systems are the interest of study in this thesis. These can be investigated using simulation methods like Molecular dynamics (MD) and Monte Carlo (MC) methods. There are qualitative differences between molecular dynamics and Monte Carlo simulations. Molecular dynamics requires finalizing approximate numerical solution of Newton's equations of motion of the macroscopic system. It employs on this context the known algorithms to solve ordinary differential equation to the required approximation. These methods correspond to actual evolution of the system with a given dynamic perception, and has advantages in examining the time evolution of the system. Both thermodynamic and kinetic data can be generated by appropriate prescription of the equilibrium condition on the distribution of velocities. Monte Carlo can be thought of as a prescription for sampling configurations from a statistical equilibrium ensemble. This principle of Monte Carlo is based on the equivalence of averages over equilibrium ensemble of microstates to the long time averages on a given macroscopic system in equilibrium. Energy is the primary physical property to prescribe the probabilistic distribution of microstates belonging to a given canonical ensemble. The choice of either MC or MD for a given simulation largely depends on the type of information to be extracted from the model system, and in the case of equal suitability the computational effort needed essentially decide the choice. This thesis employs MC methods to study confined liquid crystal systems. A brief introduction to the MC methods is presented encompassing to Metropolis algorithm and non-boltzmann sampling methods in the next sections of this chapter.

In 1945 the building of the first computer brought about a renascence of a mathematical technique known traditionally as statistical sampling; in its new formulation and owing to its nature, such problems have come to be known as the Monte Carlo method. During this

wartime period, a team of scientists, engineers, and technicians were working furiously on the first electronic computer. N. Metropolis suggested an obvious name for the statistical method a suggestion not unrelated to the fact that Stan had an uncle who would borrow money from relatives because he just had to go to Monte Carlo. A well written history *i.e.* account of the development of the Monte Carlo method was presented in [4].

2.2 Monte Carlo Simulations

Monte Carlo method is a numerical technique that depends on random numbers. It provides approximate solutions to a variety of mathematical problems by performing statistical sampling experiments on a computer, and applies to problems with no probabilistic content as well as to those with inherent probabilistic structure. Monte Carlo technique belongs to a class of computational algorithms that rely on repeated random sampling and relies on our ability to generate in principle, a truly random sequence of numbers. These methods are often used to simulate physical system based on mathematical models. Because of their reliance on repeated computation and random (or pseudo-random) numbers, Monte Carlo techniques are most suited for calculation on a computer, and offer an efficient valuable and acceptably approximate methodology particulary, when an exact solution with a deterministic algorithm is not feasible.

An experimentally measured equilibrium macroscopic property is a time averaged quantity of a given system over a larger period of observation time [5]. This experimental time average can be equated to an average over a suitable static Gibbs ensemble of microstates, provided the time evolution is ergodic. When in equilibrium the macroscopic properties of a system do not change. These corresponds to the physical properties averaged over the equilibrium ensemble. However, the physical properties do fluctuate under equilibrium conditions, and are less prominent the larger the system is. The associated fluctuations are inversely proportional to the square root of the system size and are not observable under normal condition in macroscopic system. The task of computing the thermal average

over many– particle systems is thus reduced to the job of sampling microstates from an appropriate canonical ensemble through MC sampling technique and computation of statistical properties of different physical parameters over this ensemble. Different algorithms were proposed to obtain a large enough ensemble over which the thermal properties can be averaged, of which Metropolis algorithm is widely used.

2.3 Metropolis Algorithm

This algorithm was introduced by Nicolas Metropolis and his coworkers in a paper on simulations of hard-sphere gases in 1953 and is essentially an importance sampling algorithm based on a long sequence of random numbers.

Consider a closed system, and let the set of all the microstates of the system be represented by Ω_{CS}. Starting from an arbitrary initial state C_0, a Markov chain of microstates is represented as

$$C_o \rightarrow C_1 \rightarrow C_2 \rightarrow .....C_k \rightarrow C_{k+1} \rightarrow ..... \tag{2.3.1}$$

The sequence of the micro – states appearing in the Markov chain is probabilistic condition. A Markov process is defined as a random evolution of a memoryless system, the future state depends only on the present, and not on the past, states. For example the state C_2 depends on C_1 and not on C_0. The probability of such a process is given as

$$P(C_k, C_{k-11}, C_{k-2}, ...C_3, C_2, C_1) = P(C_k|C_{k-1}) \quad \forall \quad k = 1, 2, ...n. \tag{2.3.2}$$

The past has no influence over the future once the present is specified. Restricting the decision to a Markovian process, one needs to specify thus only conditional probability of the following type to predict the evolution of the system as a Markov sequence:

$$P(C_k|C_{k-1}) = W_{ij} \quad \forall \quad k = 1, 2, ...n \tag{2.3.3}$$

where W_{ij} defines the transition probability from the state C_i to state C_j in a single step. W_{ij} is a $(i \times j)^{th}$ element of a $\Omega_{CS} \times \Omega_{CS}$ square matrix. By insisting on the ergodicity of the system, and by imposing conversation of probabilistic measure (sum of all elements

in a row of W is unity), W becomes a stochastic matrix with very special properties. The principle of ergodicity is the possibility to attain every configurations of the system starting from any arbitrary initial configuration.

The sequences of states follow a time ordered path, here the time is referred to as 'Monte Carlo time'. The time dependent behavior is described by a master equation

$$\frac{\partial P_n(t)}{\partial t} = -\sum_{n \neq m} \left[P_n(t) W_{n \to m} - P_m(t) W_{m \to n} \right], \tag{2.3.4}$$

where $P_n(t)$ is the probability of the system in being in state n at time t. In equilibrium $\left(\partial P_n(t)\right)/\partial t = 0$ and so,

$$\sum_{n \neq m} P_n(t) W_{n \to m} = \sum_{n \neq m} P_m(t) W_{m \to n} \tag{2.3.5}$$

This is called the detailed balance condition corresponding to the stationary nature of equilibrium distribution function. A more stricter condition results, known as microscopic detailed balance, by demanding that this balance be satisfied by any pair of states separable *i.e.*

$$P_n(t) W_{n \to m} = P_m(t) W_{m \to n} \tag{2.3.6}$$

The probability of the n^{th} state occurring in a classical canonical system is given by

$$P_n(t) = \frac{e^{-E_n/k_B T}}{Z} \tag{2.3.7}$$

where Z is the partition function. Hence,

$$\begin{aligned} \frac{W_{n \to m}}{W_{m \to n}} &= \frac{e^{-E_m/k_B T}/Z}{e^{-E_n/k_B T}/Z} \\ &= (E_n - E_m)\beta \\ &= \Delta E \beta \end{aligned} \tag{2.3.8}$$

where $\beta = 1/(k_B T)$. The probability is usually not known because the denominator is not known, but this is avoided in the Metropolis method by generating a Markov chain of states which depends only on the ration of the probabilities of the states involved. If we

produce the n^{th} state from the m^{th} state, the relative probability is the ratio of the individual probabilities and the denominator conveniently cancels.

In a simple way the Metropolis algorithm can be summarized as:

1. Consider an initial arbitrary state C_o from the set of micro-states Ω_{CS}. $E(C_o)$ is the energy of this initial configuration C_o.

2. The orientation of a selected molecule (spin) changed resulting in a trial state C_t. $E(C_t)$ is the energy of this trial state.

3. Compute $\Delta E = E(C_t) - E(C_o)$.

4. Accept the trial state as the next state in the Markov chain, i.e. $C_t \rightarrow C_1$, if $\Delta E \leq 0$. Otherwise accept C_t with a probability $\exp(-\beta\Delta E) \geq \xi$. ξ a random number generated.

It may be seen that this is a generalized form of importance sampling with the importance function impartially chosen as the canonical distribution function at the chosen temperature. The actual flipping of the microstate in step 2 depends on the system of study. In the Ising model the spin has only two orientations either it is up or down and hence the random steps involving a given step in the configurational spin has only two possibilities. In this thesis the system studied comprises of liquid crystal molecules, and they have continuous orientational degrees of freedom yielding a continuum of configurations to sample from . For such systems, the orientation is changed randomly by a suitable algorithm, like for example the procedure suggested for such systems by Barker and Watts [6].

2.4 Boltzmann sampling

Boltzmann sampling refers to the construction of a canonical ensemble of microstates, in contrast to the non – Boltzmann sampling (see following section) wherein the microstates are ideally generated by making a uniform random walk in energy space. In the first sampling procedure unbiased steps are proposed in the configuration space, and are accepted

or otherwise depending on the relative probabilities of the two microstates according to metropolis prescription. The system of interest is the thermotropic LC, often confined to a specific geometry and boundary conditions; and the phenomenon of interest is the nature of the phase transition between an isotropic state and nematic state. Because only the orientational degrees of freedom are relevant, lattice Hamiltonians are preferred to investigate these problems. This section describes details of MC simulations carried out in this work.

Initially a micro-state is chosen at random, – the initial state C_o, and the energy of this state is computed as $E(C_o)$ using the chosen Hamiltonian. The energy of this configuration is changed by changing the orientation of the LC molecules (spin) using Barker Watts [6] algorithm. The energy of the new trial micro-state (C_t) is referred to as $E(C_t)$. The difference between the energies of the two microstates is computed as $\Delta E = E(C_t) - E(C_o)$. If $E(C_t) \leq E(C_o)$ then $C_t \rightarrow C_1$. If not, then the state C_t is accepted with Boltzmann probability $\exp(-\beta\Delta E)$, where $\beta = 1/k_BT$ (k_B is the Boltzmann constant and T is the temperature). We generate a random number ξ, and check if $\xi \leq exp(-\beta\Delta E)$, so that $C_t \rightarrow C_1$. If $\xi > \exp(-\beta\Delta E)$, then we reject the trial state, include C_o in the ensemble and proceed with the random walk to generate another trial state C_t. This is the Metropolis algorithm, and the probability with which the state C_t is accepted depends on the desired type of ensemble. The energy of the microstates is plotted as a function of Monte Carlo steps to check for equilibration. It is expected that, starting from an arbitrary initial microstate, the system evolves through a series of transient states towards equilibrium, and the macroscopic properties in equilibrium are computed after the sequence of microstates in the Markov chain respectively follow canonical distribution. These microstates rejection of the initial transient states, and collect data only subsequently referred to as production run. During the production run, the physical quantities of interest show fluctuations about a mean value which is a constant. The larger the number of microstates collected in the production run, the better is the reliability of the average. An average of a parameter A can be computed as

$$\langle A \rangle = \frac{A_{sum}}{N} \tag{2.4.1}$$

Here, N is the number of microstates collected during the production run and A_{sum} is the addition of the physical parameter A over all the production run. Such MC simulations can be repeated at every desired temperature, and thus all relevant physical properties can be computed as a function of temperature. This way every parameter can be computed and plotted as a function of temperature. Computation of various order parameters will be discussed in detail as a subsequent section in this chapter. The canonical ensemble can be visualized as a result of competition of two probability distributions in the phase space. The first arises from the density of states $D(E)$ and is a consequence of the Hamiltonian and boundary conditions imposed. This is normally an increasing function of microstate energy. The second probability distribution is due to equilibrium with the surrounding at a given temperature and is described by Boltzmann factor. This is a decreasing function of microstate energy. A given microstate has a resultant probability of existence, decided by the product of these two distributions evaluated for that microstate. The equilibrium distribution will thus be a sharply peaked function in phase space, its location being determined by the canonical distribution function through the temperature. This is illustrated in the figure 2.1. The error in these simulations is avoided by considering a ensemble of about 1 million microstates in the production run over which the different physical parameters are computed. The energy distribution in a canonical ensemble is thus described as $P(E) \propto D(E)exp(-\beta E)$. However, such Boltzmann sampling is not efficient in certain physical conditions and requires considerable computational effort to yield reliable MC estimates of physical properties. These may be summarized as [7]:

1. In second order transitions, very large correlations among microstates are present at the transition. Single step algorithms are not suitable to overcome these correlations, cluster algorithms were proposed. First order transitions (thermally driven) pose a challenge even to cluster algorithms, as the free energy profile could develop significant barriers between the two co -existing phases, making canonical algorithm in efficient due to quasi – ergodic regions in the configuration space connection the two

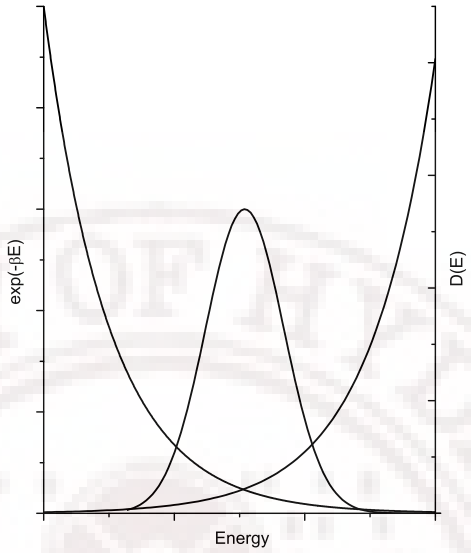

Figure 2.1: An illustrative plot for Boltzmann sampling

sets of microstates.

2. The correlation time τ diverges as $T \rightarrow T_C$ (transition temperature), and this means that finite sample Monte Carlo estimates of macroscopic properties of the system tend to become unreliable when the temperature of the system is very close to the critical value. The divergence of τ as $T \rightarrow T_C$ is called critical slowing down. This can be overcome by using non-Boltzmann sampling methods.

3. In studying critical phenomenon in detail, one needs to compute physical properties at several closely spaced temperatures and canonical sampling techniques require that each such ensemble be constructed separately. This is a very computer intensive exercise,and canonical methods are not very efficient in this respect.

4. Even though obtaining estimate of entropy and hence free energy, as a function of relevant control parameters is not within the reach of canonical sampling technique, it would be useful if this issue can be addressed by suitable algorithm, and such an exercise provides valuable insight into the physics of the system.

2.5 Non-Boltzmann Sampling

In view of importance of non – Boltzmann sampling technique as mentioned above, a brief account of methodology of constructing entropy ensemble is given below. Canonical ensemble at the desired temperature can be extracted from the microstates of the non – Boltzmann ensemble through the so – called reweighting procedure. We start this discussion by noting that the partition function is given by

$$\begin{aligned} Z(\beta) &= \sum_{C} \exp[-\beta E(C)] \\ &= \sum_{E} \exp\left[\frac{S(E)}{k_B} - \beta E\right] \end{aligned} \tag{2.5.1}$$

where $S(E)$ is the micro-canonical entropy. Here the first summation is over all the microstates, while the second is over the energy range. The probability for the closed system to be in a microstate C is given by

$$P(C) \backsim \exp[-\beta E(C)]. \tag{2.5.2}$$

The probability of the system to have an energy E is given by

$$P(E) \propto \exp\left[\frac{S(E)}{k_B} - \beta E\right]. \tag{2.5.3}$$

The Metropolis algorithm helps to sample from the above distribution and obtain a canonical ensemble. If the interest is to sample from another distribution given by say,

$$P_{\alpha}(E) \propto \exp\left[\frac{S(E)}{k_B} - \alpha(E)\right] \tag{2.5.4}$$

then the local updation of a current state C to a trial state C_t is accepted with the probability

$$p = \min\left(1, \exp\left[-\left\{\alpha\left(E\left(C_t\right)\right) - \alpha\left(E\left(C\right)\right)\right\}\right]\right). \tag{2.5.5}$$

If $\alpha(E) = \beta E$ then canonical sampling is recovered. For any other choice of $\alpha(E)$, an ensemble, not satisfying the Boltzmann distribution results and is called the non – Boltzmann ensemble. Entropic sampling is obtained when $\alpha(E) = S(E)/k_B$, which renders $P(E)$

the same for all E. Sucha sampling corresponds to random walk uniform with respect to energy. Such a choice $\alpha(E)$ entropic function, is not known *a priori*. A special algorithm has to devised to build this $\alpha(E)$ in an iterative way, depending on the microstates visited during a relatively short run. In entropic sampling, a simple random walk in done in energy space, where the energies are uniformly sampled over the energy range. Since unweighting - reweighting is done extracting the canonical ensemble of microstates, even a reasonable approximate estimate of the entropic function $\alpha(E)$ would suffice: $\alpha(E)$ should be as close to $S(E)/k_B$ as possible. A histogram of microstates generates with the above prescription leads to a fairly a flat distribution with respect to energy.

Let (E_{max}, E_{min}) be the energy range over which a uniform distribution of energy microstates is to be obtained. This range of energy is split into bins of equal energy. Let E_i be the energy of the i^{th} bin, and $\alpha(E_i) = f_o$, some initial value chosen at the beginning of the simulation. The modification factor f is reduced in a particular way, can be for example $f_1 = \sqrt{f_0}$ or $f_1 = f_0/2$, until $f = 0.00000001$. For continuous systems like liquid crystal this process is repeated a large number of times in order to obtain a fully formed density of states [8].

After the density of sates is obtained a production run is done to obtain an ensemble of equally sampled states in the energy space. We get an entropic ensemble of microstates $C_i : i = 1, N$. The canonical ensemble average of a macroscopic property say $O(C)$ at a desired temperature $T = 1/[k_B T]$ can be obtained by from the entropic sample unweighting (divide by $\exp[-\alpha(E(c_i))]$) followed by reweighting (multiply by $\exp[-\beta E(C_i)]$) ***i.e.***

$$\langle O_\beta \rangle = \frac{\sum_{i=1}^{N} O(C_i) exp[-\beta E(C_i) + \alpha(E(C_i))]}{\sum_{i=1}^{N} exp[-\beta E(C_i)] + \alpha(E(C_i))}. \tag{2.5.6}$$

Using the above method, all the physical parameters can be obtained at any chosen temperature. Free energy profiles and entropy may also be computed using the non – Boltzmann methods [7].

2.6 Computer simulations of Liquid Crystals

In liquid crystal context key quantities such as order tensor or the composition profile are the strength of simulations [9]. These are often difficult to resolve experimentally and are only accessible to relatively coarse-grained theories. At continuum length scales, LCs are characterized by a large number of experimentally observable parameters: viscosities, determined by the Leslie coefficients; orientational elasticity, controlled by the Frank constants; substrate - LC orientational coupling, governed by anchoring coefficients and surface viscosities. Given a full set of these parameters, mesoscale simulations are now able to incorporate much of this complex behavior into models of real systems.

LCs are fascinating systems to study because, like much of soft-condensed matter, their behavior is characterized by the interplay of several very different effects which operate over a wide range of time and length-scales. These effects range from changes in intramolecular configurations, through molecular liberations to many-body properties such as mass flow modes and net orientational order and ultimately to the fully equilibrated director field observed at the continuum time and length-scales. The extent of the associated time and length-scale spectra dictate that no single computer simulation model will ever be able to give a full atom-to-system description for even the simplest mesogen.

Computer simulation can contribute to our understanding of liquid crystals by relating detailed molecular structure to observed phase behavior and properties. It also helps in testing, in a microscopic way, the basis of theories of phase transitions, structure and dynamics. Using molecular dynamics and Monte Carlo techniques, and employing simple molecular models, one can hope to get insight into general features of phase equilibria, structure, and dynamics of liquid crystals. Different from the case of ordinary fluids, a simulation of liquid crystal systems should be able to yield the various phases of interest (isotropic, nematic, smectic etc.) and their transitions and to provide relevant anisotropic properties (that would reduce to a scalar for normal liquids), for a certain choice of molecular features.

Simulations of liquid crystals reported so far are carried out using two kinds of widely

divided models. Firstly, the off-lattice models, where the particles are free to move and can have any orientations [10]. The Gay-Berne (GB) potential that represents molecules as uniaxial or biaxial ellipsoids, can be regarded as a generalized anisotropic and shifted version of the Lennard-Jones (LJ) interaction which is commonly used for simple fluids, with attractive and repulsive contributions that decrease as 6 and 12 inverse powers of the intermolecular distance [11]. Extensive simulations of the Gay - Berne family of molecular models, in which potential parameters are adjusted to vary the molecular length-to-width ratio in a systematic way are studied. Simulation study of the approach to the isotropic nematic phase transition, using a large system size and lengthy runs on the T3D parallel supercomputer were reported earlier [12]. Such flexible modeling of liquid crystal gave rise to models with molecules that are biaxial in shape [13]. The progress towards accurate atomistic modeling of nematics has been discussed [14], pointing to improvements in force fields made recently and discussing the progress towards accurate prediction of material properties.

The second widely used and simple models are the lattice models, where the position of the molecule is fixed, but it can have any random orientation. Such models are useful only to describe a nematic–isotropic transition. Lattice models have a advantage over the off – lattice model when it comes to computing time [15]. These are simpler models to simulate and are adequate to study the relevant parameters at the nematic-isotropic transition. Lattice spin models are systems of simple interacting spins placed at every lattice point of say a cube. These spins are represent as unit vectors, with a continuously varying orientation. One model that is most widely used for the study of liquid crystals is the LL model [16], and has been extensively investigated in confined liquid crystals with specific effect on isotropic – nematic transition. Many modifications were suggested to this Hamiltonian to make it realistic and more appropiate in the context of a liquid crystal [17]. LL model is discussed in detail in the previous chapter of this thesis. Lattice models were also proposed for the study of more complex systems like biaxial liquid crystals [18].

Using these models the thermal averages of various physical parameters are computed

using the algorithms discussed previously. This thesis mainly deals with lattice Hamiltonians and the different parameters required for our study of liquid crystal systems are vividly discussed in some detail below.

2.7 Computation of the different parameters

2.7.1 Period Boundary Conditions

One of the ubiquitous problems is the choice of the boundary conditions, i.e. of what to surround the simulated sample with. Tackling it is unavoidable since computer simulations are usually performed on relatively limited number of particles. Even for lattice models, typical number of particles is of the order $10^3 - 10^6$, in comparison to a real bulk system with numbers as the to the Avogadro scale. Then, apart from choosing a lattice size as large as possible, it is very important to adopt some artifact at the sample surfaces so as to minimize the effects of finite size system. The appropriate choice of the boundary conditions becomes then essential, especially when small systems are investigated. The most often used constraints are the so called periodic boundary conditions (PBC), where the sample box is surrounded by exact replicas of itself. Although this kind of boundary conditions introduces a non-existent periodicity and thus some spurious correlations. PBC effectively reduce the effect of the finite size of the sample surfaces a long as the sample size is larger than the correlation lengths that can develop in the system during different simulation conditions. Due to greater correlation among sites it is expected that periodic boundary conditions might overestimate the transition temperature (T_C) . The opposite case arises when the correlation between the sites is underestimated as in the case of free boundary surfaces. Consequently periodic and free boundaries yield, respectively, upper and lower bounds for the transition temperature.

2.7.2 Average Energy and Specific Heat (C_V)

The total configuration energy is taken as the sum of the intermolecular pairwise interactions. The average energy at every temperature is computed as the average of the energy

of all microstates in the ensemble. These microstates are collected during the production run of the Monte Carlo simulation, after neglecting the initial transient states (i.e. after equilibration). Thus, the average energy is computed as

$$\langle E \rangle = \frac{E_{total}}{N_p}. \tag{2.7.1}$$

Here, E_{total} represents the sum of the energy E over the ensemble and N_p the number of microstates collected during the production run.

The specific heat capacity (at constant volume) is obtained when the average energy is differentiated with temperature under constant volume. This can also be expanded in terms of the square mean fluctuation of energy.

$$\begin{aligned} C_V =& \left(\frac{dU}{dT}\right)_V \\ =& \frac{1}{k_B T}(\langle U^2 \rangle - \langle U \rangle^2) \end{aligned} \tag{2.7.2}$$

where k_B is the Boltzmann constant, T is the temperature. As mentioned earlier, the temperature is always measured in the units of the coupling between the neighbors and hence one employs the reduced temperature T^* instead, expressed in dimensionless units as,

$$T^* = \frac{k_B T}{\varepsilon}. \tag{2.7.3}$$

The temperature at which the peak occurs is considered as the transition temperature and this peak defines the transition in these Monte Carlo simulations.

2.7.3 Order parameters

The second rank Legendre polynomial $\langle P_2 \rangle$ is calculated by averaging $P_2(\cos\beta)$ over the probability $P(\beta)$ of finding the molecule at orientation β with the director. This method is useful if the director orientation $\hat{\mathbf{n}}$ is known *a priori*. In the present MC computations, we work in an arbitrary laboratory frame with no applied aligning field. Thus we do not know the orientation of the director in each configuration and it changes with the evolution of the microstate. This means that computation of $\langle P_2 \rangle$ requires *a priori* knowledge of the principal axes system in which the ordering tensor is diagonal.

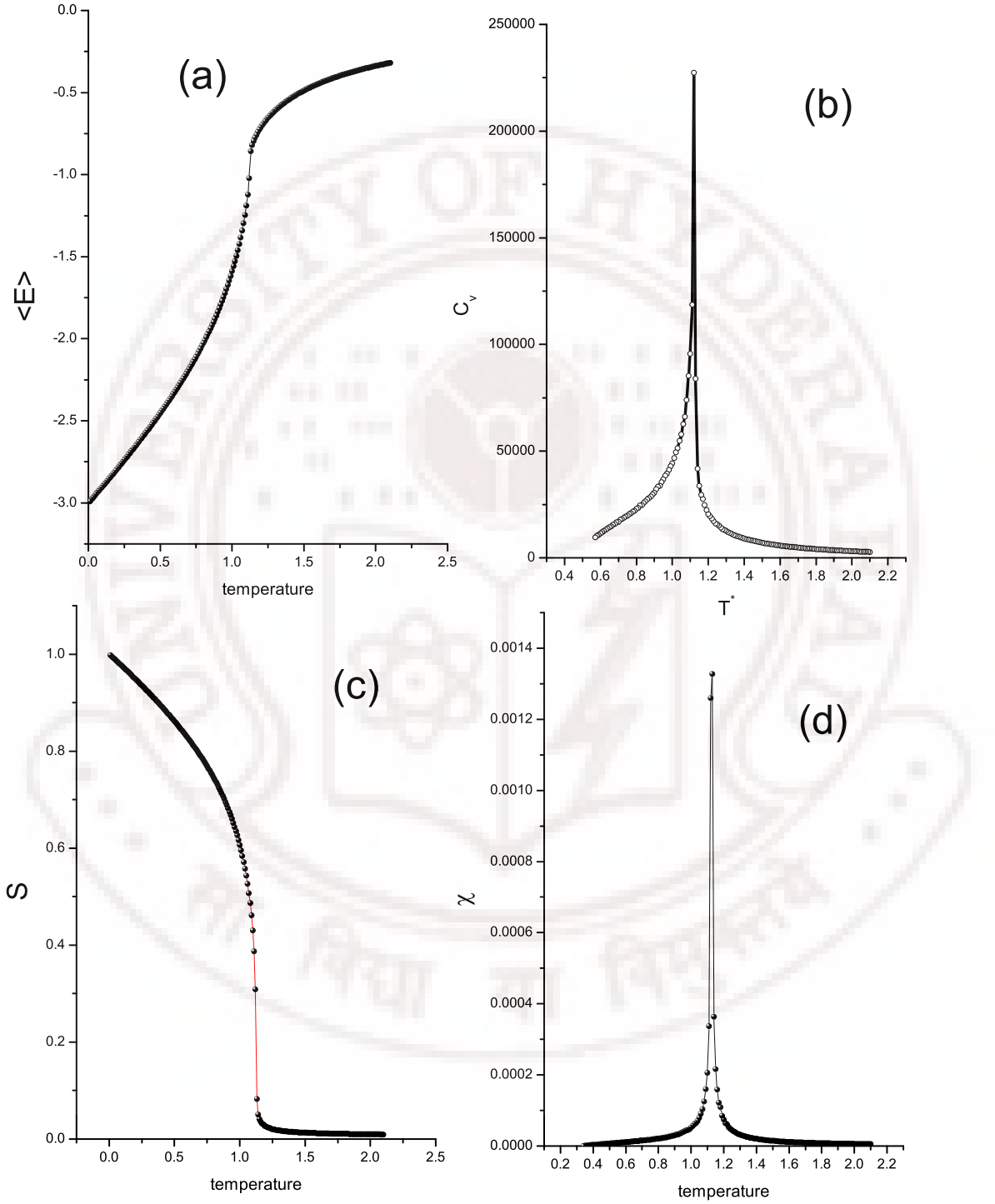

Figure 2.2: The different parameters computed for a $25 \times 25 \times 25$ cubic LL system with the variation in temperature: (a) average energy (b) specific heat (c) The order parameter (d) the nematic susceptibility (fluctuations in S) (χ)

To model such molecules we need an orthonormal set of vectors say e_x, e_y, and e_z, which represent the geometry of the molecules. The system considered has N number of particles, so N orthonormal sets are to be considered, $e_x^{(i)}, e_y^{(i)}, e_z^{(i)}$ for $i = 1.....N$. Order parameter of the system, a second rank tensor, is built by taking a direct product of the vectors in every direction. Consider $e_z^{(i)}$ axis to be the long axis of the molecule. $e_y^{(i)}$and $e_x^{(i)}$ lie in a common plane ($X-Y$ plane) but define a preferred axis each. Considering each axis of every molecule we define three order parameters Q_{xx}, Q_{yy}, Q_{zz} where Q_{zz} defines an ordering tensor considering the $e_z^{(i)}$s, similarly Q_{xx} from $e_z^{(i)}$s and Q_{xx} from $e_z^{(i)}$s.

For symmetrical molecules

Let **A** be a molecular matrix property whose only non vanishing component is along the molecule symmetry axis e_x [19]

$$A_{ab}^{MOL} = \delta_{az}\delta_{bz}. \tag{2.7.4}$$

Now, considering molecules that are rotationally symmetric about their long axes e_z, *i.e.* $e_x = e_y$, the relevant ordering matrix is Q_{zz} averaged over the sample, and is given by

$$Q_{zz} = \frac{1}{N}\sum_{i=1}^{N}\begin{pmatrix} e_{zx}^2 - \frac{1}{3} & e_{zx}e_{zy} & e_{zx}e_{zz} \\ e_{zx}e_{zy} & e_{zy}^2 - \frac{1}{3} & e_{zy}e_{zz} \\ e_{zx}e_{zz} & e_{zy}e_{zz} & e_{zz}^2 - \frac{1}{3} \end{pmatrix}. \tag{2.7.5}$$

Here, Q_{zz} a is symmetric and traceless. The average of A is obtained by relating the components of A to the molecular frame fixed components and summing over all the particles *i.e.*

$$\langle A_{ab}^{MOL}\rangle_S = Q_{zz} + \frac{1}{3}\delta_{ab}. \tag{2.7.6}$$

The diagonalization of Q_{zz} with respect to rotation matrix U identifies the director frame. Rotating and diagonalization of $\langle A^{LAB}\rangle$ is equivalent to defining the director frame of Q. The director itself is defined by the eigenvectors corresponding to the maximum eigenvalue λ_{max}. The second rank order parameter is given as $\langle P_2\rangle_\lambda = \frac{3}{2}\lambda_{max}$. The difference in the other two eigen values is the measure of the macroscopic biaxiality due to orientational ordering of the uniaxial molecule, called the phase biaxiality.

For molecules without rotational symmetry

To define the overall director of the system, we find the dominant eigen values of each Q_{xx}, Q_{yy}, Q_{zz} (say W_{xx}, W_{yy}, W_{zz}) and their associated eigen vectors $(\varsigma_{xx}, \varsigma_{yy}, \varsigma_{zz})$. The eigen vector of the most dominant eigen value W_1 from among (W_{xx}, W_{yy}, W_{zz}) defines the direction of the primary director. This is labeled as $'Z'$. The most dominant eigen value W_1 provides the primary order parameter of the system. For rod – like molecules, the directions correspond to the average direction of alignment of the long axes of the molecules.

To define the second relevant axis of the system, we construct a right handed orthonormal system with axis X, Y, Z. The direction of Z is already defined as above. The other two preferred directions X and Y are obtained from Q_{xx} and Q_{yy}. The second direction Y is obtained by considering the eigen vectors of Q_{xx} and Q_{yy} (corresponding to the respective dominant eigen value of these tensors) and projecting the on to a plane orthogonal to the system director. The eigen vector so projected orthogonal to Z is taken as $'Y'$, the eigen vector of the next dominant eigen value. The $'X'$ direction is obtained by completing the set of axes to a right handed orthogonal system.

The measure of biaxiality is given by

$$B = R^2_{22} = \frac{1}{3}[X^T Q_{xx} X + Y^T Q_{yy} Y - X^T Q_{yy} X - Y^T Q_{xx} Y] \tag{2.7.7}$$

where $X^T Q_{xx} X$ measures the extent to which the molecules x-axis are aligned along laboratory X, similarly $Y^T Q_{yy} Y$. $X^T Q_{yy} X$ gives the extent to which molecules y-axis aligned along X similarly $Y^T Q_{xx} Y$. A non-zero value of B indicates degree of biaxiality in the system.

Hence the different order parameter can be defined as

$$R^2_{00} = Z^T Q_{zz} Z \tag{2.7.8}$$

the system order parameter, the most dominant eigen value.

$$R^2_{20} = f_2^T Q_{zz} f_2 - f_3^T Q_{zz} f_3 \tag{2.7.9}$$

the phase biaxiality, non-zero only in the biaxial phase. This order parameter is computed as the difference between the other two eigen values of Q_{zz} ordering matrix, f_2 and f_3, the eigen values of Z. The molecular biaxiality is given as

$$R_{02}^2 = X^T Q_{xx} X - Y^T Q_{yy} Y, \tag{2.7.10}$$

the difference between the maximum eigen values of matrices Q_{xx} and Q_{yy}. This order parameter is non-zero only in the uniaxial phase. This order contributes to the order present along the Z direction due to the biaxiality present in the system.

The various parameters of interest of a LC that can be computed using LL model are depicted in the figure 2.2.

Bibliography

[1] C.Chiccoli, P.Pasini, G.Skacez, S.Zumer, and C.Zannoni. *Computer simulations of Liquid crystals and Polymers*. Kluwer Academic Publishers, Dordrecht, 2005.

[2] M. Ronen and M. Eliahu. Simulation a bridge between theory and reality: the case of electric circuits. *Journal of Computer Assisted Learning*, 16:14–26, 2000.

[3] S. Martellucci and A.N. Chester. *Phase tranisitons in Liquid Crystals*. Plenum Press, 1989.

[4] N. Metropolis. Tthe beginning of the monte carlo method. *Los Alamos Science Special Issue*, page 125, 1987.

[5] D. P. Landau and Kurt Binder. *A guide to Monte Carlo simulations in Statistical Physics*. Cambridge University Press, 2000.

[6] Barker J.A and Watts R.O. *Chem. Phys. Lett.*, 3:144, 1969.

[7] K.P.N.Murthy. *Monte Carlo Methods in Statistical Physics*. Universities Press, 2004.

[8] D.Jayasri, V.S.S.Sastry, and K.P.N.Murthy. Wang-landau monte carlo simulation of isotropic-nematic transition in liquid crystals. *Phys. Rev. E*, 72:036702, 2005.

[9] C M Care and D J Cleaver. Computer simulation of liquid crystals. *Reports On Progress In Physics*, 68:26652700, 2005.

[10] Claudio Zannoni. Molecular design and computer simulations of novel mesophases. *Jr. Material Chemistry*, 11:2637 – 2646, 2001.

[11] J.G. Gay and B.J. Berne. *J. Chem. Phys.*, 74:3316, 1981.

[12] Michael P Allen, Julian T Brown, and Mark A Warren. Computer simulation of liquid crystals. *J. Phys.: Condens. Matter*, 8:94339437, 1996.

[13] Roberto Berardi, Luca Muccioli, Silvia Orlandi, Matteo Ricci, and Claudio Zannoni. Computer simulations of biaxial nematics. *J. Phys.: Condens. Matter*, 20:463101, 2008.

[14] Mark R. Wilson. Progress in computer simulations of liquid crystals. *International Reviews in Physical Chemistry*, 24(34):421455, 2005.

[15] P.Pasini, C.Chiccoli, and C.Zannoni. *Advances in the Computer Simulations of Liquid crystals*. Kluwer Academic Publishers, Dordrecht, 1998.

[16] P.A. Lebwohl and G. Lasher. *Physical Rev. A*, 6:426, 1972.

[17] C.Chiccoli, P.Pasini, and C.Zannoni. A monte carlo simulation of inhomogenous lebwhol-lasher model. *Liq. Cryst.*, 2(1):39, 1987.

[18] F. Biscarini, C. Chiccoli, P. Pasini, F. Semeria, and C. Zannoni. Phase diagram and orientational order in a biaxial lattice model. a monte carlo study. *Phys. Rev. Lett.*, 75:1803–1806, 1995.

[19] C.Zannoni. *Advances in the Computer Simulations of Liquid crystals*. Kluwer Academic Publishers, Dordrecht, 1998.

Chapter 3

Structures and Transitions in Hybrid Film of Uniaxial Molecules

3.1 Planar Hybrid Film

Liquid crystals confined between substrates with incompatible boundary conditions, as a result of which the orientational order in different direction percolates into the liquid crystal system. In hybrid cells, the two bounding surfaces induce mutually perpendicular order as a result of surface anchoring. This leads to a possible equilibrium director configurations where the extent and direction of order is non homogenous and varies in the film. Technologically, hybrid films play a very important role in optical switches. They are of interest to theoretical modeling to understand the anchoring effects of the confining substrates.

Hybrid conditions can be induced in to the system in many ways. The well known methods of preparing a hybrid liquid crystal system are (figure 3.1):

1. A confined nematic liquid crystal between two planar substrates that are prepared in such a way to induce homeotropic direction at one surface and lateral at the other.

2. Liquid crystal deposited on a solid substrate that induces a in-planar ordering with a LC-air interface. LC-air interface normally induces a strongly aligned homeotropic order in the system.

3. Liquid crystal confined in a cylinder, with homogenous anchoring at the surface.

Different organizations can be obtained as a function of some suitable external driving parameters by changing the easy axis at the boundaries (e.g. by irradiation of azobenzene

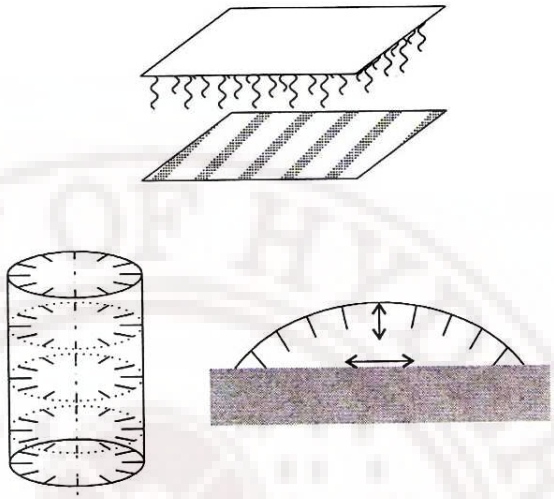

Figure 3.1: The different ways a hybrid nature can be induced in to a liquid crystal system

covered surfaces, [1]) or, more frequently, just by applying an external field or changing the temperature. A typical example of confinement leading to competing mechanisms [2] [3] is that shown by hybrid nematic films [4] [5] [6], where a liquid crystal layer is placed between two plates, typically with lateral dimensions much greater than the thickness, and with antagonistic boundary conditions: homeotropic at $z = d$ to planar at $z = 0$. The order induced by the substrates lies in the $x - y$ plane and the z axis is perpendicular to the substrate planes. In this system two limiting structural organizations can exist. The first corresponds to a continuous deformation of the director across the sample between the two easy axis directions. The other is a "biaxial" or "director-exchange" configuration with uniaxial alignment close to each of the two substrates and a sudden switch from one to the other [2] [3] [6]].

Possible technological applications have increased the interest in different hybrid nematic geometries. Experimental studies of confined systems were done using atomic force microscope and light scattering experiments [7] [8] [9]. Theoretical studies using mean field methods and phenomenological methods were undertaken to understand the order fluctuations in confined systems [10] [11] [12]. Study of defects in confined systems gained

evoked considerable interest both in theoreticians as well as to experimentalists [13]. The spatial variation of the order induces a subsurface variation of the average molecular orientation and an intrinsic contribution to the anchoring when the splay and bend elastic constants are different from the twist elastic constant [14]. Another study of interest in confined system is the induction of randomness into the liquid crystal by using random substrates [15] [16] [17]. Using molecular dynamics it was shown that a uniaxial nematic liquid crystal can exhibit an unusual ordering that appears within a few molecular lengths from a rough surface. A degree of biaxiality is seen between the Smectic C and the bulk nematic, when confined on a such rough surface [18]. Magnetic resonance and calorimetric studies were carried out to understand liquid crystals confined in random networks of pores [19]. To study the dependence of the isotropic – nematic phase transition temperature on the thickness of planar and hybridly confined films, a quasi-elastic light scattering experiments were preferred [8] and stability of ordered structures in a hybrid nematic film was obtained by spreading a droplet of liquid crystal on solid substrates. In the above experiment, the confining substrates were set to have unequal anchoring strengths. The critical cell thickness ($\sim 4\mu m$) they obtained was in good agreement with the theoretical study [20]. The existence of certain critical thickness of a surface aligned nematic film below which the nematic isotropic transition becomes continuous was shown using Landau – de Gennes theory [21]. In the frame work of Frank elastic theory, an extensive study of pretransitional director dynamics in a hybrid cell was studied by Stalling *et. al.* [22]. Using the director description of the nematic liquid crystalline ordering, the relaxation times of tilt and twist fluctuations in hybridly aligned structure and director fluctuations in uniform director field structure were studied. For the first time it was shown that order in a hybridly aligned can be a biaxial with a step – like profile of director tilt angle or the director field bent continuously [5]. Using continuum theory with the minimization of Frank free energy [5] [23] it was observed that, these opposite boundary conditions are expected to cause, for sufficiently thin films, a structural transition from the bent-director to the biaxial structure. A more detailed description of nematic order in planar hybrid films was provided

by Galabova *et. al* [24]. The biaxial structure is known to be formed only when the thickness of the liquid crystal film is below a certain critical thickness value (estimated at 47 nm for the nematic 5CB [25] [6]). On the other hand, at fixed thickness, a transition from a biaxial organization to a structure with continuous variation of the director orientation across the cell, is expected when the temperature of the system is lowered [23] [25].

Planar hybrid films were studied in detail using mean field methods and other theoretical methods. Analytical methods get difficult when the minimization of the free energy has to be done considering the various constraints and biaxiality in the system. A biaxial phase in such systems has not been observed experimentally till date, and could possibly be because the biaxial phase is stable only for a very short temperature range. Computer simulation studies stand out, behavior of confined system under such constraints are to be predicted by employing specific models to study different systems under given set of constraints. Biaxial symmetry of the system, if induced under certain controlling conditions, can be detected during the simulations. Such systems were conveniently studied by computer simulations of a Lebwohl – Lasher type lattice model [26] [27]. Computer simulations are a powerful tool for studying ordering and structural transitions in uniaxial [28] and biaxial [29] nematics and their defects [26] [2] [25] [30], particularly when the effect of complex boundaries and temperature have to be investigated. For instance, multiple organizations were also predicted and confirmed by Monte Carlo simulations [26] [2] on a closely related system with degenerate, rather than uniform boundary condition, at the planar anchoring surface. A detail Monte Carlo study was done on hybrid film of 10 layers [25]. A biaxial phase was confirmed with the increase in the biaxiality order parameter for certain range of temperature, which was not indicative in plotting the layer-wise director's tilt angle with temperature. Figure 3.2 gives an director tilt angle of each layer with temperature variation. For a better understanding of this system a non-Boltzmann sampling method is used to look out for different signature for biaxiality. A non-Boltzmann algorithm was developed for discrete model [31], that was later extended to continuous systems [32]. The physics of this algorithm was discussed in detail in the 2^{nd} chapter of the thesis.

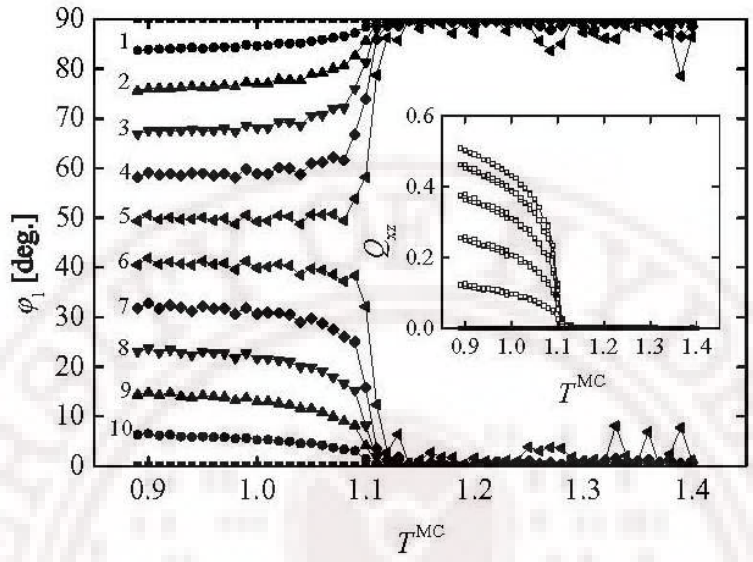

Figure 3.2: Director's tilt angle with respect to the z-direction in a h = 10-layer hybrid cell as a function of MC temperature [25].

In such hybrid films of liquid crystals three structures are known to form depending on the temperature, thickness of the liquid crystal film and anchoring strengths of the substrates. A hybrid cell confinement induces a deformation in the director field, and the elastic distortions in such films are studied within Frank elastic theory. Transition from one director state to the other can occur in a hybrid film with the change in temperature and the film thickness. The commonly known structures are:

1. Bent Structure: (Figure 3.3(a)) In a planar hybrid film, in the deep nematic phase due to the antagonist boundary conditions a bent – like structure is formed. The director takes a bent structure from one substrate to the other substrate. The nematic order is assumed to be uniaxial with the director field continuously bent from one substrate to the other. The bent director configuration exists only if the film is thicker that the critical thickness, $d_c \equiv K(1/W_2 - 1/W_1)$ [20] where K is the elastic constant in the one-elastic constant approximation and $W_2 < W_1$ are the out-of-plane strengths of the surface interaction at the two confining substrates, respectively. It has been

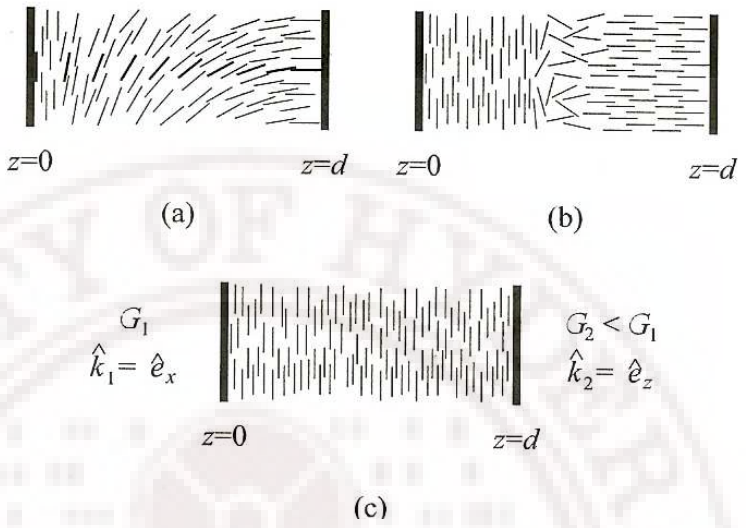

Figure 3.3: Schematic representation of three possible ordered configurations in a hybrid film: (a) the bent-director structure, (b) biaxial structure with director exchange, and (c) uniform director structure

a practice [33], in the bent director structure the biaxiality can be neglected and the scalar order parameter corresponds to its bulk value. Due to the elastic deformations of the director field the temperature of the hybrid system effectively increases. The increase of the effective temperature results in a smaller degree of order along the director with respect to the degree of order in the bulk where there are no elastic deformations. The scalar order parameter varies with distance from one substrate, the director tilt-angle in not changing linearly as in the case of uniform scalar order parameter. However, the difference is very small, and as expected, decreases further with increasing film thickness and when the boundary value of the scalar order parameter is getting closer to the value $S_b = S_{bulk}(\theta)$.

2. Uniform director structure: (Figure 3.3(c)) If the antagonist anchorings are very different in magnitude it is energetically more favorable to disobey one of the surface anchoring than subject to elastic deformations. In thinner films the director field is uniform with the nematic director in the direction of the easy axis of the substrate

with stronger anchoring ($G_2 > G_1$) in order to minimize surface contribution to the free energy.

3. Biaxial Structure: (Figure 3.3(b)) In a hybrid film with one easy axis of the substrate in the direction of the x axis and the other parallel to the z axis, the director lies in the plane (x, z). The configuration can be described by two amplitudes, let us choose Q_{xx} and Q_{zz} which refer to the scalar order parameters with respect to the director $\hat{n} = \hat{e}_n$ and $\hat{n} = \hat{e}_z$ respectively. With equally strong but orthogonal anchoring, on the average, near the first surface the liquid crystal molecules are oriented parallel to the x axis while they are parallel to z axis close to another substrate. In the vicinity of the surface the order is uniaxial however, with increasing distance from the substrate it becomes slightly biaxial. In the case of equal anchoring strengths, the order parameter profiles are symmetric with respect to the middle of the film, the *exchange region*, whereas for the unequal anchoring strength this region moves towards the substrate with the weaker anchoring. The maxima of the biaxiality profile the molecular ordering is characterized by director $\hat{n} = \hat{e}_y$ and a negative order parameter. There is a structural transition to the low-temperature bent-director field configuration that occurs with the change in temperature.

3.1.1 System studied and Model used

The system studied here is a thin planar hybrid film of uniaxial liquid crystal molecules. In the simulation, a hybrid film is constructed out of appropriate lattice consisting of LC molecules. The anchoring effects at the bonding surfaces are simulated by placing additional layers of LC molecules at the location of the substrate but with fixed orientation appropriate to boundary conditions. These layers (referred to as ghost layers in the literature) do not participate in the Monte Carlo simulations. These layers as simulated induce order in perpendicular directions into the liquid crystal system. The systems studied here are of dimensions $15 \times 15 \times d$ $(x \times y \times z)$ where $d = 10, 6, 5$ and 4 and represents the liquid crystal film thickness. Figure 3.4 gives a picture as to how this system was modeled.

In order to induce hybrid boundary conditions on the system, all the molecules in the first

Figure 3.4: A model of planar hybrid film.

layer along $(z = 1)$ are fixed along the *x*-direction. The molecules in the last layer $(z = nz)$ are fixed along the *z*-direction. The model considered here to study this system is a lattice model proposed by Lebwohl and Lasher (LL) [27]. The Hamiltonian used is

$$U_{ij} = -\epsilon_{ij} P_2(u_i.u_j) \tag{3.1.1}$$

where $\epsilon = \epsilon_i > 0$ for nearest neighbors and is zero otherwise; u_i, u_j represent the directors of the interacting molecules. A detailed description of this model is given in the first chapter of this thesis. The objective is to investigate this system, already simulated earlier based on the model using canonical methods, with entropic sampling method using Wang–Landau algorithm [32] to obtain more details about the transition behavior involving the biaxial phase in a small intermediate temperature range.

Different order parameters were computed to understand the structures and transitions in the system. Average energy and its fluctuations (C_V) were computed for the system as a function of very finely controlled temperature making use of the non – Boltzmann ensemble obtained through entropic sampling. The system order parameter (S) was computed by diagonalization of the ordering matrix of the system (chapter 2 section 1.7.3). The fluctuations in the order parameter were also computed with the variation in temperature. Another

order parameter that turns out to be of interest in the system, biaxiality parameter (P), was also evaluated; it is the difference between the minor two eigen values (*i.e.* excluding the maximum eigen value). The maximum eigen value corresponds to the uniaxial order (S) in the system. All these order parameters and the different eigen values were computed for every layer of the system along $'z'$. These plots provide a detailed representation to the structures, and the interesting transitions. The director tilt angle (ϕ) and its fluctuations were also computed and plotted along with its temperature variation. The director tilt angle is the angle made by the director of every layer with the laboratory *Z*-axis. All the above parameters were computed with high temperature resolution. These films of uniaxial molecules were investigated by changing the following control parameters: temperature, anchoring strength of the substrates (ξ) and thickness of the liquid crystal layers *(d)*.

The physical quantities that were calculated are the average energy, its fluctuations (variance) and order parameters and their fluctuations. This gives us an idea about the percolation of two competing orders, one from either substrates of the confined film, and the progressive influence of disordering thermal effects. The presence of biaxiality is indicated by the in-equivalence of the two minor eigenvalues of the ordering tensor in its principal axes system. This property is a measure of the loss of axial symmetry around local ordering direction, arising due to the azimuthally asymmetric distribution of the molecules around the local director. Even though we have considered each liquid crystal molecule to be represented by a single headless unit vector u_i, in reality each such 'spin' actually represents an elemental volume comprising of several molecules, and in such a case u_i represents the local director.

3.1.2 Effect of change in temperature

The system studied has the dimensions $15 \times 15 \times 10$ in lattice units. This was taken as a prototype system to study the effect of change in temperature. The initial configuration of the system at the beginning of the simulation was taken as random. The density of states

of the systems was gotten after many long Wang – Landau iterations and a non – Boltzmann ensemble was collected (figure 3.5). A production run was done using this density of states to collecte micro-states that were equally sampled in the energy space. Any minor deviation from the flatness is automatically corrected during the reweighting procedure since the histogram is an outcome or the representation of the density of states obtained *apriori*. Unweighting the density of states and reweighting with the Boltzmann factor for every micro-state collected, leads to the construction of a canonical ensemble of microstates appropriate to the reweighting temperature and, the different physical parameter were obtained as usual as an average over these ensembles. In the histogram of energy an average of about two million micro-states were collected so that to yield at least 10^5 microstates in a canonical ensemble so extracted. Every physical parameter was computed over the temperature range 0.6 to 2.0 in steps of 0.01, by constructing canonical ensemble (derived from the non – Boltzmann ensemble) at each of these finally constructed temperatures

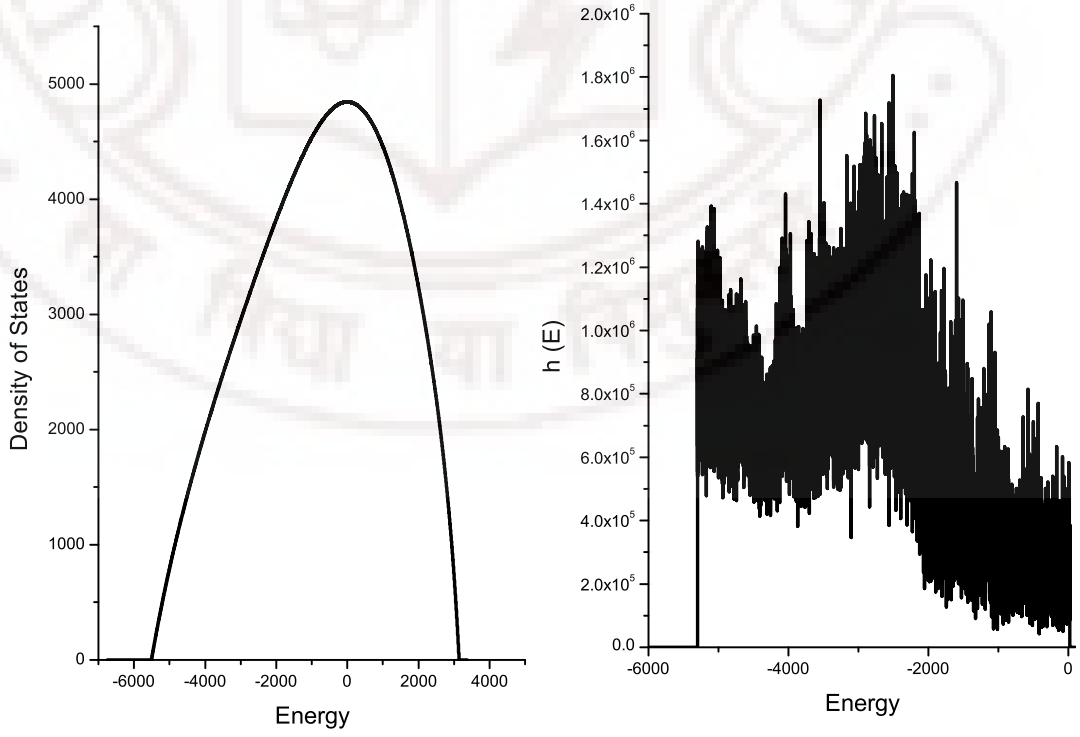

Figure 3.5: The density of states and histogram for a $15 \times 15 \times 10$ system with energy

The specific heat was plotted with temperature, two transitions were observed. The first at a temperature $T^*_{C1} = 1.09$ from one ordered nematic phase to another. The second transition at $T^*_{C2} = 1.183$ is seen from the second ordered nematic phase to a completely disordered phase (isotropic) – can be known as an ordering transition. All the parameter were plotted for all the 10 layers of the system, by extracting the three eigenvalues of ordering matrix for each of these layers. The primary order parameter reflecting the major order did not leave useful signatures at the temperatures scanned through in these transitions (figure 3.6 (a),(b)). The biaxiality parameter however has been found sensitive to the changes in the symmetry across the transitions (figure 3.6 (c), (d)). The director tilt angle with respect to the z-axis gave a clear evidence to the formation of the different phases that were formed and could be mapped to the respective physical scenario. The first at the minimum temperature a bent-layer nematic structure. In the bent-layer structure due to the substrates it is seen that the system director tilts from one substrate to other. A biaxial phase is present at a higher temperature, where there is order present in the other direction too. This phase is clearly indicated with the increase in the biaxial order parameter both for the system as well as in the layer-wise order parameter (figure 3.6 (c), (d)). The highest temperature phase is a disordered phase where the order in the system is almost zero. This is clearly indicated by the director tilt angles, all collapsing to an angle around the magic angle 53.5^o (figure 3.7). This disordered phase was also confirmed by plotting the layer-wise order parameter with temperature, which goes to a zero value (figure 3.6 (b)). The effect of confinement was observed clearly in the layers next to the substrates. There was a development of order even before the nematic phase had set in -a para-nematic phase. This initial simulation gave a insight to the different phases that were formed with change in temperature in agreement to with the literature [25]. With this as a motivation, the effect of change in anchoring strength (ξ) of the substrates was studied in detail for a system with lesser number of liquid crystal layers.

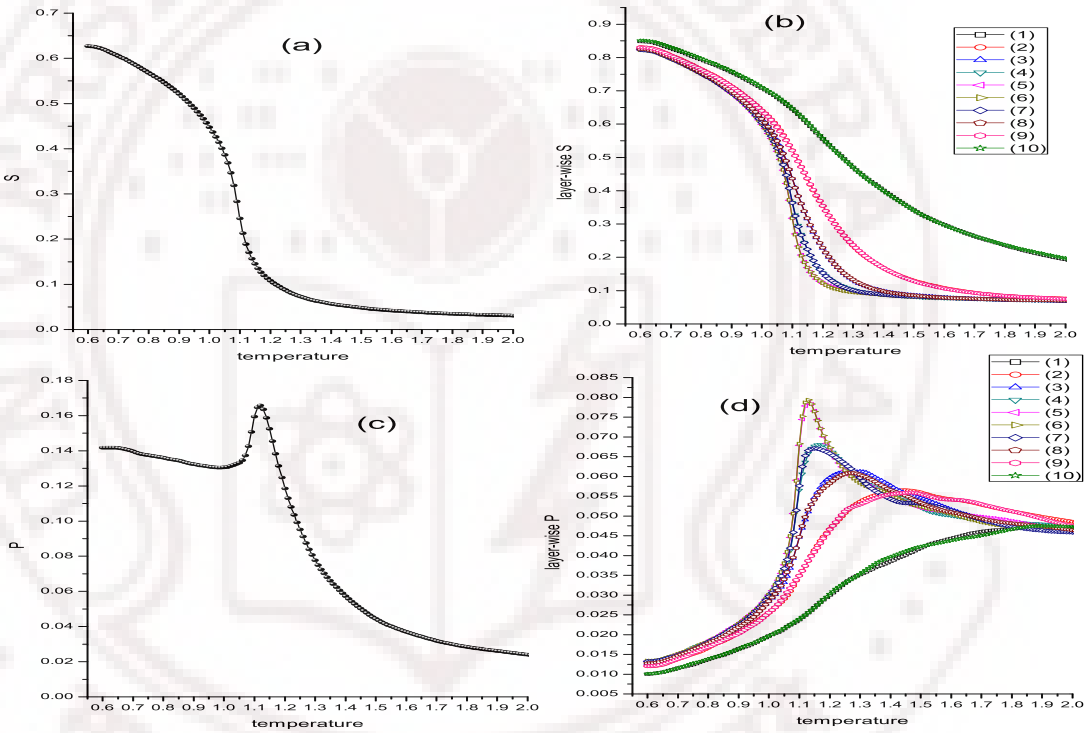

Figure 3.6: The variation of (a) system order parameter (b) layer-wise order parameter (c) system biaxiality parameter (d) layer-wise biaxiality parameter for a $15 \times 15 \times 10$ system with the variation in temperature.

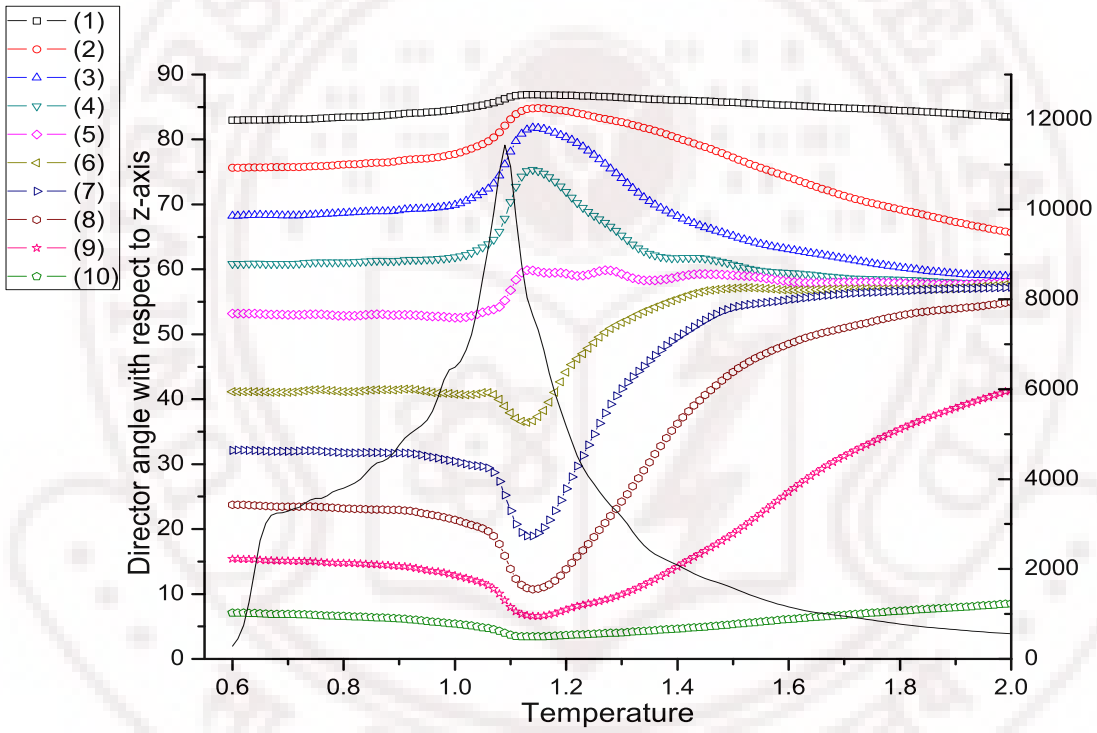

Figure 3.7: The variation of the director tilt angle (ϕ) with the z-axis for $15 \times 15 \times 10$ system and specific heat with temperature

3.1.3 Effect due to change in anchoring strength (ξ_1, ξ_{nz}) of both the substrates

Observation of the presence of two nematic phases, as the temperature is lowered, led to the possibility of carrying out the simulation now as a function of another control parameter, *viz.* the anchoring strength at the surface. The anchoring strengths of both the substrates of the system were varied systematically. For simulational purpose, variation of anchoring strength is effected by setting the energy scale of the interaction between the LC molecules (ϵ in the LL model) to unity, and the varying the strength of interaction between the LC molecules and the molecules in the 'ghost' layer within the limit from 0 to 1. The system size considered here correspond to a lattice of dimension $15 \times 15 \times 6$, with 6 layers of liquid crystal molecules. The easy axis of the ghost layers were fixed, molecules of the substrate at $z = 1$ along *x*-direction, and those at $z = nz$ along the *z*-direction. The different order parameters were computed for every layer of the system to observe the direction configuration within the film closely. The anchoring strength of the two substrates was independently varied in steps of 0.25 from 1 to 0, and then considering a total of 4 different anchored films.

For each anchoring strength a detailed study was done. A convergent density of states was obtained by using Wang – Landau algorithm modified for liquid crystals [32]. Using this density of states a histogram representing a random walk in the energy space was collected for about two million data points which is a non – Boltzmann ensemble of microstates. Canonical ensemble comprising of 290 temperatures between 0.6 and 2.00 (in reduced units) was constructed from the non – Boltzmann ensemble and all the corresponding order parameters were computed and tabulated. On an average every canonical ensemble consisted of atleast 100000 micro-states at every temperature. All the physical parameters were plotted against temperature for every system.

Figure 3.8 gives a converged density of states and a histogram for the system with dimension $15 \times 15 \times 6$ and anchoring strengths of the two substrates set at unity ($\xi_1 = \xi_{nz} =$

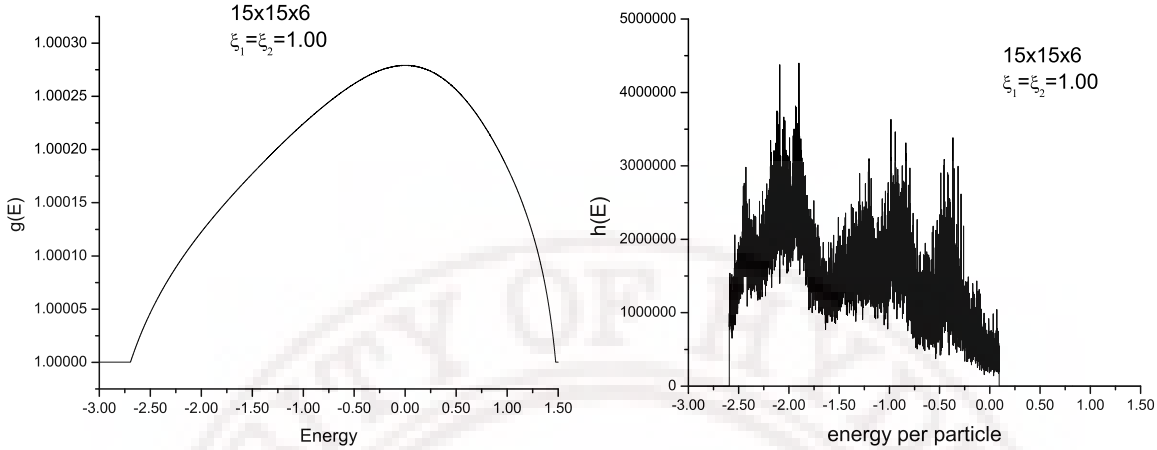

Figure 3.8: The density of states and histogram of $15 \times 15 \times 6$ system with variation in energy ($\xi_1 = \xi_{nz} = 1.00$)

1.00). Similarly, for every anchoring strength the density of states and the histogram of energy were plotted. It was seen that the biaxiality parameter of the system assumed its maximum value exactly at the temperature in between the transition temperatures ($T_{C1} = 1.0599$ and $T_{C2} = 1.699$) (figure 3.9). This showed clearly that with the decrease in temperature a biaxial nematic phase was formed when confined in a hybrid cell. This biaxial phase was formed due to the order induced by the two substrates although the liquid crystal molecules here are uniaxial by nature. This phase was seen in all the systems even when the anchoring strength of the substrates was reduced (figures 3.10 (c) (d)). It was observed that with the decrease in the anchoring strength (ξ) the second transition from biaxial phase to bent director phase was not observed in the specific heat. In order to observe a possible signature of this transition, the fluctuations of the tilt angle ϕ was considered. The plots of the director angle and specific heat (figure 3.11 (a)) with the variation in temperature gives an indication to the onset of the transition not observed in the C_V plot. It is observed a peaks occurs at a temperature T_{C1} and a dip occurs at T_{C2}. Hence, can be concluded that, these director fluctuations can be used to find the transition temperature for systems where the signature is not visible in the fluctuations of energy (figure 3.11 (b)). The transition from disordered state to biaxial phase is clearly seen. Figures 3.10 (a) and (b) gives the layer-wise biaxiality parameter and the order parameter. This figure clearly depicts the biaxiality

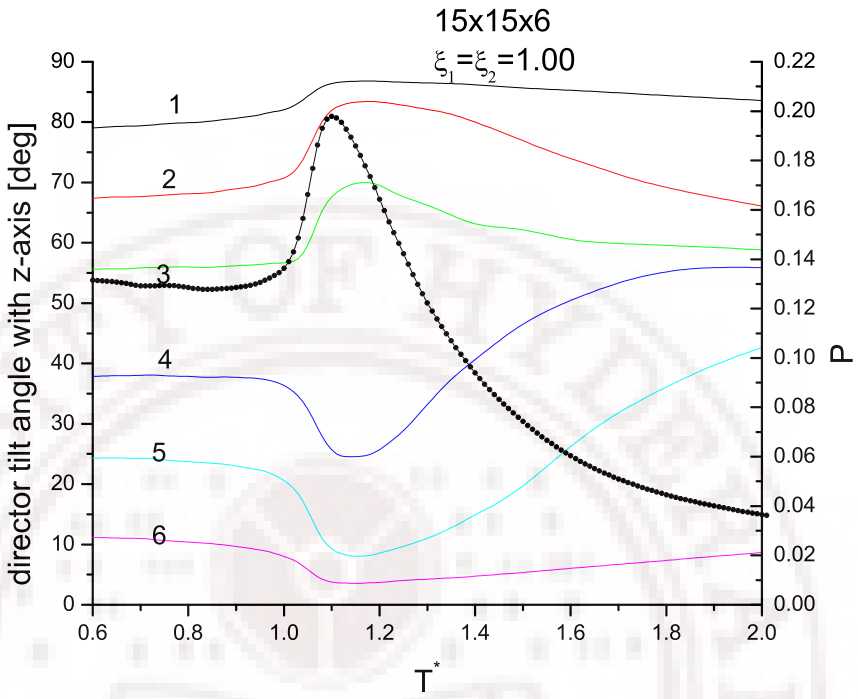

Figure 3.9: The variation of the director tilt angle (ϕ) with the z-axis for $15 \times 15 \times 6$ system and system biaxiality with temperature ($\xi_1 = \xi_{nz} = 1.00$)

is maximum in the layer 3 and 4, and the system order is minimum for these two layers, similarly for layers 1 and 6.

3.1.4 Effect due to the variation in the thickness of the liquid crystal layers -'d'

The next study done was based on variation in the thickness of the liquid crystal film (*d*). When the thickness of the liquid crystal film '*d*' is lesser than a critical thickness d_c, it is known that a bent-structure phase cannot be observed. In the present study, the thickness of the liquid crystal film was changed, and three values of '*d*' were considered (d= 6, 5 and 4). The different systems considered here were therefore: $15 \times 15 \times 6$, $15 \times 15 \times 5$, $15 \times 15 \times 4$. For each of the systems all the parameters were computed for every temperature and was further extended by changing the anchoring strengths also. Table 3.1 below gives the details of the study. Figure 3.12 gives the energy, its fluctuations and the order parameter for two

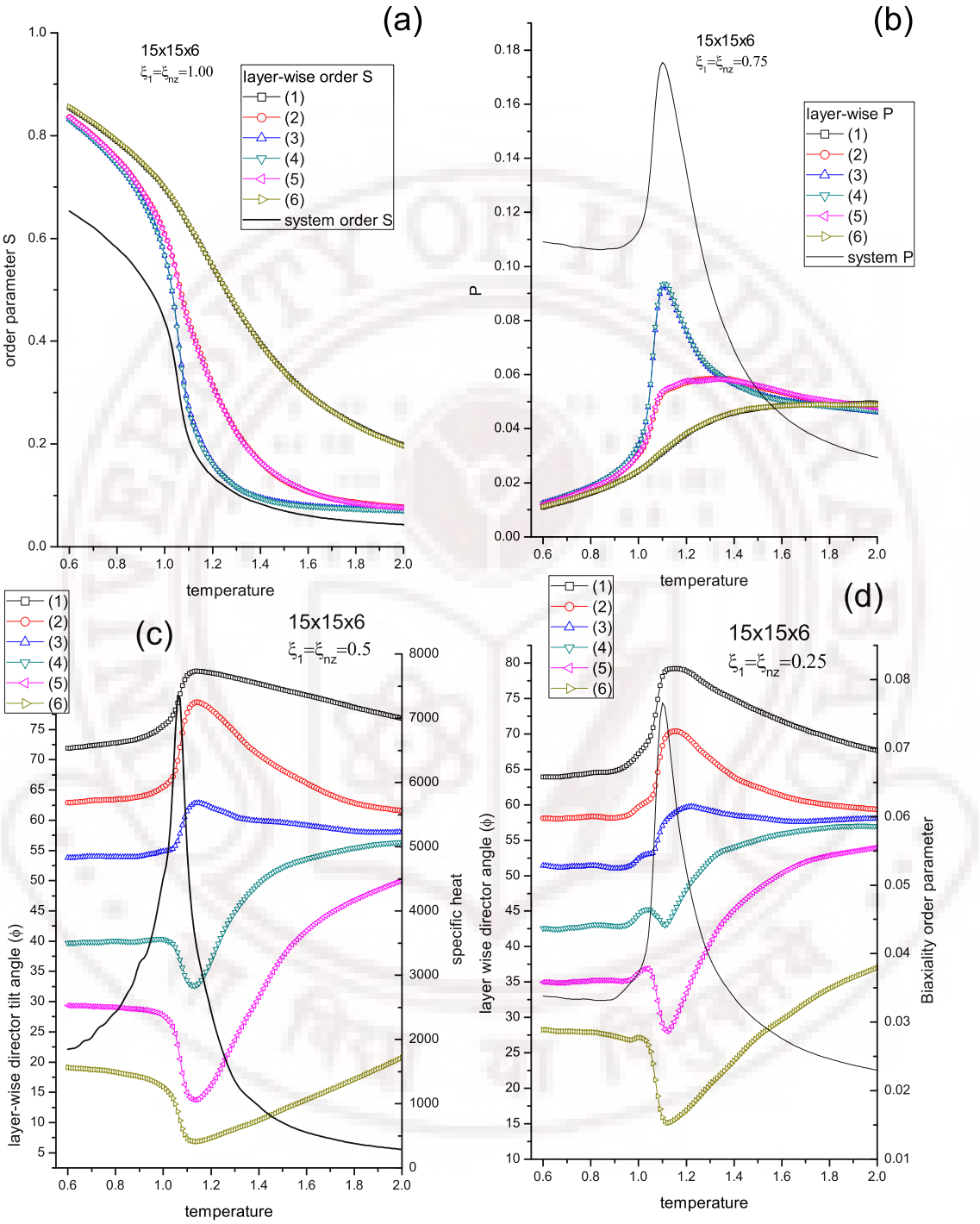

Figure 3.10: (a) Variation of system and layer–wise order parameter with temperature for a $15 \times 15 \times 6$ system with anchoring $\xi_1 = \xi_{nz} = 1.00$, (b)Variation of system and layer–wise biaxiality parameter with temperature for a $15 \times 15 \times 6$ system with anchoring $\xi_1 = \xi_{nz} = 0.75$, (c) Variation of specific heat and director tilt angle with temperature for a $15 \times 15 \times 6$ system with anchoring $\xi_1 = \xi_{nz} = 0.5$, (d) Variation of biaxiality parameter and director tilt angle with temperature for a $15 \times 15 \times 6$ system with anchoring $\xi_1 = \xi_{nz} = 0.25$,

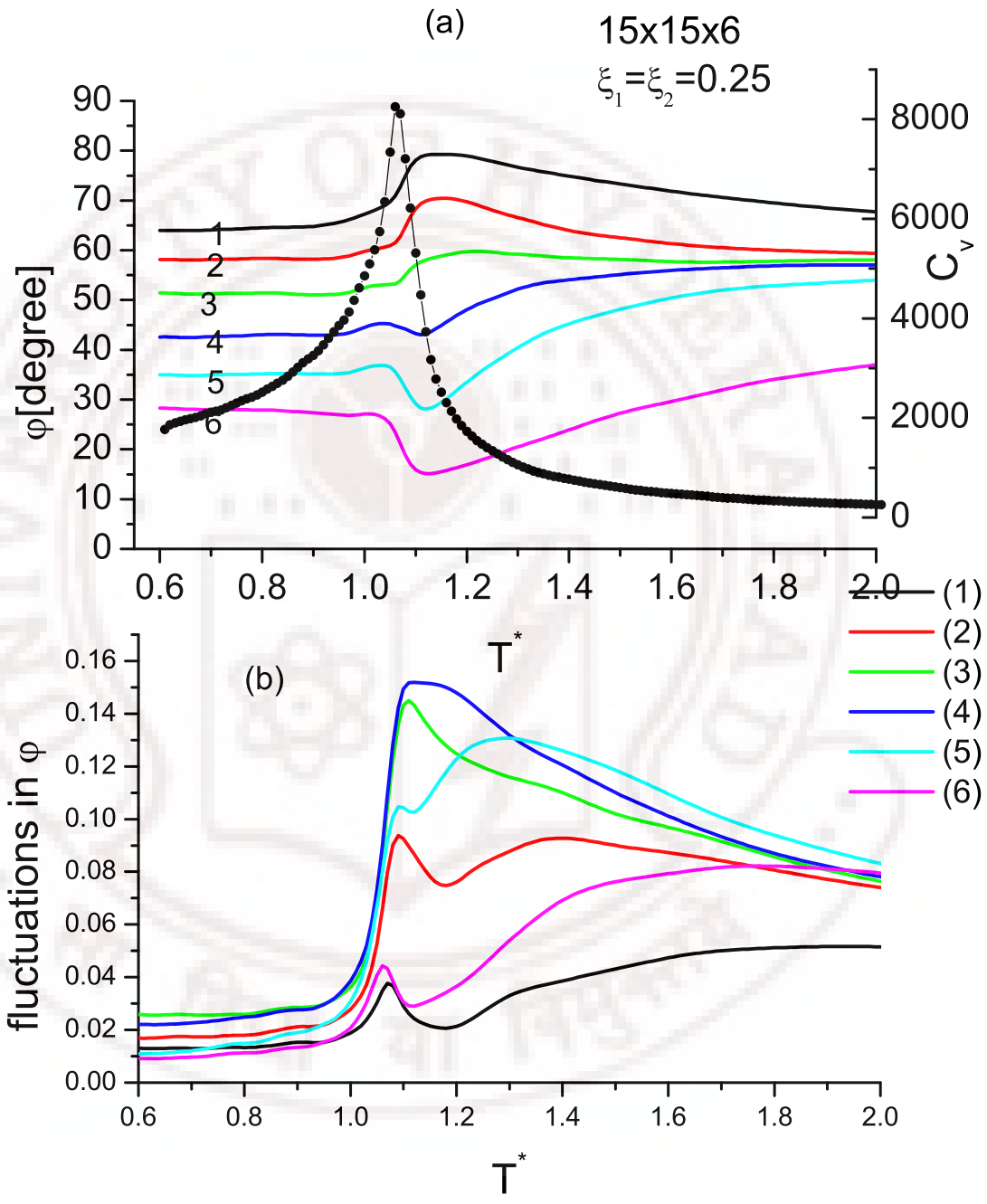

Figure 3.11: (a)The variation of the director tilt angle (ϕ) with the z-axis and specific heat C_V with temperature for $15 \times 15 \times 6$ system with anchoring strength $\xi_1 = \xi_{nz} = 0.25$ (b) Fluctuations in the director tilt angle with temperature when $\xi_1 = \xi_{nz} = 0.25$ for system $15 \times 15 \times 6$.

of the systems studied.

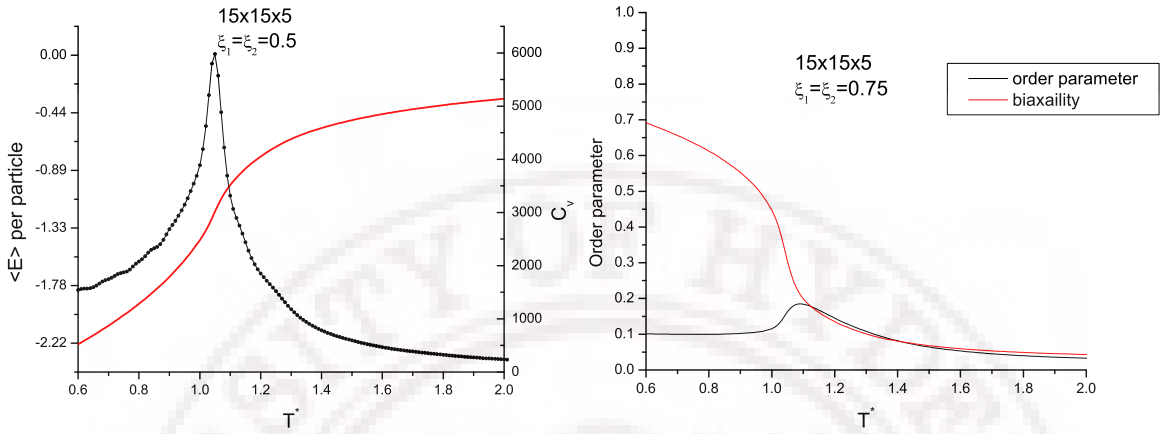

Figure 3.12: Variation of energy, fluctuations in energy,order parameter and biaxiality parameter with temperature for a $15 \times 15 \times 5$ system.($\xi_1 = \xi_{nz}$)

Table 3.1: The different planar hybrid films studied with their anchoring strength (ξ)

Set	System size	Anchoring strengths (ξ) $\xi_1 = \xi_{nz} = \xi$
1	$15 \times 15 \times 10$	1.00
2	$15 \times 15 \times 6$	1.00, 0.75, 0.50, 0.25
3	$15 \times 15 \times 5$	1.00, 0.75, 0.5, 0.25
4	$15 \times 15 \times 4$	1.00, 0.75, 0.50, 0.25

For every set given in the Table 3.4, detailed simulation described above were carried out, and the relevant physical variable were computed as a function of temperature and combination of anchoring strength, for different system sizes (figures 3.13,3.14). Figure 3.15 shows the variation of the director angle with temperature when the LC-substrate interaction is equal to LC-LC interaction (i.e. $\xi_1 = \xi_{nz} = 1.00$). It is noticed that the

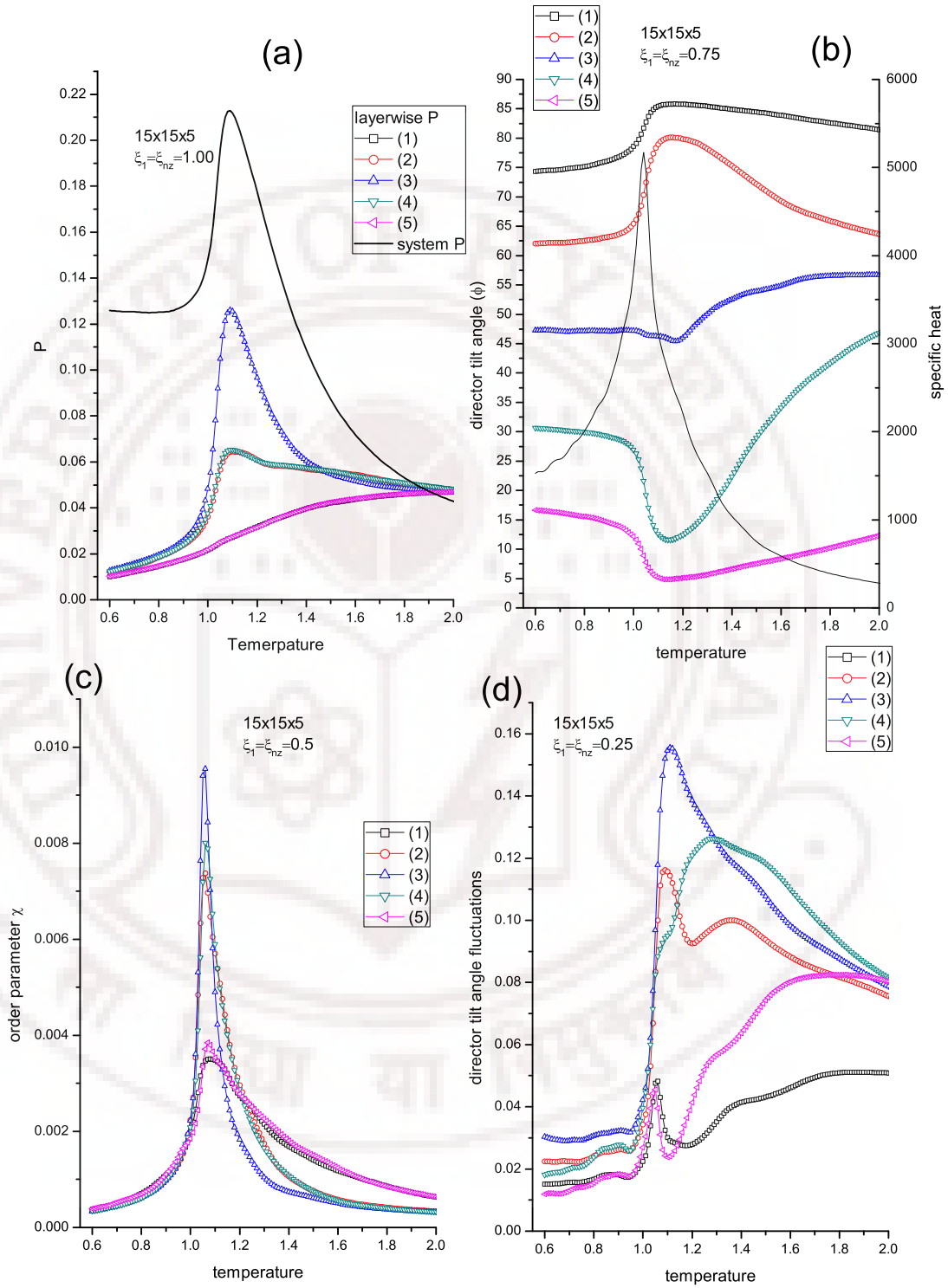

Figure 3.13: (a) Variation of system and layer-wise biaxiality parameter with temperature for a $15 \times 15 \times 5$ system with anchoring $\xi_1 = \xi_{nz} = 1.00$, (b)Variation of specific heat and director tilt angle with temperature for a $15 \times 15 \times 5$ system with anchoring $\xi_1 = \xi_{nz} = 0.75$, (c)Variation of system and layer-wise order parameter with temperature for a $15 \times 15 \times 5$ system with anchoring $\xi_1 = \xi_{nz} = 0.5$, (d) Variation of the fluctuations of director tilt angle with temperature for a $15 \times 15 \times 5$ system with anchoring $\xi_1 = \xi_{nz} = 0.25$,

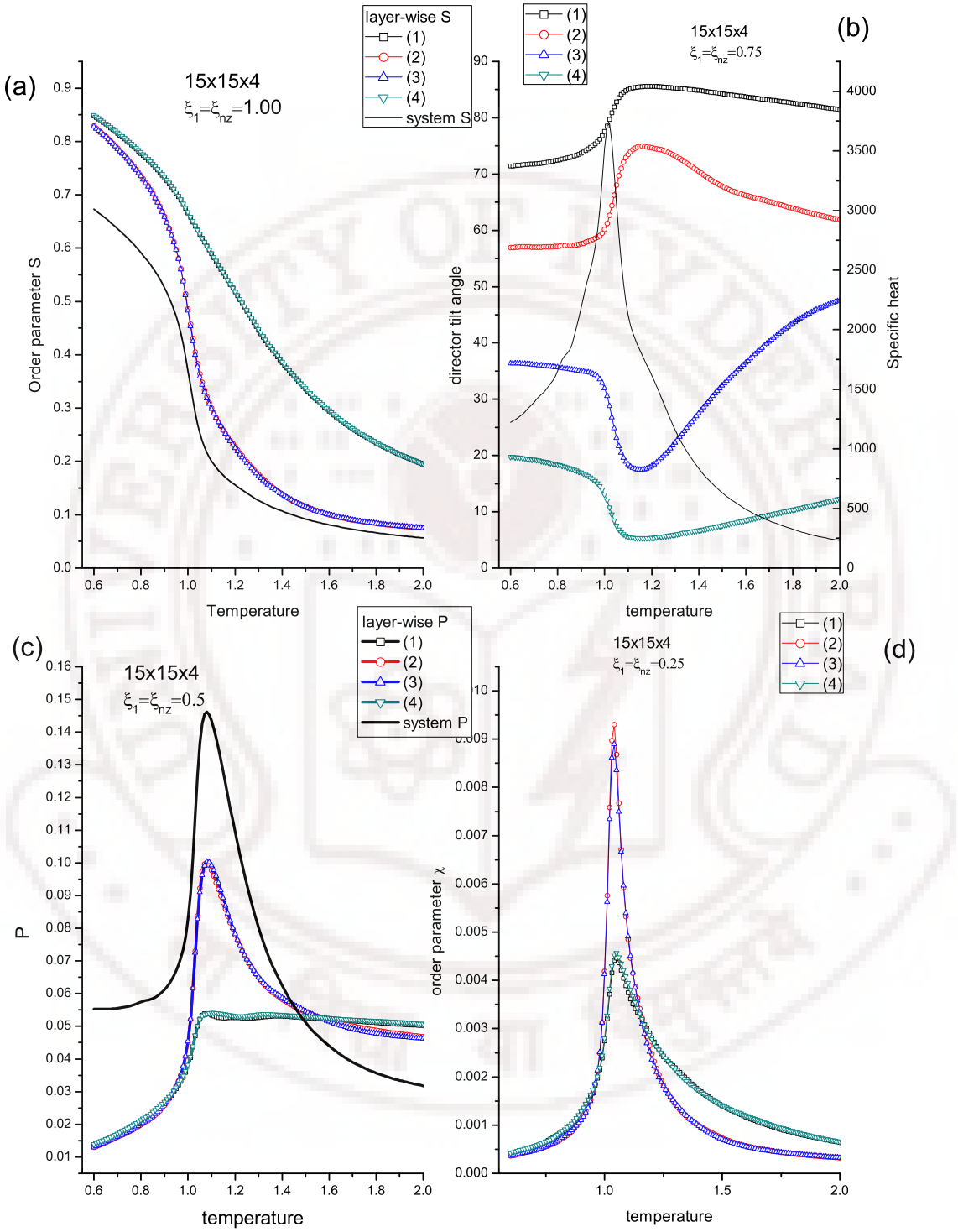

Figure 3.14: (a) Variation of system and layer–wise order parameter with temperature for a $15 \times 15 \times 4$ system with anchoring $\xi_1 = \xi_{nz} = 1.00$, (b)Variation of specific heat and director tilt angle with temperature for a $15 \times 15 \times 4$ system with anchoring $\xi_1 = \xi_{nz} = 0.75$, (c) Variation of system and layer-wise biaxiality parameter with temperature for a $15 \times 15 \times 4$ system with anchoring $\xi_1 = \xi_{nz} = 0.5$, (d) Variation of layer-wise order parameter susceptibility with temperature for a $15 \times 15 \times 4$ system with anchoring $\xi_1 = \xi_{nz} = 0.25$,

director angle fluctuations needed to be computed for each of these systems too, as the specific heat did not show any signature at the isotropic-biaxial transition for the systems with lower anchoring strengths ($\xi_1 = \xi_{nz} = 0.25$). These plots represents the fluctuations in angle director are needed to specify the transition temperatures (figure 3.16). In order to observe the different structures that can be seen for a system with lesser number of liquid

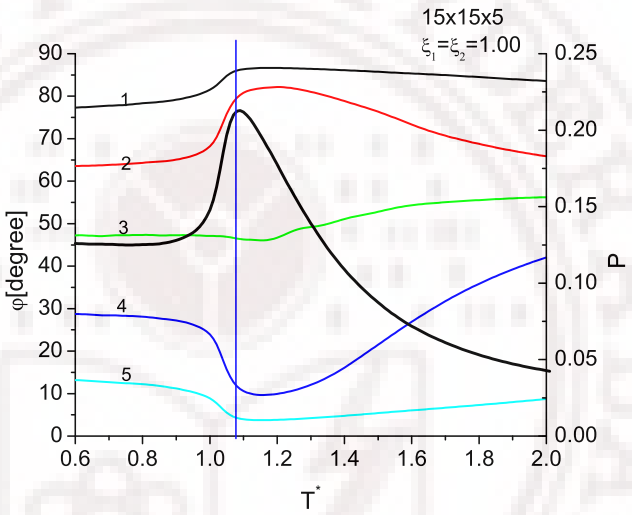

Figure 3.15: Angle director variation with temperature for $15 \times 15 \times 5$ system ($\xi_1 = \xi_{nz} = 1.00$)

crystal layers, a $15 \times 15 \times 4$ system was studied. Set 4 in table 3.1 gives the details of the study done on this system. A bent structure was observed when the temperature was reduced, which is in agreement to previously done Monte Carlo studied [25]. However, the result obtained is not in an agreement to the theoretical studies perviously done [20], but agrees with the canonical Monte Carlo results in this context [25](figure 3.17).

To understand the relative effects of confinement and anchoring, a comparative study was done, by observing the thermal behavior of different physical parameters. The transition from bent-structure to biaxial structure seems to become sharper with the decrease in anchoring strength (ξ), this is seen in both the specific heat and the Binder's cumulant. The order parameter and the biaxiality parameter show a decrease in order with an increase in the anchoring strength (figure 3.18). The biaxiality parameter (figure 3.19) for all the

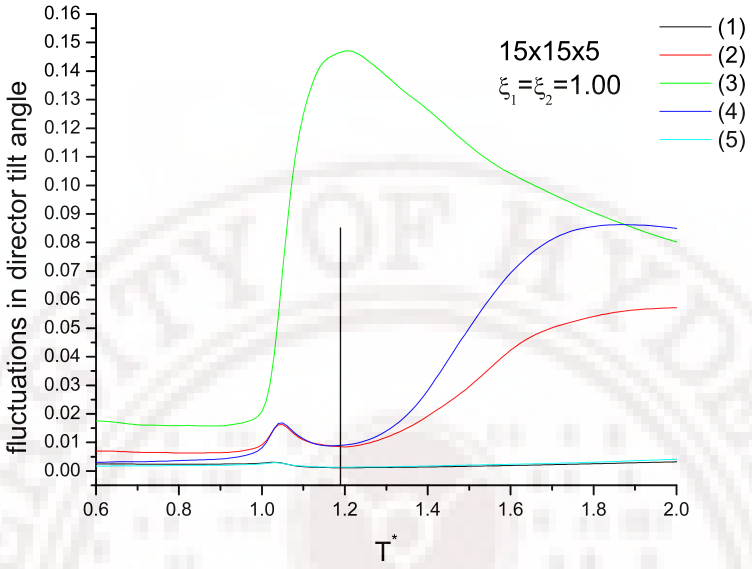

Figure 3.16: Fluctuations of the director angle with temperature for $15 \times 15 \times 5$ system $(\xi_1 = \xi_{nz} = 1.00)$

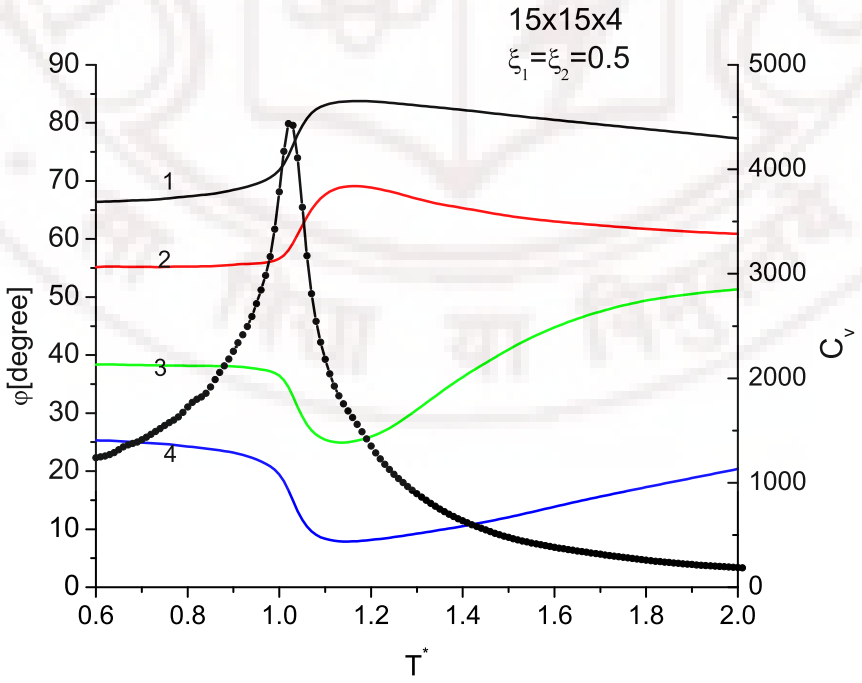

Figure 3.17: The director angle with temperature for $15 \times 15 \times 4$ system $(\xi_1 = \xi_{nz} = 0.5)$

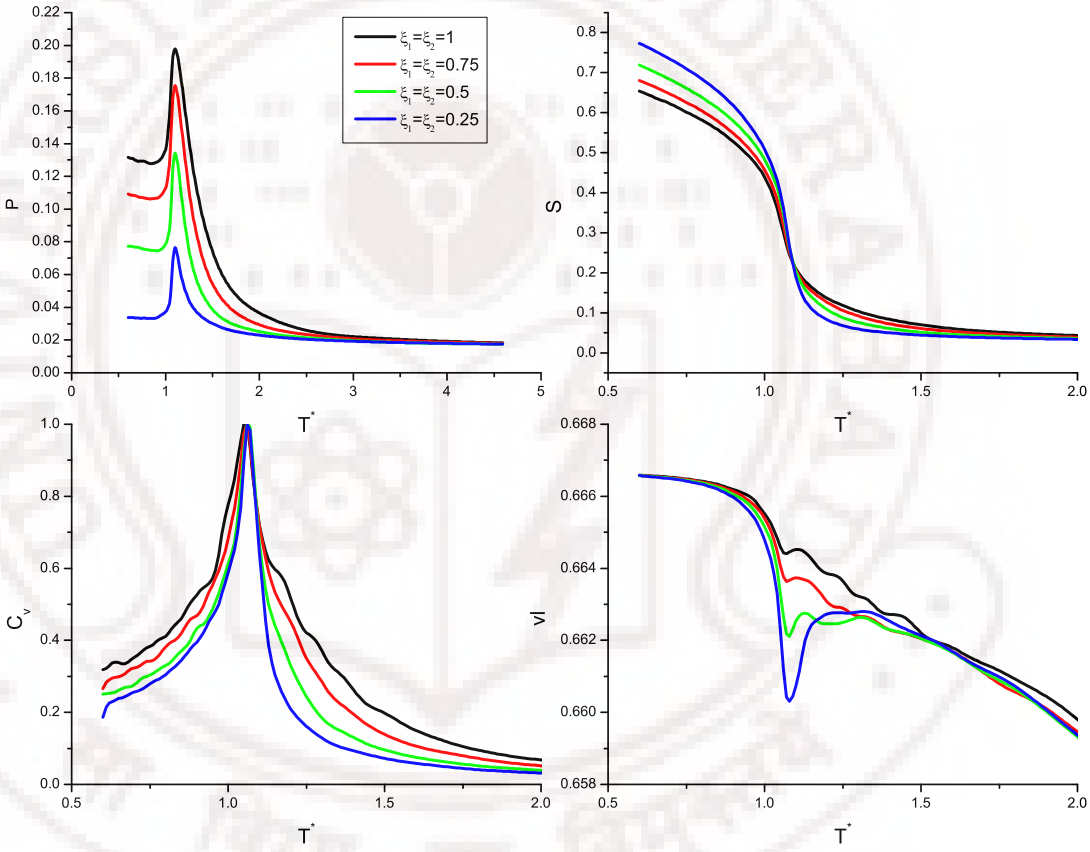

Figure 3.18: The variation of different parameters with temperature for $(\xi_1 = \xi_{nz})$ changing from 0.25 to 1.00

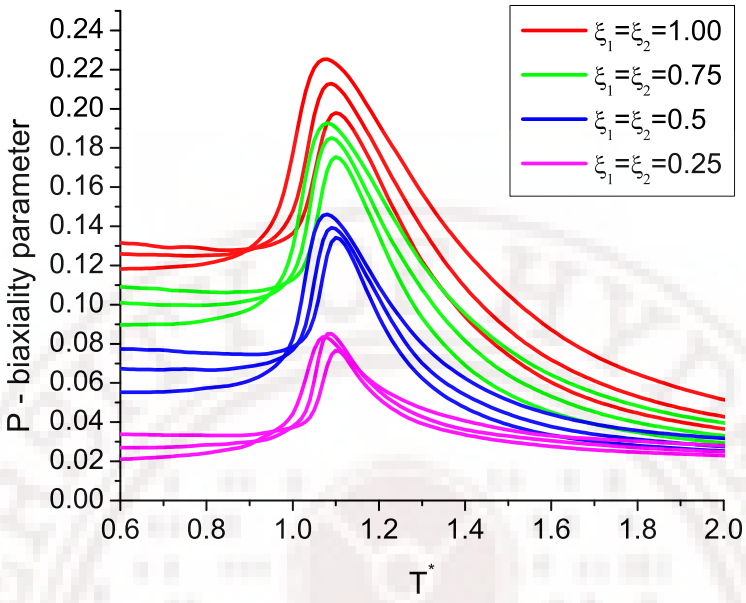

Figure 3.19: The variation of biaxiality with temperature for the different anchoring strength at the lower temperatures.

systems in the set 2, 3 and 4 of the table 3.2 were plotted with temperature variation. It is observed that even in the bent-structure phase a finite degree of biaxiality is still present. It is seen that the biaxiality of the system depends on the anchoring strength of the substrates and is independent of the thickness of the liquid crystal film. A graph was obtained by taking the minimum value of the biaxiality parameter for the $15 \times 15 \times 6$ system at the least temperature and plotted against the anchoring strength (ξ) (figure 3.20). This graph showed that biaxiality increased with the increase in anchoring strength, clearly bring out the role of anchoring in the producing observed phase biaxiality. The transition temperature (T_{C1}) was observed to increase with the increase in the system size (figure 3.21). Another interesting feature seen in confinement is the deviation from linearity in the director angles as a finction of the layer index in the system (figure 3.22). As may be expected the least anchored system shows maximum deviation, since the intermediate 'bulk' system is least perturbed in this case, and hence prefers a more uniform director angle within this region [34].

A special case of a hybrid film is studied, where the liquid crystals are confined in

cylindrical hybrid films.

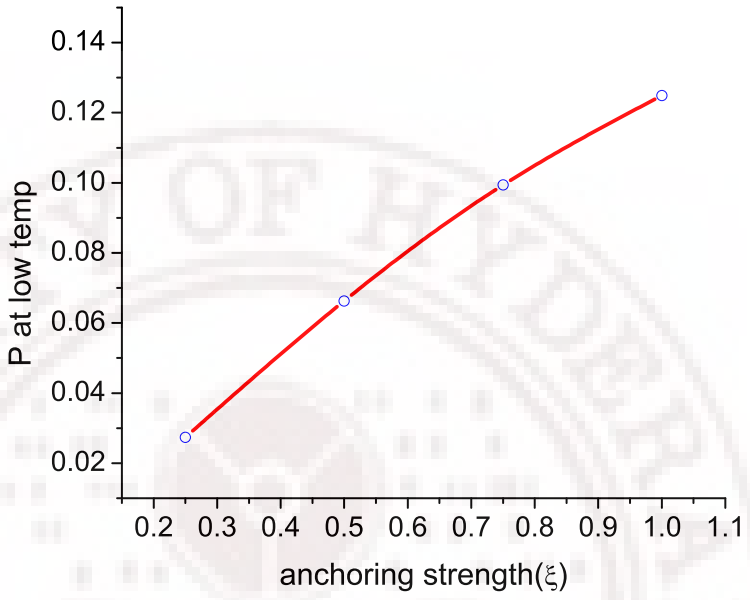

Figure 3.20: The variation of biaxiality with anchoring strength ξ

3.2 A Special Case – Cylindrical Hybrid films:

Non-linear optical methods were used to study the effect of confinement of liquid crystals in capillaries. One feature reported here is the observation of a stable regime looking like a waveguide under certain conditions [35]. Xenon NMR spectroscopy was used to study nematic liquid crystal confined in cylindrical submicron cavities [36]. To study the organization of the liquid crystal in nanocavities a NMR study showed the presence of a paranematic phase formed in the isotropic phase due to the confinement [37]. In such confined systems when either the radius of the cavity, temperature or the strength of the applied field was changed a radial structure transformed into an axial structure or vice-versa [38]. Using numerical minimization of free energy of uniaxial nematic crystal, different nematic structures were observed when liquid crystal molecules are confined in a long cylindrical cavity with homeotropic surface anchoring [39]. The stability regions of the escaped radial and planar polar nematic structures confined to a cylindrical cavity for different external

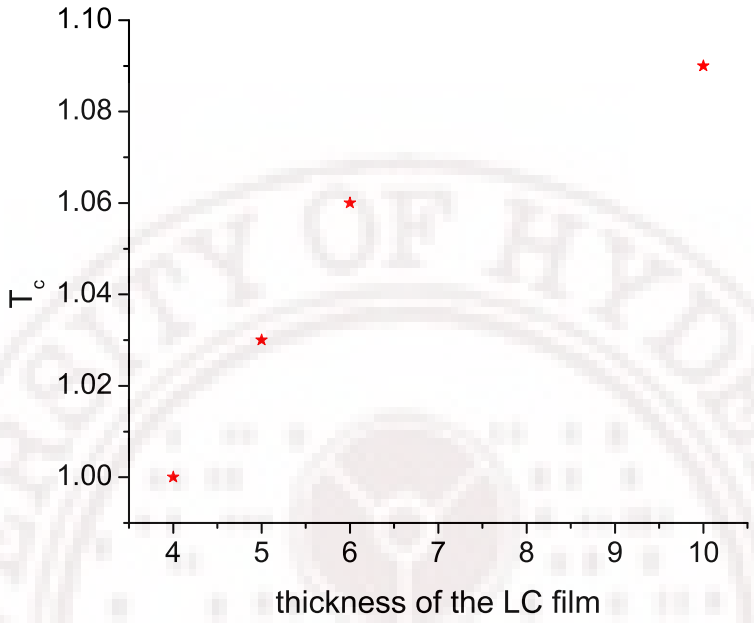

Figure 3.21: Variation of T_{C1} with the thickness of the liquid crystal film d

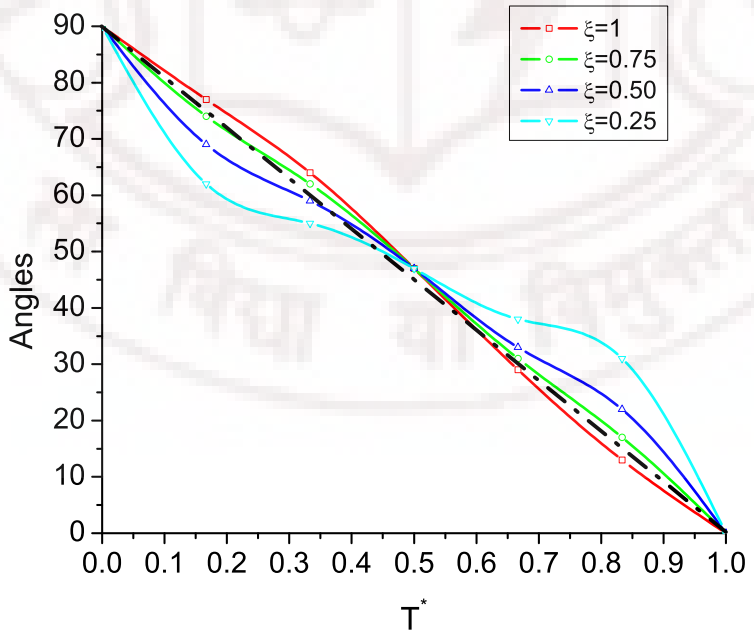

Figure 3.22: Deviation of bent -director angle with change in the anchoring strength of the substrates

magnetic field strengths, anchoring strengths and ration of the elastic constants were investigated. Numerical study based on Landau-de-Gennes free energy was done to consider the effects of different surface anchoring interactions and director configurations [40]. In this study, both the scalar and the orientational order parameters were considered to vary independently. It was observed that a plane polar configuration is essentially more favorable over a polar radial for small radii. Conditions for orientational transitions between radial – planar – radial, planar polar and escaped radial structures was determined for a liquid crystal confined in submicron cylindrical cavity [41]. Molecular dynamics was used to simulate nematic liquid crystal structures confined in a submicron cylinders. Different liquid crystal structures were observed by varying the cylindrical size, anchoring strength and anisotropy constant [42]. An isotropy fluid of needle like hard spherocylinders of length *L* near hard spherical of cylindrical wall using Onsager second viral approximation was studied [43]. The most recent computer simulation of a liquid crystal confined to a spherical cavity deals with an interplay of surface order and elasticity [44]. With the increase in the density, first a uniaxial surface film is formed and then a biaxial surface film, which eventually fills the entire cavity.

The configuration of a nematic liquid crystal confined between two concentric cylinders of radii r_1 and $\rho r_1 > r_1$ with homeotropic anchoring conditions at the walls was studied using theoretical methods [45]. Under certain conditions either a axial configuration or an escape into the third dimension is observed. This represents a geometrically induced Freedericksz transition. The curvature of the confined substrates gives rise to these different structures. In the light of the above studies on cylindrical LC films, we consider here MC simulation (based on canonical sampling) of such a film but subjected to hybrid boundary condition at the two solid substrates.

As a special case a hybrid film was modeled with two concentric cylinders. The hybrid nature in the system was brought about by making one cylindrical substrate induce order within a plane perpendicular to the axis, say the radial order and the other to induce order along the the axis of the cylinder, say axial order order. The effect of the surfaces is thus

to induce incompatible order – one along the cylindrical axis and the other perpendicular to it, – thus testing a hybrid cylindrical film. These system was studied to understand the different structures that can be formed in this system, with temperature and anchoring strength.

3.2.1 Modeling of hybrid films enclosed between two concentric cylinders:

A cylindrical film is carved out of a suitable cuboid, whose dimensions are determined by the thickness and the length of the film. The cuboid dimensions are chosen in such a way it embeds the film as well as the substrate layers (ghost layers) to introduce anchoring effects. Since the dimensions of interest are only the radii, periodic boundary conditions are imposed along the axis of the film enclosed between the two concentric cylindrical substrates.

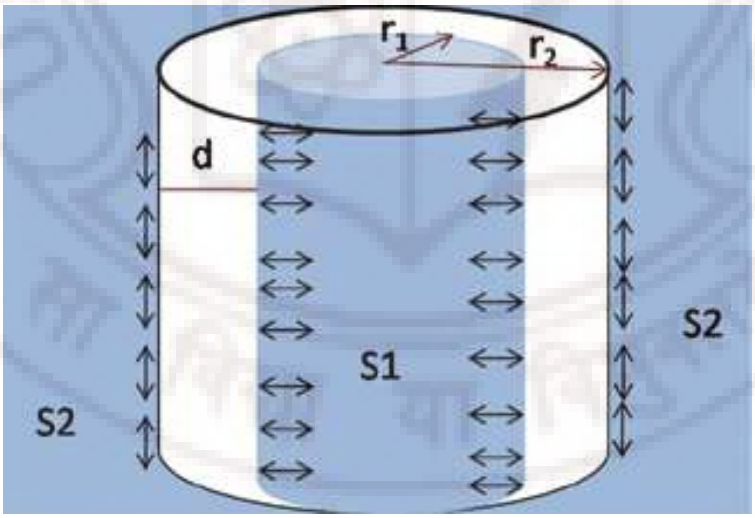

Figure 3.23: A cartoon depicting how a cylindrical hybrid film is modeled (the blue indicating the ghost molecules).

Consider that the radius of the outer cylinder is r_2 and inner cylinder is $r_1(r_2 > r_1)$. A flag is used to differentiate the substrate molecules from the liquid crystal molecules. All the molecules with their radius more that r_2 are considered as the substrate of the outer

cylinder - surface $S2$. All the molecules with their radii lesser than r_1 are considered as the molecules of the inner substrate - surface $S1$. The molecules belonging to $S1$ and $S2$ are considered as ghost layers and their orientations are fixed according to the problem we are studying. The fixed orientations of the spins at the two surfaces then define the anchoring nature of the substrates. For convenience of discussion, the condition of the orientation at the inner surface of the cylinder (in contact with the liquid crystal molecules) is referred to as X_1; at the outer surface as X_2. The anchoring strengths of the inner and outer surfaces are designated as ϵ_1 and ϵ_2, respectively. The thickness of the liquid crystal molecules is denoted as d where $d = r_2 - r_1$. The liquid crystal molecules embedded in the interstitial space between these two cylindrical substrates have been assigned random orientation at the beginning of the Monte Carlo simulations. Hybrid nature of the film can be generated, for example, by forcing at X_1 and X_2, the anchoring conditions at the two substrates to be mutually perpendicular. Accordingly, axial (A) or radial (R) boundary conditions are imposed, at either of the surfaces. In this notation, A_1 denotes that inner surface is imposing axial boundary condition; R_1 denotes that it is imposing a radial boundary cindition, etc. For convenience, with this definition, we will follow the notation $[r_1, r_2; X_1, X_2; \epsilon_1, \epsilon_2]$ to specify compactly the conditions of simulation, X standing for A (axial) or R (radial) boundary conditions, as case may be.

Another important point considered here is the way this system is made to mimic a real system. In order to make the system imitate a real system as closely as possible periodic boundary conditions (PBC) are considered. Periodic boundary conditions in this system are imposed along the axis of the cylinder i.e along the height of the cuboid, keeping in view the symmetry of the film. This system was studied by constructing canonical ensembles (Boltzmann ensembles) at different temperatures, using Metropolis algorithm. A equilibration run composed of about 20000 Monte Carlo lattice sweeps and the system energy equilibrates subsequently. An ensemble of 150000 microstates was collected after equilibration representing the canonical ensemble. All averages are preferred over this ensemble.

The substrates are fixed to induce a hybrid order in the liquid crystal system. The simulations was started at the highest temperature 2.00, reduced by 0.02 until the minimum value of 0.05 is reached. The last equilibrium microstate of the higher temperature was used as the initial state for the next lower temperature which makes the convergence of the next ensemble to its equilibrium faster.

As before, the energy is measured in units of the interaction constant in the LL potential between two neighboring LC molecules. The anchoring strength is now made variable by making the interaction of the LC molecules with the respective substrates to vary as per the prescribed value. Thus, the strength of interaction is a tunable parameter $0 < \epsilon_s < 1$, and is referred to as the surface anchoring strength. The anchoring strengths ϵ_1 and ϵ_2 compared to this parameters on inner and outer surfaces, respectively. The anchoring strength on the inner substrate ϵ_1 is varied, while keeping $\epsilon_2 = 1$. A detailed investigation of the director structures for different values of ϵ_1 and ϵ_2 (in the range 0 to 1) and with different types of orientations of anchoring in the two surfaces (A_1, R_2 or R_1, A_2) was carried out to look for physically interesting combinations of these which have the potential to induce 'biaxial' features. It turned out that physically curious systems requires radial anchoring at the inner surface and axial anchoring at the outer surface. Thus, the main system of our further study was one with radial ordering on the inner substrate and axial ordering on the outer substrate. While these two substrates try to induce ordering in antagonistic directions, the interactions among liquid crystal molecules would prefer uniaxial symmetry. These three ordering mechanisms compete in the system, and could be made comaprable by changing the geometric parameters *r* and *d*. One of the immediate goals of this work is to explore and find out a physically interesting system with appropriate values of these two model parameters such that these two competing ordering mechanism, are tuned so that their effects in the (concentric) middle layers tends to possible biaxial structure like in the case of planar hybrid film. The conflict however becomes practically irrelevant when *d* is very large, and in this limit the system recovers its bulk-like features.

Thus, it is clear that the response of the thin film to these conflicting and competing

influences will crucially depend on the number of liquid crystal molecules in the plane perpendicular to the axis, the degree of conflicting influence of the substrate and of course, the reduced temperature T^* which essentially sets the relative importance of entropy in relation to energy of the system. This study was done by considering the liquid crystal to be represented by a lattice model [27] (equation 3.1.1) that mimics the nematic-isotropic transition in a simple way.

3.2.2 Results and Discussion on cylindrical hybrid films

The system which we studied is a cylindrical film embedded between two concentric cylinders representing the confining substrate. The inner cylinder has a radius r_1 (lattice units) and the outer cylinder has a radius r_2 . For purposes of computation of data and understanding the spatial variation of the different features, and keeping the axial symmetry of the system in view, we divide this confined cylindrical film into concentric cylindrical layers of unit thickness, and compute physical parameters of each of the sub-layers so as to obtain information on the spatial variation of the director field. In the Monte Carlo simulation, obviously only those 'spins' located at lattice points within this concentric cylindrical shell will participate, while the 'spins' located at rest of the lattice points in the cube (corresponding to the substrate) are held fixed. The fixed orientations of the spins at the two surfaces then define the anchoring nature of the substrate. Based on the results obtained from the initial chosen boundary conditions on this cylindrical system, and also on the earlier analysis of similar data on thin hybrid planar films, we carried out extensive simulations (as a function of temperature) for different anchoring conditions imposed on the nature and extent of the anchoring at the two surfaces, as well as different sizes of the films by varying r_1 and r_2 [46]. For convenience, with this definitions, we will follow the notation [r_1 **,** r_2 **;** $X1, X2$; ε_1 **,** ε_2] to specify compactly the conditions of simulation as mentioned earlier. The following sections describe the results of our simulations on several cylindrical films (of various sizes) with different experimental conditions imposed at the inner and outer surfaces.

In order to provide a perspective of the different input parameters used to obtain results on hybrid films of varying character, a summary of the systems investigated in this study is provided in the following Table 3.2, following the above notation for denoting the system under consideration.

Table 3.2: The different cylindrical hybrid film systems studied by varying the boundary conditions

System	Simulation Condition
1	[2, 8 ; A1, R2 ; 1.0, 1.0]
2	[2, 8 ; R1, A2 ; 1.0, 1.0]
3	[2, 8 ; A1, R2 ; 0.5, 1.0]
4	[2, 8 ; A1, R2 ; 0.0, 1.0]
5	[2, 8 ; R1, A2 ; 0.5, 1.0]
6	[2, 8 ; R1, A2 ; 0.0, 1.0]
7	[3, 9 ; R1, A2 ; 1.0, 1.0]
8	[2, 8 ; R1, A2 ; 1.0, 1.0]

Here, a film of inner radius of 2 (in lattice units), outer radius of 8, and a length of 28 lattice units, carved out of a cubic lattice of dimensions $18 \times 18 \times 28$ is considered. While keeping the anchoring strengths at the two surfaces equal (unity), we experiment

with the effect of imposing two different antagonistic boundary conditions at the two surfaces, thereby creating a hybrid cylindrical film. We report here our results arising out of these two sets of boundary conditions: 1. the substrate molecules at the inner boundary are orientated along the cylindrical axis and hence try to impose orientational order in the liquid crystal medium along the axis (say, z-axis) of the cylinder (axial order); and 2. the substrate molecules contained in each $[x, y]$ plane at the outer surface point to the center of the cylinder lying in that plane, introducing what we can refer to as radial order in the system. Another interesting hybrid film by simply interchanging the nature of the boundary conditions (inner substrate imposing radial order and the outer one imposing an axial order) were studied, to provide contrasting effects, representing a different experimental condition. An initial study with reference to Table 3.2 was done in detail to look for a system that showed interesting features [46] [47]. It is seen that only system - 3(table 3.2) showed the effect of confinement on the intermediate layers. Considering this as a starting point a detailed study was done by changing the anchoring strength of the substrate imposing the axial anchoring.

3.2.3 Cylindrical Hybrid films [2, 8 ; *A*1, *R*2; 0.5, 1.0]

We present results of a film of $r_1 = 2$ and $r_2 = 8$ with an axial anchoring at the inner surface, with relative strength 0.5 and radial anchoring at the outer surface with strength 1.0. Periodic boundary conditions are impressed along the axis of the cylinder.

Specific heat and Energy

(Figure 3.24 (f)): The specific heat, and the average energy are plotted with the variation in temperature. In this system the inner substrate induces an axial order with anchoring strength (ϵ_1) 0.5. The other substrate induces a radial order with anchoring strength 1 (ϵ_2). The specific heat plot shows up with a shoulder on the higher temperature side at $T^* = 1.06$ other than the peak that occurs at $T^* = 0.98$. However, these features are not readily observable in the variation of average energy with reference to temperature.

Order parameter 'S'

(Figures 3.24 (a), (b)): Figure 3.24 (a) gives the overall order parameter present in the system due to the confinement. The order parameter of a bulk LL model which is normally a slow monotonically increasing function with the decrease in temperature, showed a qualitative different profile due to the hybrid nature of confinement. It may be recalled that the system order parameter is given by the maximum eigen value of the ordering tensor but for a scale factor. A sudden rise is seen in the order parameter profile at $T^* = 0.98$, after which the order remains constant. The layer-wise order parameter was also plotted with change in temperature. At the higher temperatures, the order in the layers -1 and -6 rises, indicating the building of order in the system with the decrease in temperature. At the transition the order parameter profile of the layer - 1 had a dip and then rises sharply unlike layer - 6. The layer - 2 being more influenced by substrate *1* follows a similar path as layer - 1. Layer - 4 and layer - 5 show a peak at the transition temperature, after which they decrease. The layer - 3 shows an interesting feature: there is a peak occurring at the transition temperature, after which the order in the layer decreases. The order parameter of this layer at the lower temperature is zero.

Radial and Axial Order

(Figure 3.24 (c), (d)): The layer-wise radial and the axial order of the system seem to increase as expected. The innermost layer (layer - 1) has the maximum radial order and outermost layer (layer - 6) has the highest axial order and vice versa. The layer - 5 follows layer - 6 with more axial order than radial order. The most interesting among all the layers is the layer - 3, where axial order is zero but the radial order is 0.5. The molecules are not aligned axially but have a little amount of radial order. The axial order being zero is also verified by the overall order parameter of this layer tending tos zero at the minimum temperature.

Biaxiality

(Figure 3.24(e)): The biaxiality is given as the difference in the smaller two eigen values of the ordering tensor. It is observed from figure 3.24 (e) that biaxiality is present when the layer is aligned radial. Layer 6, 5 and 4 have considerable amount of biaxiality reaching 0.34, 0.28, 0.17 at the minimum temperature, respectively. While layer - 1, 2 and 3 reach a minimum (~ 0) at the lowest temperature. The layer - 3 seems to be most interesting and this is discussed in detail.

Discussing the layer - 3 in particular at temperature 0.05, it is seen that the order parameter is zero, and the biaxiality is zero too. The axial order is zero and the radial order is 0.5, which gives an idea with regard to the alignment of the molecules in this layer. From these order parameters values it may be concluded that the molecules are randomly aligned, and the layer has an isotropic alignment. This is seen as a consequence of the percolation of competing order from the two substrates, and this particular layer with the specific geometry and anchoring strength chosen, seems to be preferring an isotropic symmetry to satisfy two interfacial conditions between two competing, qualitatively different, ordering mechanisms.

Noticing this feature in this system (system 3 Table 3.2), a detailed study was done by changing the anchoring strengths (ϵ_1) in steps of 0.1. Table 3.3 gives the details of the study. The anchoring strength ϵ_1 was changed from 0.0 to 1.00 for the inner substrate imposing axial order while keeping the anchoring strength ϵ_2 of the outer substrate was kept at 1.00 (imposing radial). This study was done to understand the effect of anchoring ϵ_1 on the various parameter as an indication to an anchoring transition.

Every system in table 3.3 was studied in detail by computing all the layer-wise parameters along with the system properties.

3.2.4 Cylindrical Hybrid films [2, 8 ; *A*1, *R*2; 0.48, 1.0]

We discuss the results of a film of $r_1 = 2$ and $r_2 = 8$ with an axial anchoring at the inner surface with relative strength 0.48, and radial anchoring at the outer surface with strength

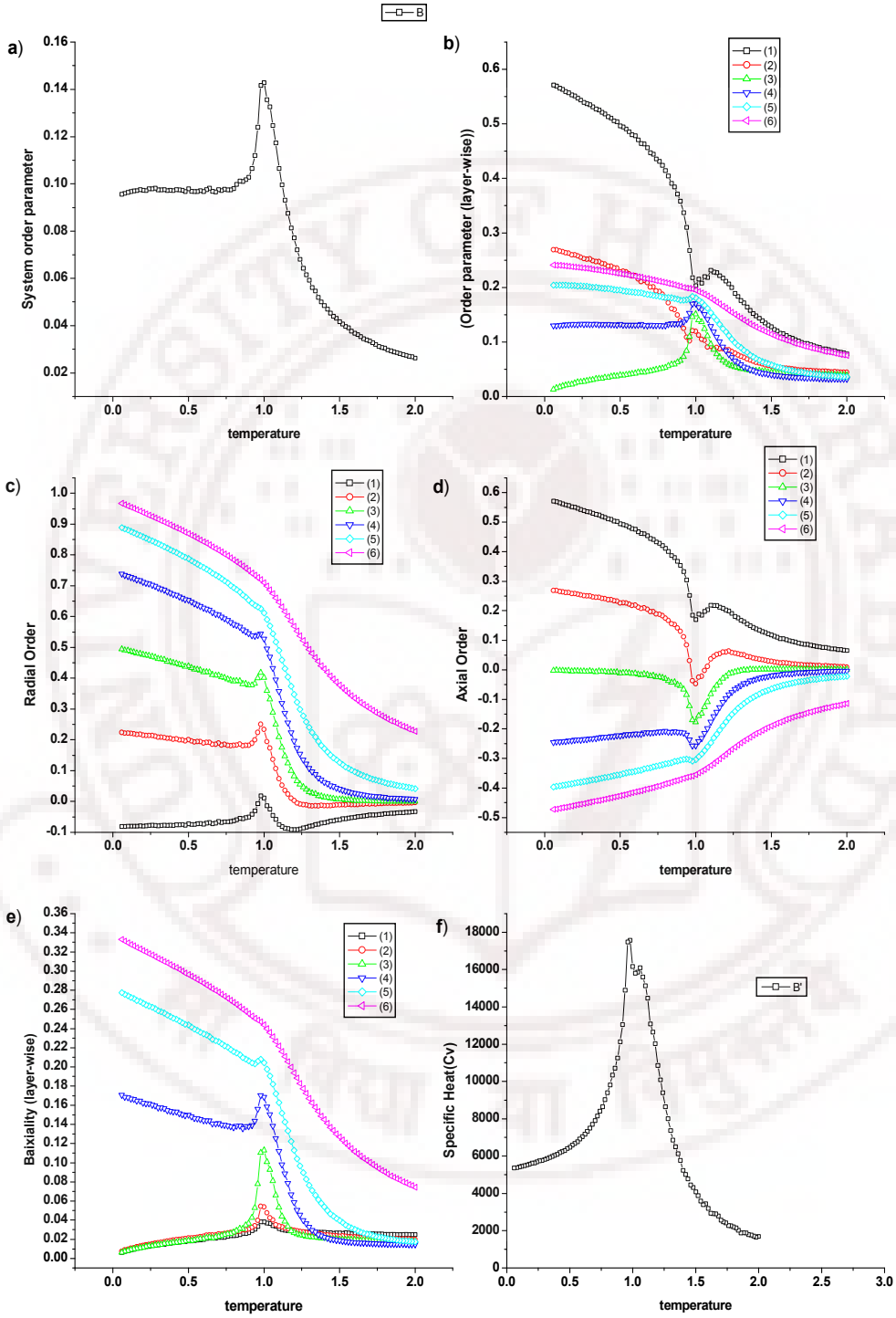

Figure 3.24: (a) Order parameter of the bulk film b) Layer-wise order parameter c) Layer-wise radial order parameter d) Layer-wise order parameter along z-axis e) Layer-wise bi-axiality of system layer-wise and f) Specific Heat (C_V) [r_1 = 2, r_2 = 8; ε_1 =0.5 with axial boundary conditions and ε_2 = 1.0 with radial boundary conditions]

Table 3.3: Simulation Study 2: Varying ϵ_1 with axial anchoring while keeping the anchoring strength of the outer substrate constant.

System	Simulation Condition
1	[2, 8 ; A1, R2 ; 0.0, 1.0]
2	[2, 8 ; A1, R2 ; 0.22, 1.0]
3	[2, 8 ; A1, R2 ; 0.32, 1.0]
4	[2, 8 ; A1, R2 ; 0.42, 1.0]
5	[2, 8 ; A1, R2 ; 0.44, 1.0]
6	[2, 8 ; A1, R2 ; 0.45, 1.0]
7	[2, 8 ; A1, R2 ; 0.46, 1.0]
8	[2, 8 ; A1, R2 ; 0.48, 1.0]
9	[2, 8 ; A1, R2 ; 0.50, 1.0]
10	[2, 8 ; A1, R2 ; 0.52, 1.0]
11	[2, 8 ; A1, R2 ; 0.54, 1.0]
12	[2, 8 ; A1, R2 ; 0.62, 1.0]
13	[2, 8 ; A1, R2 ; 0.82, 1.0]
14	[2, 8 ; A1, R2 ; 1.00, 1.0]

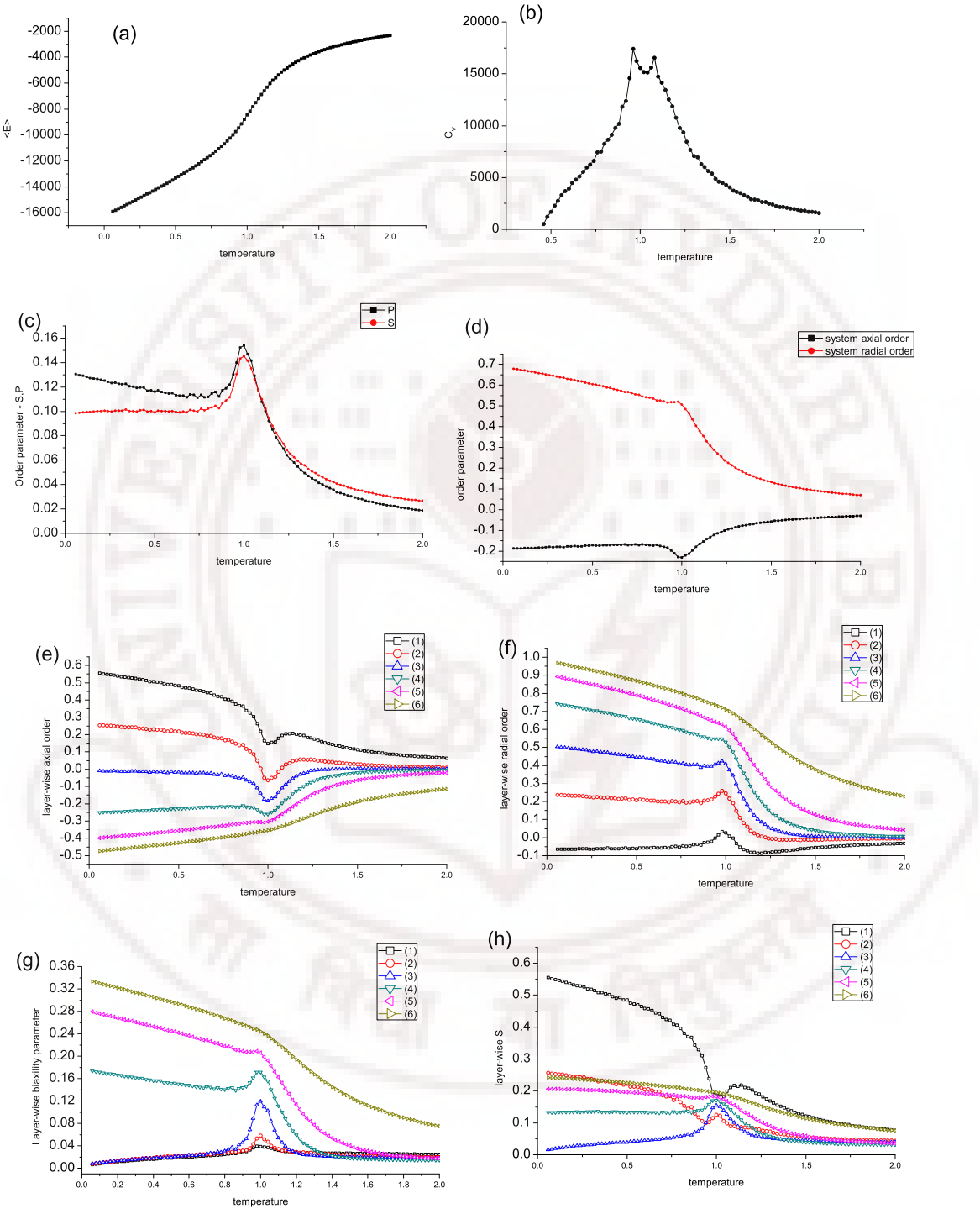

Figure 3.25: (a) Average energy b) specific heat c) system order parameters - S and P d)system radial and axial order parameters e) layer-wise axial order parameter f) Layer-wise radial order parameter g) layer-wise biaxiality parameter h) layer-wise order parameter S *[r_1 = 2, r_2 = 8; ε_1 =0.48 with axial boundary conditions and ε_2 = 1.0 with radial boundary conditions]*

1.0 (figure 3.25).

Average energy and specific heat

(Figures 3.25(a), (b)): The average energy and the specific heat are plotted against temperature. The specific heat plots show clearly the presence of two transitions occurring at, $T_{C1} = 0.96$ and $T_{C2} = 1.08$.

System order parameters

(Figure 3.25 (c),(d)): The system order parameters (overall order parameter, biaxial, radial, axial) computed for this systems are plotted against temperature. The system order parameter shows a very curious profile: normally for a bulk system at the least temperature the order rises to about ~ 0.9. Here the order parameter takes a value of 0.1. The biaxiality parameter has a higher value than the system order parameter. The radial and axial order give a better story to the ordering in the system. The molecules in the system are more radially ordered than axially ordered, hence the system order parameter S has a very low value.

Layer-wise radial and axial order

(Figure 3.25 (e), (f)): Figures 3.25 (e) gives the layer-wise axial order of the system, depicting the orientation of the molecules along the z-axis. It is clearly seen that most of the layers have a negative value for the order and have a complimentary positive radial order (figure 3.25(f)). Only layer -1 has a slight radial order, indicating that this layer is more axially ordered than radially ordered. The layer -3 similar to the above discussed system has a zero value axial order and has radial order of 0.5.

layer-wise order parameter and the biaxiality parameter

(Figure 3.25(g), (h)): The layer-wise order parameter is plotted with temperature in the figure 3.25 (g). It is observed that the layer 1, 2, and 3 have almost zero value of biaxiality parameter at the least temperature (figure 3.25(g)). There is non – zero order present in

all the layer except the layer-3, at the least temperature. The inability of this layer to orientational order, even at the very low temperature (~ 0.05) is curious. It points out that any such ordering of this layer is not compatible with the two competing boundary conditions, tuned suitably.

From table 3.3 it is noticeable that a study was done with a intricate variation in ϵ_1. The system order parameter (figure 3.26 (b)) does not give any indication to a transition but with the increase in ϵ it is observed that order in the system decreases at the least temperature. With the variation in temperature there is observable change in the order parameter profile, a peak occurring due to the competing boundary conditions. The biaxiality parameter with the change in temperature similar to the order parameter develops a peak indicating the competing boundary conditions (figure 3.26(b)). The only observable change with change in ϵ_1 is the increase in the sharpness of the peaks. Figures 3.26 (c) and (d) give the system radial and axial order parameter with the change in temperature for various values of ϵ_1. The effect of increasing the ϵ_1 is indicative in the plots. The effect of changing ϵ_1 is observed when the specific heat plots were clubbed together (figure 3.27). The main noticeable feature was the development of a double peak in the specific heat with the increase in ϵ_1. The specific heat for the $\epsilon_1 = 0.00$ showed a peak in the specific heat, which developed into a double peak for $\epsilon_1 = 0.48$ and again collapsed to a single peak for $\epsilon_1 = 1.00$ (figure 3.27). The development of the double peak clearly noticeable as a variation in the competing forces due to the substrates.

To get an understanding about the different transitions occurring the layer-wise biaxiality parameter was plotted with temperature and super imposed with the specific heat for the system [2, 8 ; $A1$, $R2$; 0.48, 1.0] (figure 3.28). This plot showed that the biaxiality peaked exactly in between the two peaks of the specific heat. With the understanding in the planar hybrid films this can deciphered as transition between three stable states. The first peak at higher temperature can be referenced to transition from a disordered state to an ordered state-1 and the second one corresponds to a transition from ordered state-1 to an ordered state-2. From figure 3.28 this shows that ordered state-1 corresponds to a biaxial

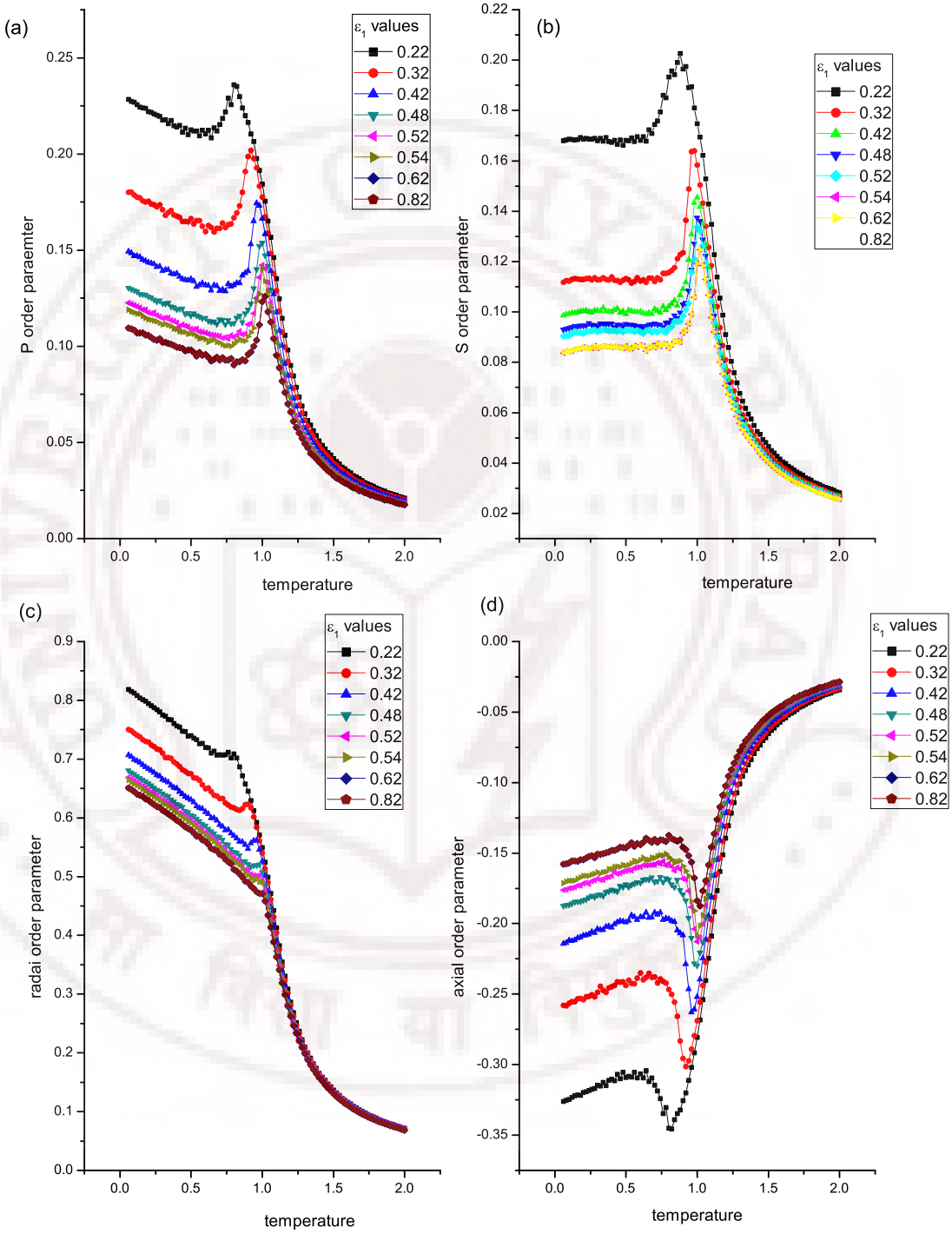

Figure 3.26: (a)Biaxial order parameter (b) System order parameter (c) Radial order parameter (d) Axial order parameter against temperature for different values of ϵ_1 with axial ordering keeping $\epsilon_2 = 1.00$ with radial anchoring.

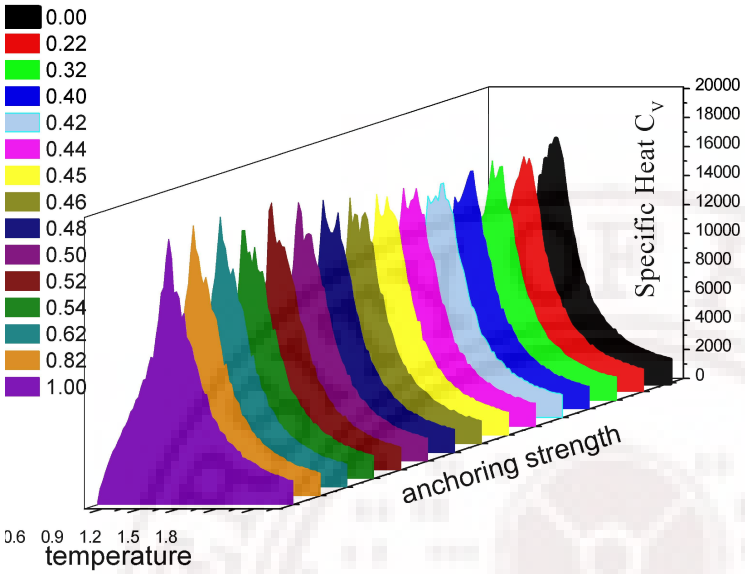

Figure 3.27: Variation of specific heat with temperature for all the systems in table 3.3

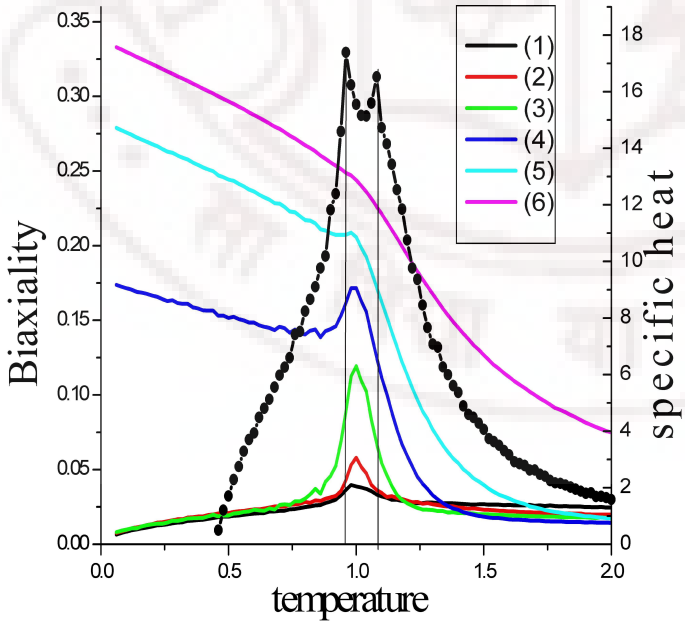

Figure 3.28: Variation of layer-wise biaxiality with temperature with the specific heat for the system [2, 8 ; A1, R2 ; 0.48, 1.0]

phase. Ordered phase 2 can correspond to a stable phase like the bent phase in a planar hybrid film.

A cylindrically confined hybrid film of liquid crystal molecules is more competitive to study than a planar hybrid film. The curvature in these system play very important role by effecting the splay elastic constant K_1 of the system. In this system the area of the substrates are not equal as in a planar hybrid film, hence parameters like that anchoring strength play a monumental role. In this study the anchoring strength ϵ_1 had to be tuned independently in order to observe a biaxial phase, which was simple to observe in a planar hybrid film and observed for every anchoring strength. This study also indicated the importance of the boundary conditions, all boundary conditions assumed in table 3.2 showed that a biaxial phase appeared only when the right boundary condition with the apparent anchoring was assumed.

3.2.5 Conclusions

A planar hybrid film of uniaxial liquid crystal molecules was studied using Monte carlo simulations. Simulations were performed based on LL model and entropic sampling method was employed to obtain higher resolution in temperature, and to overcome some of the known limitations of canonical sampling techniques. These results are discussed in the light of MC simulations performed earlier to get further insight into the model. It was seen that there are two transitions occurring, a higher temperature one being a isotropic to a biaxial phase. The most interesting feature in this study was the presence of biaxiality seen due to hybrid confinement in a system of uniaxial molecules. The lower temperature transition is a structural transition from a biaxial phase to a bent director phase. A study was done also by changing the thickness 'd' of the liquid crystal film and also changing the anchoring strength of the confining substrates ϵ_1 and ϵ_2. Along with the specific heat and the average energy, the order parameters (system order parameter, biaxial order parameter) were studied for every layer to get a detailed understanding of the transitions occurring in the system with changes in temperature.

Using canonical sampling methods a hybrid film confined between concentric cylindrical substrates was studied. A biaxial phase was observed for a particular boundary condition when the anchoring strength was tuned very finely. This film is more complex to study compared to planar hybrid film because of the curvature. Firstly, the area of the two substrates are unequal and secondly, the cost of energy per unit area due to distortion is unequal at the two bounding surfaces due to the curvature. Under these circumstances the subtle balancing of the influence of the bonding surfaces on the middle layers requires a detailed tuning of the anchoring conditions, in order to observe biaxial effects as were observed in planar films more readily due to simpler boundary conditions.

The biaxial phase discussed above in the case of the hybrid films, is solely due to the antagonist boundary condition imposed by the substrates. The LC molecules modeled here with LL model represent cylindrically symmetric uniaxial molecules. The biaxial order parameter observed in these studies is known commonly as the phase biaxiality order parameter (R^2_{20}) . This study lead us to focus on systems with molecules that are biaxial *i.e.* lack of cylindrical symmetry about the long axis. The next two chapters deals with a study of such molecules in predicting their properties in bulk, and under confinement.

Bibliography

[1] A. V. Zakharov and M. Iwamoto. Homeotropic-planar anchoring transition induced by trans-cis isomerization in ultrathin polyimide langmuirblodgett films. *J. Chem. Phys.*, 118:10758, 2003.

[2] C. Chiccoli, O. D. Lavrentovich, P. Pasini, and C. Zannoni. Monte carlo simulations of stable point defects in hybrid nematic films. *Phys. Rev. Lett.*, 79:4401, 1997.

[3] C. Chiccoli, P. Pasini, and C. Zannoni. Hybridly aligned liquid crystal films. a monte carlo study of molecular organization and thermodynamics. *Mol. Cryst. Liq. Cryst.*, 336:123, 1999.

[4] T. Rasing and I. Musevic, editors. *Surfaces and Interfaces of Liquid Crystals*. Springer Verlag, Berlin, 2004.

[5] P. Palffy-Muhoray, E. C. Gartland, and Kelly. A new configurational transition in inhomogeneous nematics. *Liq. Cryst.*, 16:713, 1994.

[6] A. Sarlah and S. Zumer. *Surfaces and Interfaces of Liquid Crystals*. Springer, Berlin, 2004.

[7] K. Kocevar, R. Blinc, I. Musevic, and J. Stefan. Atomic force microscope evidence for the existence of smecticlike surface layers in the isotropic phase of a nematic liquid crystal. *Phys. Rev. E*, 62(3):R3055, 2000.

[8] M. M. Wittebrood, Th. Rasing, S. Stallinga, and I. Musevic. Confinement effects on the collective excitations in thin nematic films. *Phys. Review Lett.*, 80(6):1232, 1998.

[9] T.Bellini, N.A.Clark, and D.W.Schaefer. Dynamic light scattering study of nematic and smectic-a liquid crystal ordering in silica aerogel. *Phys. Review Lett.*, 74(14):2740, 1995.

[10] P. Ziherl, A. Sarlah, and S. Zumer. Collective fluctuations and wetting in nematic liquid crystals. *Phys. Rev. E*, 58(1):602, 1998.

[11] P. Ziherl and S. Zumer. Fluctuations in confined liquid crystals above nematic-isotropic phase transition temperature. *Phys. Review Lett.*, 78(4):682, 1997.

[12] A. Borstnik and S. Zumer. Forces in an inhomogeneously ordered nematic liquid crystal: Stable and metastable states. *Phys. Rev. E*, 56(3):3021, 1997.

[13] N.Schopohl and T.J.Sluckin. Defect core structure in nematic liquid crystal. *Phys. Review Lett.*, 59(22):2582, 1987.

[14] G. Skacej, A. L. Alexe-Ionescu, G. Barbero, and S. Zumer. Surface-induced nematic order variation:intrinsic anchoring and subsurface director deformations. *Phys. Rev. E*, 57(2):1780, 1998.

[15] N.Nobili and G.Durand. Disorientation-induced disordering at a nematic-liquid-crystal-solid interface. *Phys. Review A*, 46(10):R6174, 1992.

[16] Hao Li and Mehran Kardar. Fluctuations induced fordes between rough surfaces. *Phys. Review Lett.*, 67(23):3275, 1991.

[17] R.Barberi and G.Durand. Order parameter of nematic liquid crystal on rough surfaces. *Phys. Rev. A*, 41(4):2207, 1990.

[18] J. Stelzer, P. Galatola, G. Barbero, and L. Longa. Molecular dynamics simulations of surface-induced ordering in a nematic liquid crystal. *Phys. Rev. E*, 55(1):477, 1997.

[19] G.S.Iannacchione, G.P.Crawford, S.Zumer, J.W.Doane, and F.Finotello. Randomly constrained orientational order in porous glass. *Phys. Rev. Lett.*, 71(16):2595, 1993.

[20] G.Barbero and R.Barbieri. *J.Phys (Paris)*, 44:609, 1983.

[21] Ping Sheng. Phase transitions in surface aligned nematic films. *Phys. Rev. Lett.*, 37(16):1059, 1976.

[22] S.Stalling, M.M.Witterbrood, D.H.Luijendijk, and T.Rasing. Theory of light scattering by thin nematic liquid crystal films. *Phys. Rev. E*, 53:6085, 1996.

[23] A. Sarlah and S. Zumer. Equilibrium structures and pretransitional fluctuations in a very thin hybrid nematic film. *Phys. Rev. E*, 60:1821, 1999.

[24] G.Galabova, N.Kothekar, and D.W.Allender. Stable configurations in hybrid nematic cells in relation to thickness and surface order. *Liq. Cryst.*, 23:803, 1997.

[25] C. Chiccoli, P. Pasini, A. Sarlah, C. Zannoni, and S. Zumer. Structures and transitions in thin hybrid nematic films: A monte carlo study. *Phys Rev. E*, 67:0507031, 2003.

[26] P. Pasini, C. Chiccoli, and C. Zannoni. *Advances in the Computer Simulations of Liquid Crystals*. Kluwer, Dordrecht, 2000.

[27] P.A. Lebwohl and G. Lasher. Nematic-liquid-crystal ordera monte carlo calculation. *Phys. Rev. A*, 6:426, 1972.

[28] U. Fabbri and C. Zannoni. A monte carlo investigation of the lebwohl-lasher lattice model in the vicinity of its orientational phase transition. *Molec. Phys.*, 58:763, 1986.

[29] F. Biscarini, C. Chiccoli, P. Pasini, F. Semeria, and C. Zannoni. Phase diagram and orientational order in a biaxial lattice model. a monte carlo study. *Phys. Rev. Lett.*, 75:1803–1806, 1995.

[30] C. Chiccoli, I. Feruli, O.D. Lavrentovich, P. Pasini, S. Shyianovskii, and C. Zannoni. Topological defects in schlieren textures of biaxial and uniaxial nematics. *Phys. Rev. E (R)*, 66:030701, 2002.

[31] F. G. Wang and D. P. Landau. Efficient, multiple-range random walk algorithm to calculate the density of states. *Phys. Rev. Lett.*, 86:2050, 2001.

[32] D.Jayasri, V.S.S.Sastry, and K.P.N.Murthy. Wang-landau monte carlo simulation of isotropic-nematic transition in liquid crystals. *Phys. Rev. E*, 72:036702, 2005.

[33] Andreja $\check{S}arlah$. PhD thesis.

[34] C. Chiccoli, S. P. Gouripeddi, P. Pasini, K. P. N. Murthy, V. S. S. Sastry, and C. Zannoni. Hybrid nematic films: A detailed monte carlo investigation. *Mol. Cryst. Liq. Cryst.*, 500:118 – 131, 2009.

[35] M.Warenghem, J.F.Henninot, and G.Abbate. Non linear induced self waveguiding structure in dye doped nematic liquid crystal confined in capillaries. *Optics Express*, 2(12):483, 1998.

[36] H.W.Long, M.Luzar, H.C.Gaede, R.G.Larsen, J.Kritzenberger, A.Pines, and G.P.Crawford. Xenon nmr study of a nematic liquid crystal confined to cylindrical submicron. *J. Phys. Chem.*, 99:11989–11993, 1995.

[37] S.G.Cloutier, J.N.Eakin, R.S.Guico, M.E.Sousa, G.P.Crawford, and J.M.Xu. Molecular self-organization in cylindrical nanocavities. *Phys. Rev. E*, 73:051703, 2006.

[38] J.E.Erdmann, S.Zumer, and J.W.Doane. Configuration transition in a nematic liquid crystal confined to a small spherical cavity. *Phys. Rev. Lett.*, 64(16):1907, 1990.

[39] S.Kralj and S.Zumer. The stability diagram of a nematic liquid crystal confined to a cylindrical cavity. *Liquid crystal*, 15(4):521–527, 1993.

[40] R.M.Marroum, G.S.Iannacchione, D.Finotello, and M.A.Lee. Numerical study of cylindrically confined nematic liquid crystal. *Phys. Rev. E*, 51(4):R2743, 1995.

[41] S.V.Burylov. Equilibrium configuration of a nematic liquid crystal confined to a ctlindrical cavity. *Jr. of Expermental and Theoretical Physics*, 85(5):873, 1997.

[42] Z.Bradac, S.Kralj, and S.Zumer. Molecular dynamics study of nematic structures confined to a cylindrical cavity. *Phys. Rev. E*, 58(6):7447, 1998.

[43] B.Groh and S.Dietrich. Fluids of rodlike particles near curved surfaces. *Phys. Rev. E*, 59(4):4216, 1999.

[44] Yu Trukhina and T.Schilling. Computer simulation study of a liquid confined to a spherical cavity. *Phys. Rev. E*, 77:011701, 2008.

[45] D.R.M.Williams and A.Halperin. Nematic liquid crystal in a tube: A freedericksz transition. *Phys. Rev. E*, 48(4):R2366, 1993.

[46] V.Vijay Kumar. A monte carlo study of hybrid cylindrical thin films of liquid crystals. Master's thesis, School of Physics, University of Hyderabad, 2006.

[47] G. Sai Preeti, Vijay Kumar V, K. P. N. Murthy, and V. S. S. Sastry. Monte carlo study of radial and axial ordering in cylindrical films of liquid crystal. *Computational Material Science*, 44:180, 2008.

Chapter 4

Phase diagram of a biaxial liquid crystal: A Monte Carlo study

It seems that the Holy Grail of liquid-crystal science has at last been found. – G.R.Luckhurst [1]

4.1 Introduction

A biaxial nematic is a spatially homogenous liquid crystal with three distinct optical axes. This is to be contrasted to a simple nematic, which has a single preferred axis, around which the system is rotationally symmetric. The symmetric group of a biaxial nematic is D_{2h}, *i.e.* corresponding to a rectangular right parallelepiped, having three orthogonal C_2 axes and three orthogonal mirror planes. Biaxial nematic schematically can be visualized as a system comprising of platelets with $\vec{m}$ as the long axis, $\vec{e}$ and $\vec{e_\perp}$ as the minor axes.

Biaxiality was for the first time experimentally observed in lyotropic liquid crystals [2] [3]. Thermotropic biaxial liquid crystal was experimentally realized for the first time in nonlinear oxadiazole units [4]. A mixture of rods and discs showed a biaxial phase using experimental methods like polarized microscopy and conoscopy. However, efforts to observe a biaxial nematic (N_B) phase in two component melts of rod-like and disk-like liquid crystals have been unsuccessful [5] [6] [7]. There have been recent papers reporting the detection of biaxiality in tetrapodes using IR spectroscopy [8]. Experimental detection of biaxiality has always been rather difficult owing to the artifacts introduced in the detection itself [8], [9]. Using X-ray diffraction methods a biaxial nematic phase

was observed, which was in agreement with the calculation of the form factor of bent-core shaped molecules and the structure factor of the nematic phase [10].

Research in biaxial liquid crystal is of equal importance to both experimentalists as well to theoreticians. Computer simulations have made a great deal of mark in understanding biaxial liquid crystals. Based on two simple models of uniaxial liquid crystals, biaxial liquid crystal models have been developed. First, model based on the Gay – Berne potential which permits both translational and orientational degrees of freedom. A biaxial version of Gay-berne potential, originally used to model uniaxial anisotropic molecules was developed [11]. This biaxial model can be used to deal with molecules of different attractive and repulsive contributions along the three axes. This was further developed into a generalized potential describing interactions between two arbitrary, not necessarily identical, ellipsoidal particles [12]. Using these improvements, it is realized that a biaxial orthogonal smectic phase could also be observed in addition to the uniaxial and biaxial nematic phases [13]. When this model was extended to discotic particles, it was observed that a biaxial phase was seen when the well depth anisotropies have the same sign [14]. A molecular dynamics simulation was carried out to study the response of a bulk biaxial liquid crystal to an external field [15]. Application of this potential to investigate biaxial systems has been reviewed in detail recently [16].

Monte Carlo simulation using hard ellipsoids [17] was done to obtain the phase diagram of a system comprising of biaxial liquid crystal molecules [18]. Bent – core molecule were formed by joining two hard spherocylinders with chosen length – breadth ratio. Computer simulation and theoretical studies were carried out on these molecules [19]. Extending these spherocylinders by adding an ideal tail was studied using computer simulations. It was observed that a smectic A phase was formed with no presence of a biaxial nematic phase [20]. Some models that really influenced experimental studies were the modeling of bent-shaped molecules. Most known was the Monte Carlo simulation of a generic model to look for biaxiality in the bulk system [21]. Bent shaped molecules usually have core molecules in between due to which a biaxial phase can in principle be formed. Further

improvements of this model were effected by adding a bending potential to it. This helped to investigate the relationship between the flexibility of the bent-core molecule and inability to form a biaxial nematic phase [22].

Second model for studying the biaxial nematic liquid crystals is based on Lebwohl-Lasher model, which has only orientational degrees of freedom. A pair potential was developed using the complete set of Euler angles to describe the molecular orientations. This model uses the London-de Boer-Heller approximation for dispersive forces, and has a control parameter in the form of molecular biaxiality λ. Setting this parameter to 0.2, detailed computer simulation studies were done to investigate the order parameters [23]. Using mean field approximations, a pair-wise inter-molecular potential for an ensemble of particles with lower symmetry was developed. This model gave results very much in agreement with the experimental data [24]. With further developments, a pair-wise additive lattice model was proposed, and Monte Carlo simulations were done in order to compute the four order parameters (a brief introduction to these was previewed in chapter 1) [25]. This effort led to the determination of the phase diagram, with a triple point where a direct isotropic to biaxial nematic transition occurs. A more detailed study at this transition point showed that the $I - N_B$ transition is a second order transition [26]. For values of the biaxiality parameter lesser than $1/\sqrt{6}$, the molecules are mapped to prolate geometry, else oblate. Using this model a Monte Carlo study of defects [27], [28] was done with reference to the Schlieren textures gotten experimentally [29].

Monte Carlo simulation studies of an equal mixture of rod-like and disc-like liquid crystals [30] showed that at lower temperatures the system split into two phases of rod-like and disc-like uniaxial nematic, rather than forming a biaxial nematic [31]. The interaction between the rod – like and disc – like molecules was further changed in order to see if a biaxial order could be observed [32]. A computer experiment of hard spherocylinders to model a continuous mixture of rods and discs was attempted, demixing occurred in these system [33].

A real liquid crystal molecule is always inherently biaxial in its symmetry, even though

the appearance of macroscopic biaxiality comprising of such constituents is a rare phenomenon. Curiosity among the physicists rose as to why microscopic biaxiality does not get translated to macroscopic biaxial symmetry, almost as a rule. The formation of biaxial phases is mostly over taken by other mechanisms like crystal formation or layering. Based on the theoretical studies and computer simulations done, molecular modeling of a biaxial liquid crystal was attempted [24], [34] in order to possibly determine microscopic criteria for fanning a realistic biaxial liquid crystal. In this context, it was found useful to define a molecular biaxiality parameter in terms of the length, breadth and width of the liquid crystal molecule. It is noted that unambiguous acceptance of an experimental finding of a biaxial phase could be a challenging question to be resolved [35]. A number of applications have already been envisaged for the biaxial nematic phase. For example, it is to be expected that rotation of the minor directors might be relatively rapid and possibly faster than the primary director $\hat{n}$. Technological applications of biaxial particles are a very challenging.

There has to be considerable amount of opposition in finding an experimental method to detect biaxiality in a liquid crystals system. Deuterium NMR has been known to be one of the most powerful methods to detect orientational order, particularly biaxiality, in a liquid crystal system [9]. The biaxial nematic phase was recently observed in different thermotropic liquid crystals, namely bent-core compounds, side-chain polymers, bent-core dimers, and organosiloxane tetrapodes [36]. A nuclear magnetic resonance NMR spectra are collected for a nematic organosiloxane tetrapode. The sample was continuously rotated around an axis perpendicular to the magnetic field. In conjunction with the analysis of a deuterium NMR experiment on the same system reported earlier has been discussed. The three principle components of any tensorial property are different for a biaxial nematic phase, refractive index being such a representative property, which can be measured readily. Using conoscopy, isogyres for a uniaxial phase are two dark lines forming a cross; however, if the phase is biaxial the isogyres open and so do not cross in the center of the image. A definitive identification of the nematic phase as biaxial could not be confirmed since for thin films the surface can induce an optical biaxiality in the sample even if the bulk

phase is uniaxial is a problem. An alternative method, free from the influence of surface forces on the director orientation, needed to establish the symmetry of the nematic phase could be deuterium NMR spectroscopy. In the isotropic phase, the NMR spectrum of a sample containing a set of equivalent deuterons contains a single line. However, on entering the liquid crystal phase, it splits into a doublet because of the quadrapolar interaction of the deuteron under the presence of a long range orientation order. The magnitude of the splitting depends both on the (second rank) orientational order parameters of the medium and the orientation of the director with respect to the external magnetic field. If the nematic phase is biaxial the ratio of the splitting when the magnetic field is along n to that when it is parallel to l or m deviates from the ratio expected of a uniaxial medium, *viz.* $2:1$. Therefore, it would be necessary to prepare a monodomain sample of the nematic and then change its orientation with respect to the magnetic field to establish the phase symmetry. In practice this can be difficult because one of the directors will always be aligned with the magnetic field of the spectrometer and so a competing electric field would be necessary to change its orientation. Possible detection of biaxiality through NMR measurements continues to be a challenging experimental problem

A simple treatment to deal with an ensemble of biaxial particles using mean field methods was proposed [34] and is based on generalized Maier – Saupe theory for asymmetric molecules [37]. Four order parameters were found to be necessary to define the biaxial phase of liquid crystals. It was seen that there existed another second order transition, other than the uniaxial nematic to isotropic $(N_U - I)$ transition, at a much lower temperature from uniaxial nematic N_U to a biaxial nematic N_B [38].

Using the models of Straley [34], a simple pair-wise interactive model was proposed,

wherein every anisotropic molecule is considered to have uniaxial (q) and biaxial (b) components. Thus, anisotropic part of every molecular biaxial tensor has two traceless, orthogonal components, defined as

$$\begin{aligned} q :=& m \otimes m - \frac{1}{3} I \\ b :=& e \otimes e - e_{\perp} \otimes e_{\perp}. \end{aligned} \tag{4.1.1}$$

Here, m is the long axis of the molecule, and e and $e_{\perp}$ represent the other two axes. The q tensor is uniaxial around m and the other is biaxial. Considering two molecules, the interaction Hamiltonian between them is given as

$$V = -U_o\{q.q' + \gamma(q.b' + q'.b) + \lambda(b.b')\} \tag{4.1.2}$$

The incremental energy δV, relative to the state of alignment of two molecules, when constrained to be positive definite restricts (γ, λ) space to a fan-shaped plot (figure 4.1). On further restrictions applicable to *calamitic* molecules, with the long molecular axis $\overrightarrow{m}$ harder to orient than the other two axes $\overrightarrow{e}$ and $\overrightarrow{e_{\perp}}$, only a part of the fan-shaped plot (the shaded triangle region in figure 4.1) is availbale for the parameter (γ, λ). Dispersion forces approximation [25] [26] further restrict the space to a parabolic trajectory corresponding to $\lambda = \gamma^2$, yeilding a suitable set of parameters in the above potential (equation 4.1.2). A phase diagram was proposed using mean field methods when the second term was neglected *i.e.* $\gamma = 0$ (figure 4.1). This plot showed the presence of a tri – critical and a triple point. A tri – critical point occurs at $\lambda_C = 0.20$, where the $N_B - N_U$ transition changes from second order to first order transition. A triple point is seen at $\lambda_T = 0.22$, where the three phases (isotropic (I), uniaxial nematic (N_U) and biaxial nematic (N_B)) coexist. A more elaborate phase diagram was proposed by extending the variation of the parameter λ up to 1, keeping however, $\gamma = 0$ [40]. By defining a criterion for a tri – critical point for a biaxial particles, another tri-critical point was shown to exist when the $I - N_B$ transition changes from first order to second order for a higher value of λ (figure 4.2). The existence of the second tri – critical $(I - N_B$ point was also predicted using bifurcation analysis

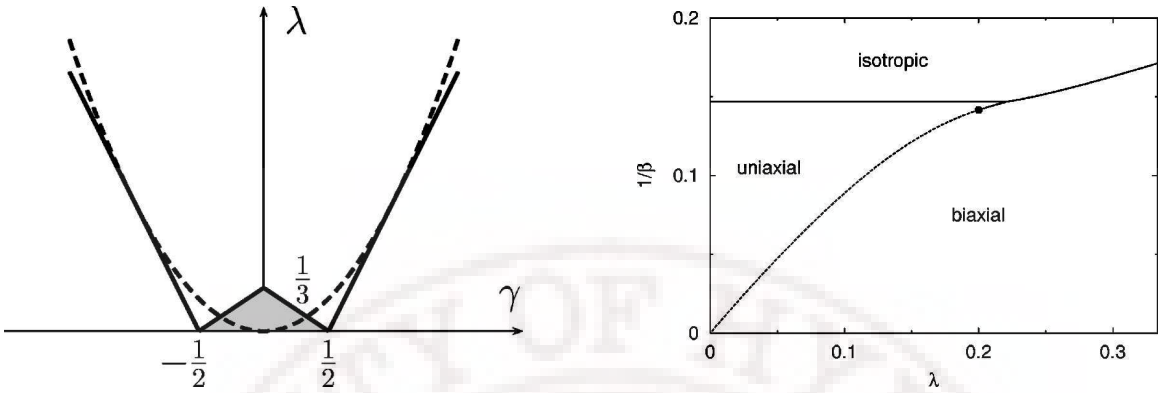

Figure 4.1: Admissible values for the dimensionless parameter γ and λ in equation 4.1.2. The phase diagram with change in λ with $\gamma = 0$ (Ref [39] figure 2, figure 4)

) [41]. Monte Carlo simulations confirmed the appearance of these different phases, with changes in λ. These developments were further generalized to find a thermodynamically exact criterion that governing a biaxial phase [42]. It was shown that the complete phase diagram proposed is universal. A identical phase diagram was proposed using quadrupolar approximations [43]. A parameter $\rho = T_{N_B - N_U}/T_{(N_U - I)}$, is defined as ratio of transition temperature $N_B - N_U$ to $I - N_U$ [44]. It was found that ρ was almost independent of the parameter γ, and interpreted as a quantitative indication that the term λ is the dominant biaxial interaction (equation 4.1.2). Hence a tri-critical line could be drawn in figure 4.3 (the thick black line intersecting at C). This parameter is not defined beyond $\lambda = 0.22$, as a uniaxial nematic phase does not exist and a direct $I - N_B$ transition occurs. Hence a triple point line can be defined in the triangle that intersects at C (figure 4.3). Moving in the triangle along either γ or λ axis gave a understanding to the occurrence of tri – critical and triple point. Bifurcation analysis was done to obtain a profile of free energy using the equilibrium free energy for λ=0.174 and γ=0.193. Its seen that a definite first order transition occurred from isotropic to uniaxial nematic region. The order of uniaxial nematic to biaxial nematic did depend on the values of the parameters (λ,γ).

This present work attempts to study the biaxial lattice Hamiltonian by generating the phase diagram in the (γ, λ) space and tries to look for a criteria that stabilizes or otherwise, a biaxial phase. In our attempt to do this we have used a pair-wise interaction potential

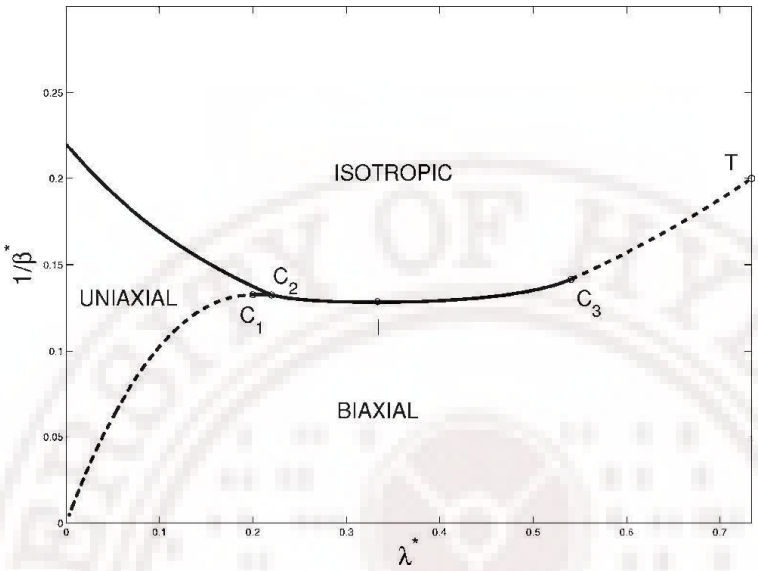

Figure 4.2: The phase diagram proposed with the parameter $\gamma = 0$ and varying λ (reference [43] figure 6)

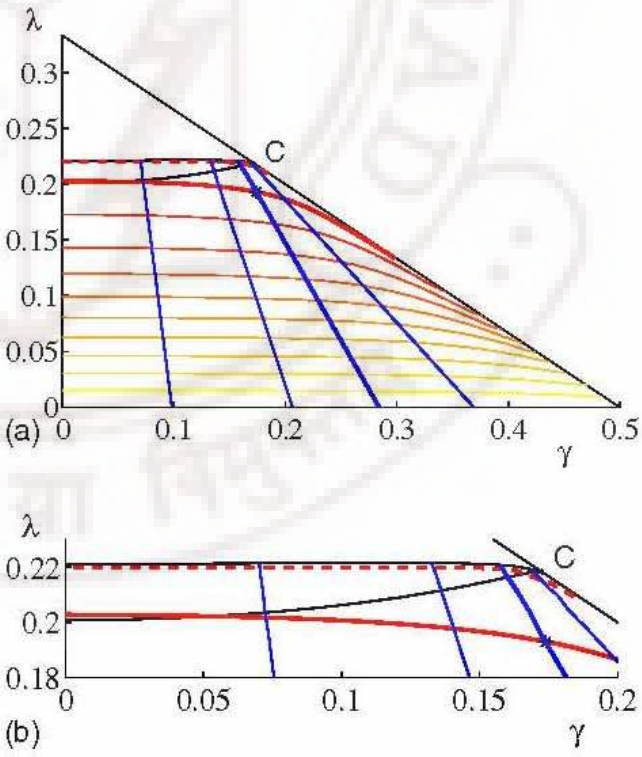

Figure 4.3: Contour map of the ratio ρ:= $T_{N_B - N_U}/T_(N_U - I)$ between the biaxial-uniaxial temperature and isotropic-uniaxial temperature as a function of the parameters (γ,λ) restricted to the triangle.(reference [44] figure 3(a))

(equation 4.1.2).

4.2 Model Used and Computational details.

From this simple model 4.1.2 a Hamiltonian was derived where the orientations of the spins determine the interaction energy between two particles [39]. Consider classical, identical particles, possessing D_{2h} symmetry, whose centers of mass are associated with a three-dimensional (simple-cubic) lattice N^3; let $x_\mu \in N^3$ denote the coordinate vectors of their centers of mass. The interaction potential will be isotropic in orientation space, and restricted to nearest neighbors, involving particles or sites labeled by μ and ν, respectively. The orientation of each particle can be specified via an orthonormal triplet of 3-component vectors (e.g. eigenvectors of its inertia tensor), say $\{w_{\mu,j}, j = 1, 2, 3\}$; in turn these are defined by an ordered triplet of Euler angles $\omega_\mu = \{\phi_\mu, \theta_\mu, \psi_\mu\}$; particle orientations are defined with respect to a common, but otherwise arbitrary, Cartesian frame. The two molecules can be represented as u_j for $w_{\mu,j}$ and v_k for $w_{\mu,k}$. Here, for a given j, u_j and v_j have the same functional dependence on ω_μ and ω_ν, respectively. Let $\tilde{\Omega}$= $\Omega_{\mu\nu}$ denote the set of Euler angles defining the rotation transforming u_i to v_j. Then we define,

$$f_{jk} = (u_j.v_k), \qquad G_{jk} = P_2(f_{jk}) \tag{4.2.1}$$

where P_2 denotes the second Legendre polynomial. The continuous interaction potential used for this study is defined by appropriate linear combinations of terms G_{jk} , which can be cast in the form,

$$U = -\epsilon\{G_{33} - \Gamma[G_{11} - G_{22}] + \Lambda[2(G_{11} + G_{22}) - G_{33}]\}. \tag{4.2.2}$$

Here ϵ denotes a positive constant setting the energy scales. The reduced temperature in turn is defined in terms of this energy scale as $T^* = k_B T/\epsilon$. $|\Gamma|$ and $|\Lambda|$ are often taken lesser than one. The parameters Γ and Λ in the equation 4.2.2 have a one – to – one mapping to the parameters γ and λ in the equation 4.1.2. Setting these two terms to zero of course corresponds to reducing the above potential to Lebwohl-Laser model. It was shown that a

biaxial phase does not appear when a simulation is done keeping the third term as zero, *i.e.* $\Lambda = 0$ [23]. An approximation proposed on equation 4.2.2 , is the London-de Born-Heller approximation where, $\Lambda = \Gamma^2$.

Monte Carlo simulations using this model (equation 4.2.2) were carried out earlier in detail setting the parameter $\Gamma = 0$. Based on the mean field considerations it is argued that a second order uniaxial to biaxial transition occurs for $0 < \Lambda \lesssim 0.22$, a first order transition for $0.20 < \Lambda \lesssim 0.22$, and finally a direct transition from isotropic to biaxial nematic phase for $\Lambda > 0.22$ [39]. It was seen that for simulations within $\Lambda = 0.24$ did not show a direct transition from N_B to isotropic, but there was a uniaxial nematic present for a small range of temperature [45]. A direct transition from $I - N_B$ did occur at $\Lambda = 0.30$. This simulation showed that there is one point of Λ where two transitions collapsed into one in the region $0.24 \leq \Lambda \leq 0.30$ for $\Gamma = 0$.

In the light of these earlier prediction and simulations, we take up in this study a detailed simulation of the above model spanning the parameter space (Γ, Λ), but without restricting the Hamiltonian to dispersive force approximation. In this context, we consider a $20 \times 20 \times 20$ cubic lattice of biaxial molecules interacting through a pair-wise, restricted to a nearest neighbors, through the potential (equation 4.2.2) as mention above. Every lattice points is considered as biaxial molecule defined by a set of orientation vectors (us or vs). These do not have the translational degrees of freedom. Each distinct system is characterized by the specifications of the values of Γ and Λ. Metropolis algorithm with Boltzmann sampling is used to equilibrate this system, typically requiring 250,000 Monte Carlo lattice starting from an arbitrary initial condition of the orientation of different molecules. Equilibrium ensembles were collected over 250,000 microstates at every temperature. The temperature is varied from 4.0 to 0.05 in steps of 0.0395. The equilibrium ensemble is used to compute average of different relevant quantities, such as $R^2_{00}, R^2_{02}, R^2_{20}$ [46] [47] [17], average energy and the specific heat (Details on the computation of these parameters is discussed in Chapter 2).

Γ/Λ		a 0.0	b 0.1	c 0.2	d 0.3	e 0.4	f 0.5	g 0.6	h 0.7	i 0.8	j 0.9	k 1.0
1	0.0	1a	1b	1c	1d	1e	1f	1g	1h	1i	1j	1k
2	0.1	2a	2b	2c	2d	2e	2f	2g	2h	2i	2j	2k
3	0.2	3a	3b	3c	3d	3e	3f	3g	3h	3i	3j	3k
4	0.3	4a	4b	4c	4d	4e	4f	4g	4h	4i	4j	4k
5	0.4	5a	5b	5c	5d	5e	5f	5g	5h	5i	5j	5k
6	0.5	6a	6b	6c	6d	6e	6f	6g	6h	6i	6j	6k
7	0.6	7a	7b	7c	7d	7e	7f	7g	7h	7i	7j	7k
8	0.7	8a	8b	8c	18	8e	8f	8g	8h	8i	8j	8k
9	0.8	9a	9b	9c	9d	9e	9f	9g	9h	9i	9j	9k
10	0.9	10a	10b	10c	10d	10e	10f	10g	10h	10i	10j	10k
11	1.0	11a	11b	11c	11d	11e	11f	11g	11h	11i	11j	11k

Table 4.1: The values of all the Γ and Λ values used in equation 4.2.2. (4f system - system with Γ=0.3 Λ=0.5, second column refers to Γ values, columns a to k gives the Λ values)

4.3 Results and Discussion

The effect of the two parameters (Γ and Λ) was studied by choosing systematically different values of them, and simulating the resulting systems . For the various systems in the table 4.1, the relevant physical parameters were computed as a function of temperature. The parameter Γ was varied from 0 to 1 in steps of 0.1. For every Γ, Λ was changed from 0 to 1 in steps of 0.1; a variation with a resolution of 0.01 was effective if necessary for a a more detailed study. Table 4.1 gives the details of the variation of the two parameters along with the nomenclature followed to refer to a specific system of study.

4.3.1 Simulation details for $\Gamma = 0.0$

From the Table 4.1 for the value of $\Gamma = 0.0$, it is seen that Λ is changed from 0.0 to 1.00. For $\Lambda = 0.0$ this system is just the LL model as in the Hamiltonian 4.2.2, the terms with the biaxial interactions being set to zero. Increasing the value of Λ to 0.1, it is seen that there are two transitions occurring: first transition from uniaxial nematic (N_U) to a biaxial nematic phase (N_B) occurring at $T_{C1} = 0.6$, a second transition from a disordered phase to a uniaxial nematic phase N_U at $T_{C2} = 1.1165$. Figure 4.4 gives the details of the various parameters obtained for this set of parameters $\Gamma = 0.0$ and $\Lambda = 0.1$ (Set 1b in Table 4.1). The biaxiality parameter R^2_{22} for this set of parameter $\Gamma = 0.00$ and $\Lambda = 0.1$ has a maximum value of 0.65 at the low temperature indicating the least temperature phase is a biaxial nematic phase (N_B). For $\Lambda = 0.2$ it is seen that $T_{C1} = 1.119$ and $T_{C2} = 1.195$, the uniaxial nematic phase is still present though for a small range of temperature. For values of Λ beyond 0.26, it is seen that there exits only one transition, a $I - N_B$. It is observed in figure 4.5, that there is just one peak in the specific heat, and both R^2_{00} and R^2_{22} become non – zero at this transition temperature. Plotting all the specific heat profiles corresponding to different Λ values for $\Gamma = 0.0$, it is seen that for lower values of Λ there are two transitions and for higher values of Λ there is only one transition (figure 4.6). In the figure 4.7, plotting the transition temperatures T_C values (obtained from the location of

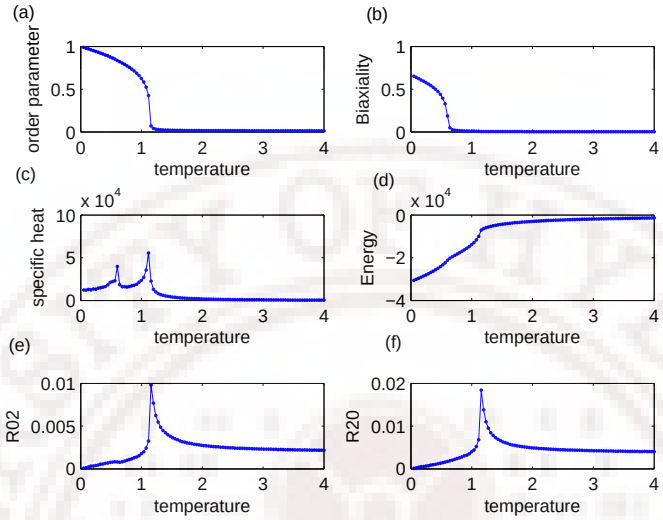

Figure 4.4: Variation of (a) order parameter, (b) biaxiality parameter, (c) specific heat (C_V), (d)Energy, (e)R^2_{02}, (f)R^2_{20} with temperature for a system with the parameter $\Gamma = 0.0$ and $\Lambda = 0.1$

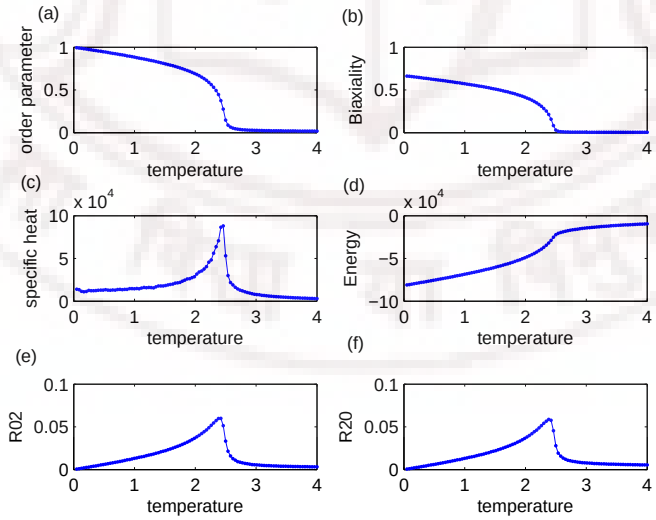

Figure 4.5: Variation of (a) order parameter, (b) biaxiality parameter, (c) specific heat (C_V), (d)Energy, (e)R^2_{02}, (f)R^2_{20} with temperature for a system with the parameter $\Gamma = 0.0$ and $\Lambda = 0.8$

C_V peaks) against Λ, a phase diagram at $\Gamma = 0.0$ is obtained. With the initial increase in Λ, there are two transitions present, first from a uniaxial nematic phase to a biaxial nematic phase, and the second from uniaxial nematic phase to the isotropic phase.

As the value of Λ is increased, the specific heat peaks comes closer and collapses into a single peak at $\Lambda = 0.26$. When Λ was increased beyond 0.26, a direct transition occurs from biaxial nematic (N_B) to isotropic phase (I). The phase diagram simulated here for $\Gamma = 0.00$, is in agreement to that obtained through mean filed consideration [43]. A direct $I - N_B$ transition occurred after Λ was increased beyond 0.26, in agreement with reference [45]. It may be noted that in the earlier Monte Carlo simulations [45] also two transitions occurred at $\Lambda = 0.24$, which is beyond the value predicted by mean filed studies. Our present results are in agreement with these simulation results.

4.3.2 Simulation details for $\Gamma = 0.1$

Increasing Γ to 0.1 indicates that the interaction between the uniaxial and biaxial terms in the Hamiltonian (Equation 4.2.2) increases. For lower values of Λ it is seen that there are two transitions occurring, at the first the order parameter R^2_{00} becomes non zero, and at the second R^2_{22} also becomes non – zero value. Figure 4.9 gives the different order parameters that were computed for the systems with $\Gamma = 0.1$ with various values of Λ (Table 4.1: systems 2a to 2k). It is seen that for lower values of Λ there exists two transitions: first T_{C1} from biaxial nematic N_B to a uniaxial nematic N_U. The higher transition temperature T_{C2} corresponds to the transition from uniaxial nematic to a isotropic phase (figure 4.10). Plotting the specific heat against temperature for different values of Λ, it is observed that in this case the range of Λ values over which a direct transition from isotropic to biaxial phase reduces considerably (figure 4.11). With the increase in Λ till 0.25, two transitions are observed. The two transitions collapsed to a single transition after $\Lambda = 0.25$, indicating a direct transition occurring from a isotropic phase to a biaxial nematic phase. Unlike $\Gamma = 0.0$, it is seen that there are again two transitions possible beyond $\Lambda = 0.5$, first from the isotropic to uniaxial nematic and then from uniaxial nematic to a biaxial nematic phase.

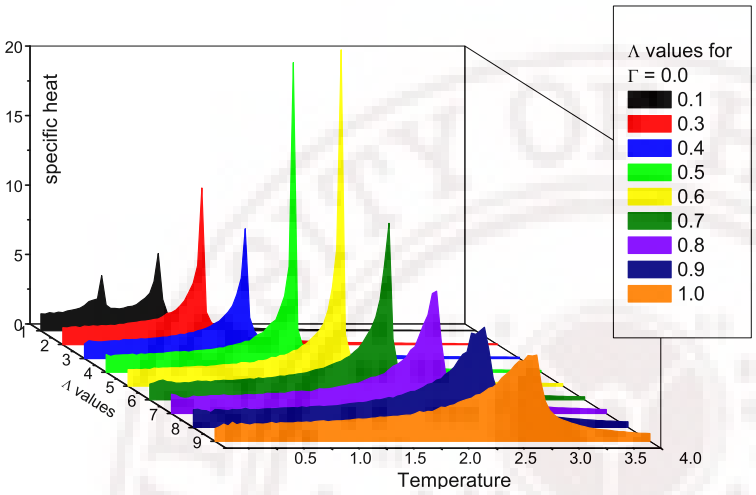

Figure 4.6: The specific heat with temperature at different Λ values.

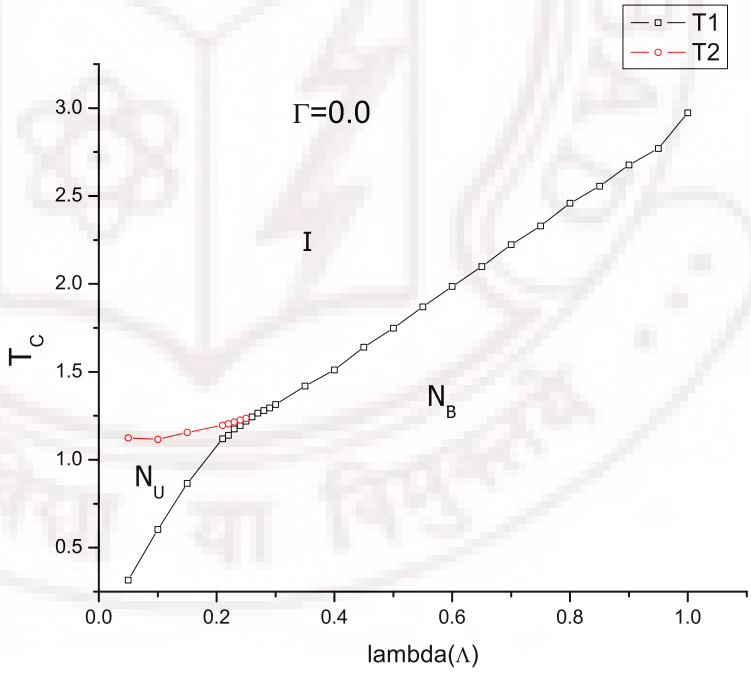

Figure 4.7: The phase diagram for Γ=0.00, taking the transition temperature from the peak position(s) of the specific heat data for every system by changing the Λ value ($T1$ – transition temperature from state N_U to N_B and $T2$ – transition temperature from N_U to isotropic phase).

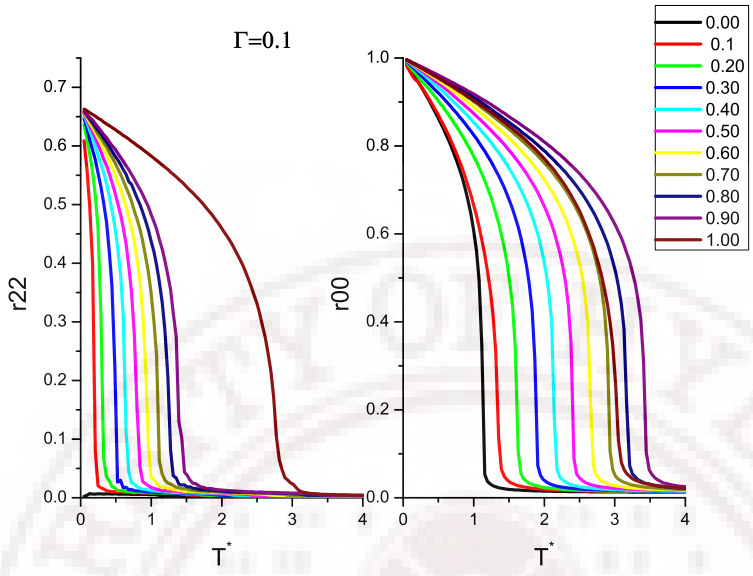

Figure 4.8: R^2_{00} and R^2_{22} with variation in temperature for different values of Λ keeping $\Gamma = 0.1$

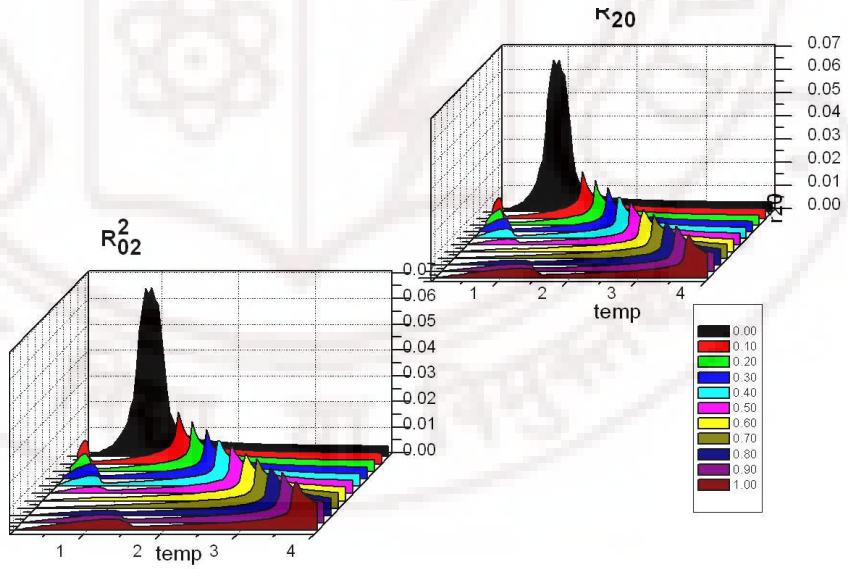

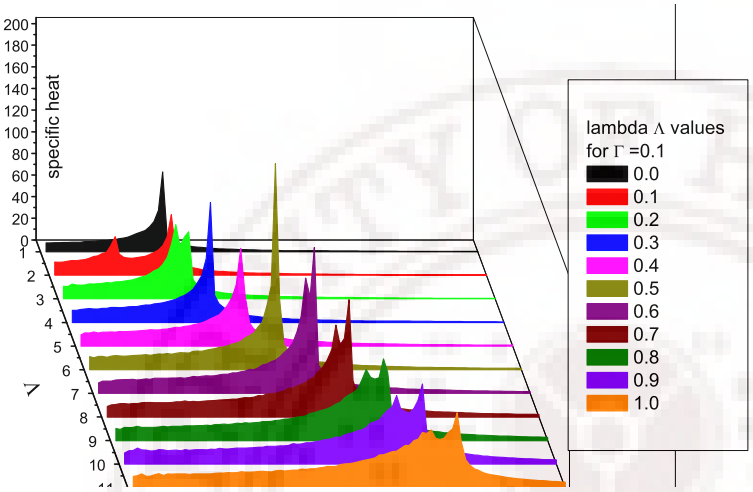

Figure 4.10: The specific heat with temperature at different Λ values.

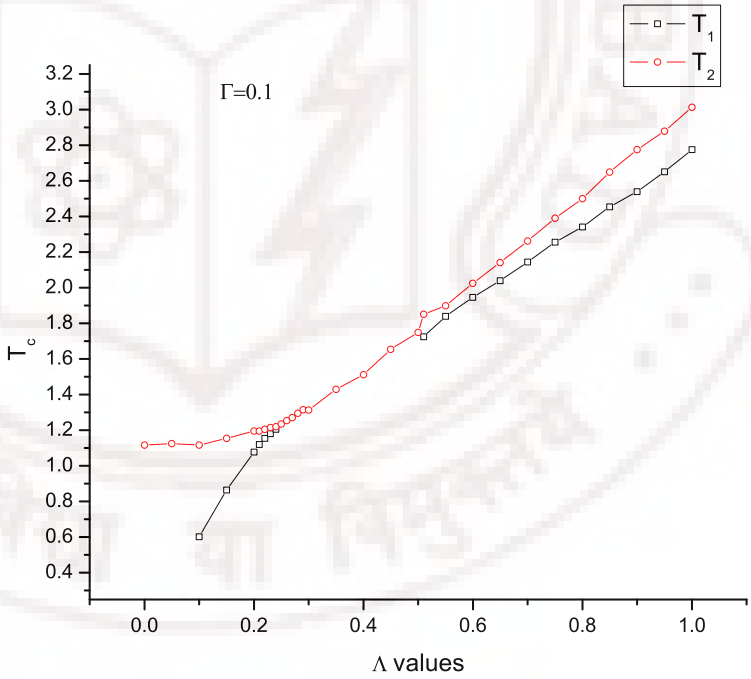

Figure 4.11: The phase diagram for Γ=0.10, taking the transition temperature from the peak position(s) of the specific heat data for every system by changing the Λ value ($T1$ – transition temperature from state N_U to N_B and $T2$ – transition temperature from N_U to isotropic phase).

4.3.3 Simulation details for $\Gamma = 0.2$

This section deals about the 11 systems studied by keeping the parameter $\Gamma = 0.2$ corresponding to the systems 3a to 3k in the Table 4.1. Keeping $\Gamma = 0.2$, Λ was changed from 0 to 1.00. The specific heat plots against temperature for the different values of Λ were plotted together to look for the different phases formed (figure 4.12). Considering the transition temperatures from the specific heat profiles a phase diagram was plotted for the different values of Λ (figure 4.13). It is observed that beyond $\Lambda = 0.2$ there is only one transition, – a direct isotropic – biaxial nematic transition. A more detailed study was done around this point to determine more accurately the value of Λ where the two transitions ($N_U - N_B$ and I – N_U) collapsed to one (I - N_B). Similarly for values of Λ beyond 0.5, similar study with a finer variation in the value of Λ was carried out to obtain an accurate estimate of Λ value where the single transition splits into two. Figures 4.14 and 4.15 give the different parameters computed for two systems with the parameters ($\Gamma = 0.2$ and $\Lambda = 0.22$) and ($\Gamma = 0.2$ and $\Lambda = 0.23$), respectively. It is clear from these plots how the phases of the system change qualitatively with the change in Λ for the specific value of Γ.

4.3.4 Simulation details for $\Gamma = 0.3$

Figure 4.16 gives the various physical parameters computed for the system with $\Gamma = 0.3$ and $\Lambda = 0.0$. It is seen that the biaxiality parameter is nearly negligible (~ 0) at the lowest temperature. There is only one transition occurring at $T_{C2} = 1.116$, and the order parameter R^2_{00} becomes non – zero at this T_{C2}. It is seen that Λ is a very important for the formation of a biaxial phase, this is in agreement to the perviously done Monte Carlo studies [48] and theoretical studies [44]. A non – zero value of Λ is necessary to observe a biaxial phase. By just increase the Λ value by 0.1, a very stable biaxial phase is observed for $\Gamma = 0.3$ (figure 4.17). A phase diagram for the parameter $\Gamma = 0.3$ is plotted by considering the transition temperatures from peak positions of the specific heat plots (figure 4.18). The transition temperatures are plotted against the Λ values for $\Gamma = 0.3$ (figure 4.19). It is evident from this plot there exist two triple points, where the three phases (I, N_U, N_B)

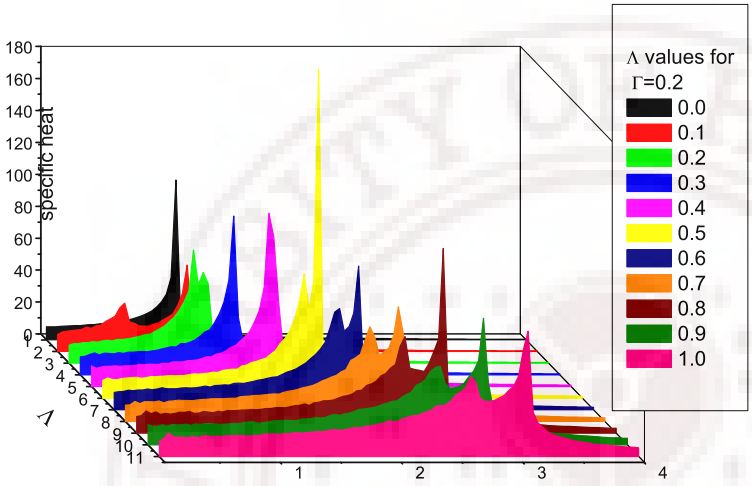

Figure 4.12: The specific heat with temperature for different Λ values.

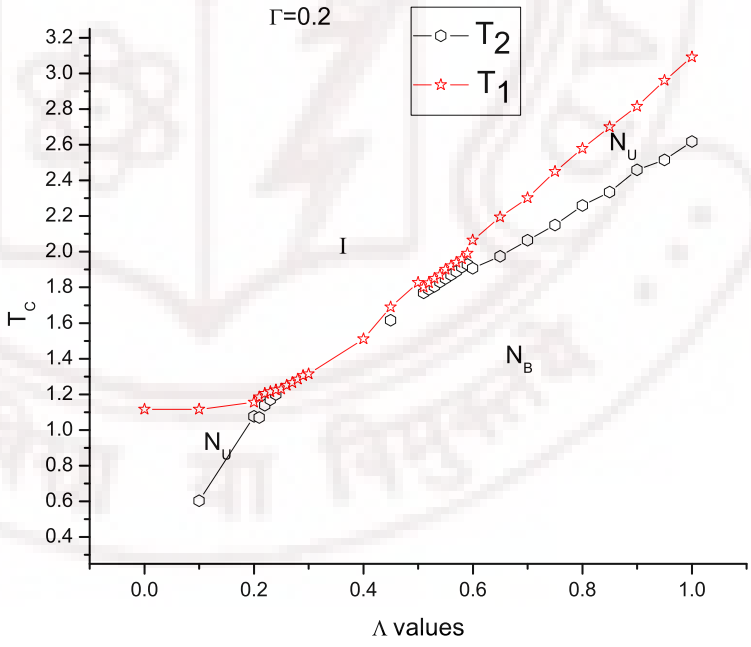

Figure 4.13: The phase diagram for Γ=0.2, considering the transition temperature from the specific heat for every system by changing the Λ value.

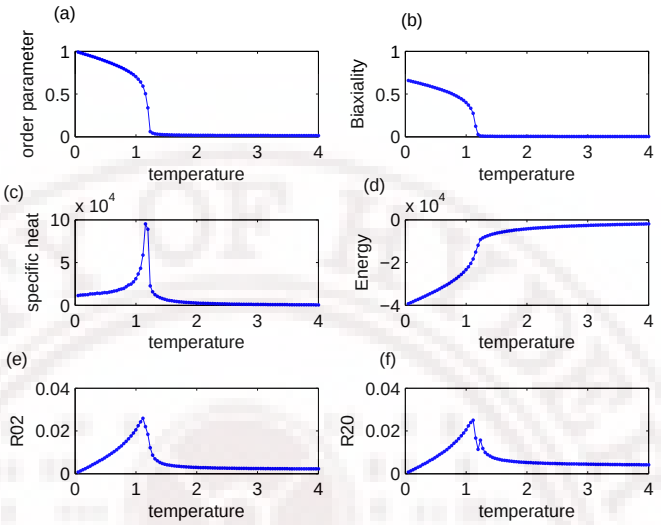

Figure 4.14: Variation of (a) order parameter, (b) biaxiality parameter, (c) specific heat (C_V), (d)Energy, (e)R^2_{02}, (f)R^2_{20} with temperature for a system with the parameter $\Gamma = 0.2$ and $\Lambda = 0.22$

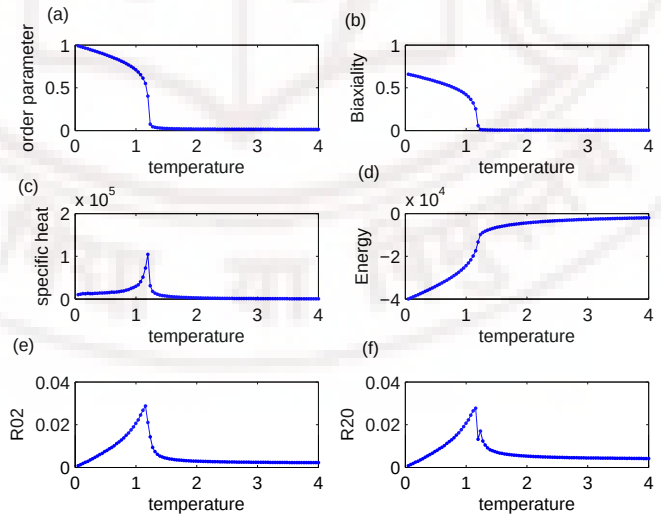

Figure 4.15: Variation of (a) order parameter, (b) biaxiality parameter, (c) specific heat (C_V), (d)Energy, (e)R^2_{02}, (f)R^2_{20} with temperature for a system with the parameter $\Gamma = 0.2$ and $\Lambda = 0.23$

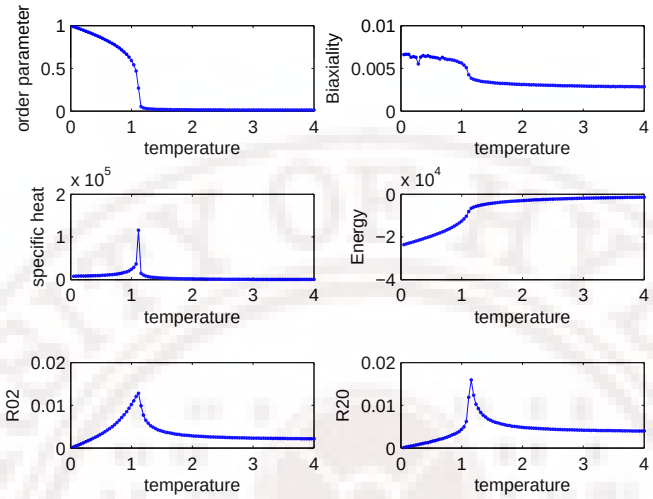

Figure 4.16: Variation of (a) order parameter, (b) biaxiality parameter, (c) specific heat (C_V), (d)Energy, (e)R^2_{02}, (f)R^2_{20} with temperature for a system with the parameter $\Gamma = 0.3$ and $\Lambda = 0.00$

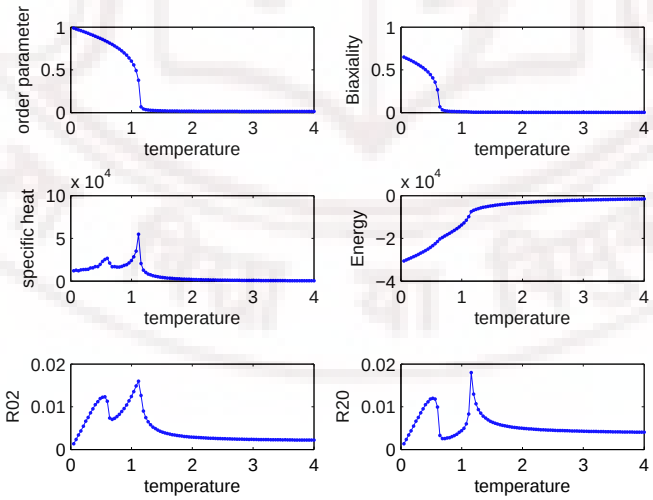

Figure 4.17: Variation of (a) order parameter, (b) biaxiality parameter, (c) specific heat (C_V), (d)Energy, (e)R^2_{02}, (f)R^2_{20} with temperature for a system with the parameter $\Gamma = 0.3$ and $\Lambda = 0.1$

.

coexist, first at $\Lambda_C = 0.25$ and the other at 0.3. In the intermediate range of Λ a direct I – N_B transition occurs, is evident from the specific heat profile. For a direct $I - N_B$ transition order parameters becoming non – zero at this transition temperature T_C.

4.3.5 Simulation details for $\Gamma = 0.4$

With the increase in Γ to 0.4, it is observed that the range of Λ values over which a direct transition occurs from a isotropic to biaxial nematic phase are decreases. Figure 4.20 gives the specific heat computed with a temperature variation for different values of Λ keeping $\Gamma = 0.4$. Initially for the lower values of Λ two transitions are visible, T_{C1} a $N_B - N_U$ transition and the second T_{C2} a $I - N_U$ transition. There are values around $\Lambda = 0.2$ where a direct transition occurs $I - N_B$. For $\Lambda = 0.2$, a direct transition is observed from isotropic phase I to a biaxial nematic phases N_B. This direct transition is confirmed by both the order parameters R^2_{00} and R^2_{22} becoming non – zero at the transition temperature $T_C = 1.156$ (figure 4.22). From these simulations there is a narrow range of Λ values (0.19 – 0.21)where a direct transition to N_B (for $\Gamma = 0.4$). It is observed that with the increase in Γ from 0.1 to 0.4 the two triple points come closer, shrinking gradually the range of Λ over which a direct N_B phase is possible starting with the isotropic phase. It may be noted that under dispersion approximation, a direct transition is possible only for a specific value of Λ ($1/\sqrt{6} \sim 0.416$) [25].

4.3.6 Simulation details for $\Gamma = 0.5$

Increasing Γ value to 0.5, two transitions were observed when the specific heat with temperature was plotted for different values of Λ (figure 4.23). The triple points observed for $\Gamma = 0.4$, do not appear any more on further increasing the Γ value beyond 0.4. The phase diagram for $\Gamma = 0.5$ was plotted by considering the transition temperatures from the specific heat profiles (figures 4.23, 4.24). Plotting order parameters R^2_{02} and R^2_{20} against temperature, the signatures for the two transitions is observed (figure 4.25). Figure 4.25 (a) and (b) give the order parameter R^2_{00} and biaxiality parameter R^2_{22} for the system with

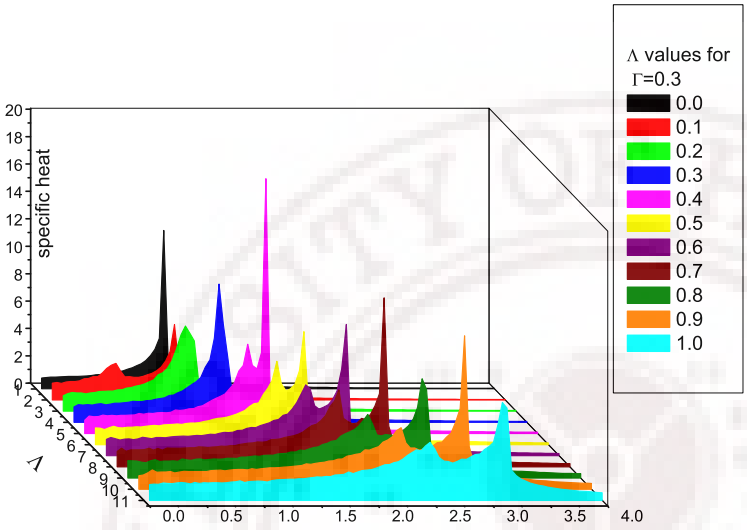

Figure 4.18: The specific heat with temperature at different Λ values.

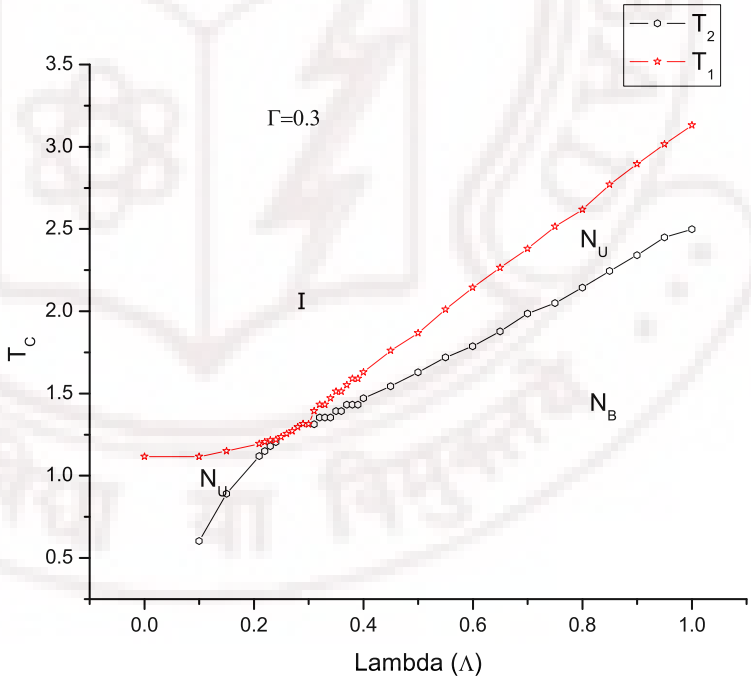

Figure 4.19: The phase diagram for Γ=0.3, taking the transition temperature from the peak position(s) of the specific heat data for every system by changing the Λ value ($T1$ – transition temperature from state N_U to N_B and $T2$ – transition temperature from N_U to isotropic phase).

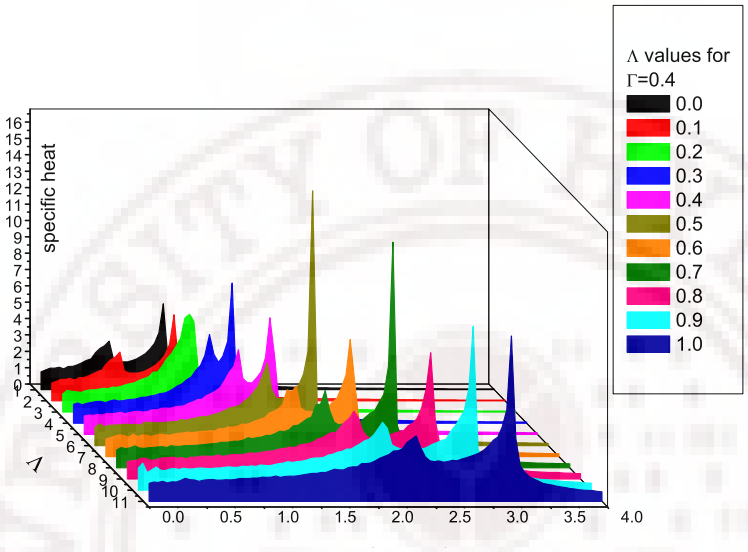

Figure 4.20: The specific heat with temperature at different Λ values.

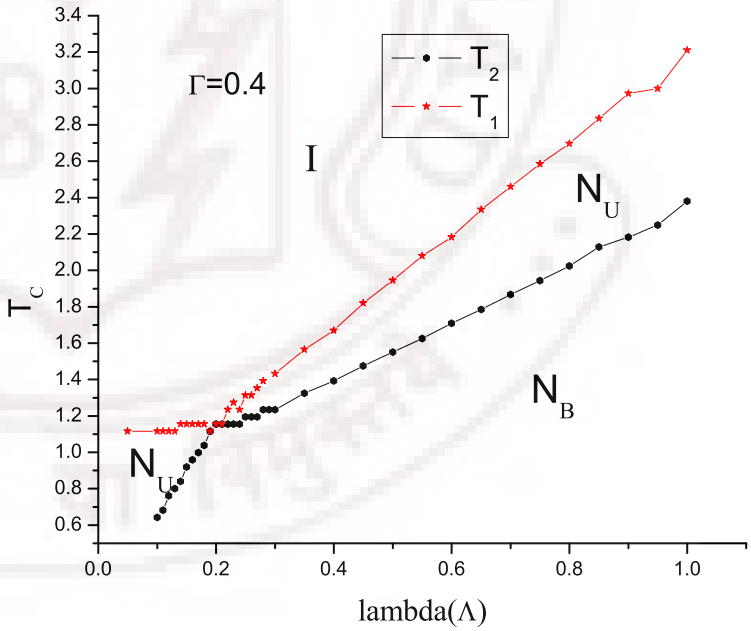

Figure 4.21: The phase diagram for Γ=0.4, taking the transition temperature from the peak position(s) of the specific heat data for every system by changing the Λ value ($T1$ – transition temperature from state N_U to N_B and $T2$ – transition temperature from N_U to isotropic phase).

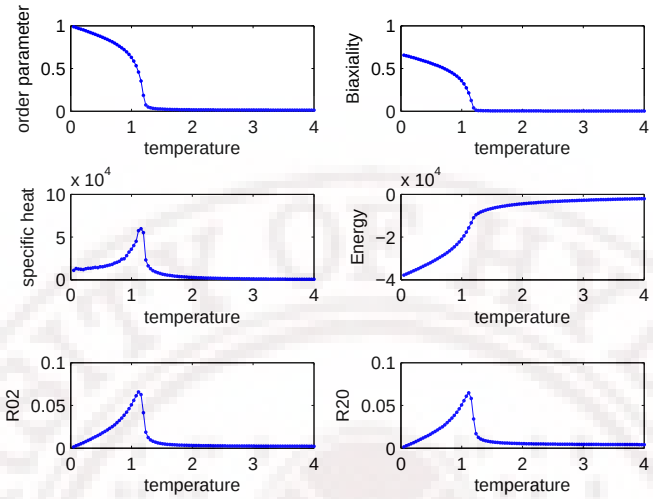

Figure 4.22: Variation of (a) order parameter, (b) biaxiality parameter, (c) specific heat (C_V), (d)Energy, (e)R^2_{02}, (f)R^2_{20} with temperature for a system with the parameter $\Gamma = 0.4$ and $\Lambda = 0.2$

.

parameters $\Gamma = 0.5$ and $\Lambda = 0..9$.

4.3.7 Simulation details for $\Gamma = 0.6$

For $\Gamma = 0.6$ similar to $\Gamma = 0.5$, it is observed that there is always a uniaxial nematic phase present for every Λ value. The lowest temperature phase can be reached through uniaxial nematic phase, i.e. the phase sequence is always $I \rightarrow N_U \rightarrow N_B$. It is seen that on increasing Γ the interaction between uniaxial part and biaxial part increases, leading to more stable biaxial phases. The phase diagram for $\Gamma = 0.6$ was plotted by considering the transition temperatures from the specific heat profiles (figures 4.26, 4.27). On increasing Λ, it is observed that the uniaxial phase becomes more stable too for a particular value of Γ. The order parameter R^2_{00} and the biaxiality parameter R^2_{22} become non – zero at a higher temperature with the increase in Λ (figure 4.28) i.e. the transition temperatures T_{C1} and T_{C2} increase with the increase in Λ value. The order contributed to along the Z direction due to the biaxiality at the molecular level R^2_{02} and the phase biaxiality parameter are also

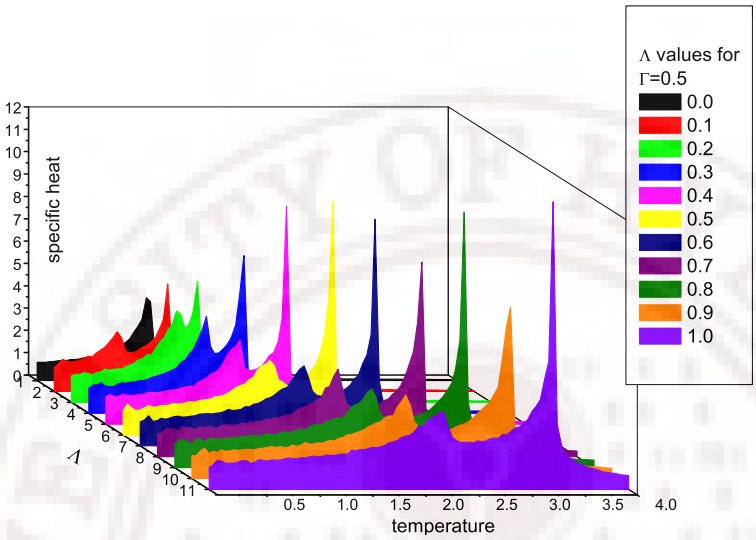

Figure 4.23: The specific heat with temperature at different Λ values.

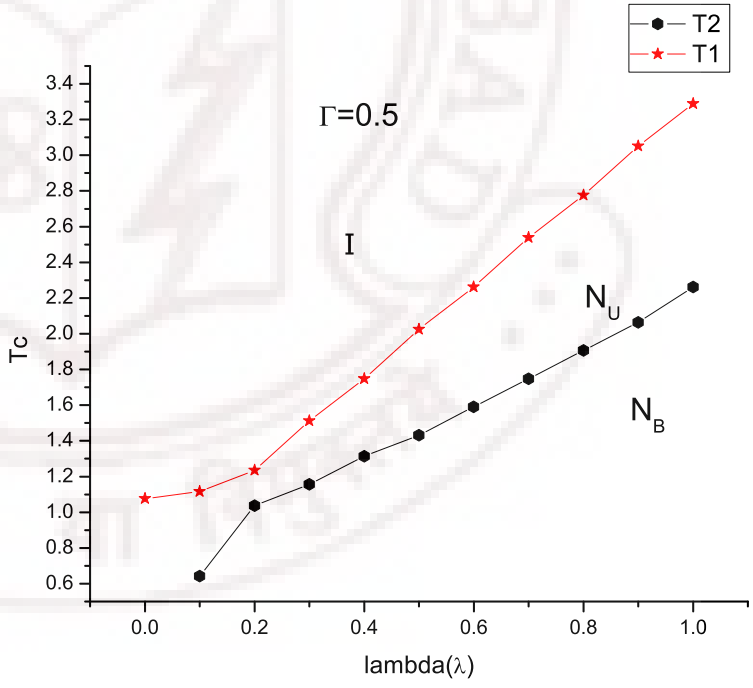

Figure 4.24: The phase diagram for Γ=0.5, taking the transition temperature from the peak position(s) of the specific heat data for every system by changing the Λ value ($T1$ – transition temperature from state N_U to N_B and $T2$ – transition temperature from N_U to isotropic phase).

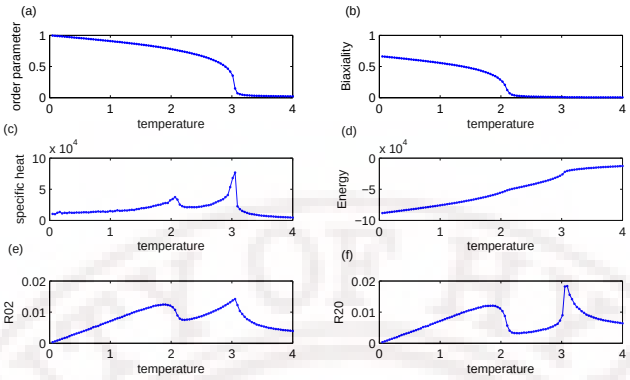

Figure 4.25: Variation of (a) order parameter, (b) biaxiality parameter, (c) specific heat (C_V), (d)Energy, (e)R^2_{02}, (f)R^2_{20} with temperature for a system with the parameter $\Gamma = 0.5$ and $\Lambda = 0.9$

plotted as a function of temperature for different values of Λ at $\Gamma = 0.6$.

4.3.8 Simulation details for $\Gamma = 0.7$

When the $\Lambda = 0.7$, it is seen that a biaxial phase is not observable (figure 4.30). The biaxiality parameter is negligible at the least temperature, there is only one transition observed at $T_C = 1.077$. These results are in agreement with the earlier Monte Carlo studies, and also predictions based on mean – filed considerations. These point out the dominant value of the term in the Hamiltonian in the formation of biaxial phase. This phenomenon is observed for all Γ with $\Lambda = 0.0$. The phase diagram showed that a very stable uniaxial nematic phase is present for all the values of Λ. It is seen that increasing the value of Γ from 0.5 to 0.7, a more stable uniaxial nematic phase forms. Figures 4.31 and 4.32 give the specific heat profiles with temperature for different values of Λ and the phase diagram obtained for $\Gamma = 0.7$, respectively.

4.3.9 Simulation details for $\Gamma = 0.8$

Considering the different values of Λ from the Table 4.1 for $\Gamma = 0.8$, a phase diagram was plotted by considering the transition temperatures from the specific heat profiles (figures 4.33, 4.34). The uniaxial nematic phase becomes stable with the increase in Λ. The

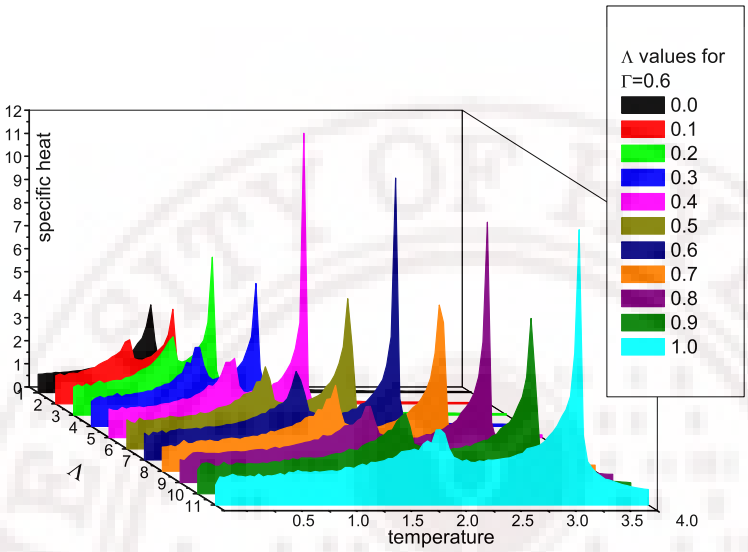

Figure 4.26: The specific heat with temperature at different Λ values.

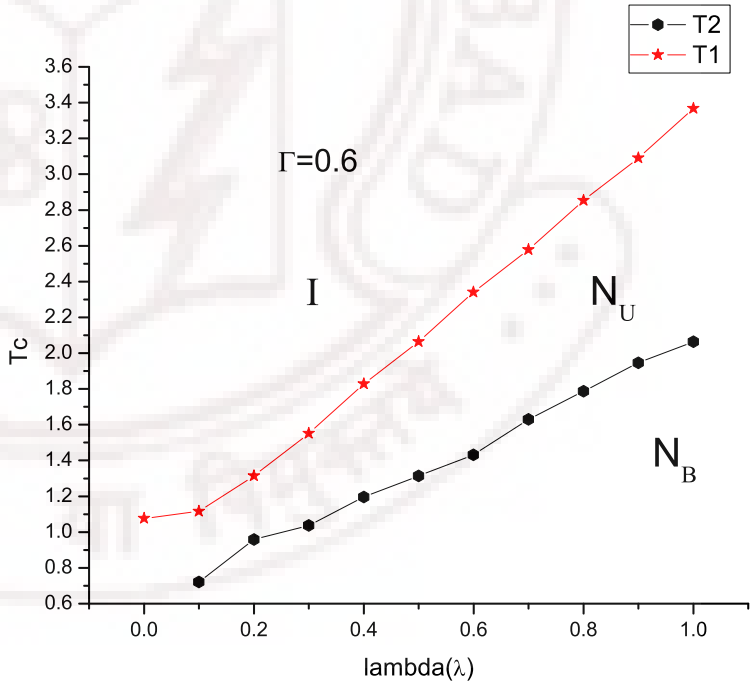

Figure 4.27: The phase diagram for Γ=0.6, taking the transition temperature from the peak position(s) of the specific heat data for every system by changing the Λ value ($T1$ – transition temperature from state N_U to N_B and $T2$ – transition temperature from N_U to isotropic phase).

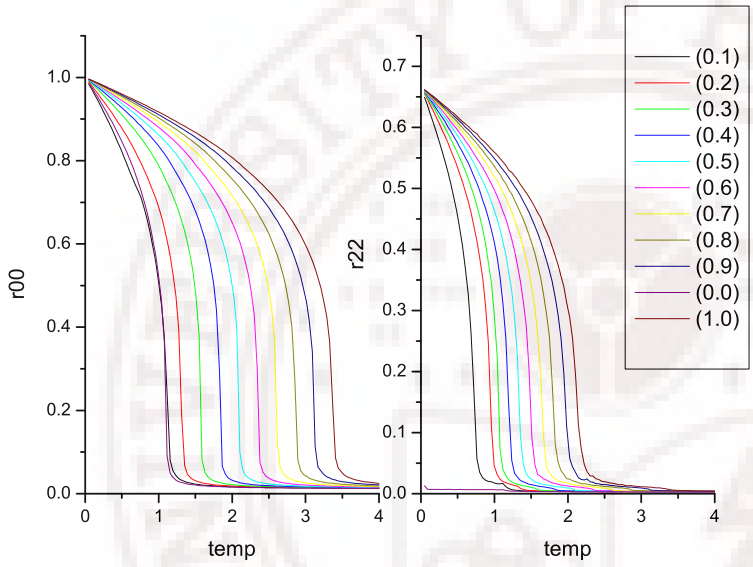

Figure 4.28: R^2_{00} and R^2_{22} with variation in temperature for different values of Λ keeping $\Gamma = 0.6$

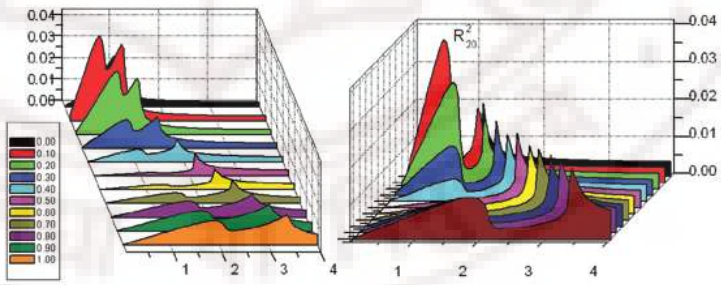

Figure 4.29: R^2_{20} and R^2_{20} with variation in temperature for different values of Λ keeping $\Gamma = 0.6$

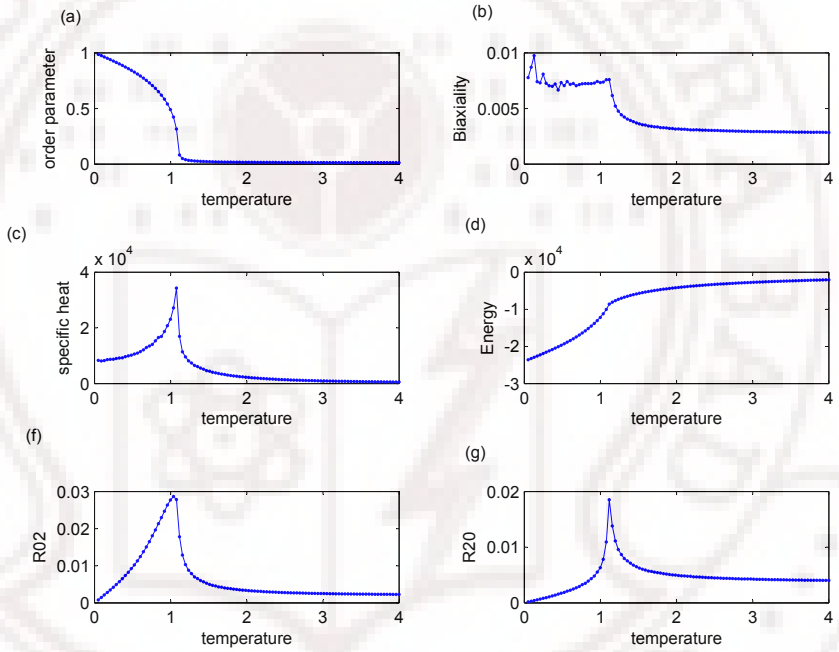

Figure 4.30: Variation of (a) order parameter, (b) biaxiality parameter, (c) specific heat (C_V), (d)Energy, (e)R^2_{02}, (f)R^2_{20} with temperature for a system with the parameter $\Gamma = 0.7$ and $\Lambda = 0.0$

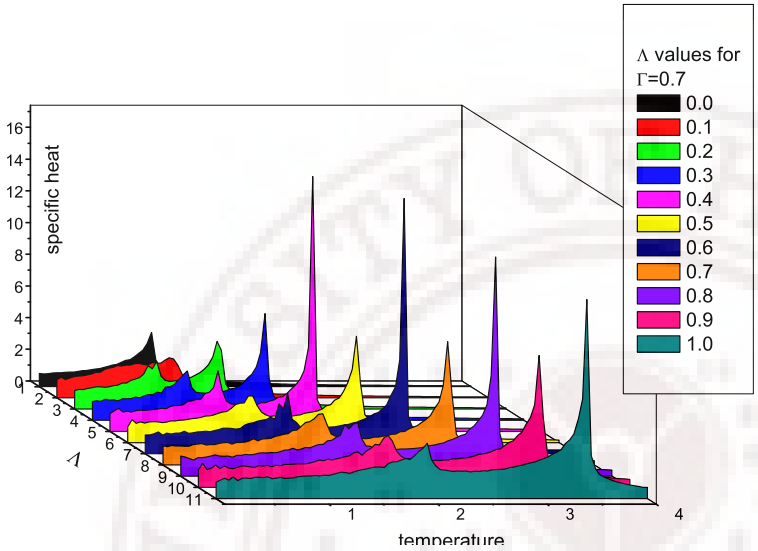

Figure 4.31: The specific heat with temperature at different Λ values.

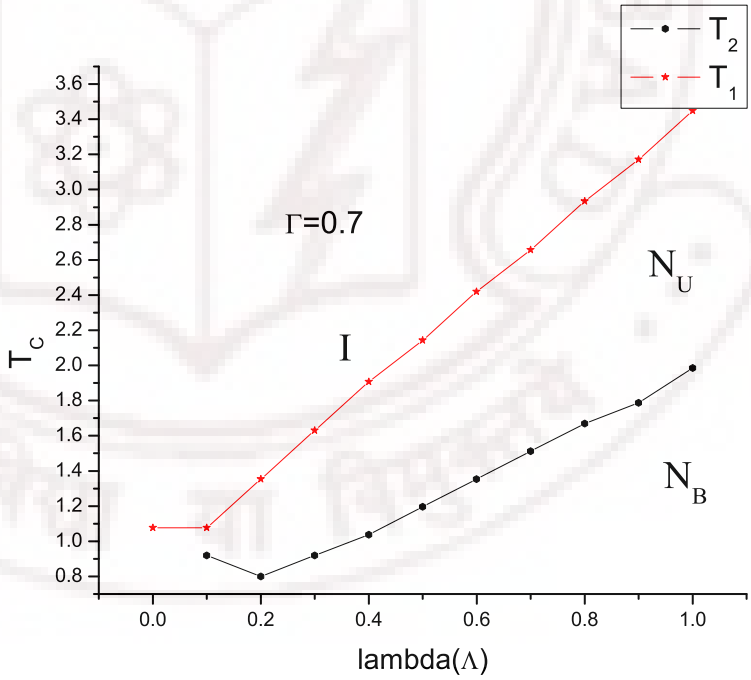

Figure 4.32: The phase diagram for Γ=0.7, taking the transition temperature from the peak position(s) of the specific heat data for every system by changing the Λ value ($T1$ – transition temperature from state N_U to N_B and $T2$ – transition temperature from N_U to isotropic phase).

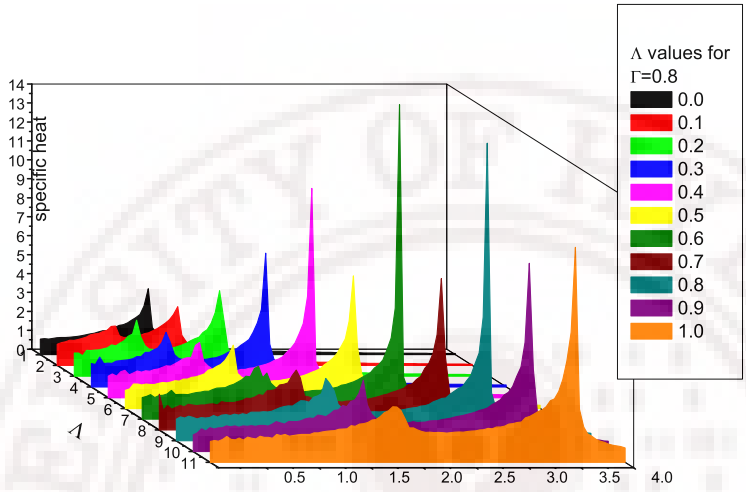

Figure 4.33: The specific heat with temperature at different Λ values.

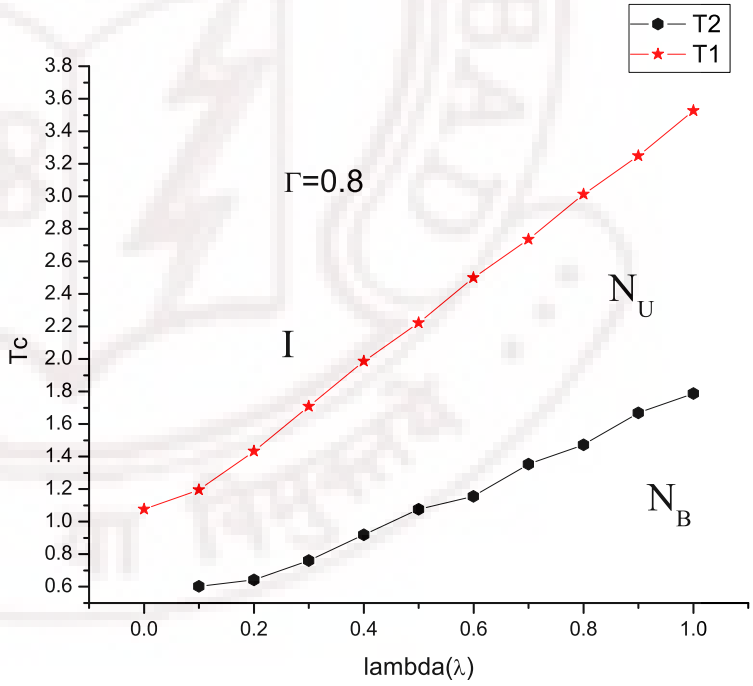

Figure 4.34: The phase diagram for Γ=0.8, taking the transition temperature from the peak position(s) of the specific heat data for every system by changing the Λ value ($T1$ – transition temperature from state N_U to N_B and $T2$ – transition temperature from N_U to isotropic phase).

$R^2_{00}, R^2_{02}, R^2_{20}$ and R^2_{22} are plotted against temperature for different values of Λ for $\Gamma = 0.8$ (figures 4.35, 4.36).

4.3.10 Simulation details for $\Gamma = 0.9$

For this particular value of $\Gamma = 0.9$, Λ values are varied from 0.0 to 1.00 in steps of 0.1 (systems 10a to 10k). For these different values of Λ specific heat was plotted against temperature. It is observed that there were always two transitions present. The first one occurs at a lower temperature T_{C1} - a transition from $N_U - N_B$. The second transition occurs at a higher temperature T_{C2} a transition from isotropic phase to a N_U phase. The lower transition in some cases is seen only as shoulder in the specific heat profile, but can be readily confirmed by the variation of the biaxiality parameter R^2_{22}. Figure 4.39 shows the plots of the different parameters obtained for the system 10g in the Table 4.1. Signatures of the first transition (T_{C1}) are seen in the order R^2_{02} and R^2_{20} order parameters also.

4.3.11 Simulation details for $\Gamma = 1.0$

For $\Gamma = 1.00$, similar to the lower values of Γ all the parameters were computed. In the Hamiltonian 4.2.2, considering $\Gamma = 1$, is considering the interaction between the uniaxial and biaxial terms between the neighboring particles on equal terms as the interaction between the uniaxial terms (the energy being always measured in units of ϵ). The biaxial phase is observed as a very stable phase for all values of $\Lambda > 0$. The biaxial order parameter R^2_{22} reaches a value of ~ 0.6 for the least temperature. The system order parameter becomes non – zero at the T_{C2}, indicating the onset of a nematic phase. The other two order parameters R^2_{02} and R^2_{20} give a clear evidence of the phases (figure 4.40). Figures 4.42 gives the phase diagram for $\Gamma = 1.00$ by considering the transition temperatures from the specific heat profiles for the different Λ values (figure 4.41).

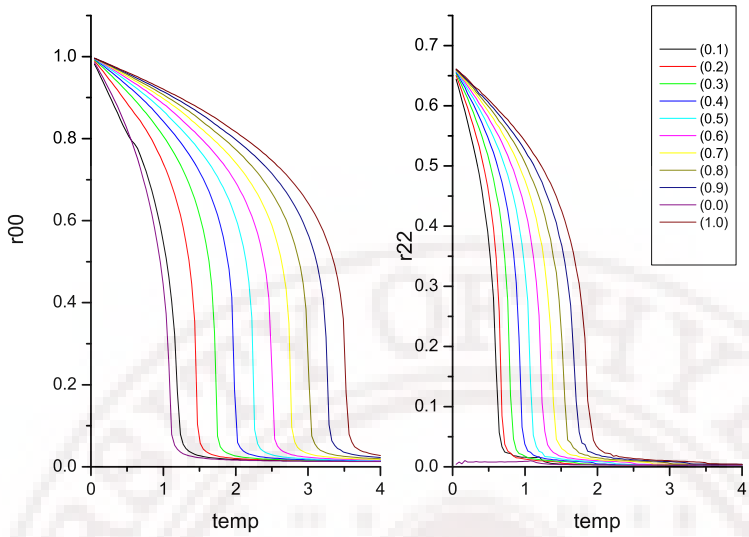

Figure 4.35: R^2_{00} and R^2_{22} with variation in temperature for different values of Λ keeping $\Gamma = 0.8$

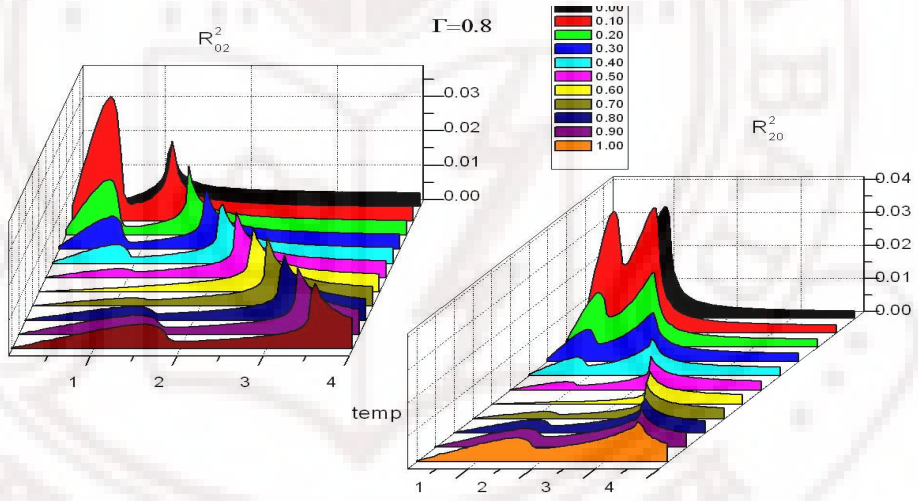

Figure 4.36: R^2_{20} and R^2_{20} with variation in temperature for different values of Λ keeping $\Gamma = 0.8$

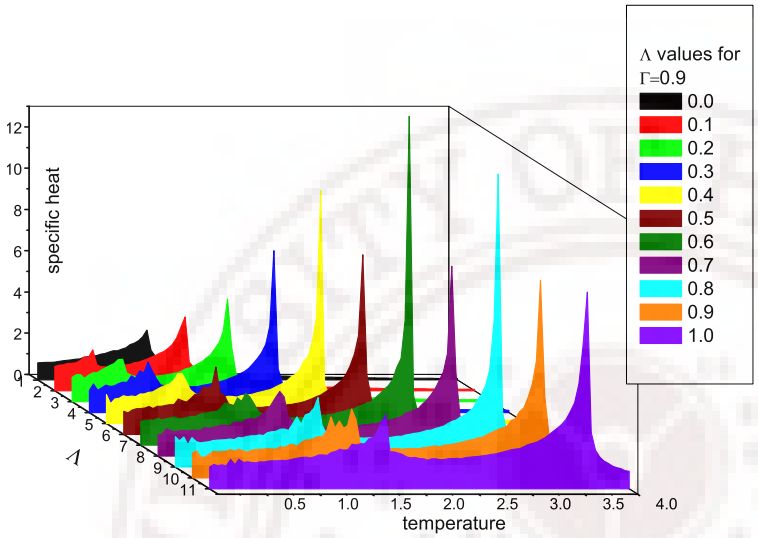

Figure 4.37: The specific heat with temperature at different Λ values.

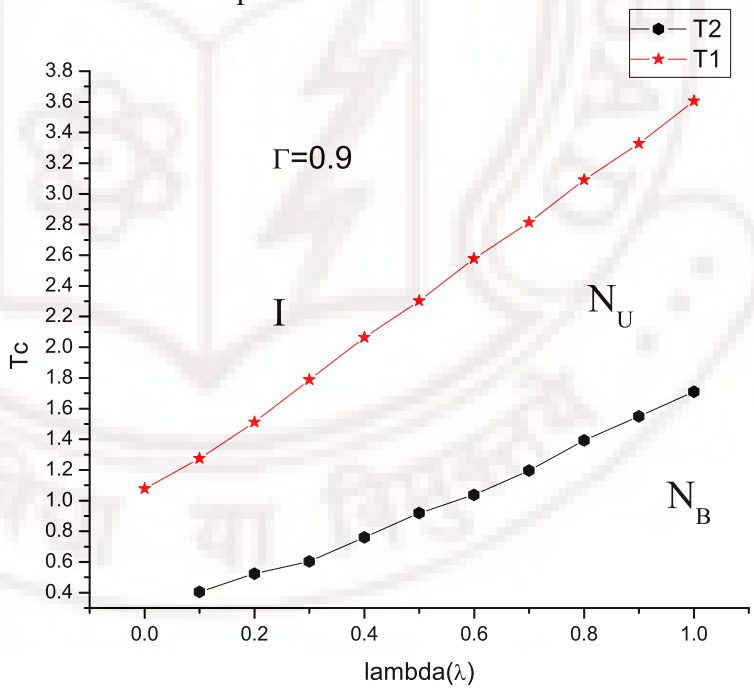

Figure 4.38: The phase diagram for Γ=0.9, taking the transition temperature from the peak position(s) of the specific heat data for every system by changing the Λ value ($T1$ – transition temperature from state N_U to N_B and $T2$ – transition temperature from N_U to isotropic phase).

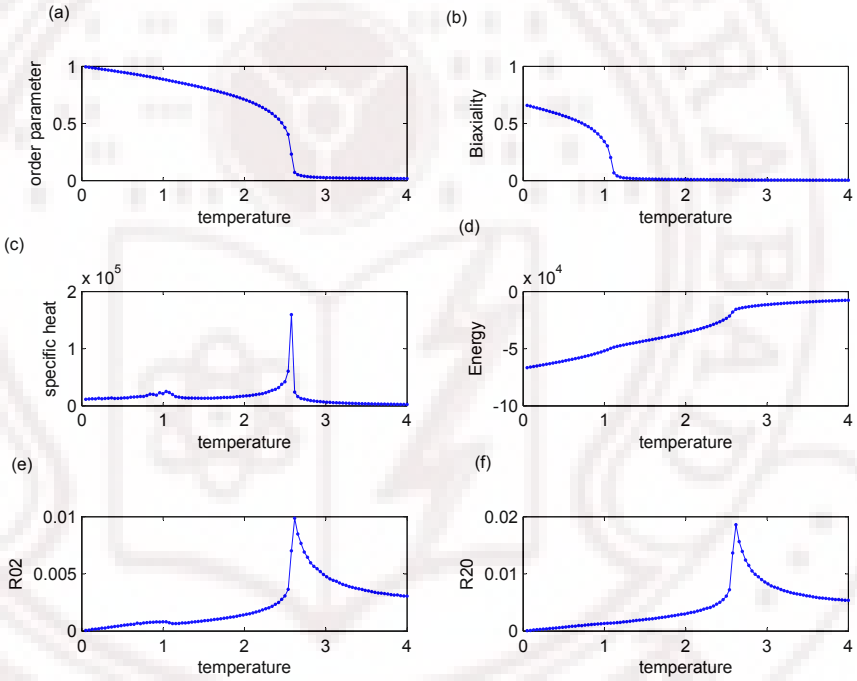

Figure 4.39: Variation of (a) order parameter, (b) biaxiality parameter, (c) specific heat (C_V), (d)Energy, (e)R^2_{02}, (f)R^2_{20} with temperature for a system with the parameter $\Gamma = 0.9$ and $\Lambda = 0.6$

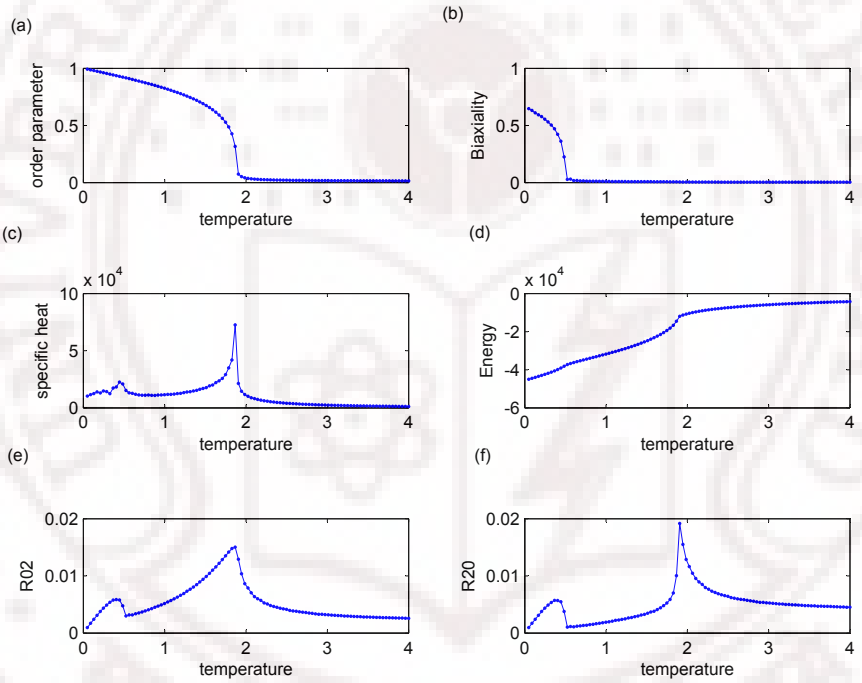

Figure 4.40: Variation of (a) order parameter, (b) biaxiality parameter, (c) specific heat (C_V), (d)Energy, (e)R^2_{02}, (f)R^2_{20} with temperature for a system with the parameter $\Gamma = 1.00$ and $\Lambda = 0.3$

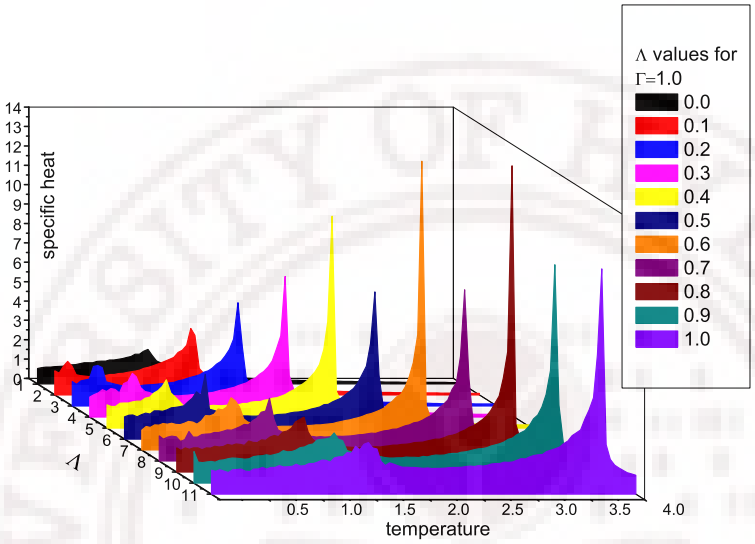

Figure 4.41: The specific heat with temperature at different Λ values.

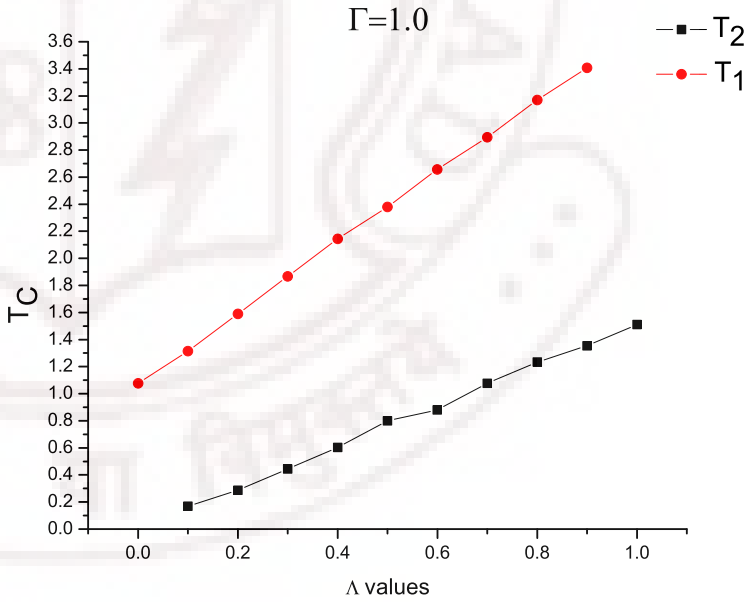

Figure 4.42: The phase diagram for Γ=1.00, taking the transition temperature from the peak position(s) of the specific heat data for every system by changing the Λ value ($T1$ – transition temperature from state N_U to N_B and $T2$ – transition temperature from N_U to isotropic phase).

4.4 Conclusions

With the change in Γ it was observed there were subtle changes in the phase diagrams obtained. For $\Gamma = 0.00$ and lower values of Λ two transitions were observed, first a transition $N_U - N_B$ and then a higher temperature transition from $I - N_B$. It is realized that with the further increase in Λ beyond 0.6 only a direct isotropic to a N_B transition is observed. Increasing Γ to 0.1 (Figure 4.11, 4.10), two triple points are observed when the phase diagram was plotted with Λ variation, first at $\Lambda = 0.25$ and other at $\Lambda = 0.5$. It is seen that there is line of Λ values where a direct transition occurs from biaxial nematic (N_B) to an isotropic phase. For the lower and the higher values of Λ, there was a uniaxial nematic phase present between a isotropic and a biaxial nematic phase. Further increasing Γ to 0.2, two triple points are observed at $\Lambda = 0.25$ and $\Lambda = 0.4$ (Figure 4.19, 4.18). The phase diagram for $\Gamma = 0.3$ (Figure 4.19, 4.18) showed two triple points appearing at $\Lambda = 0.24$ and $\Lambda = 0.30$ in a similar way as $\Gamma = 0.2$. Increasing the Γ parameter, the two triple points come closer to each other. The range of Λ values for which a direct transition from N_B to I occurs decreases. With the increase in Γ the two peaks $(N_U - N_B$ and $I - N_U)$ come closer. Further for Γ to 0.4 it is seen that there exists much lesser values of Λ for which a direct $I - N_B$ transition occurs (Figure 4.21, 4.20). Further increasing Λ beyond 0.21 for $\Gamma = 0.4$, no direct $I - N_B$ transition is observed. For $\Gamma = 0.5$ (Figure 4.24, 4.23) the phase diagram was plotted by considering the transition temperatures from the specific heat plots (Figure 4.23). It was observed that there were no values of Λ for which a direct $I - N_B$ transition occurred. With further increase in Γ the uniaxial nematic phase became more stable. There are always two transitions occurring first an $I - N_U$ and a $N_U - N_B$ with a temperature variation for every value of Λ. For $\Gamma = 0.6$ (Figure 4.27, 4.26), it is realized from the plot of the phase diagram that the uniaxial nematic phase is stable over a larger range of temperature compared to the plot of $\Gamma = 0.5$. A similar phenomenon is observed for $\Gamma = 0.6, 0.7, 0.8, 0.9, 1.0$ (Figures 4.27, 4.32 4.34, 4.38, 4.42) that a stable biaxial phase is present with the change in temperature, and occurs as a transition from a

uniaxial nematic phase. For $\Gamma = 1$ (Figure 4.42), the uniaxial phase becomes more stable, i.e. exists over a larger range of temperature. A stable biaxial phase is observed for higher values of Γ, but can be approached only from a uniaxial nematic phase.

Comparing the Monte Carlo study with the mean field work [39] and the bifurcation analysis [44] done, there are some new results obtained by doing a Monte Carlo simulations of a lattice model for biaxial liquid crystal systems . It is seen in figure 4.3 that a uniaxial nematic and a biaxial nematic phases are formed with the change in Λ for different Γ. It is observed that there are Λ values for which a direct $I - N_B$ transition occurs, which is not mentioned in the perviously done studies. These Monte Carlo simulations are in agreement with reference [48], where two transitions occur for $\Lambda = 0.24$ (model B1 in [48] [45]) and a $I - N_B$ transition for $\Lambda = 0.30$ (B2 model in [48] [45]). After a certain Λ it is seen for a given Γ there is a direct $I - N_B$ transition. Initially for lower values of Γ, say for $\Gamma = 0.1$ two transitions occur first $I - N_U$, then $N_U - N_B$, these are in agreement to what has been observed using simulations. From figure 4.3, an $I - N_B$ occurs at $\Lambda = 0.22$ for $\Lambda = 0.1$, whereas in the Monte Carlo simulation $\Lambda_{I-N_B} = 0.25$. Our simulations show that only until $\Gamma = 0.4$, there is at least a value of Λ for which an $I - N_B$ can occur. For Γ greater than 0.4 a uniaxial nematic phase is always present and becomes stable with increase in Γ. The bifurcation analysis studies dealt with the values of Γ and Λ that lay in the triangle ($0 \geq \lambda \geq 0.33$ and $0 \geq \gamma \geq 0.25$). Both the parameters Γ and Λ are equally important to decide the kind of transitions occurring in a biaxial liquid crystal system. This study indicates that there exists a range of (Γ, Λ) parameter where the biaxial phase cannot be reached directly from isotropic phase. In real systems a biaxial phase has not been realized in principle due to the competing mechanisms stabilizing other phases (like layered phases) after the onset of N_U phase.

Monte Carlo simulations are carried out based on the Hamiltonian (equation 4.2.2) covering systematically useful range of the model parameter $[\Gamma, \Lambda]$. Resultant phase diagrams are presented for the biaxial systems. This simulation shows a triple point occurring for Γ=0.0, two triple points for Γ=0.1, 0.2, 0.3 that move closer with increase in Γ. Increasing

Γ=0.4, only one triple point is observed. With further increase of Γ there always exists two transitions, $I - N_U$ and $N_U - N_B$. This simulation shows that both the parameters are important in mediating the transitions occurring in a biaxial nematic system.

Further study of this system can be undertaken with a more improved non-Boltzmann sampling methods. Due to the many degrees of freedom present, obtaining a density of states becomes a difficult task. Using these advanced techniques the order of the transitions and the exact transition temperature can be obtained from the free energy profiles.

Bibliography

[1] G. R. Luckhurst. Liquid crystals - a missing phase found at last? *Nature*, 430:413, 2004.

[2] L.J.Yu and A.Saupe. Observation of biaxail nematic phase in potassium laurate-1-decanol-water mixutres. *Phys. Review Lett.*, 45(12):1000, 1980.

[3] R.Bartoliono, T.Chiaranza, and M.Meuti. Uniaxial and biaxial lyotropic nematic liquid crystals. *Phys. Rev. A*, 26(2):1116, 1982.

[4] L. A. Madsen, T. J. Dingemans, M. Nakata, and E. T. Samulski. Thermotropic biaxial nematic liquid crystals. *Phys. Rev. Lett.*, 92:145505–1, 2004.

[5] H. H. Wensink, G. J. Vroege, and H. N.W. Lekkerkerker. Biaxial versus uniaxial nematic stability in asymmetric rod-plate mixtures. *Phys. Rev. E*, 66:041704, 2002.

[6] A.G. Vanakaras and D. J. Photinos. Theory of biaxial nematic ordering in rod-disc mixtures revisited. *Mol. Cryst. Liq.Cryst.: Sci. Tech. A*, 299:65–71, (1997).

[7] S. Varga, A. Galindo, and G. Jackson. Ordering transitions, biaxiality, and demixing in the symmetric binary mixture of rod and plate molecules described with the onsager theory. *Phys. Rev. E*, 66:011707, 2002.

[8] K. Merkel, A. Kocot, J. K. Vij, R. Korlacki, G. H. Mehl, and T. Meyer. Thermotropic biaxial nematic phase in liquid crystalline organo-siloxane tetrapodes. *Phys. Rev. Lett.*, 93:237801, 2004.

[9] J. L. Figueirinhas, C. Cruz, D. Filip, G. Feio, A. C. Ribeiro, Y. Frere, T. Meyer, and G. H. Mehl. Deuterium nmr investigation of the biaxial nematic phase in an organosiloxane tetrapode. *Phys. Rev. Lett.*, 94:107802, 2005.

[10] B. R. Acharya, A. Primak, and S. Kumar. Biaxial nematic phase in bent-core thermotropic mesogens. *Phys. Rev. Lett.*, 92:145506–1, 2004.

[11] R. Berardi, C. Fava, and C. Zannoni. A generalized gay- berne intermolecular potential for biaxial particles. *Chem. Phys. Lett.*, 236:462, 1990.

[12] R. Berardi, C. Fava, and C. Zannoni. A gay- berne potential for dissimilar biaxial particles. *Chem. Phys. Lett.*, 297:8, 1998.

[13] R. Berardi and C. Zannoni. Do thermotropic biaxial nematics exist? a monte carlo study of biaxial gay - berne particles. *Jr. Chem. Phys.*, 113(, pages = 5971), 2000.

[14] R. Berardi and C. Zannoni. Biaxial discotic gay - berne mesogens and biaxial nematics. *Mol. Cryst. Liq. Cryst.*, 396 PN Part 1:177, 2003.

[15] R. Berardi, L. Muccioli, and C. Zannoni. Field response and switching times in biaxial nematics. *J. Chem. Phys.*, 128:024905.1–.12, 2008.

[16] Roberto Berardi, Luca Muccioli, Silvia Orlandi, Matteo Ricci, and Claudio Zannoni. Computer simulations of biaxial nematics.

[17] M. P. Allen. Computer simulation of a biaxial liquid crystal. *Liq. Cryst.*, 8:499, 1990.

[18] P.J.Champ and M. P. Allen. Phase diagram of hard biaxial ellipsoid fluid. *J. Chem. Phys.*, 106:6681, 1997.

[19] P.J.Champ, M. P. Allen, and A.J.Masters. Theory and computer simulation of bent-core molecules. *J. Chem. Phys.*, 111(21):9871, 1999.

[20] J.S.V.Duijneveldt and M.P.Allen. Computer simulatio study of flexible-rigid-flexible model for liquid crystal. *Mol. Phys.*, 92(5):855–870, 1997.

[21] M.A.Bates and G.R.Luckhurst. Biaxial nematic phases and v-shaped molecules: A monte carlo simulation study. *Phys. rev. E*, 72:051702, 2005.

[22] M.A.Bates. Influence of flexibility on the biaxail nematic phase of bent core liquid crystal: A monte carlo simulation study. *Phys. rev. E*, 74:061702, 2006.

[23] G. R. Luckhurst and S. Romano. Computer simulation studies of anisotropic systems uniaxial and biaxial nematics formed by noncylindrically symmetric molecules. *Mol. Phys.*, 40:129, 1980.

[24] G. R. Luckhurst, C. Zannoni, P. L. Nordio, and U. Segre. Molecular field theory for uniaxial nematic liquid crystals formed by noncylindrically symmetric molecules. *Mol. Phys.*, 30:1345, 1975.

[25] F. Biscarini, C. Chiccoli, P. Pasini, F. Semeria, and C. Zannoni. Phase diagram and orientational order in a biaxial lattice model. a monte carlo study. *Phys. Rev. Lett.*, 75:1803–1806, 1995.

[26] C. Chiccoli, P. Pasini, F. Semeria, and C. Zannoni. A detailed monte carlo investigation of the tricritical region of a biaxial liquid crystal systems. *Int. J. Mod. Phys. C*, 10:469–476, 1999.

[27] C. Chiccoli, I. Feruli, O. D. Lavrentovich, P. Pasini, and C. Zannoni S.V. Shiyanovskii. Topological defects in schlieren textures of biaxial and uniaxial nematics. *Phys. Rev. E Rapid Comm.*, 66:030701–030701.4, 2002.

[28] C. Chiccoli, P. Pasini, Ivan Feruli, and C. Zannoni. Simulation of topological defects in nematic liquid crystal films. *Mol. Cryst. Liq. cryst.*, 398:195–206, 2003.

[29] S. Chandrasekhar, Geetha G. Nair, D. S. Shankar Rao, S. Krishna Prasad, K. Praefcke, and D. Blunk. A thermotropic biaxial nematic liquid crystal. *Curr. Sci.*, page article21, 1998.

[30] D.Apreutesei and G.H.Mehl. Completely miscible disc and rod shaped molecules in the nematic phase. *Chem. Commun.*, pages 609–611, 2006.

[31] R.Hashim, G.R.Luckhurst, and S.Romano. Computer simulation studies of anisotropic systems xii. mixture of rods and plates- a biaxial nematic? *Mol. Phys.*, 53(6):1535–1539, 1984.

[32] R.Hashim, G.R.Luckhurst, F.Prata, and S.Romano. Computer simulation studies of anisotropic systems xxii. an equimolar mixture of rods and discs: A biaxial nematic? *Liq. Cryst.*, 15(3):283–309, 1993.

[33] A.Galindo, A.J.Haslam, S.Varga, G.Jackson, A.G.Vanakaras, D.J.Photinos, and D.A.Dunmur. The phase behavor of a binary mixture of rodlike and disclike mesogens: Monte carlo simulation, theory and experiment. *J. Chem. Phys.*, 119(10):5216, 2003.

[34] J.P.Straley. Ordered phases of a liquid of biaxial particle. *Phys. Rev. A*, 10(5):1881, 1974.

[35] G.R.Luckhurst. Biaxail nematic liquid crytsal: fact or fiction? *Thin Solid Films*, 393:40–52, 2001.

[36] C. Cruz, J. L. Figueirinhas, D. Filip, G. Feio, A. C. Ribeiro, Y. Frre, T. Meyer, and G. H. Mehl. Biaxial nematic order and phase behavior studies in an organosiloxane tetrapodes using complementary deuterium nmr experiments. *Phys. Rev. E*, 78:051702, 2008.

[37] M. J. Freiser. Ordered states of nematic liquid. *Phys. Rev. Lett.*, 24(19):1041, 1970.

[38] M. J. Freiser. Successive transitions in a nematic liquid. *Mol. Cryst. Liq. Cryst.*, 14:165–182, 1971.

[39] A.M.Sonnet, E.G.Virga, and G.E.Durand . Dielectric shape dispersion and biaxial transitions in nematic liquid crystals. *Phys. Rev. E*, 67:061701, 2003.

[40] G. De Matteis and E. G. Virga. Tricritical points in biaxial liquid crystal phases. *Phys. Rev. E*, 71:061703–1, 2005.

[41] G. De Matteis, S. Romano, and E. G. Virga. Bifurcation analysis and computer simulation of biaxial liquid crystals. *Phys. Rev. E*, 72:041706, 2005.

[42] L.Longa, P.Grzybowski, S.Romano, and E.Virga. Minimal coupling model of the biaxail nematic phase. *Phys. Rev. E*, 71:051714, 2005.

[43] F. Bisi, E. G. Virga, E. C. Gartland, G. De Matteis, A. M. Sonnet, and G. E. Durand. Universal mean-field phase diagram for biaxial nematics obtained from a minimax principle. *Phys. Rev. E*, 73:05170, 2006.

[44] Fulvio Bisi, Geoffrey R. Luckhurst, and Epifanio G. Virga. Dominant biaxial quadrupolar contribution to the nematic potential of mean torque. *Phys. Rev. E*, 78:021710, 2008.

[45] Silvano Romano. Mean-field and computer simulation study of a biaxial nematogenic lattice model mimicking shape amphiphilicity. *Physics letters A*, 333:110119, 2004.

[46] Riccardo Rosso. Orientational order parameters in biaxial nematics: Polymorphic notation. *Liq. Cryst.*, 34(6):737–748, 2007.

[47] Robert J Low. Measuring order and biaxiality.

[48] Silvano Romano. Computer simulation of a biaxial nematogenic model on a three-dimensional lattice and based on a recently proposed interaction potential. *Physica A*, 337:505 519, 2004.

Chapter 5

Structures and transitions in hybrid films of biaxial molecules

5.1 Introduction

A thin film of liquid crystal when confined between two substrates (with larger surface dimension than the thickness) with antagonistic boundary conditions is a hybrid film. In a typical hybrid planar film nematic order is induced by the two substrates in mutually perpendicular directions along, say laboratory z – axis, one in the homeotropic direction at $z = d$ (thickness of the film) and the other in the lateral (planar) direction at $z = 0$. Here we consider such thin film of biaxial liquid crystal molecules, confined in such a geometry. Monte Carlo simulations are carried out to look for details of director structures, and possible orientational transitions, as the sample is cooled from its isotropic phase.

Biaxial nematic phases continue to attract considerable attention [1] [2] both from theoretical [3] [4] [5]and experimental [6] [7] [8], points of view. Interest in biaxial liquid crystals led to many models being proposed, and these were investigated using computer simulations [9] [10]. Biaxial liquid crystals deviate from cylindrical symmetry, usually being broad-like in structure. Besides the usual ordering of long axes of the molecules (along the primary director, say) orientational ordering of the remaining axes of the molecules (leading to secondary directors, say) is an interesting possibility. This leads to an in principle possibility of using switching of the secondary direction for effecting changes in the optical properties of the medium. It is expected that rotation of the minor directors might be relatively rapid and possibly faster than for the director $\hat{n}$. This could possibly lead to

a display with a fast response and based on in-plane switching [2]. Thus, confined biaxial liquid crystals are fascinating objects of study in liquid crystal research. Such confinement effects can be mimicked in computer simulations by introducing suitable anchoring conditions at the surfaces. One such confined system recently studied is a biaxial nematic droplet [11]. The optical textures of this droplet were studied, looking for defects that can be formed in such systems. One of the well known and well investigated confined systems of liquid crystal is the hybrid film.

Interest in confined liquid crystal research is shown by both experimentalists and theoreticians. Theoretical studies using mean field methods, minimization of Franks free's energy were studied in detail to understand the different transitions and structures that are formed [12]. Experimentalists have used different methods to understand such systems in more detail [13] [14]. Detailed investigation were also carried out by using computer simulations methods, wherein liquid crystals were modeled by lattice based models like LL model [15] or off – lattice models like Gay – Berne [16] models [17] [13] [18]. Other models used were hard spherocylinders to understand the effects of different types of substrates on liquid crystal film. Attempts were made to understand the effect of confinement comparing their differences from bulk systems. Optical textures of confined systems were simulated for both uniaxial and biaxial particles [19] [20] [21].

5.2 Hybrid film of Uniaxial Molecules

The stability of different structures of a nematic liquid crystal in a planar hybrid film was examined within the framework of a Gaussian description of order fluctuations [22] [23]. In a very thin film the director field is not bent smoothly between the two orientations induced at the two substrates, but exhibits a step-like change if the anchorings at the confining substrates are strong and comparable in magnitude. A (dis)continuous structural transition to the bent-director state, which occurs with increasing film thickness or decreasing temperature, is governed by the lowest bending director fluctuation mode. The (dis)continuity

of the structural transition depends on the temperature and film thickness. The analysis of nematic liquid crystals confined to highly constrained hybrid films with a biaxial structure has revealed a soft-mode or soft-mode-like dynamics in the vicinity of the structural transition toward hybridly aligned (bent-director) structure.

With this backdrop, Monte Carlo simulations were earlier preformed using the LL [15] lattice model. A hybrid film of liquid crystal (10 layers) was studied [24]. The existence of a biaxial phase was observed when the temperature is decreased from the isotropic phase. With further decrease in the temperature a bent – like structure is formed, that remains stable, a structural transition from biaxial- bent phases. This biaxial phase is stable only for a small range of temperature. The structural transition was monitored both by the change in order parameters and by the fluctuations in energy. These films were also investigated as a function of their thickness, and the findings are constant with prediction from phenomenological studies. To get a better understanding of this system a deeper study was undertaken using JSM modified Wang Landau algorithm [25] (Chapter 3 of the thesis). A clearer picture of the system was obtained by computing the bulk and the layer-wise order parameter at the transition. The layer-wise director angles (ϕ) were plotted with temperature change to map out the different structures that were formed. The exact transition temperature was confirmed by examining the features of the free energy profiles. This work is discussed in detail in the pervious chapter of this thesis (Chapter 3). A similar study of a thin film of liquid crystal confined between two cylindrical hybrid film was carried out based on canonical Monte Carlo sampling methods (as reported in Chapter 3 earlier) [26]. A biaxial phase was realized for specific chosen anchoring strengths of the substrates in an intermediate range or temperatures.

The main interest in the present study lies in understanding a confined biaxial system and this was studied in detail keeping in mind the different structures seen in a hybrid film of uniaxial molecules. The objective is to look for possible effects on the self – organization of the biaxial molecules in a thin planar geometry, when subjected to a competing boundary conditions at the two surfaces. Such a film was studied based on canonical Monte

Carlo methods, as a function of temperature. All the relevant order parameters and their fluctuations were examined to look for signatures of possible intermediate stable structures which are direct consequence of hybrid boundary conditions. The motivation for this is qualitatively similar to the study of confined planar hybrid films. These simulations on biaxial systems were augmented by extending these simulation to film with variable relative anchoring strength.

5.3 Model Used and System studied

The system studied here is a planar geometry hybrid film of biaxial molecules. A hybrid film is built by inducing order into the liquid crystal system in perpendicular directions. Let us assume that $'XYZ'$ represent the laboratory frame and $'xyz'$ represent the molecular frame. In order to get a hybrid nature in the liquid crystal system, the molecules of the first $(k = 1)$ and the last layer $(k = nz)$ of a cuboid are assumed as substrates or as ghost layers. The molecules at $k = 1$ layer are all fixed along the laboratory frame i.e. x is along X, y along Y and z along Z. The molecules on the substrate at $k = nz$ are all fixed at orientations obtained by rotating the direction of the molecules on the ghost layer $k = 1$ by π about the X axis, i.e. x is along X, y along $-Z$ and z along Y (figure 5.1). The molecules on these two substrates of course do not participate in the Monte Carlo steps. Periodic boundary conditions are considered along the X and Y directions, in order to minimize the finite size effects. The system considered here is of the size $15 \times 15 \times 8$ $(X \times Y \times Z)$. The anchoring strengths of the two substrates are represented as ϵ_1 and ϵ_{nz}. As usual, we represent the energy of the system in units of the coupling constant in LL potential, thereby representing the temperature of the system by a convenient dimensionless variable T^*. The anchoring strength at the substrates which is the interaction constant between LC and substrate molecules is then also measured in the same units as T^*.

A pairwise additive lattice Hamiltonian is used for this study [27]. The model chosen here is a lattice based Hamiltonian which has contributions from both the biaxial terms,

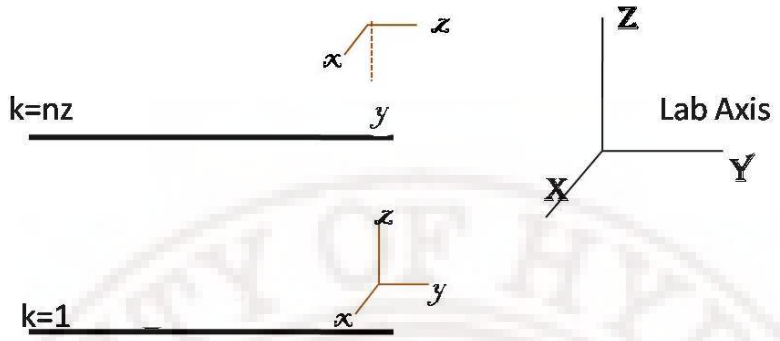

Figure 5.1: The system for biaxial hybrid film.

but requires only a simple parameter λ for simplification. This corresponds to dispersion approximation, and has a phase diagram with a Landau point, is given as

$$U_{ij} = -\epsilon(\frac{3}{2}V_{33} - \lambda\sqrt{6}(V_{11} - V_{22}) + \lambda^2(V_{11} + V_{22} - V_{12} - V_{21}) - \frac{1}{2}) \qquad (5.3.1)$$

ϵ, λ are positive constants, with ϵ being set to unity as mentioned above. λ is the biaxiality parameter, and defines the amount of molecular biaxiality in the system. In this problem the study is done by considering the biaxiality parameter as $\lambda = 0.35$. Below the tri-critical [28] point the molecules are known to be prolate in shape. Considering the biaxiality parameter as 0.35 has a certain significance, at this value of λ the two transitions were clearly apart, with a range of temperature having a biaxial phase (figure 5.2).

This model was preferred over other that proposed by Romano [29] for the ease of computation and, is based on the Born-de-London's approximation. This model was earlier studied in detail using Monte Carlo methods and mean field methods [28] [27]. It is known from the previously done Monte Carlo studies that the molecules are known to be prolate in shape for values of λ below the tri – critical point $(\lambda = 1/\sqrt{6})$ and oblate else. Using the above mentioned Hamiltonian a droplet was studied using Monte Carlo simulations [11].

A hybrid film of biaxial molecules was studied using Markov Chain Monte Carlo methods with Metropolis algorithm (Chapter2 of the thesis for the details). This system was equilibrated for half a million Monte Carlo runs and a productions run of half a million

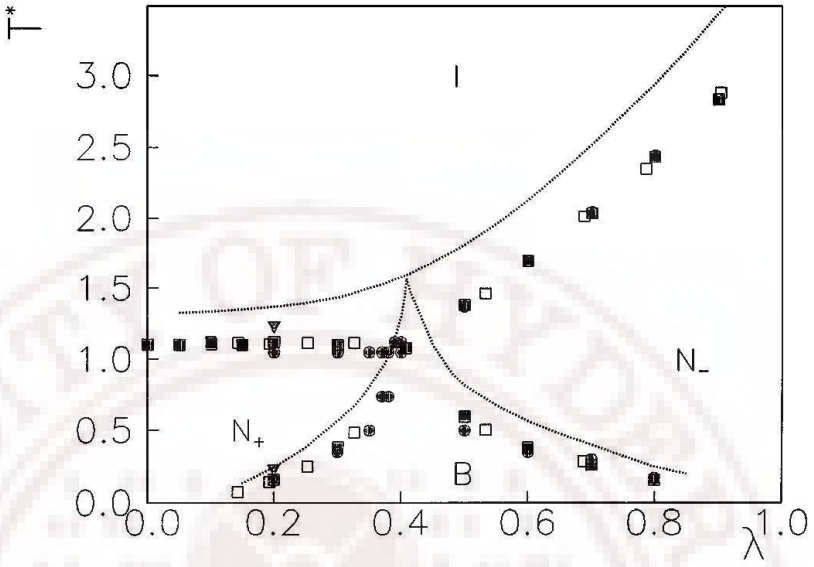

Figure 5.2: Phase diagram proposed for the hamiltonian 5.3 [28]

runs also. The average energy and the fluctuations in energy (specific heat) were computed for the system. Different order parameters $R^2_{00}, R^2_{02}, R^2_{20}, R^2_{22}$ were computed along with their fluctuations for the system [30]. The way these parameters are computed is given in detail in Chapter2 of this thesis and Chapter 1 of this thesis contains the physical meaning of every parameter.

5.4 Results and Discussions

A planar thin film with dimensions $15 \times 15 \times 8$ in lattice units is considered for the present study, with periodic boundary conditions being imposed in the x and y directions. A layer of liquid crystals are placed at the two bounding surfaces in the Z – direction, called the ghost layers to represent the effect of substrates. These substrate molecules are oriented suitably to induce boundary conditions of choice and are held fixed thoughout the simulation (figure 5.1). The initial configuration of the LC system is taken as random *i.e.* all the liquid crystal molecules are initialized in random directions. The system is simulated at different temperatures (reduced units) 2.00 to 0.01, in steps of 0.005, yielding 400 data sets to investigate temperature dependencies. The system was equilibrated for 50,000 Monte

Carlo sweeps at every temperature, the last configuration of the higher temperature being taken as the initial configuration for the next lower temperature in order to reach the equilibrated configuration at the earliest. Canonical Monte Carlo sampling with Metropolis algorithm was used for this study (discussed in chapter 2 of this thesis).

The different physical parameters computed for this confined system are: average energy $\langle E \rangle$, the specific heat capacity C_V, the different order parameters: R^2_{00} – primary system order parameter along the Z – axis arising from the orientational order of the long axes of the molecule, R^2_{02} – the order along the Z direction due to the biaxiality components of the molecules, R^2_{20} – the phase biaxiality parameter, R^2_{22} – the biaxiality parameter arising from molecular biaxiality. The computation of these order parameter is discussed in chapter 2 of the thesis and are equilibrated over an ensemble of at least 1,00,000 microstates. For obtaining details of director variation in the film, each of these parameters was computed for every layer of this system. Thus the film is divided, for computational progress, into 8 distinct layers indexing it from the substrate at $k = 1$. Other useful parameters not defined before but provided a clearer understanding to this system are angle φ_z is computed as the angle made by primary molecular axis *viz.* z – component of the molecule with respect to the laboratory Z – axis, and then angle φ_y is computed by considering average the angle made by molecular y axes with laboratory Z axis.

In this study, the biaxiality parameter is set at $\lambda = 0.35$, a convenient value from the phase diagram (figure 5.2) and the above parameters are computed as a function of finely varied temperatures. To explore this system further , the effect of anchoring strength on the director structure is investigated by repeating the above simulations as a function of anchoring strength at the surface. The results are discussed in detail below.

5.4.1 Variation of director configuration with temperature

In this section the hybrid film $(15 \times 15 \times 8)$ comprising of biaxial molecules, subjected to equal anchoring conditions at the two surfaces $(\varepsilon_1 = \varepsilon_{nz} = 1.00)$, is investigated as a function of temperature (T^* is varied from 2.00 to 0.01 in steps of 0.005). The different

physical properties computed include: bulk and layer – wise variation with temperature of $R^2_{00}, R^2_{20}, R^2_{02}$ and R^2_{22} and variation in them. Further, the layer – wise tilt angle of the primary director (associated with R^2_{00}) with respect to the layer normal (Z – axis) is also computed with temperature. These results are presented and discussed in this section.

As shown in figure 5.5 the specific heat profile shows two transitions, first at $T_{C1} = 1.01$ and the second at $T_{C2} = 0.51$. Figure 5.3 gives the plots of the variation of the different order parameters with temperature. The order parameter R^2_{00} shows a step – like change in

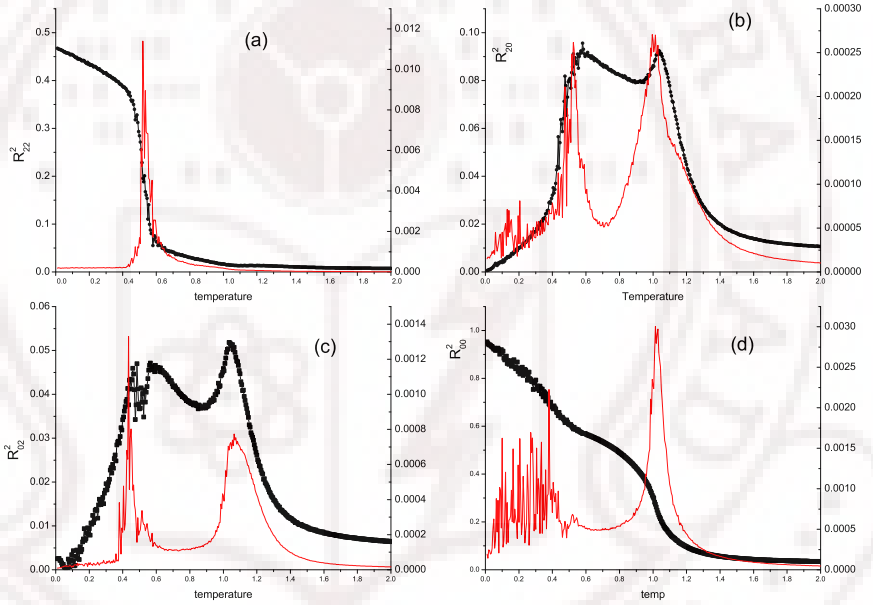

Figure 5.3: (a) R^2_{22}, (b) R^2_{20}, (c) R^2_{02}, (d) R^2_{00} with the variation in temperature. (The plots in red indicate the respective fluctuations)

profile after T_{C2} (figure 5.3 (d)). This change in R^2_{00} profile at the lower temperature, shows up as a fluctuations in order parameter susceptibility. The biaxiality parameter R^2_{22} is plotted with temperature variation in the figure 5.3 (a). It is observed that R^2_{22} becomes non – zero at T_{C2} that shows up as a peak in its fluctuations (*i.e.* the corresponding susceptibility). The contribution to the order along Z due to the biaxiality present in the molecule (R^2_{02}) and the phase biaxiality parameter (R^2_{20}) have maximum values between the two transition temperatures T_{C1} and T_{C2} (figure 5.3 (b) and (c)). It is seen that, there are significant

fluctuations persisting in both R^2_{02} and R^2_{00} susceptibilities at the lower temperatures. The susceptibilities of the order parameters R^2_{02} and R^2_{22} do not show such fluctuations at the lower temperatures, temperatures lower than T_{C2}. This seems to be significant.

The different layer – wise order parameters were plotted in figure 5.4 each layer being indexed from one of the substrates programmed with index $k = 1$ (figure 5.1). Compared to this expected bulk values, none of these order parameters seems to be significantly affected by confinement. Referring to figure 5.4 (b), the layer – wise R^2_{00} showed no large fluctuations in the parameter compared to the bulk parameter as shown in figure 5.3 (d). It is interesting to note that while the layer – wise R^2_{00} has fairly high value (~ 1.0) without appreciable fluctuations at very low temperatures, the bulk R^2_{00} has a relatively lower value (~ 0.95) and shows dominant fluctuations. A further insight emerges by a study of layer – wise director tilt – angle with respect to Z – axis, as shown in figure 5.5. It is seen that that on cooling the sample below T_{C2} (= 0.51) two quantities changes occur: the spread of the layer angles proportionally decrease due to the onset of the low temperature phase (by about 5^O); and the intermediate layers (particulary layers with indices 5 and 6, figure 5.5) show considerable fluctuations of director tilt – angles. It is interesting that while the amount of the order R^2_{00} in each of the layer does not seem to fluctuate principally, its orientation fluctuate and is more so in the intermediate layers. These are reflected in the observation of the wild fluctuations in the R^2_{00} value (figure 5.3 (d)) at the corresponding temperatures. This presents a scenario where the different layers are fairly completely ordered (as far as long axis of the molecules are concerned), but their directors are fluctuating. Thus we should expect another order parameter to be affected by such collective fluctuation of the long axes, *viz.* R^2_{20} – the so called phase biaxiality (*i.e.* biaxiality indexed due to the biaxial alignment of the molecular long axes). The simulated data as indexed show that such is indeed in the case (figure 5.3 (b)). The other two parameters, R^2_{02} and R^2_{22}, arise due to the difference in the ordering of the other two molecular axes (x and y, as per our notation), and hence their fluctuations are expected to be insensitive if the statistical fluctuation about the axes are similar (unlike R^2_{00} and R^2_{20}). We see that the fluctuations in R^2_{02} and R^2_{22} are

indeed relatively very small, confining the structure and dynamics in the film that emerges from these studies. The director tilt angle was plotted for every layer with the variation in temperature. The director tilt angle φ_z is computed as the average of all the tilt angles made

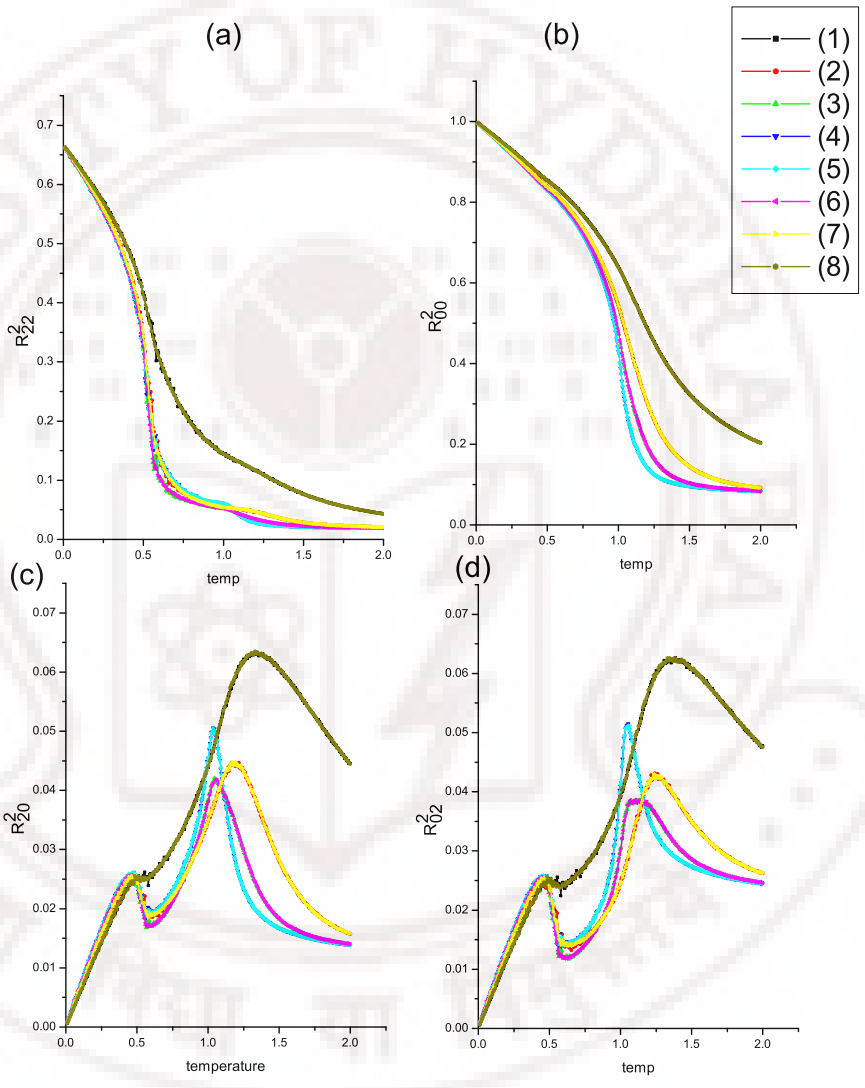

Figure 5.4: The variation of (a) R^2_{22}, (b)R^2_{00}, (c)R^2_{20}, (d)R^2_{02} with temperature.

by every molecular z – axis with the laboratory Z – axis. At high temperatures where the order is zero (*i.e.* in disordered phase), the φ_z value relatively yields the value of the magic angle when $3\cos^2\theta - 1 = 0.00$. With the decrease in temperature, the effect of confinement is observed by the increase in the layer – wise order and the change in φ_z. The tilt – angle

after the second transition T_{C2} shows significant changes. The spread of the tilt angle over the layers decreases by 5^O, indicating the layers tilting closer to each other.

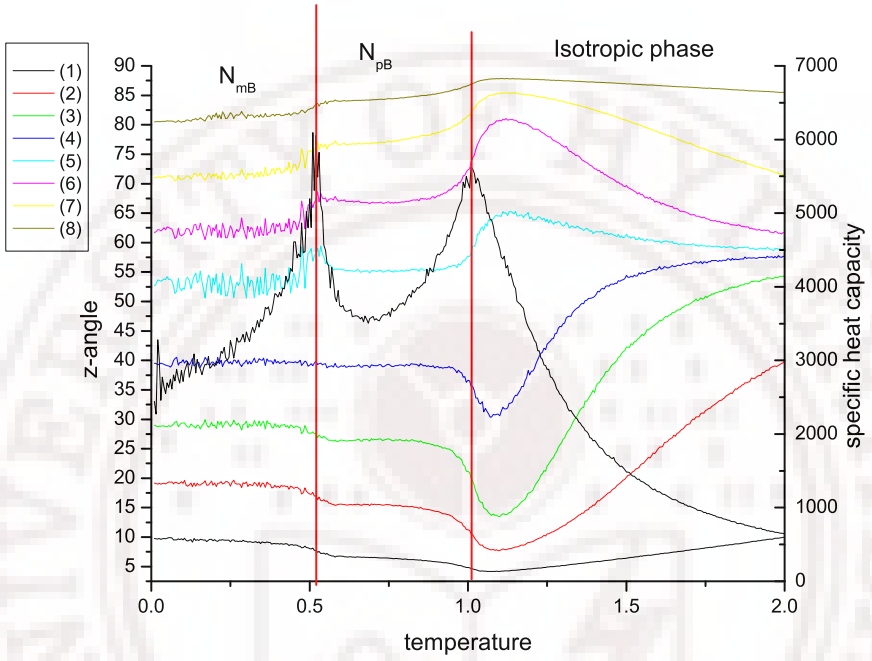

Figure 5.5: The variation of the z-angle ϕ with temperature overlapped by the specific heat plot to represent the different phases formed.)

From this study it can be inferred that there are two ordered systems under confinement, formed due to variation of temperature. The first – a higher temperature phase is characterized entirely by the phase biaxiality – we refer to this nematic phase as N_{pB}. With further decrease in temperature, there is another transition occurring from N_{pB} to another biaxial phase say N_{mB}. The second order phase is now entirely characterized by the molecular biaxiality and is indicated by the onset of R^2_{22}. It may further be seen that the order parameter R^2_{02} is also non – zero only in the N_{pB} phase, indicating that there could be a small contribution to the order in the Z – direction only as long as molecular biaxial components are arranged to zero in this nematic phase. Onset of R^2_{22} seems to discourage the ordering R^2_{02}.

From the above plots and the discussions it can be concluded that the fluctuation in the

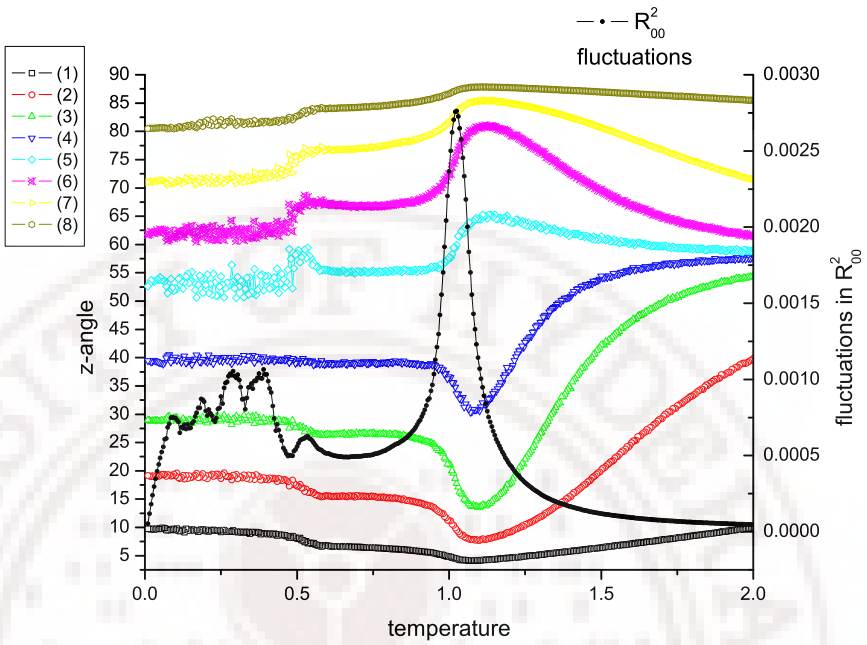

Figure 5.6: Variation of the angle made by the molecular z axis with the laboratory Z axis and the R^2_{00} fluctuations with temperature.

tilt angle φ are a result of confinement of all the molecular axes (x, y, z). This restrictive confinement seems to lead to an appreciable frustration of the intermediate layers, and as is well known under the circumstances they exhibit significantly higher amount of fluctuations. Another way of stating this is to say that the free energy profile becomes more shallow with respect to these degrees of freedom. These fluctuations are observed only in the absolute order parameters (R^2_{00} and R^2_{20}), the order parameter that are computed considering the $z-$ component of the molecules. The profiles of order parameters considering the relative order parameters (R^2_{02} and R^2_{22}), considering the difference in the order components along the x and y directions, do not show such signatures of these fluctuations. It can also be inferred from the above plots that the order in the layers does not fluctuate whereas the layer 4, 5, and 6 is tilt angles (φ) fluctuate. This indicates that the overall system order parameter R^2_{00} fluctuates because the layer – wise angle director fluctuates but having a constant (magnitude) layer – wise order. The effect of confinement is observed as these fluctuations in the layer – wise tilt angles and the absolute order parameters (R^2_{00} and R^2_{20}).

It is interesting to visualize this scenario as arising due to a very curious free energy surface which has at once sharp minimum with respect to the magnitude of the layer – wise uniaxial order, but relatively shallow when it comes to the corresponding director orientations. In other words this corresponds to the presence of fluctuating collecting modes (as contrasted to individual molecular orientations), permitted by the frustration caused by very restrictive hybrid boundary conditions imposed on these biaxial molecules at the substrates.

These thermal effects at the fixed anchoring strengths ($\varepsilon_1 = \varepsilon_2 = 1.00$) point out to a possibly more complex structures, obtainable by a careful tuning of the relative anchoring strengths. The next section represents the effect of anchoring strength on the phase transition in these hybrid films.

5.4.2 Variation of director configuration with anchoring strength (ϵ_{nz})

The objective of these simulations is to vary the relative anchoring influence of the two substrates. To this end, we fix one of the anchoring strengths say ε_1 (at $k = 1$, figure 5.1) at 1.0, and vary the other value ε_{nz} systematically in the range 0 to 1.0 in convenient steps. For every such combinations of anchoring strengths (there are 11 systems generated as indicated in Table 5.1), MC simulations as described above were carried out. The physical parameters computed are summarized in Table 5.1. In these systems one additional physical property was also monitored: the variation of tilt angle φ_y corresponding to the average distribution of molecular Y – axis in each layer relative to the laboratory Z – axis (figure 5.1). Out of the 11 systems studied, we discuss specifically 4 systems, due to the features exhibited.

System 1 (Table 5.1): [$\varepsilon_1 = 1.00$ and $\varepsilon_{nz} = 0.00$]

The system 1 in the Table 5.1 defines a $15 \times 15 \times 8$ system, where $\varepsilon_1 = 1.00$ and $\varepsilon_{nz} = 0.00$. The anchoring strength due to the substrate 2 $(k = nz)$ is set to zero , *i.e.* the system is strongly anchored on one side and is left free on the other. The system order parameters ($R^2_{00}, R^2_{02}, R^2_{20}$ and R^2_{22}) for the system are plotted in the figure 5.9. It is observed that the

Table 5.1: Change ϵ_{nz}

System No.	ϵ_1	ϵ_{nz}	Parameters studied
1	1.00	0.00	$\langle E \rangle$, C_V, system and layer-wise order parameters: $R^2_{00}, R^2_{02}, R^2_{20}$ and R^2_{22} with their fluctuations, the tilt angles φ_z and φ_y
2	1.00	0.1	$\sim do \sim$
3	1.00	0.2	$\sim do \sim$
4	1.00	0.3	$\sim do \sim$
5	1.00	0.4	$\sim do \sim$
6	1.00	0.5	$\sim do \sim$
7	1.00	0.6	$\sim do \sim$
8	1.00	0.7	$\sim do \sim$
9	1.00	0.8	$\sim do \sim$
10	1.00	0.9	$\sim do \sim$
11	1.00	1.0	$\sim do \sim$

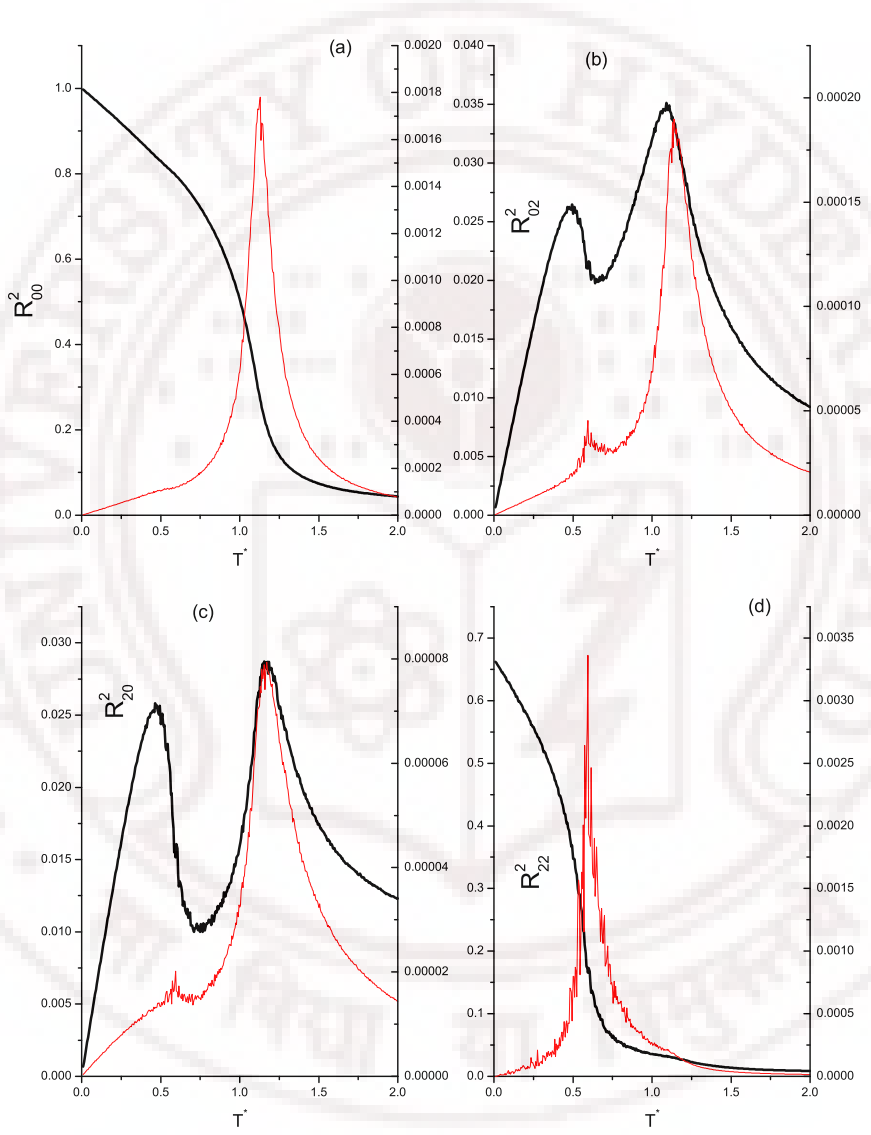

Figure 5.7: Variation of (a) R^2_{00}, (b)R^2_{02}, (c)R^2_{20}, (d)R^2_{22} with temperature for a system with $\varepsilon_1 = 1.00$ and $\varepsilon_{nz} = 0.00$

order parameter R^2_{00} has an abrupt change at $T_{C1} = 1.10$. Effect of transitions are also observed both in the susceptibilities of R^2_{20} and R^2_{02} at the same transitions temperature T_{C1}. This temperature (T_{C1}) corresponds to a transition from a disorder phase to nematic phase. The biaxiality parameter R^2_{22} becomes non – zero at a temperature different from T_{C1}, at $T_{C2} = 0.5$, which corresponds to transition from a uniaxial nematic phase to a biaxial nematic phase (figure 5.2). The lower temperature transition is seen in the specific heat also at this temperature T_{C2} (Figure 5.8). Figure 5.8 gives the variation of the tilt angle

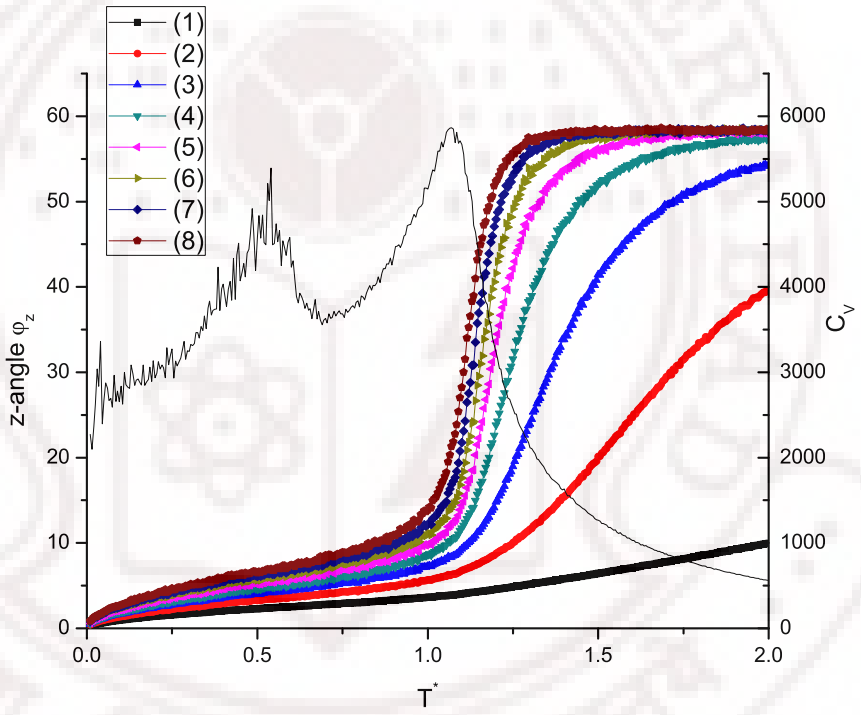

Figure 5.8: Variation of the z tilt angle φ_z and the specific heat C_V with temperature for a system with $\varepsilon_1 = 1.00$ and $\varepsilon_{nz} = 0.00$

made by the molecular z – axis with the laboratory Z axis. It is clear from the behavior of these tilt angles with temperature that with the onset of a nematic phase the layers tend to align along the substrate that induces anchoring. In the isotropic phase, layers 2 and 3 are influenced by the anchoring substrates at $k = 1$, while the other have a non – zero orientational order, reflected by the tilt – angles (very near to to the magic angle). This is to be contrasted to the low temperature nematic phase, where all the directions in the

different layers are aligned fairly above the laboratory Z – direction. Referring to figure 5.9, it is seen that the layer – 1 is perfectly anchored. The effect of anchoring is seen in the different order parameters plotted for layer – 1. The order for the layer – 1 is around 0.25 even before a nematic phase set in (figure 5.9). With the decrease in temperature the order sets into the system as a nematic phase. The R^2_{22} order parameter for the free layer (layer - 8) sets in only at the lowest temperature (figure 5.10 (c)). This clearly shows that biaxiality is developing in the system and percolating over a temperature range. The R^2_{02} parameter is the highest for the tightly confined layer, and with the decrease in temperature the order in every layer comes to a zero value. Increasing the anchoring strength ε_{nz} subtle changes are observed in the systems. As seen in the Table 5.1, ε_{nz} is increased in steps of 0.1, a system with $\varepsilon_{nz} = 0.2$ is discussed next.

System 3 (Table 5.1): [$\varepsilon_1 = 1.00$ and $\varepsilon_{nz} = 0.2$]

Increasing the anchoring strength $\varepsilon_{nz} = 0.2$ corresponds to a gradual increase of the influence of the competing substrate at $k = nz$ on the liquid crystal system. It is expected that this increase in anchoring strength will lead to different director configurations. The order parameters of the system when plotted with temperature variation, a transition from isotropic to a uniaxial nematic is seen as a peak in the R^2_{00} fluctuations. A transition from uniaxial nematic phase to biaxial nematic phase is observed at $T_{C2} = 0.535$ indicated by increase in R^2_{22}. The layer – wise order parameters are plotted with the variation in temperature in the figure 5.10. The transition from isotropic phase to uniaxial nematic phase is clearly observed by plotting the tilt – angle with the molecular z axis (figure 5.11). The specific heat profile indicates the presence of two transitions with the variation in temperature (figure 5.11). Plotting the title angle, it is clear that at T_{C2}, there is order setting in to the system, and also indicated by the onset of the system order parameter R^2_{00}. For system 4 (Table 5.1) with $\varepsilon_{nz} = 0.3$, it seen that all the physical parameters have the similar profiles as system 3.

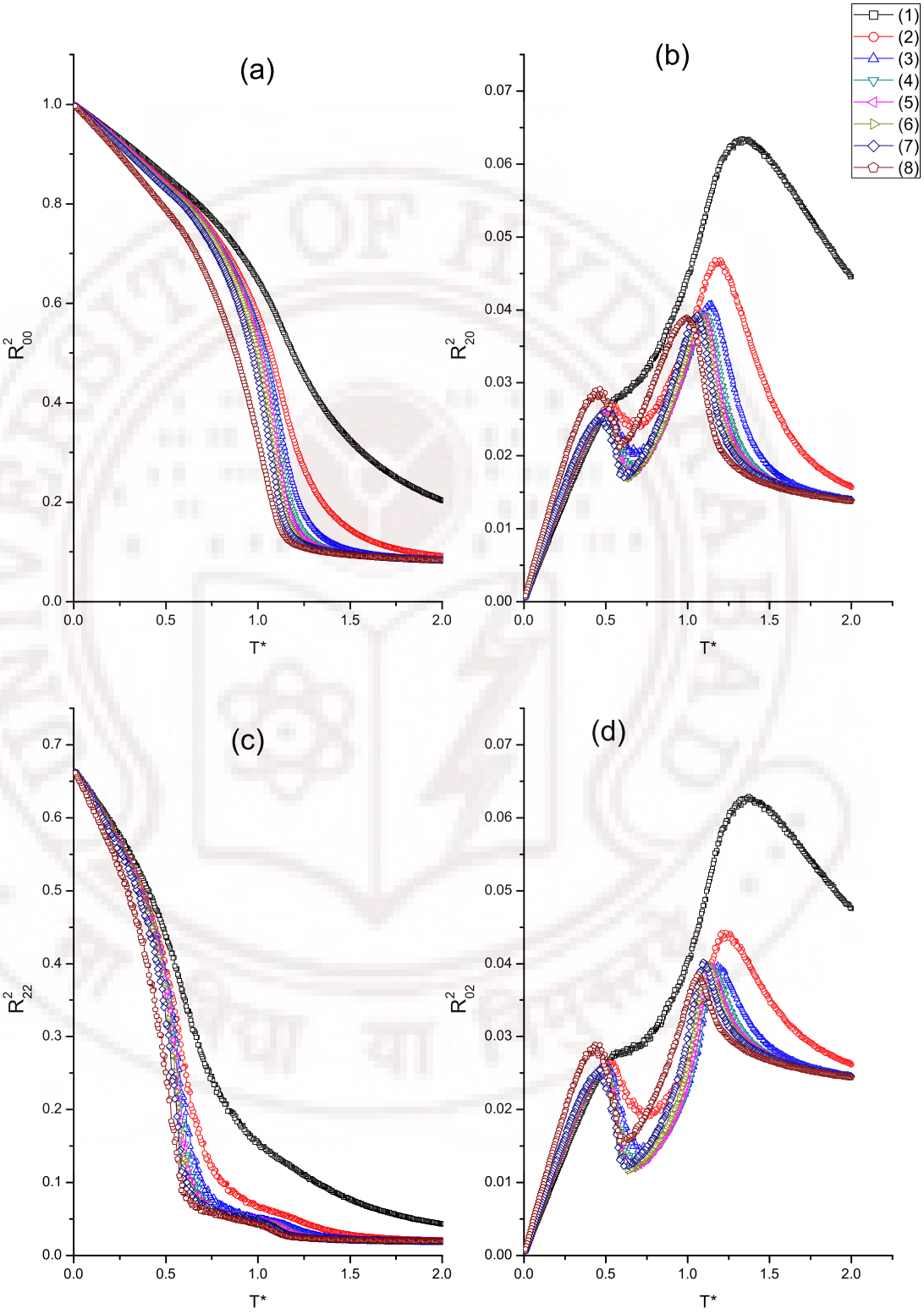

Figure 5.9: Variation of layer – wise (a) R^2_{00}, (b)R^2_{02}, (c)R^2_{20}, (d)R^2_{22} with temperature for a system with $\varepsilon_1 = 1.00$ and $\varepsilon_{nz} = 0.00$

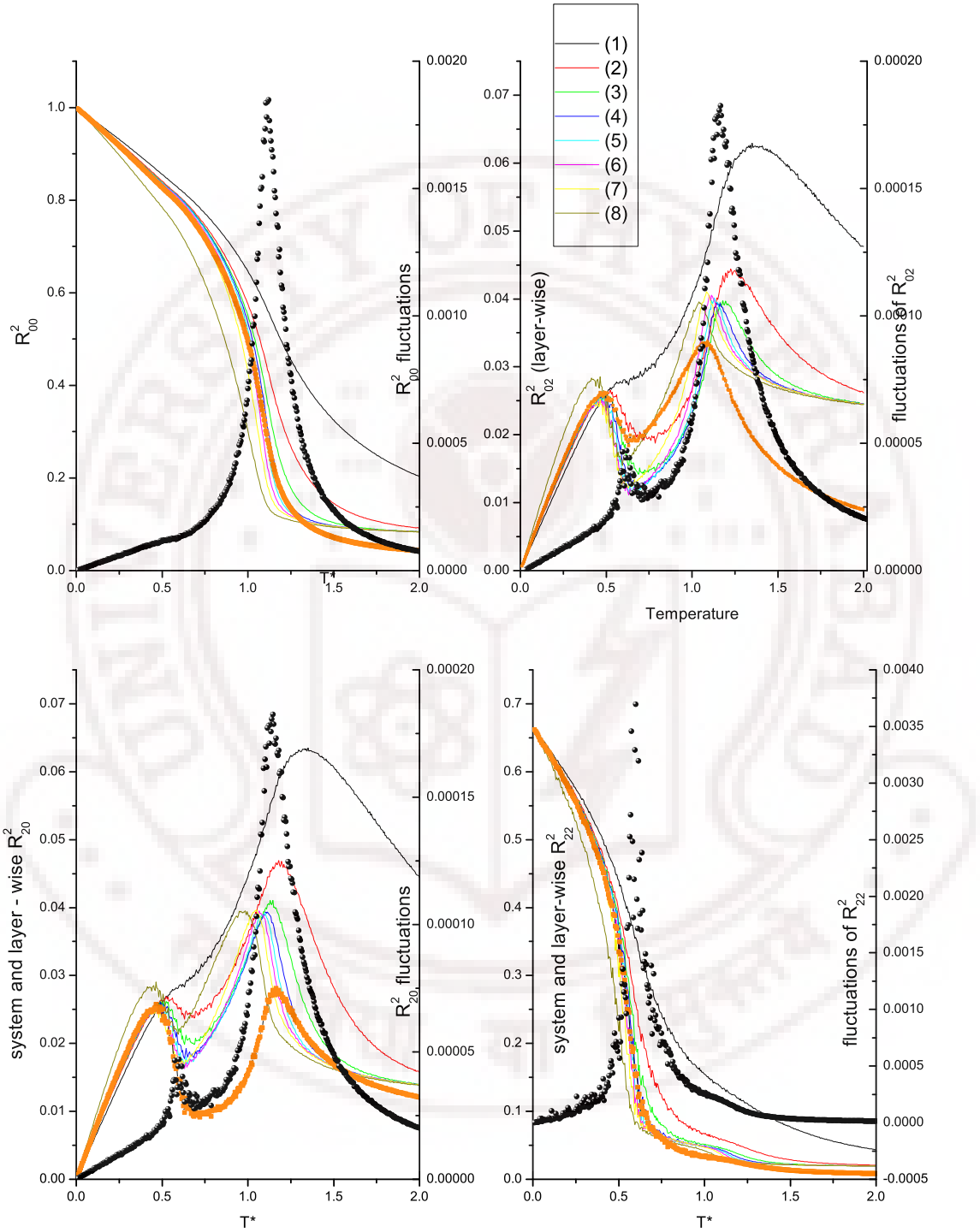

Figure 5.10: Variation of system and layer – wise (a) R^2_{00}, (b)R^2_{02}, (c)R^2_{20}, (d)R^2_{22} and the system order fluctuations with temperature for a system with $\varepsilon_1 = 1.00$ and $\varepsilon_{nz} = 0.2$ (orange – system order parameter; scatter black – system order fluctuations; lines – layer – wise order parameters)

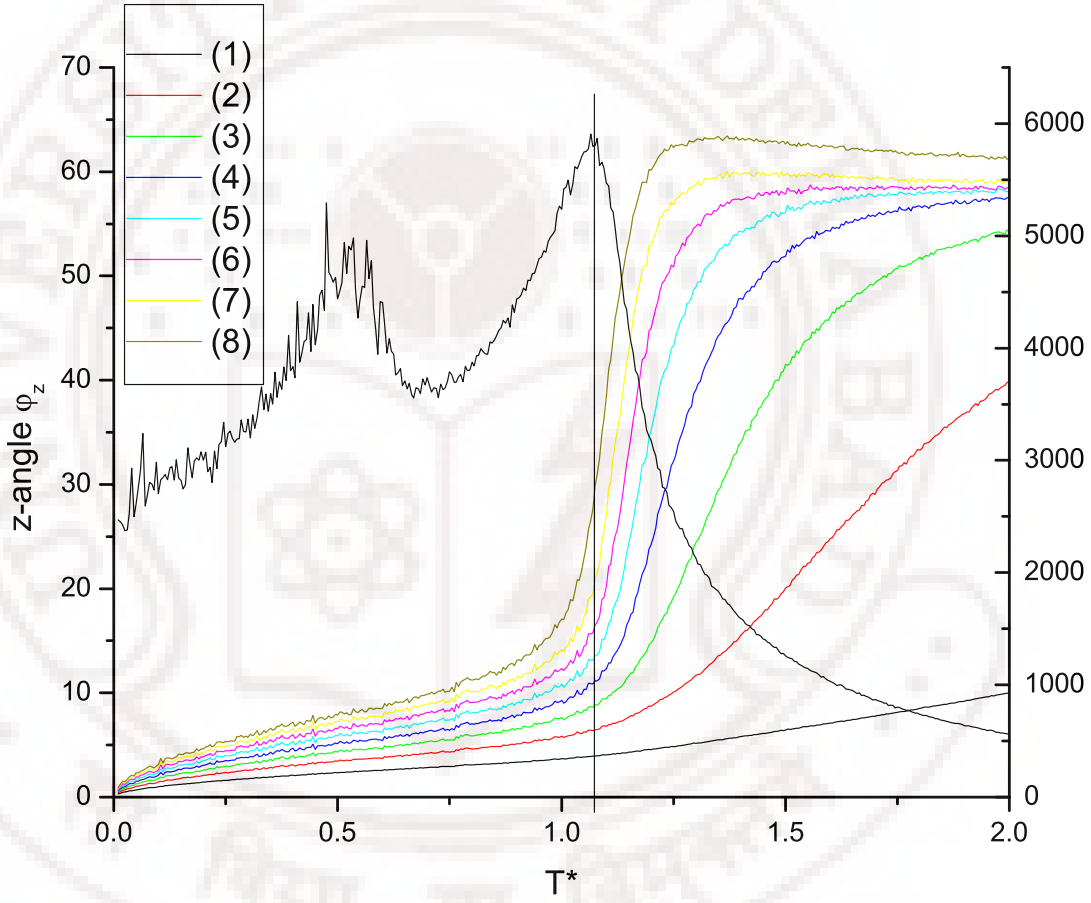

Figure 5.11: Variation of the z tilt angle φ_z and the specific heat C_V with temperature for a system with $\varepsilon_1 = 1.00$ and $\varepsilon_{nz} = 0.2$

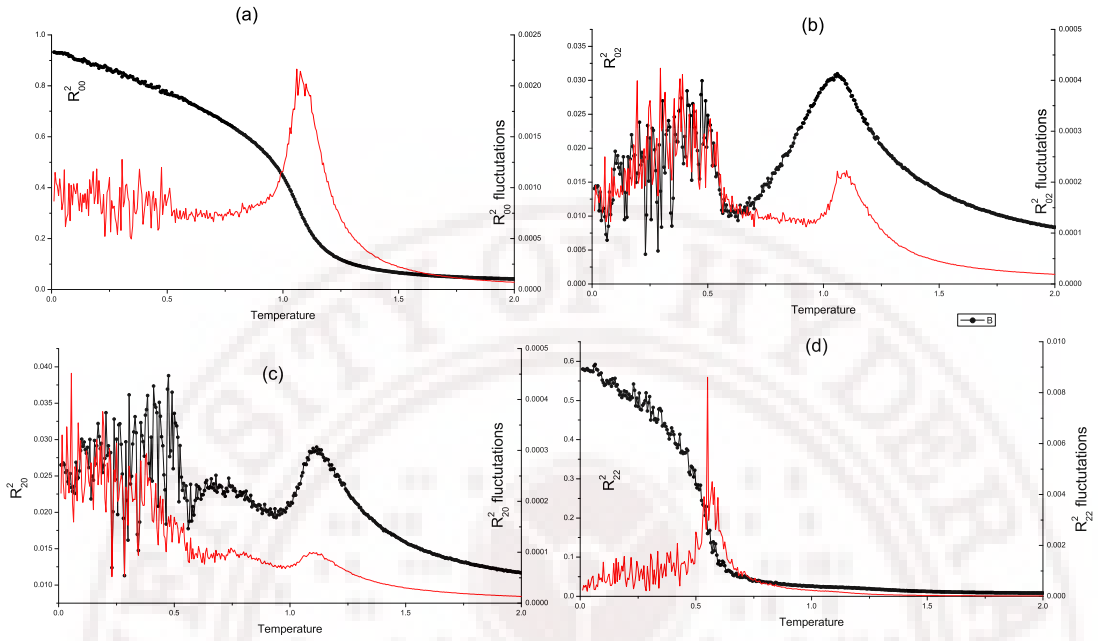

Figure 5.12: Variation of (a) R^2_{00}, (b)R^2_{02}, (c)R^2_{20}, (d)R^2_{22} and their fluctuations with temperature for a system with $\varepsilon_1 = 1.00$ and $\varepsilon_{nz} = 0.4$ (black – order parameter; red – susceptibilities)

System 5 (Table 5.1): [$\varepsilon_1 = 1.00$ and $\varepsilon_{nz} = 0.4$]

Increasing ε_{nz} to 0.4 it is observed that there were dominant changes in all the parameters computed. The specific heat profile shows up with two transitions similar to the above systems discussed. Plotting of this parameter does not give an indication to the effect of confinement. The bulk order parameters $R^2_{00}, R^2_{02}, R^2_{20}$ and R^2_{22} show quantitative changes when plotted with the variation in temperature. The system order parameter that was used to be a monotonically increasing curve with temperature shows slight fluctuation at the lower temperatures and shows up as fluctuations in the susceptibility (figure 5.12 (a)). Such a feature was observed in the R^2_{02} and R^2_{20} also, these fluctuations were observed only after the occurrence of the second transition ($T_{C1}, T^* < 0.5$). Unlike the system that is confined between substrates with anchoring strength $\varepsilon_1 = \varepsilon_{nz} = 1.00$, here the R^2_{22} has some fluctuations which was rather a smooth cure perviously (figure 5.3). It is interesting to note that the features in the layer – wise order parameters show some fluctuations that were

not present in the above studied systems. For $\varepsilon_{nz} = 1.00$, it was observed that the layer – wise order parameters were smooth plots with out any fluctuations. After the onset of the transition T_{C1}, the effect of confinement is observed as fluctuations in the layer – wise order parameters and the bulk order parameters. The profiles of all the order parameters are changed increasing the anchoring strength $\varepsilon_{nz} = 0.4$, when the temperatures are reduced lesser than 0.53. The biaxiality parameter R^2_{22}, which was a smooth increasing function until $\varepsilon_{nz} = 0.3$, shows sudden fluctuations at the lower temperatures. The phase biaxiality parameter R^2_{20} and the order induced in the Z direction due to the molecular x and y components R^2_{02} show sudden change in the profiles and their susceptibilities have high order of fluctuation at the lower temperatures (figures 5.12(b) and (c)). From plotting the z component tilt – angle the effect of the second substrate on the layers is clear by change in the layer director angles compared to the systems with lesser ε_{nz}. Figure 5.13 (b) gives the layer – wise tilt angle made by the molecular y with the laboratory Z axis. The layer – wise order parameters do not show prominent changes as the system order parameters. These various features observed by increasing the anchoring strength is due to the sudden effect of confinement on the film. This anchoring strength $\varepsilon_{nz} = 0.4$, seem to be a threshold anchoring strength, as there are notable changes in all the order parameters. With the further increase in ε_{nz} the fluctuation in the order parameter reduce, giving rise to new phases as discussed above section.

System 9 (Table 5.1): [$\varepsilon_1 = 1.00$ and $\varepsilon_{nz} = 0.8$]

Increasing the anchoring strength to about 80% of the LC – LC interaction ($\varepsilon_{nz} = 0.8$), the effect of enhanced competing order induced into the system is observed. Every system order parameter (figure 5.15) shows the effect after onset of a biaxial phase. The phase biaxiality R^2_{20} shows a sudden increase, compared to system with anchoring strength lesser than 0.4 (figure 5.10). The molecular z component tilt angle gives clear understanding on the effect of confinement (figure 5.16). The onset of the biaxial nematic phase and increase of confinement make every layer tilt angle reduce by 3^o. It is interesting to note angle

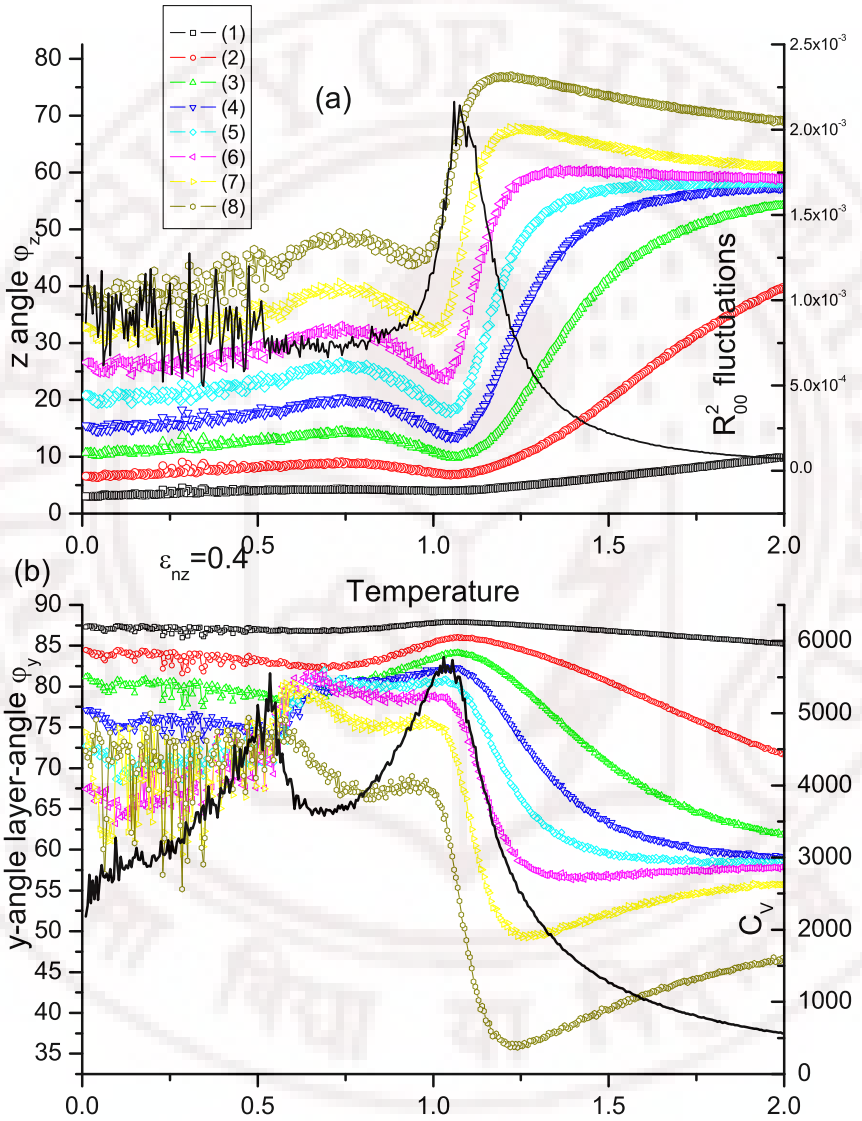

Figure 5.13: (a) Variation of z – tilt angle φ_z and R^2_{00} susceptibility with temperature (b)Variation of y – tilt angle φ_y and specific heat (C_V).

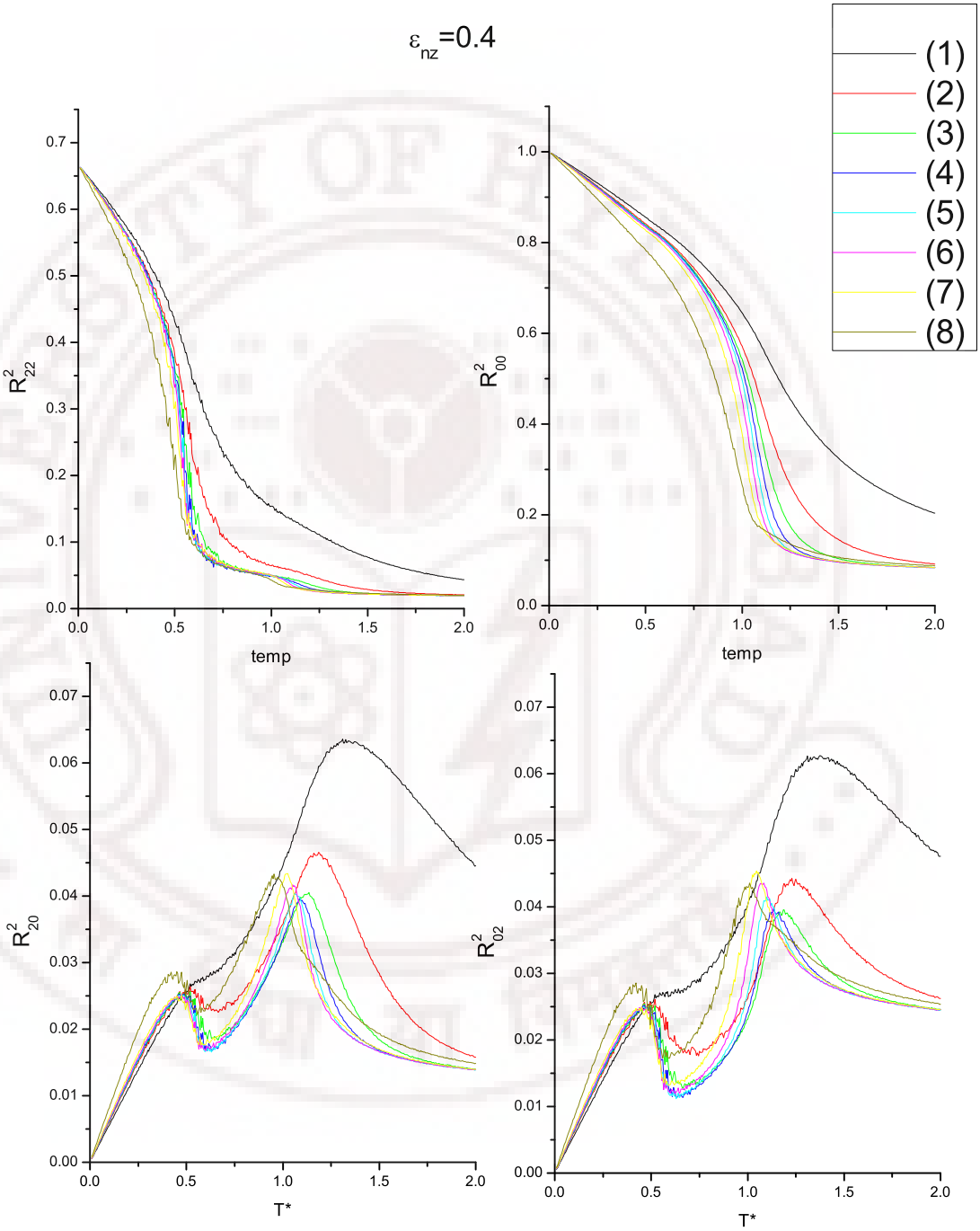

Figure 5.14: Variation of layer – wise (a) R^2_{22}, (b)R^2_{00}, (c)R^2_{20}, (d)R^2_{02} temperature for a system with $\varepsilon_1 = 1.00$ and $\varepsilon_{nz} = 0.4$

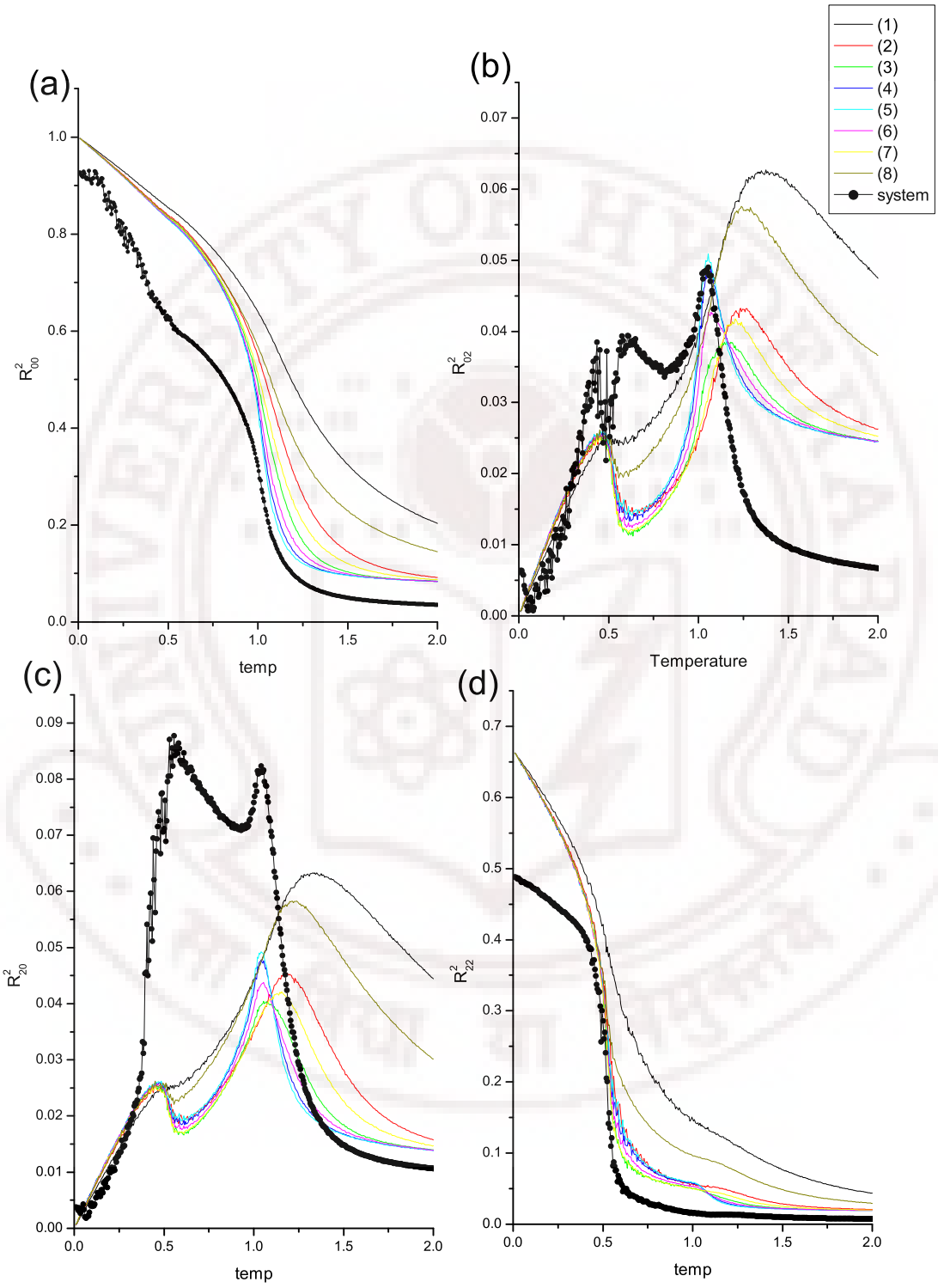

Figure 5.15: Variation of system and layer – wise (a) R^2_{00}, (b)R^2_{02}, (c)R^2_{20}, (d)R^2_{222} temperature for a system with $\varepsilon_1 = 1.00$ and $\varepsilon_{nz} = 0.8$

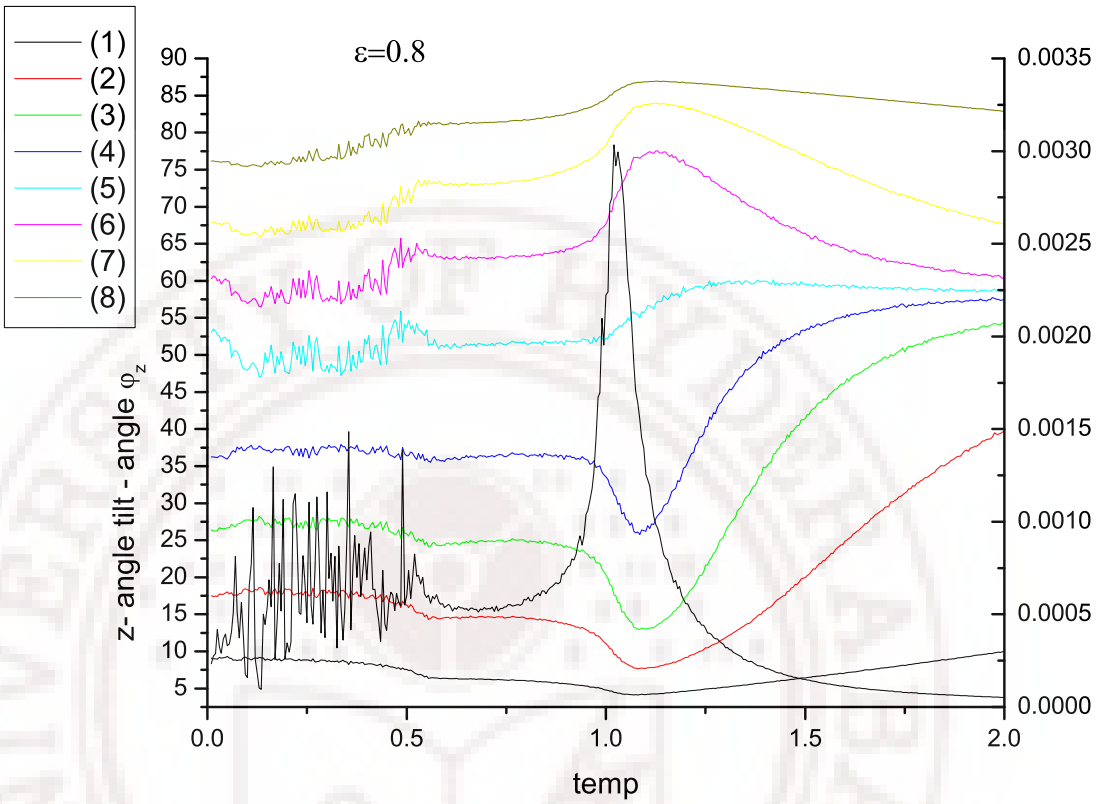

Figure 5.16: Variation of z – tilt angle φ_z and R^2_{00} susceptibility with temperature.

variations with temperatures at least temperature. The tilt angle which was trying to settle at an angle 3^o lesser tries to settle back at the angle before the onset of the biaxial phase. (figure 5.5).

The effect of increasing the anchoring strength is better brought out by plotting the various order parameters obtained for each of the 11 systems (indicated in the Table 5.1). Subtle changes were observed in every parameter from one system to another as ε_{nz} was increased, and a comparative discussion is presented below. Changes in the anchoring strength ϵ_{nz} seem to lead to many interesting new features. With the increase in ϵ_{nz} the energy profile remains the same but the minimum energy seems to decrease by 100 units for $\epsilon_{nz} = 1.00$ as compared to $\epsilon_{nz} = 0.00$. It is also observed that there is a decrease in the transition temperature T_{C1} with the increase in ϵ_{nz} from the specific heat profiles (figure 5.17). The system order parameter (R^2_{00}) shows a curious change in its profile

with the increase in anchoring strength of the substrate at $k = nz$. This order parameter, which was a smooth monotonically increasing curve for systems 1, 2, and 3, starts to show fluctuations at the lower temperatures for higher ϵ_{nz} (*i.e.* for $\varepsilon_{nz} \geq 0.3$). With further increase in ϵ_{nz} to 0.7, the order parameter shows a rapid increase in its value (figure 5.18) and develops a step – like profile. Concurrent with the change in R^2_{00}, it is observed that the fluctuations in the order (R^2_{00}) develop a second peak at these lower temperatures. For values of ϵ_{nz} greater than 0.7 another peak is observed at a temperature of about 0.365. It is seen that the (R^2_{02}) (figure 5.19) of system increases when ϵ_{nz} is increased and also exhibits changes in its profile. The corresponding fluctuations in R^2_{02} indicate the development of another peak at lower temperatures, similar to the effects observed in the case of R^2_{00}. The phase biaxiality (R^2_{20}) shows a different trend compared to the R^2_{02}, decreases at $\epsilon_{nz} = 0.4$ and then increases (figure 5.20). There is a similar change in R^2_{20} fluctuations as in R^2_{02} fluctuations, a new peak develops at the lower temperatures for higher ϵ_{nz} . The step size of biaxiality parameter R^2_{22} in the low temperature than decrease with the increase of ε_{nz} and the transition becomes sharper (figure 5.21). This change in the biaxiality parameter R^2_{22} (arises purely from molecular biaxiality) indicates clearly that the biaxial symmetry of the film is reduced by introducing increasing hybrid biaxial anchoring at the second substrate (figure 5.21).

It is seen that the effect of increasingly restricting confinement gave rise to different structures in a hybrid film of biaxial molecules while salient features of the bulk phase sequence seem to be present. A temperature variation study showed the presence of two different structures from the system order parameter and its fluctuations. It is seen that with the change in anchoring strength (ε_{nz}), the profiles of different order parameters showed the presence of new structures. The angle made by the z-component of the biaxial particles with the laboratory Z-axis gave a useful insight to the effect of anchoring. In order to understand the effect of anchoring and look out for an anchoring transition from each of the system studied in table 5.1, the data at a very low temperature, say 0.25 was considered. The different order parameters $R^2_{00}, R^2_{02}, R^2_{20}, R^2_{22}$ were tabulated and plotted (figure 5.23).

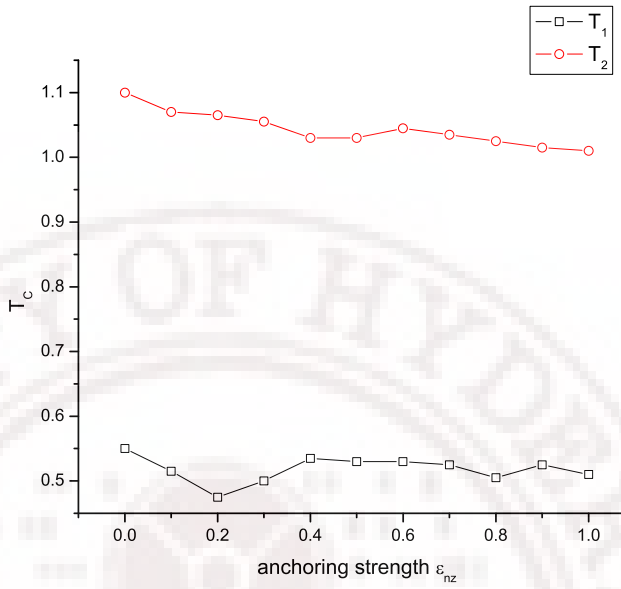

Figure 5.17: The transition temperatures of the two peaks for all the ϵ_{nz} anchoring strengths between 0 to 1 in steps of 0.1

It was seen that at $\epsilon_{nz} = 0.4$ all the order parameters show abrupt change in their profiles. The system order parameter R^2_{00} which was at the value of 0.92 reduces to around 0.82 after the critical anchoring 0.4. The biaxiality parameter R^2_{22} which was a constant at 0.56 before $\epsilon_{nz} = 0.4$ comes down to a value 0.50 from which it starts to reduce with the further increase in the anchoring strength. The phase biaxiality (R^2_{20}) shows a sudden change at the anchoring 0.4 and comes to a constant at 0.015 again. The (R^2_{02}) order parameter at $\epsilon_{nz} = 0.4$ has a sudden dip from 0.016 to 0.002 and recovers the constant value for higher anchoring. The layer – wise director angles were plotted for every anchoring strength at this temperature 0.25 (figure 5.22). It is seen that the angle slope changes as ϵ_{nz} is changed beyond 0.3. This change occur at the same ϵ_{nz} as that realized in order parameters too. These above observations point to the occurrence of anchoring induced transition in the structure of the hybrid biaxial LC film in its biaxial nematic phase. A fanning angle (θ) is defined to represent these structural changes, as the difference in the z-angle of the eighth (nz = 8) say φ_8 and the first layers (nz = 1) say φ_1 (figure 5.24). This parameter θ shows a sudden change from a zero value at $\varepsilon_{nz} = 0.4$ to a non-zero value, indicating a transition.

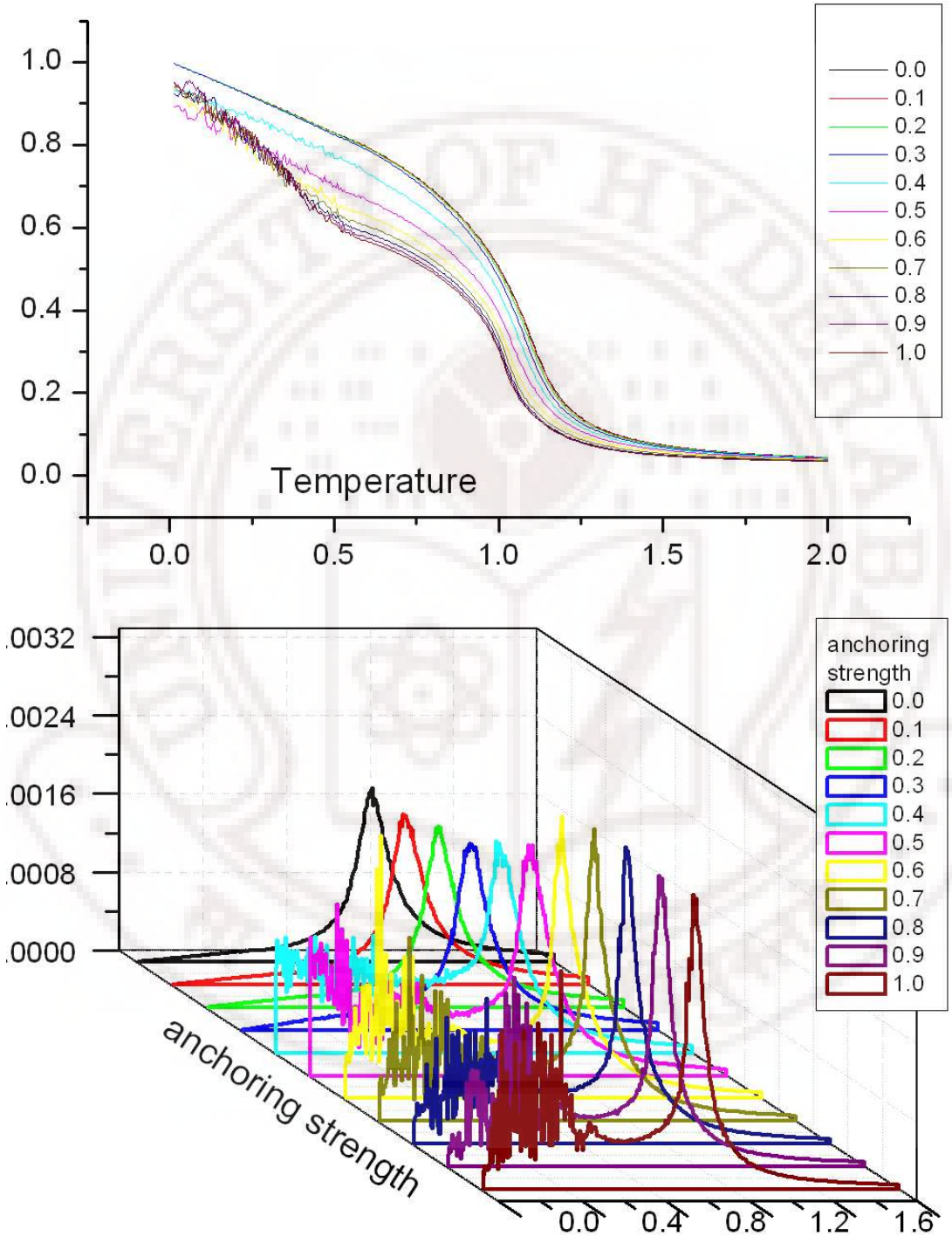

Figure 5.18: For every anchoring strength $(\epsilon_{nz}, \epsilon_1 = 1.00)$ the system order parameter R^2_{00} and its fluctuations

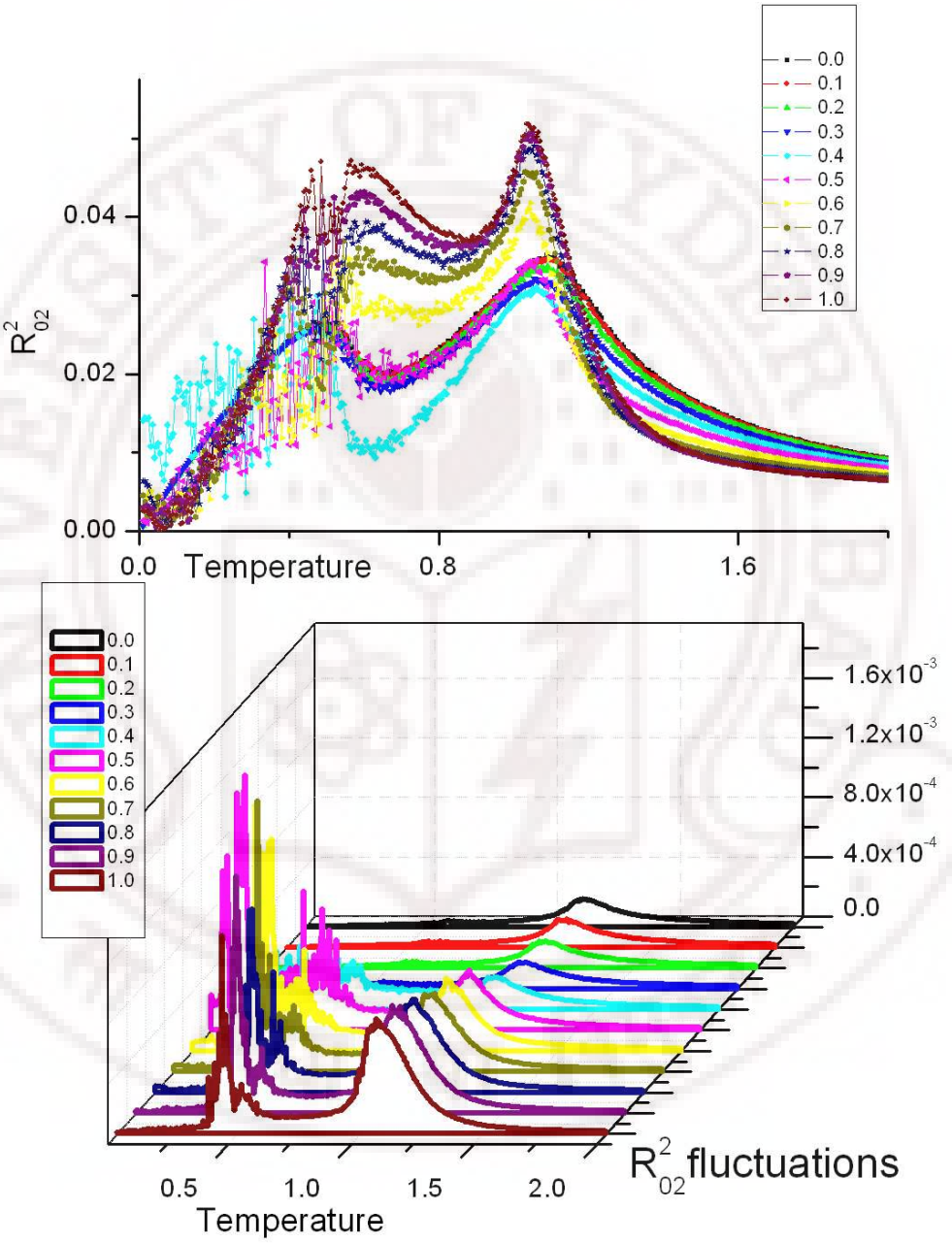

Figure 5.19: Variation in R^2_{02} and its fluctuations with temperature for all the systems (Table 5.1)

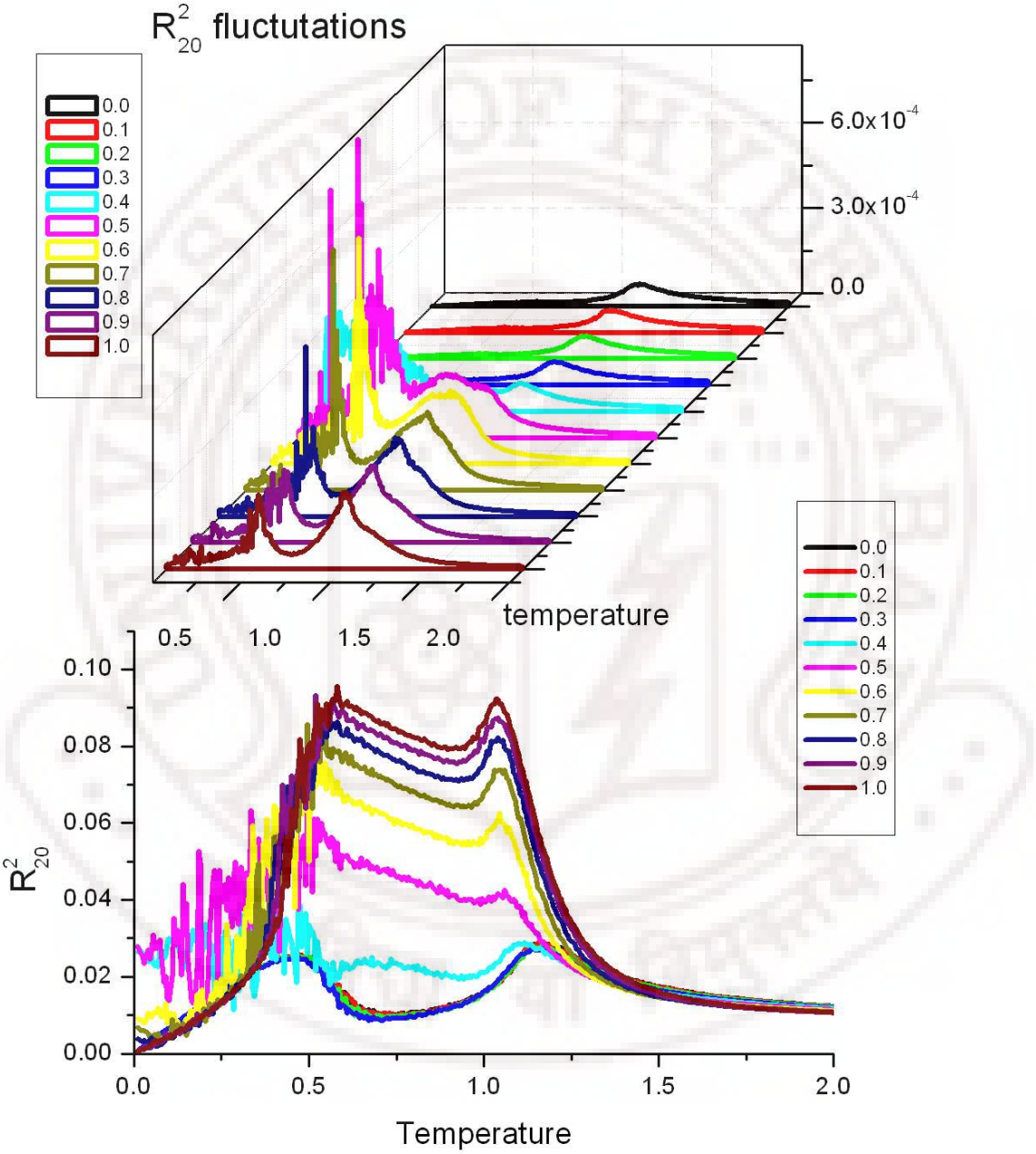

Figure 5.20: Change in phase biaxiality R^2_{20} and its fluctuations for different anchoring strength ϵ_{nz} keeping $\epsilon_1 = 1.00$.

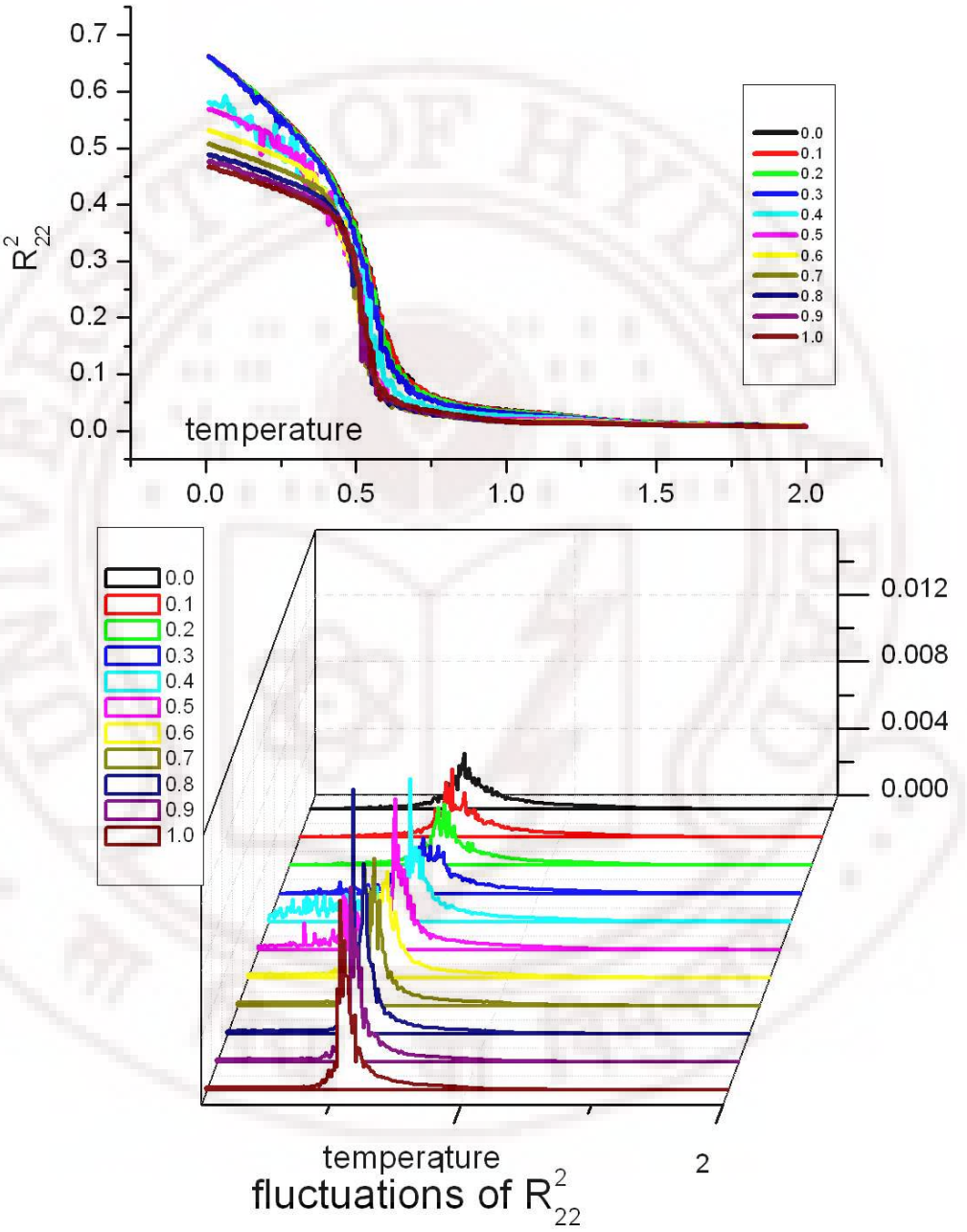

Figure 5.21: The biaxiality parameter R^2_{22} and its fluctuations for every system in table 5.1 with variations in temperature.

Considering the discussion of variation of different order parameters and their fluctuations as a function of ε_{nz}, it appears that the system is undergoing a subtle structural change, in its biaxial nematic phase as the anchoring strength is gradually scanned, thereby setting up a typical influence percolating from two surfaces.

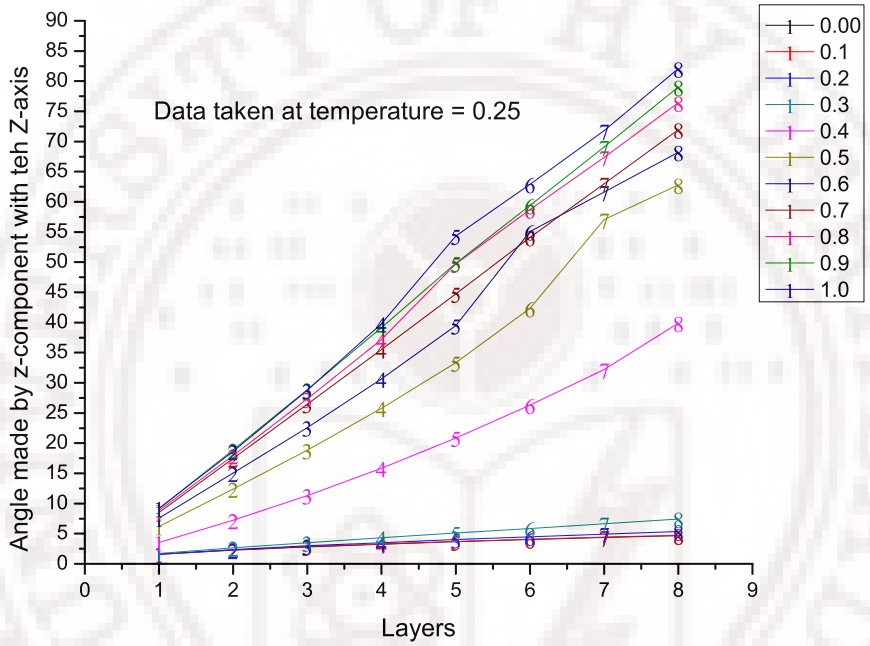

Figure 5.22: The angles for every layer plotted with the anchoring strength variation at temperature 0.25

5.5 Conclusions

A hybrid film of biaxial liquid crystal was modeled, using a lattice hamiltonian. This confinement showed the presence of a new structure when the order parameter and the director angles were plotted with temperature. The first – a higher temperature phase is characterized entirely by the phase biaxiality – we refer to this nematic phase as N_{pB}. With further decrease in temperature, there is another transition occurring from N_{pB} to another biaxial phase say N_{mB}. The second order phase is now entirely characterized by the molecular biaxiality and is indicated by the onset of R^2_{22}. It may further be seen that the

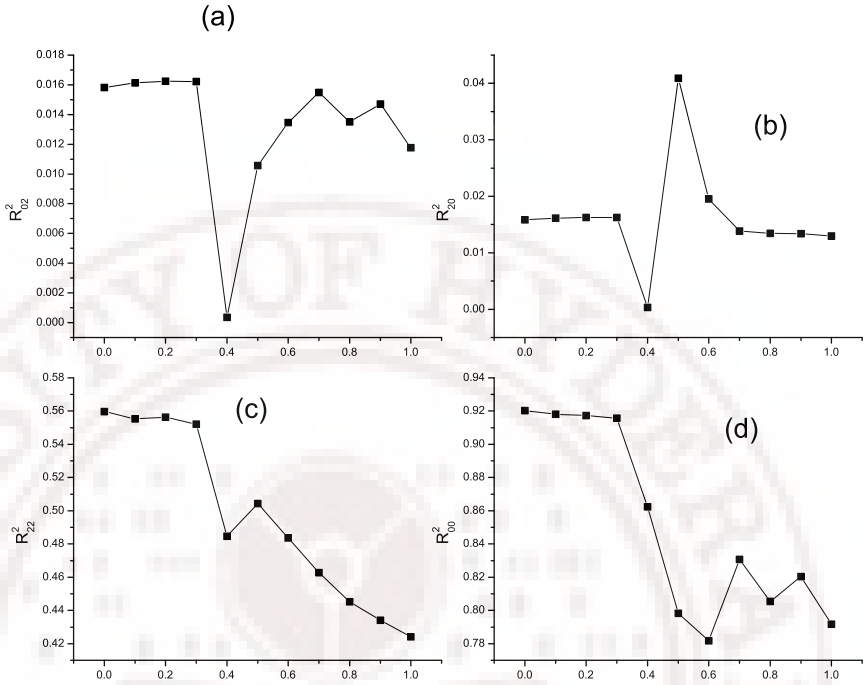

Figure 5.23: The order parameters with anchoring strength at temperature 0.25.

order parameter R^2_{02} is also non – zero only in the N_{pB} phase, indicating that there could be a small contribution to the order in the Z – direction only as long as molecular biaxial components are arranged to zero in this nematic phase. Anchoring transition was observed when the anchoring strength of one of the substrates was changed in steps of 0.1 from 0 to 1. All the parameters showed a change in their profile at anchoring strength 0.4 (ϵ_2). Variation of different order parameters and their fluctuations as a function of ε_{nz}, it appears that the system is undergoing a subtle structural change, in its biaxial nematic phase as the anchoring strength is gradually scanned, thereby setting up a typical influence percolating from two surfaces. It is observed from the R^2_{22} susceptibility that the transition gets sharper after the onset of the anchoring transition $(\varepsilon_{nz} = 0.4)$ for higher anchoring strengths ε_{nz}.

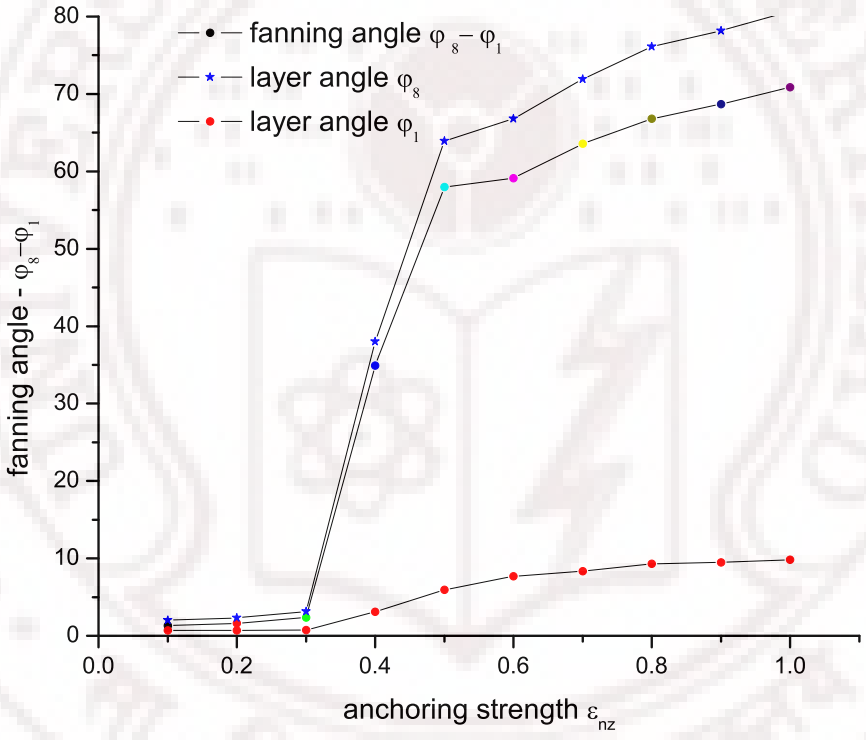

Figure 5.24: The fanning angle φ with anchoring strength variation.

Bibliography

[1] G. R. Luckhurst. Liquid crystals - a missing phase found at last? *Nature*, 430:413, 2004.

[2] G.R.Luckhurst. Biaxail nematic liquid crytsal: fact or fiction? *Thin Solid Films*, 393:40–52, 2001.

[3] J.P.Straley. Ordered phases of a liquid of biaxial particle. *Phys. Rev. A*, 10(5):1881, 1974.

[4] M. J. Freiser. Ordered states of nematic liquid. *Phys. Rev. Lett.*, 24(19):1041, 1970.

[5] M. J. Freiser. Successive transitions in a nematic liquid. *Mol. Cryst. Liq. Cryst.*, 14:165–182, 1971.

[6] B. R. Acharya, A. Primak, and S. Kumar. Biaxial nematic phase in bent-core thermotropic mesogens. *PRL*, 92:145506–1, 2004.

[7] K. Merkel, A. Kocot, J. K. Vij, R. Korlacki, G. H. Mehl, and T. Meyer. Thermotropic biaxial nematic phase in liquid crystalline organo-siloxane tetrapodes. *Phys. Rev. Lett.*, 93:237801, 2004.

[8] J. L. Figueirinhas, C. Cruz, D. Filip, G. Feio, A. C. Ribeiro, Y. Frere, T. Meyer, and G. H. Mehl. Deuterium nmr investigation of the biaxial nematic phase in an organosiloxane tetrapode. *Phys. Rev. Lett.*, 94:107802, 2005.

[9] Michael P. Allen. Computer simulation of a biaxial liquid crystal. *Liquid Crystals*, 8(4):499 – 511, 1990.

[10] R. Berardi, C. Fava, and C. Zannoni. A generalized gay- berne intermolecular potential for biaxial particles. *Chem. Phys. Lett.*, 236:462, 1990.

[11] C. Chiccoli, P. Pasini, Ivan Feruli, and C. Zannoni. Biaxial nematic droplet and their optical textures: A lattice model computer simulaiton study. *Mol. Cryst. Liq. cryst.*, 441:319–328, 2005.

[12] B.Jerome. *Rep. Prog. Phys.*, 54:391, 1991.

[13] O. Lavrentrovich. *Defects in liquid crystals: computer simulations, theory and experiments*, volume 43. Kluwer Academic Publishers, 2002.

[14] J.Cognard. *Mol. Cryst. Liq. Cryst. Suppl. 1*, 23:289, 1982.

[15] P.A. Lebwohl and G. Lasher. Nematic-liquid-crystal ordera monte carlo calculation. *Phys. Rev. A*, 6:426, 1972.

[16] J. G. Gay and B. J. Berne. Modification of the overlap potential to mimic a linear sitesite potential. *J. Chem. Phys.*, 74:3316, 1981.

[17] Claudio Zannoni and Paolo Pasini. *Advances in the Computer Simulations of Liquid Crystals*, volume 545. Kluwer Academic Publishers, December 1999.

[18] Greg D. Wall and Douglas J. Cleaver. Computer simulation studies of confined liquid-crystal films. *Phys. rev. E*, 56(4):4306–4316, 1997.

[19] C. Chiccoli, P. Pasini, O.Lavrentovich, and C. Zannoni. Monte carlo simulations of stable point defect defects in hybrid nematic films. *Phys Rev. lett.*, 79(22):4401, 1997.

[20] C. Chiccoli, P. Pasini, Ivan Feruli, and C. Zannoni. Simulation of topological defects in nematic liquid crystal films. *Mol. Cryst. Liq. cryst.*, 398:195–206, 2003.

[21] C. Chiccoli, I. Feruli, O. D. Lavrentovich, P. Pasini, S.V. Shiyanovskii, and C. Zannoni. Topological defects in schlieren textures of biaxial and uniaxial nematics. *Phys. Rev. E Rapid Comm.*, 66:030701–030701.4, 2002.

[22] A.Sarlah and S.Zumer. Equlibrium structures and pretransitional fluctuations in a very thin hybrid nematic film. *Phys Rev. E*, 60(2):1821, 1999.

[23] Andreja $\check{S}arlah$. PhD thesis.

[24] C. Chiccoli, P. Pasini, A.Sarlah, C. Zannoni, and S.Zumer. Structures and transitions in thin hybrid nematic films: A monte carlo study. *Phys Rev. E*, 67:050703(R), 2003.

[25] C. Chiccoli, S.P. Gouripeddi, P. Pasini, K.P.N. Murthy, and C. Zannoni V.S.S. Sastry. Hybrid nematic films: A detailed monte carlo investigation. *Mol. Cryst. Liq. Cryst.*, submitted, 2008.

[26] G. Sai Preeti, V. Vijay Kumar, V.S.S. Sastry, and K.P.N. Murthy. Monte carlo study of radial and axial ordering in cylindrical films of liquid crystal. *Computational Materials Science*, 44(1):180–184, 2008.

[27] C. Chiccoli, P. Pasini, F. Semeria, and C. Zannoni. A detailed monte carlo investigation of the tricritical region of a biaxial liquid crystal system. *Int. J. Mod. Phys. C*, 10:469–476, 1999.

[28] F. Biscarini, C. Chiccoli, P. Pasini, F. Semeria, and C. Zannoni. Phase diagram and orientational order in a biaxial lattice model. a monte carlo study. *Phys. Rev. Lett.*, 75:1803, 1995.

[29] Silvano Romano. Computer simulation of a biaxial nematogenic model on a three-dimensional lattice and based on a recently proposed interaction potential. *Physica A*, 337:505 519, 2004.

[30] Robert J Low. Measuring order and biaxiality. *Eur. J. Phys.*, 23:111–117, 2002.

Chapter 6

Anchoring Transition and Influence of Director Fluctuations in Liquid Crystal Droplets

6.1 Introduction

Polymer-dispersed liquid crystals (PDLC) [1] are a relatively new class of materials that hold promise for many applications ranging from switchable windows to projection displays. These materials, which are simply provide useful boundary condition for nice spherical LC droplets, are the focus of extensive research in the display industry. PDLCs consist of liquid crystal droplets that are dispersed in a solid polymer matrix. The resulting material is a sort of "swiss cheese" (Figure 6.1) polymer with liquid crystal droplets filling in the holes. These tiny droplets (a few microns across for practical applications) are responsible for the unique behavior of the material. By changing the orientation of the liquid crystal molecules with an electric field, it is possible to vary the intensity of transmitted light. These system are of great interest in technology for display [2]. These systems have been subjected of considerable research, especially from the point of view of understanding the physics of the different structures that can be formed.

Deuterium NMR was used to study submicron-size droplets of monomeric liquid crystal dispersed in solid polymer matrix [3], with special focus on the director fluctuations were monitored too. The deformations were also investigated in a PDLC sample, by applying a varying electric field was applied in addition to the magnetic filed of the NMR [4]. It was shown that for droplets of size larger than 0.35 μm (diameter) N-I transition is first

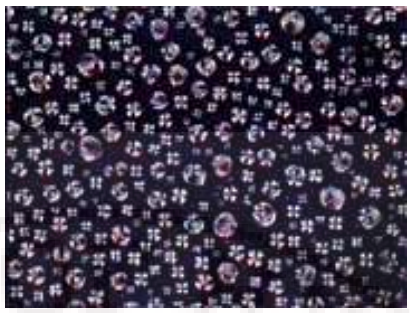

Figure 6.1: An illustrative picture of PDLC

order; and for lesser than 0.35 μm it is continuous with a paranematic phase. The deformations of spherical droplet shapes into randomly oriented rotational ellipsoids were also investigated both by theoretical and experiential methods. The orientational order in stretched polymer dispersed liquid crystal was investigated using deuterium NMR in the nematic and in isotropic phases [5]. It shows that the surface value of the order parameter turns out to be largely temperature independent and is seen to increase with increasing strain. Light scattering and electro – optic response was used to study micro – droplets of nematic liquid crystal which are spontaneously formed in a solid polymer at the time of polymerization [6]. Electro-optic properties of PDLC show a reversible optical response from an opaque state to a highly transmitting state under the action of an appropriate electric field which aligns the liquid crystal director [7]. Light control films consisting of submicron liquid crystal droplets dispersed in ultraviolet-cured polymer matrices, which can respond optically to both applied electric fields and temperature changes, were formed potentially useful for displays and light shutters [8]. The optomechanical properties of a polymer dispersed liquid crystal film were investigated by simultaneously measuring the stress-strain and polarization dependent optical transmission characteristics. The polymer alignment at the interface increases the droplet order parameter along the stretch axis, consistent with the results of the optical and mechanical experiments [9].

Holographic polymer dispersed liquid crystal materials were studied using NMR and dynamic light scattering methods, which were prepared for switchable diffractive optical

elements [10]. Their reflection peaks were tuned as a function of applied voltage [11]. Theoretical studies showed stripe pattern formation when a holographic PDLC induced phase separation via anisotropic pattern photo-polymerization [12]. In real systems, the radial structure occurs more frequently than the diametrical ones. Continuous structure transitions in a spherical chiral nematic droplet under the influence of an electric field was studied [13]. Cholesteric liquid crystal droplets embedded in a medium which enforce parallel surface anchoring was treated. The Frank's free energy was minimized to study disclination lines of integer and half-integer values [14]. Theoretical studies on the stability of uniaxial nematic liquid crystalline structure in supra-micronm-size spherical cavities that impose a weal homeotropic anchoring were carried out [15]. These predicted a triple point of radial, non singular axial and axial structure. Such a droplet was also studied using scattering matrix and nematic differential cross section [16]. Scattering patterns were calculated in detail for the three different nematic director's configurations: one characteristic of a droplet in a strong external field, the other characteristic of a droplet outside the field in the case normal surface anchoring and their characteristics of an isotropic droplet with a surface induced nematic layer. Ordering in bipolar liquid crystal droplets was also studied close to the nematic – isotropic transition. The droplet structure was obtained by minimization of Landau-de-Gennes free energy [17]. It is observed that there was a growth of a polar defect toward the center of the droplet. Similarly a spherical submicrometer droplet embedded in a solid polymer was studied using Landau-de-Gennes theory [18]. For a droplet with a radial structure, the strength of the nematic polymer interfacial interaction affects the nematic – paranematic phase transition, and may in addition induce a boundary layer nematic phase. Rayleigh-Gans approximation was used to derive the scattering matrix, differential cross section and the total cross section for a small nematic droplet [19]. Earlier simulations [20] based on LL model have clearly shown that the size of this inner uniaxial core is independent of the actual size of the droplet (assuming that it is always bigger than the core region) [21], and it is essentially determined by the nature of the Hamiltonian chosen. To make this scenario quantitative, the concept of radial order parameter S_R was

introduced to specify the degree of alignment of the LC region along the radial direction of the droplet, along with S which denotes the uniaxial ordering of the nematic phase [20]. These simulations focused on the temperature dependence of the formation of the radial order, and its propagation to the inner layers, as the nematic phase is formed. Further studies were carried out on these droplets to understand the effects of applied external field [22] at various anchoring strengths at the polymer interface. Different molecular organizations were investigated by illustrating their influence on the simulated NMR spectra. Droplets with toroidal and bipolar boundary conditions were also studied using Monte Carlo simulation for different anchoring strengths and at different external fields [23] [24] [25] [26]. More recently a droplet of biaxial molecules was investigated using MC simulations based on a suitable lattice Hamiltonian [27] for the different kinds of defects formed in such systems [28].

A simple method for the simulation of the textures of nematic liquid droplets as observed through a polarization microscope was developed [29], using basic principles of transformation matrices in optics. When the system size is bigger than a particular size, experiments cannot readily be done, and in such cases simulations become very useful and important for studying such systems. Simulation studies were used to study the different structures and the defect formation in PDLC. To study the effect of different types of orders induced, different polymers that were modeled to give radial, toroidal, and bipolar order [20], [26]. A model droplet of 304 particles with radial order percolating in to the system due to the polymer was studied using Monte Carlo simulations [23]. The whole droplet was split in to shells of unit radius and numbered from the center of the droplet. Average energy and it derivative with temperature were studied to understand the transitions occurring in this system. Other than the above mentioned two parameters the system order parameter $< P_2 >$, the fourth order polynomial $< P_4 >$ and the radial order $< P_2 >_R$ were computed. These order parameters were computed for every shell of the droplet. The LL model [30] was used to simulate the system using the Metropolis algorithm, and the effect of anchoring strength 'J' was investigated [31]. It was seen that with changes in J the

radial order in the system changes dramatically. For higher values of J a hedgehog defect formation was observed in the center of the droplet which disappeared to give an ordered domain at lower anchoring strengths. A droplet in a polymer inducing toroidal surface order [25] was studied as a function of temperature, and with changes in the anchoring strength. Another study focussed on the effect of an external field on a droplet with radial order percolating due to the substrate interactions [32]. To understand this system better, NMR spectra (of ^{2}H nuclei attached to rigid core) were computed for different director organizations using Monte Carlo methods. At stronger fields the line-shape essentially reduces to a doublet corresponding to the parallel splitting, whereas at much lower fields it is the characteristic of a powder spectrum. A detailed simulation of NMR spectrum along with the order parameters were carried out to investigate the different molecular organizations comparable with external conditions. A similar study was done with the polymer matrix inducing a bipolar order, and here the external field magnitude was varied for both positive and negative susceptivity anisotropy [24]. Droplets were also modeled using Gay-Berne potential to induce radial order, and it was observed that radial order percolated only for large enough droplets [33]. Droplets with radial, bipolar, and random boundary conditions were also considered, and examined from the point of the influence of specific molecular motion on the ^{2}H NMR spectrum [34]. The effects of molecular motion such as fluctuations of molecular long axes and translational diffusion, and on external field ordering effects were computed [35]. Using NMR as a tool the development of a defect was observed in a droplet with bipolar boundary conditions [36]. When closer to the confining substrate diffusion is significantly slower than in the bulk liquid crystal, leading to in perceptible changes in the NMR spectra. Dynamic effects were calculated especially due to translational diffusion and on its slowing-down near the surface layer [37]. Molecular dynamics of a droplet placed at the liquid crystal interface between two different regions of the solid polymer matrix was studied.The interface accordingly separates the droplet into two hemispheres: the first of these is under radial boundary conditions; the second hemisphere is under bipolar boundary conditions were studied [38]. Using a simple model for

biaxial nematics [27], [39] a droplet was modeled [28]. Polarizing textures were used to study this system in comparison to uniaxial molecules for different boundary conditions.

In particular, these droplets of micrometer size, or less, were earlier investigated [18] under different anchoring conditions imposed by the bounding polymer matrix. The motivation originated both from the point of basic issues involved in determining the equilibrium structures in such soft model systems under confinement, as well as due to their applications as optical modulators [16] [29]. Of specific interest is a droplet subjected to radially ordering conditions at the polymer-substrate interface [23]. Markov chain Monte Carlo (MC) studies based on Lebwohl-Lasher (LL) model [30] show that the droplet, in its nematic phase and under strong anchoring conditions, is essentially radially ordered but for a small spherical region at the core which has the uniaxial nematic phase [22]. The origin of this core region is attributed to the delicate balance between energy penalty imposed by the radial ordering (at that curvature) and the energy expenditure involved in maintaining an interfacial spherical region (between the inner uniaxial ordering and outer radial ordering [31]). Obviously, this is dictated on one hand by the degree of the relevant elastic distortion sustainable (in this case the splay distortions) *vis-á-vis* the influence of the inter-molecular interactions to bring about uniaxial ordering.

One of the interesting questions that arises in this connection concerns the role of anchoring strength of the bounding surface in inducing radial order (at a given temperature in the nematic phase), and nature of the transition from a wholly uniaxial structure (when the bounding surface is completely ineffective in influencing the liquid crystal inside) to an essentially radial structure, as was observed in the earlier work under strong anchoring condition. The other important considerations include the role of the relevant elastic property (splay energy represented by the corresponding coefficient K_1) in determining the nature of this transition, the size of the inner uniaxial core that emerges, and also the extent of competition that it may provide at the interfacial region, betrayed by the fluctuations in the order parameters quantifying the equilibrium structure of the medium. In other words, use of a suitable Hamiltonian which can incorporate the elastic properties of the medium

while accounting for the nematic order of the liquid crystal would be very appropriate in the study of this problem. One of the questions addressed is whether the influence of the anchoring by the surface, and consequent induced radial order, could be viewed as due to a wetting phenomenon.

In this context, it may be noted that a lattice based Hamiltonian which explicitly takes into account, the elastic properties of the medium via the three elastic coefficients (splay (K_1), twist (K_2), and bend (K_3) elastic constants) was proposed earlier [40]. This interaction is computed for nearest neighbor lattice elements. Its application to Schadt-Helfrich cell was demonstrated through detailed Monte Carlo simulations [40]. In this work, we shall adopt this model to study the equilibrium director configurations of a PDLC droplet in its nematic phase under radial boundary conditions, with specific focus on anchoring transition induced by variable coupling to the polymer matrix, and the role of splay distortion.

6.2 Hamiltonian Used and Details of simulations

The model Hamiltonian used for this study is

$$\Phi_{jk} = \lambda \left[P_2\left(a_j\right) + P_2\left(a_k\right)\right] + \mu\left(a_j a_k b_{jk} - \frac{1}{9}\right) + \nu P_2\left(b_{jk}\right) + \rho\left[P_2\left(a_j\right) + P_2\left(a_k\right)\right] P_2\left(b_{jk}\right). \tag{6.2.1}$$

Here, P_2 is the second rank Legendre polynomial. The coefficients of expansion are related to the elastic constants through the following relations, involving the chosen linear dimension Λ of the volume element in the cubic lattice to represent their local directors:

$$\begin{aligned}
\lambda =& \frac{1}{3}\Lambda\left(2K_1 - 3K_2 + K_3\right) \\
\mu =& 3\Lambda\left(K_2 - K_1\right) \\
\nu =& \frac{1}{3}\Lambda\left(K_1 - 3K_2 + K_3\right) \\
\rho =& \frac{1}{3}\Lambda\left(K_1 - K_3\right).
\end{aligned} \tag{6.2.2}$$

An interesting feature of this potential is that Λ, enters as a length scale over which the director gradient is discretized and defines the lattice parameter corresponding to the distance between the neighboring sites. By setting all the elastic constants equal to each other, say K, the above potential is reduced to the form of the Lebwohl-Lasher potential. Under these special conditions, the energy scale parameter ϵ, is equal to ΛK for the present model. In general, the total free energy of the system is then given by

$$\Psi = \frac{1}{2}\sum_{j=1}^{N}\sum_{k=1}^{6}\Phi_{jk}, \tag{6.2.3}$$

where N is the number of sites. Following the procedure adopted earlier, the scaled potential for use in simulations is obtained by dividing equation 6.2.1 by $|\nu|$. This leads to a scaled temperature, to be used in the Monte Carlo scheme, given by

$$T^* = k_B T/|\nu| = 3k_B T/(\Lambda|K_1 - 3K_2 - K_3|). \tag{6.2.4}$$

A detailed description of this Hamiltonian is discussed in the Chapter 1 of this thesis.

A sufficiently large cubic lattice is considered and a sphere of chosen radius (in lattice units) is carved out [22]. Consequently the bounding surface will be a jagged sphere due to the discrete nature of the arrangement of lattice points. Each lattice point is associated with a local director say, spin averaged over molecules enclosed in the cubic volume element of dimension Λ. Each spin is associated with a unit vector oriented along that local director. The lattice sites inside the sphere represent local directors within the liquid crystal which participate in the Monte Carlo chain dynamics, while those outside the sphere with fixed desired orientations correspond to substrate imposing the required boundary conditions (in the present case, oriented towards the center so as to impose radial boundary conditions surface anchoring). These fixed molecules, representing the substrate, hence do not participate in the simulation moves.

The flexibility of this Hamiltonian is utilized to study the effect of elastic properties on the director distribution by taking the example of a liquid crystal with known elastic constants in the nematic medium for purposes of simulation in this work. Thus, we set the

values of K_1, K_2, and K_3 from the measurements on PAA taken at a reduced temperature T/T_{NI} equal to 0.963 as $7.0 \times 10^{-12}N$, 4.3×10^{-12}N, and 17.0×10^{-12}N, respectively [40]. The energy scale is set, for a given set of elastic constants, by the dimension of the volume element over which the local director is defined, and hence the effective temperature at which the canonical ensemble is constructed is determined by this choice of equation 6.2.4. From the previous studies on planar hybrid film [44] it was concluded that the continuum results could be recovered for a choice of this dimension typically in the range of a few hundred $\mathring{A}$ and above, corresponding to a typical reduced temperature T^* of 0.10 and below. Assignment of lower values of Λ, leading to higher values of T^*, would correspond to, in physical terms, appreciable fluctuations in the director field. It was found that for such effective high temperatures, the predicted results were not consistent with the expected behavior from continuum theory based on minimization procedures. Typical value for Λ above which the fluctuations are small enough to yield satisfactory simulated results consistent with experimental results was reported to be around 700 $\mathring{A}$.

Due to the symmetry of the problem (nematic droplet subjected to radial boundary conditions) only splay distortion is operative, and this convenient situation is exploited by extending these studies as a function of relative splay energy contribution, effective by varying the value of K_1 relative to the other elastic constants. To this end, the simulations are performed for different K_1 values at fixed K_2 and K_3, and the results are then discussed for convenience in terms of the ratio (called scale factor, say α) of the assigned K_1 value to its actual value.

These studies are also aimed at examining the influence of the surface anchoring on changes in the director structure, and accordingly we introduce a variable anchoring strength ε_S (in units of the energy scale set above), ranging from 0 to 1. This defines the strength of interaction between the liquid crystal molecules and the (orientationally) fixed molecules in the substrate. Introduction of this variable facilitates a study of possible anchoring induced structural transitions in the system.

Different physical properties are computed based on these simulations, and in order

to get an insight into the director structure inside the droplet, we consider the droplet to be comprising of concentric shells of a given width indexing them in ascending order as we move away from the center of the droplet. We report ensemble averages of different properties measured within each of the layers. The variables so computed include: uniaxial orientational order S_A, (referred to the axial order in the system), the radial order S_R, (measuring the degree of alignment of liquid crystal molecules along the radial direction in the droplet, computed from $\langle P_2(\cos(\theta_i))\rangle$ where θ_i is the angle made by each of the liquid crystal molecules in the droplet with respect to the local radial direction and the angular brackets represent the ensemble average over the sample as well over the Monte Carlo runs), RMS fluctuations in these orders within each concentric layer, and the rigid lattice limit NMR spectrum of a deuterium (located on the core of the molecule) expected of the system assuming that the Zeeman field is always applied parallel to the instantaneous director. We take known typical values for deuterium quadrupole coupling constants (175 kHz) and the C-D bond angle with respect to the long axis of the molecule 60^o.

Canonical ensembles at the fixed reduced temperature of 0.01 (corresponding to K_1, K_2, and K_3 values of $7.0 \times 10^{-12}N$, 4.3×10^{-12}N, 17.0×10^{-12}N respectively and Λ = 710 $\mathring{A}$) were constructed for a droplet with a radius of 15 lattice units using the Markov chain Monte Carlo simulation based Metropolis algorithm. The data for computation of the above physical property's variables were collected over 5 million Monte Carlo steps after ignoring the first 1 million steps for equilibration. The results are discussed below.

6.3 Results and discussion

With the scale factor fixed at unity (i.e. using the typical values of the elastic coefficients of PAA as such), we see an anchoring mediated structural transition of the director configuration as depicted in figure 6.2. Both S_A and S_R show a sudden jump at $\varepsilon_S \sim 0.54$. When ε_S is close to zero, the surface does not have a significant influence on the director structure and the droplet has predominantly uniaxial director configuration represented by

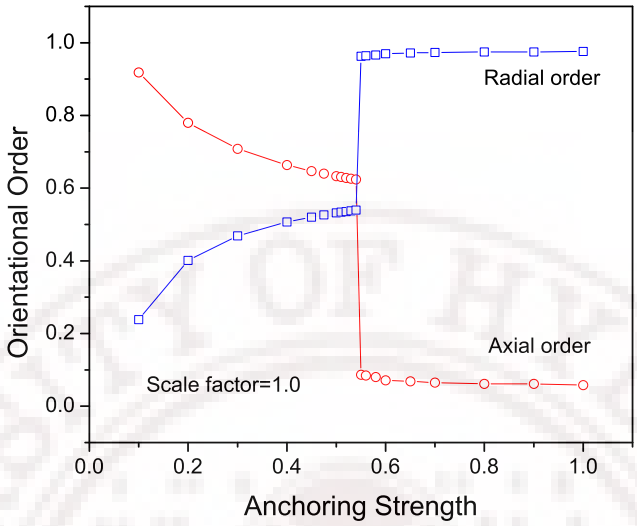

Figure 6.2: Variation of radial and axial order with anchoring strength for scale factor 1.00

a high value of S_A, and the corresponding S_R is low. As the value of ε_S is increased the uniaxial order decreases and at the threshold value of about 0.54 the axial order practically vanishes, while the radial order assumes a value very near unity. This would physically correspond to an anchoring mediated sudden change in the director structure finally culminating in an essentially radially ordered director configuration. These results are consistent with those of the earlier work carried out with LL model with $\varepsilon_S = 1$. It is interesting to see the corresponding changes in the layer-wise order parameters as a function of ε_S. These are depicted in figures 6.3 and 6.4. Both the figures, which are complementary, indicate that below the threshold ε_S the development of radial order, at the expense of the axial counterpart, is gradual as one moves out from the center of the droplet, and the droplet thus is getting gradually transforming from a pure uniaxial symmetry to a more spherical symmetry. Just at the threshold value, a sudden transition of the director structure takes place, making it essentially spherically symmetric, but for a small inner core (of a radius of about 3-4 lattice units) which still manages to have uniaxial order. This, is due to the significant elastic energy involved in forcing the radial orientations of the director to the very center of the droplet [23] [45]. Thus the minimum free energy is obtained by allowing a small core

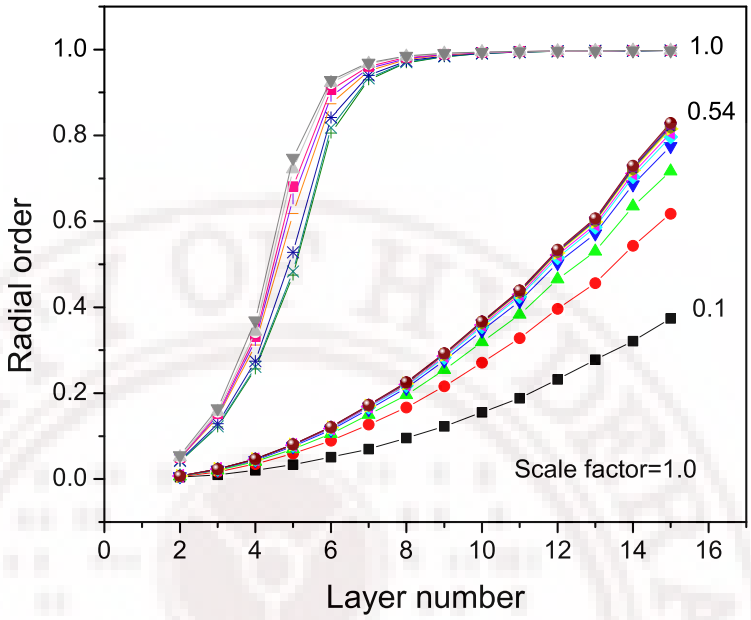

Figure 6.3: Variation of radial order with layers for the scale factor 1.00 for different anchoring strengths (the different plots correspond to different anchoring strengths ε_S, as indexed)

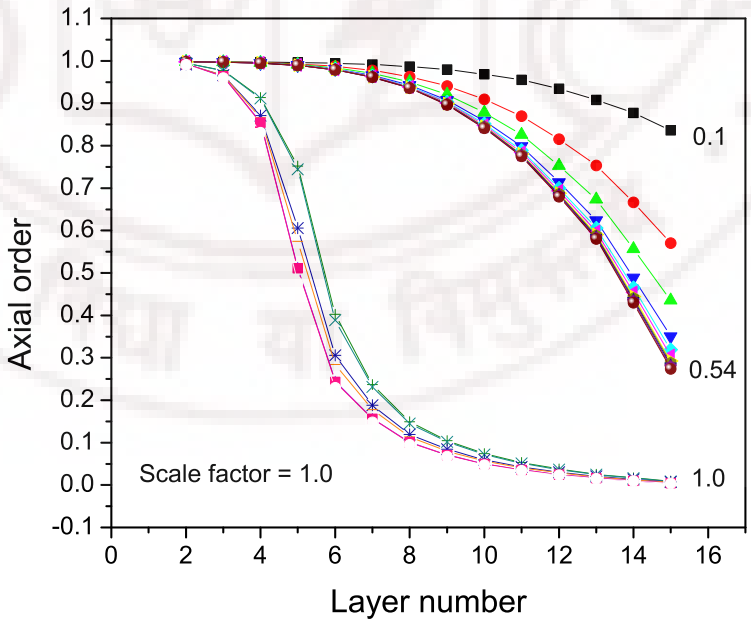

Figure 6.4: Variation of axial order with layers for the scale factor 1.00 for different anchoring strength (the different plots correspond to different anchoring strengths ε_S, as indexed)

of uniaxial region with some energy cost at the interface between two differently ordered regions of the medium.

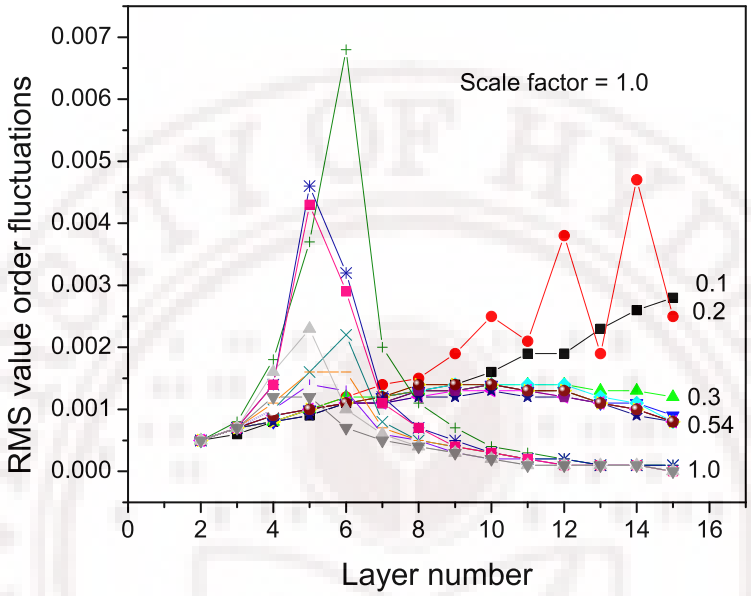

Figure 6.5: Variation of RMS value of order fluctuations with layer number for different anchoring strengths (the different plots correspond to different anchoring strengths ε_S, as indexed)

Figure 6.5 shows the RMS value of layer-wise (uniaxial) order fluctuations as ε_S is varied from 0.1 to 1.0. These fluctuations seem to provide an insight into the progression of the radial order towards the center, and are significant near the interfacial region at the delimiting surface due to frustration effects. When ε_S is low (0.1) the effect of radial anchoring seems to make the axial order fluctuate progressively more, as the confining surface is reached from the center. At $\varepsilon_S = 0.2$, there are very significant fluctuations which persist typically in the outer five layers, implying that at this anchoring value, the energy cost of percolating the radial order is competing with the interfacial energy (at the surface) involved to retain a large enough uniaxial region. It may be noted that this energy cost is relatively small at this large radius of the uniaxial droplet. However further increase of ε_S to 0.3, and up to a threshold value of about 0.54, indicates rather curiously that the fluctuations are uniform over the layers, but for a small (approximately two-fold) increase

in the middle layers of the droplet. This suggests that the uniaxial order fluctuations are smaller at the core (away from the competing boundary conditions) and at the surface (due to the pinning effect from the surface); and are somewhat more pronounced in the mid-layers, as can be expected under the circumstances. At the onset of the anchoring induced transition, beyond the threshold value of ε_S, however, the scenario changes qualitatively. The order fluctuations suddenly shift towards an inner layer (around 4-5 units) and show systematic peaks (unlike the fluctuations near the outer layers at $\varepsilon_S = 0.2$) at the interfacial surfaces, their position shifting progressively to inner layers as the anchoring strength is increased to unity beyond the threshold value. These fluctuations unambiguously show the onset of radial order, and its progression with anchoring strength; and provide the signature of the anchoring-induced structural transition in the medium. In order to correlate the above changes with experimentally observable quantities, ^2H NMR spectra expected from the different director configurations were generated for different ε_S values. Figure 6.6 shows two limiting spectra for ε_S = 0.1 and 1.0.

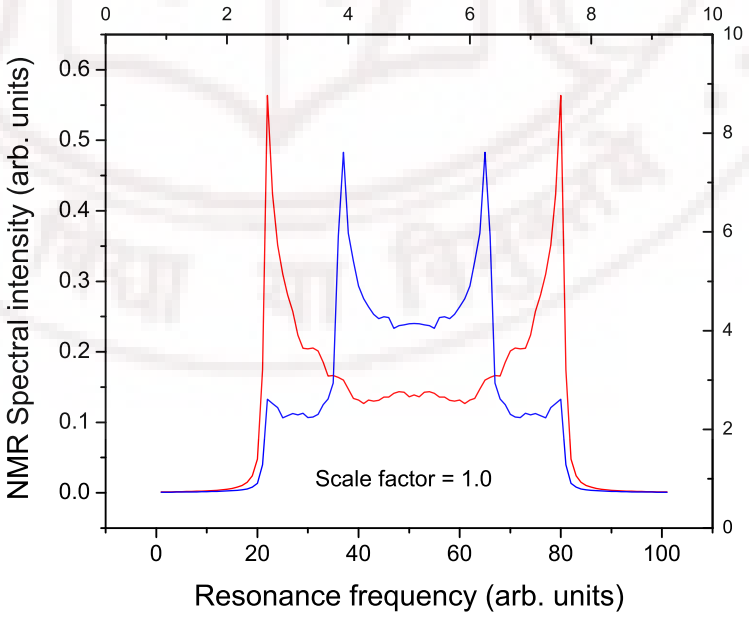

Figure 6.6: Simulated NMR spectrum for different resonant frequencies for the scale factor 1.00 (inner plot representing axial order).

The simulations were extended to find the effect of varying the energy cost of the relevant elastic distortion (*i.e.* splay constant K_1 relative to its actual value, while retaining the other two elastic constants the same) through the scale factor α, as mentioned before. Figure 6.7 shows the variation of the two orders with ε_S as α is varied from 0.1 to 3.0 in some convenient steps. It may be noted that after the onset of the anchoring-induced transition,

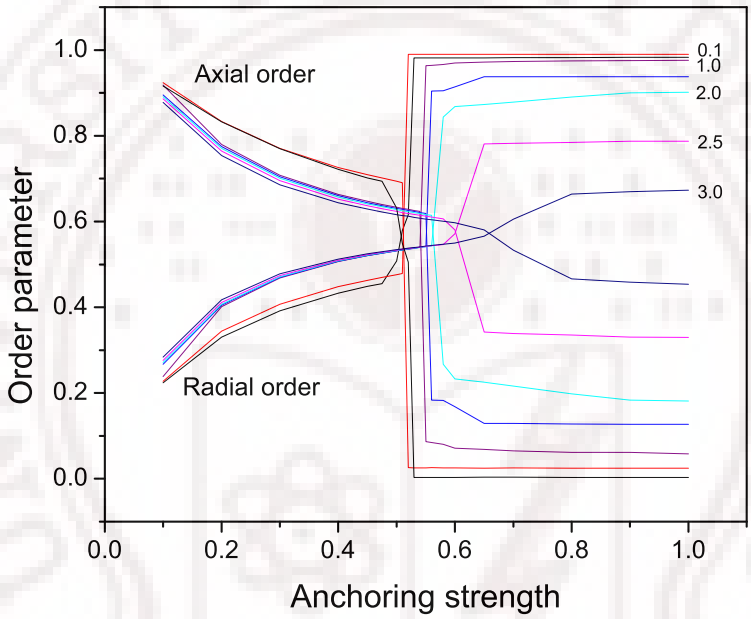

Figure 6.7: Variation of the order parameters with anchoring strength for different scale factors as indexed.

the region of interface between the uniaxial core and the outer radial region depends on the balancing of elastic energy costs involved, and in this case is determined by the splay elastic coefficient; other competing conditions kept constant. Thus, figure 6.7 shows that the effect of varying the relative value of the splay elastic constant is two fold: the threshold value for the anchoring transition increases with increase of α, and the extent of change in one type of order to the other type after the anchoring transition decreases with α. This is consistent with the picture that as K_1 is systematically increased, it requires more anchoring influence from the boundary to induce this transition, and a higher K_1 value also demands a larger uniaxial core for energy balance at the interface thus reducing the disparity between the

magnitudes of the two different types of orientational order. For comparison with the case of $\alpha = 1$ (figures 6.2 and 6.3), figures 6.8 and 6.9 show layer-wise variation of the two orders with ε_S at $\alpha = 0.1$. It is seen that the threshold value for the anchoring transition is now around 0.52 and the radius of the inner uniaxial core has diminished.

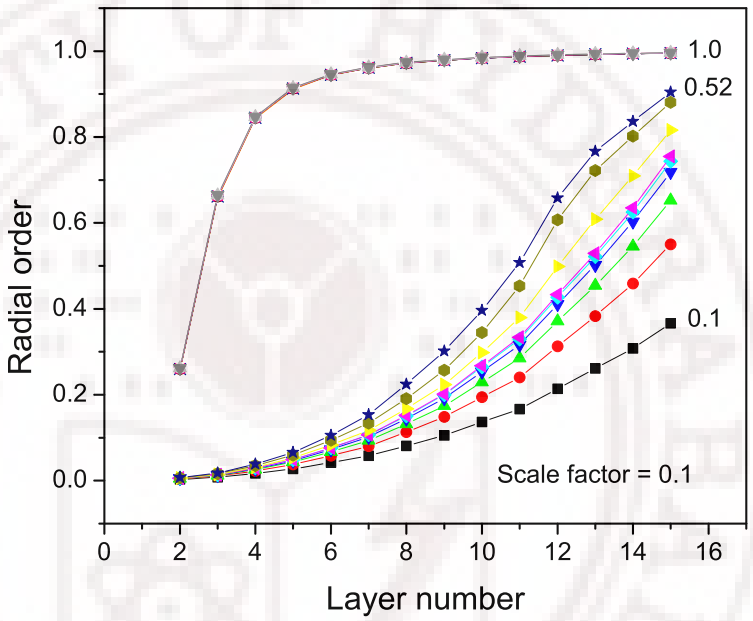

Figure 6.8: Radial order for every layer for the scale factor 0.1 for different anchoring strengths (the different plots correspond to different anchoring strengths ε_S, as indexed).

To examine the growth of the core region with uniaxial order as a function of changes in the splay constant, we show layer-wise variation of S_A as α is varied (figure 6.10). From this one can infer the typical size of the core sustaining uniaxial order and its dependence on splay elasticity. These results are plotted in figure 6.11 showing a linear variation of the radius of the spherical inner uniaxial core with scale factor α. From these results, one can also plot the variation of the threshold values of ε_S needed to induce the anchoring transition, as a function of different scale factor values (α), and thus is shown in figure 6.12. It is also illustrative to compute the ^2H NMR spectra for the different values of α, at the fixed $\varepsilon_S = 1$, to see how the corresponding layer-wise variation of the director field (figure 6.10) would reflect in an experimental situation, and this is shown in figure 6.13. To

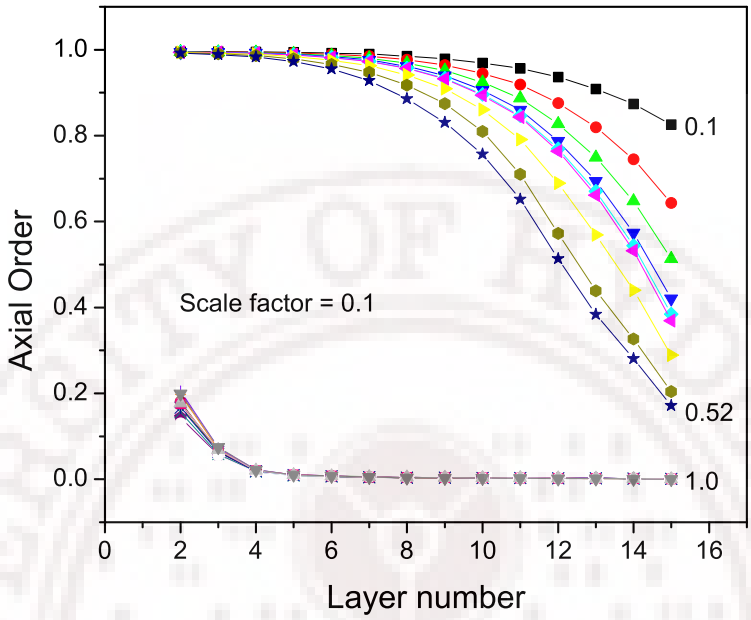

Figure 6.9: Axial order for different anchoring strength for every layer at scale factor 0.1 (the different plots correspond to different anchoring strengths ε_S, as indexed)

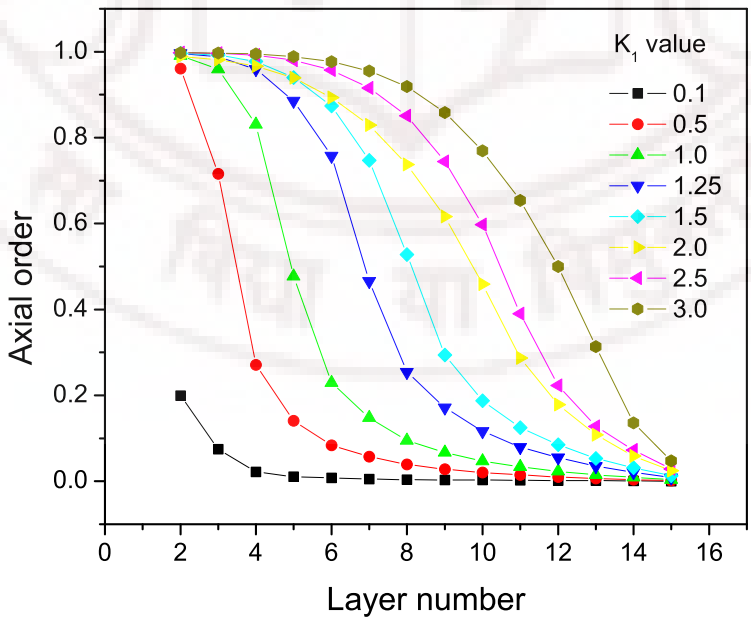

Figure 6.10: Variation of axial order for different K1 with the layer number.

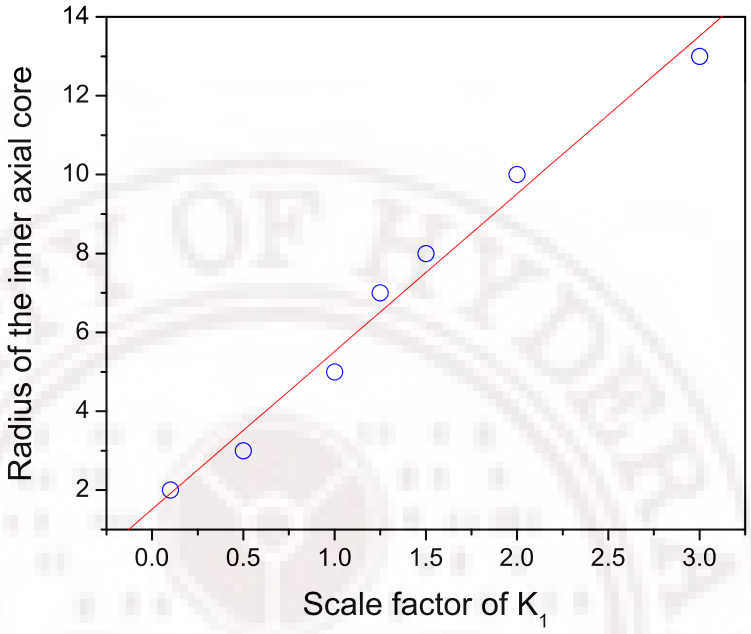

Figure 6.11: Radius of the inner axial order core with the scale factor

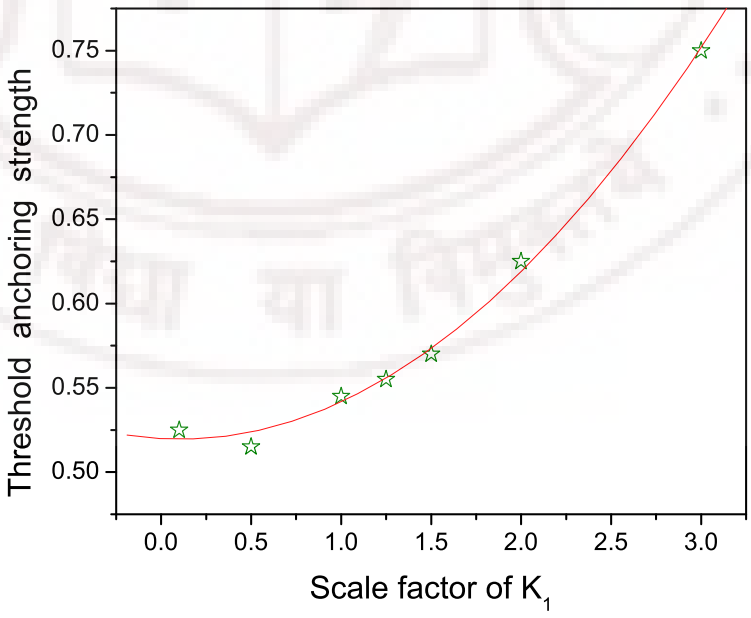

Figure 6.12: Variation of threshold anchoring strength with scale factor

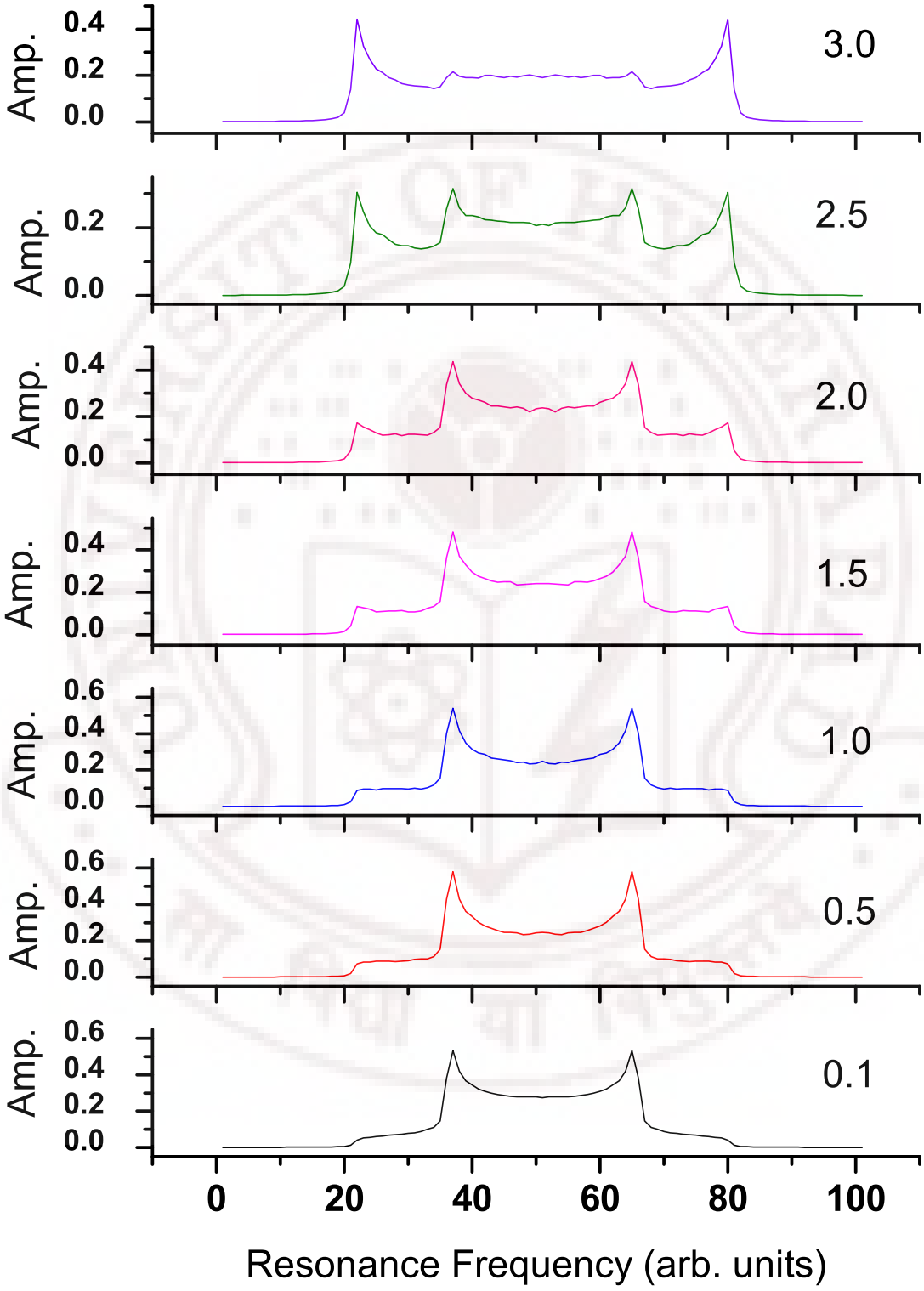

Figure 6.13: Simulated NMR spectra for various values of scale factors

look for possible hysteresis of this anchoring transition, given the abrupt changes induced by the anchoring strength, the simulations were repeated at $\alpha = 1$, by decreasing ε_S to zero starting from unity. The results are shown in figure 6.14 and it is observed that there is a strong hysteresis associated with this anchoring transition. The transition to the original uniaxial state (at the lower anchoring values) could not be located precisely, and one can only infer that it should be somewhere between 0.1 and 0.0.

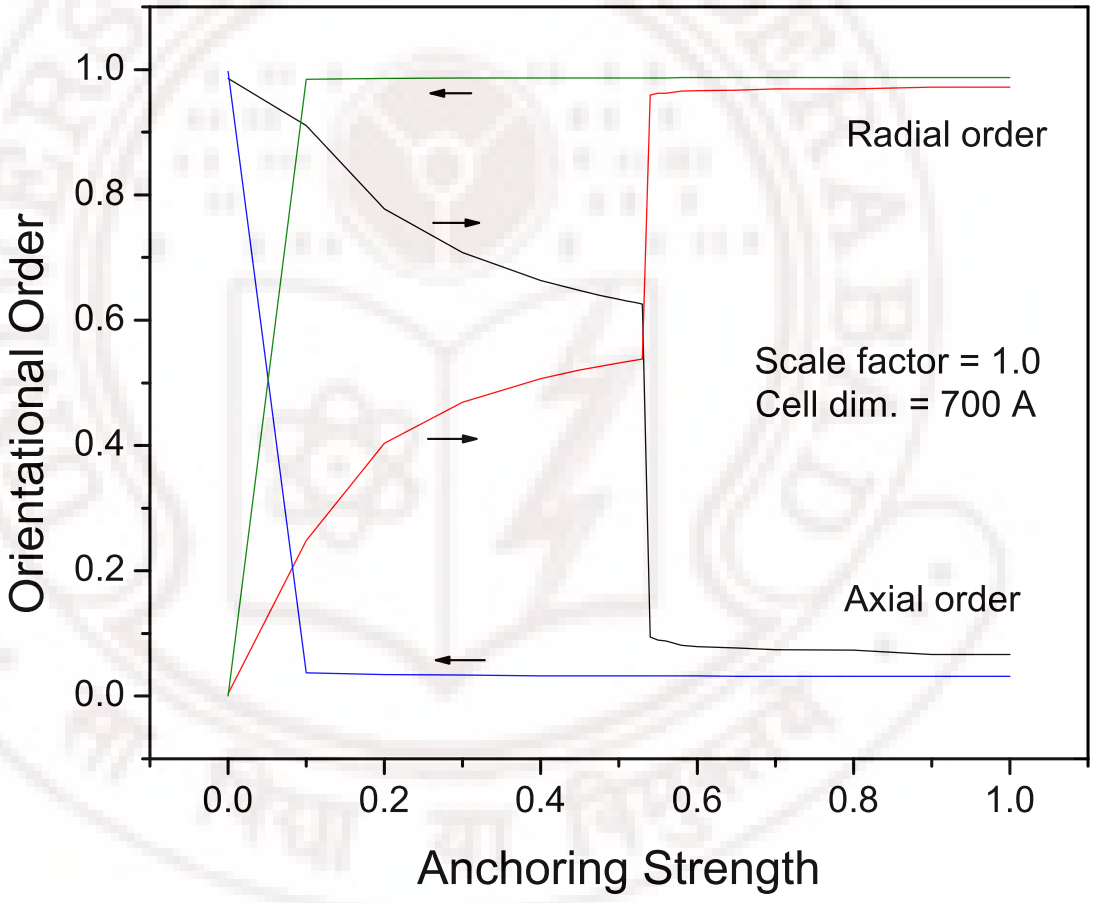

Figure 6.14: The hysteresis curve for cell dimension (Λ) 700 A

Finally, the applicability of this model depends on the the dimension of the volume element Λ chosen to represent the average director field, and it was held fixed at $700A^o$. To test limitations of this dimension on the results, simulations were also carried out, (setting $\alpha = 1$), at two other values of $\Lambda(70\mathring{A}$ and $7\mathring{A})$, and figure 6.15 summarizes the findings.

At $70\mathring{A}$ (corresponding to the reduced temperature of 0.1, it could be expected from the earlier work on planar hybrid films [44] that the volume element is too small to provide statically reliable representative director orientations (in statistical terms, the ensemble is collected at an unacceptably higher temperature), and any departures, if observed, were explained as due to the effect of large director fluctuations. The present results thus show that at lower values of Λ the effect of director fluctuations is considerable, and the transition displays a shift in the threshold anchoring strength and also apparent weakening of the transition (figure 6.15). The data at an even lower value shown in figure 6.15 proves this point convincingly.

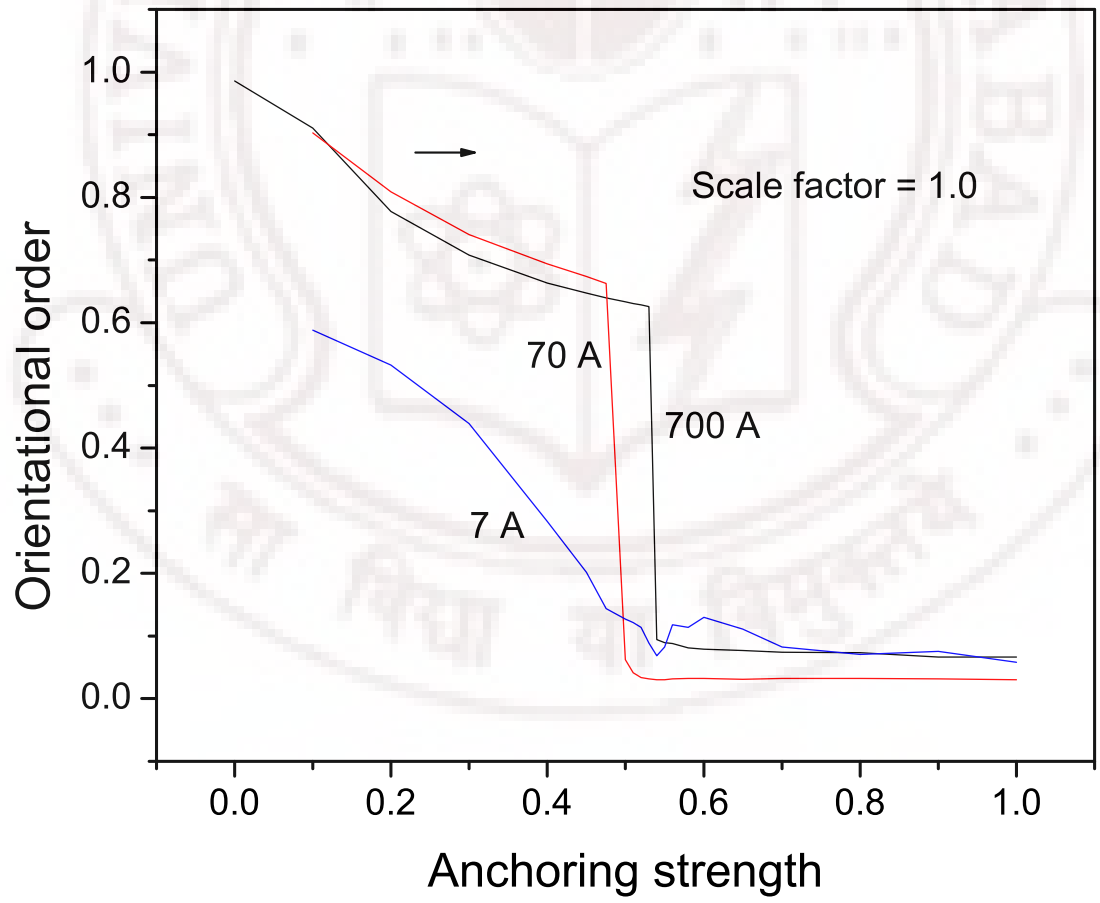

Figure 6.15: Variation of Orientational order with anchoring strength for different cell dimensions

6.4 Conclusions

Liquid crystal micro-droplet is revisited with a different Hamiltonian model which permits explicit incorporation of the elastic properties of the medium, under certain conditions. We report here a structural transition in the director field, induced by tuning the anchoring strength at the spherical boundary. The layer-wise profiles of the two orders which distinguish the two phases, as well as their layer-wise fluctuations, provide an insight into the progression of this transition. The flexibility of this model is used to simulate the effect of assigning different splay properties of the medium (via the scale parameter), and the anchoring transition is studied as a function of the scale parameter, keeping other conditions the same. This affects both the anchoring threshold for the transition, as well as the extent to which the radial order could penetrate into the droplet. These effects can be conveniently gleaned by looking at ^2H NMR spectra (under rigid lattice conditions) which represent the variations of the director fields more transparently. The anchoring transition seems to be of strong first order leading to complete wetting, and is reflected by the large hysteresis associated with this transition. This model is of course limited by the choice of the length scale connecting the volume element over which the local director is defined, and is effectively reflected in the Monte Carlo simulation via the reduced temperature that is assigned during the simulation. These limits are also examined to see the effect of director fluctuations on the anchoring transition reported.

Bibliography

[1] C.P.Grawford and S.Zummer. *Liquid crystal in complex geometries formed by polymer and porous network.* Taylor and Francis, London, 1996.

[2] J. W. Doane, A. Golemme, J. L. West, and J. B. Whitehead Jr.and B.G.Wu. Polymer dispersed liquid crystals for display application. *Mol. Cryst. Liq. Cryst*, 165:511–532, 1988.

[3] A.Golemme, S.Zumer, J.W.Doane, and M.E.Neubert. Deuterium nmr of polymer dispersed liquid crystal. *Phys. Rev. A*, 37(2):559, 1988.

[4] M. Ambrozic, P. Formoso, A. Golemme, and S. Zumer. Anchoring and droplet deformation in polymer dispersed liquid crystals:nmr study in an electric field. *Phys. Rev. E*, 56(2):1825, 1997.

[5] Ichiro Amimori, James N. Eakin, Gregor Skaej Jun Qi, Slobodan umer, and Gregory P. Crawford. Surface-induced orientational order in stretched nanoscale-sized polymer dispersed liquid-crystal droplets. *Phys. Rev. E*, 71:031702, 2005.

[6] J.W.Doane, N.A.Vaz, B.G.Wu, and S.Zumer. Field controlled light scattering from nematic droplets. *Appl. Phys. Lett.*, 48(4):269, 1986.

[7] G. Chidichimo, G. Arabia, A. Golemme, and J. W. Doane. Electrooptic properties of polymer dispersed liquid crystals. *Liquid Crystals*, 5(5):1443–1452, 1989.

[8] Nuno A. Vaz, George W. Smith, and G. Paul Montgomery Jr. A light control film composed of liquid crystal droplets dispersed in a uv-curable polymer. *Molecular Crystals and Liquid Crystals*, 146:1–15, 1987.

[9] Ichiro Amimori, Nikolai V. Priezjev, Robert A. Pelcovits, and Gregory P. Crawford. Optomechanical properties of stretched polymer dispersed liquid crystal films for scattering polarizer applications. *J. Of Appl. Phys.*, 93(6):3248, 2003.

[10] Marija Vilfan, Bostjan Zalar, Adam K. Fontecchio, Mojca Vilfan, Michael J. Escuti, Gregory P. Crawford, and Slobodan Zumer. Deuteron nmr study of molecular ordering in a holographic-polymer-dispersed liquid crystal. *Phys. Rev. E*, 66:021710, 2002.

[11] Chris C. Bowley, Pavel A. Kossyrev, Gregory P. Crawford, and Sadeg Faris. Variable-wavelength switchable bragg gratings formed in polymer-dispersed liquid crystals. *Appl. Phys. Lett.*, 79(1):9, 2001.

[12] Thein Kyu, Domasius Nwabunma, and Hao-Wen Chiu. Theoretical simulation of holographic polymer-dispersed liquid-crystal films via pattern photopolymerization-induced phase separation. *Phys. Rev. E*, 63:061802, 2001.

[13] J. Bajc and S. Zumer. Structural transition in chiral nematic liquid crystal droplets in an electric field. *Phys. Rev. E*, 55(3):2925, 1997.

[14] J. Bezic and S. Zumer. Structures of cholesteric liquid crystal droplets with parallel surface anchoring. *Liquid crystal*, 11(4):593419, 1992.

[15] S.Kralj and S.Zumer. Freedericksz transition in supra-μm nematic droplets. *Phys. rev. A*, 45(4):2461, 1992.

[16] S.Zumer. Light scattering from nematic droplets: Anomalous-diffraction approach. *Phys. Rev. A*, 37(10):4006, 1988.

[17] I.Vilfan, M.Vilfan, and S.Zumer. Orientational order in bipolar nematic microdroplets close to phase transition. *Phys. Rev. A*, 40(8):4724, 1989.

[18] S.Kralj, S.Zumer, and D.W.Allender. Nematic-isotropic phase transition in a liquid crystal droplet. *Phys. Rev. A*, 43(6):2943, 1991.

[19] S.Zumer and J.W.Doane. Light scattering from small nematic droplets. *Phys. Rev. A*, 34(4):3373, 1986.

[20] P. Pasini, C. Chiccoli, and C. Zannoni. *Advances in the Computer Simulations of Liquid Crystals*. Kluwer, Dordrecht, 2000.

[21] C. Chiccoli, P. Pasini, F. Semeria, T.J. Sluckin, and C. Zannoni. *J. Phys. II France*, 5:427, 1995.

[22] E. Berggren, C. Zannoni, C. Chiccoli, P. Pasini, and F. Semeria. Monte carlo study of the molecular organization in model nematic droplets-field effects. *Chem. Phys. Lett.*, 197:224–230, 1992.

[23] C. Chiccoli, P. Pasini, F. Semeria, and C. Zannoni. A computer simulation of nematic droplets with radial boundary conditions. *Phys. Lett. A*, 150:311–314, 1990.

[24] E. Berggren, C. Zannoni, C. Chiccoli, P. Pasini, and F. Semeria. Computer simulations of nematic droplets with bipolar boundary conditions. *Phys. Rev. E*, 50:2929–2939, 1994.

[25] C. Chiccoli, P. Pasini, F. Semeria, and C. Zannoni. Computer simulations of nematic droplets with toroidal boundary conditions. *Mol. Cryst. Liq. Cryst.*, 221:19–28, 1992.

[26] C. Chiccoli, P. Pasini, G. Skacej, S. Zumer, and C. Zannoni. *Lattice spin models of polymer-dispersed liquid crystals in Computer Simulations of liquid crystals and polymers*. Kluwer, Dordrecht, 2005.

[27] F. Biscarini, C. Chiccoli, P. Pasini, F. Semeria, and C. Zannoni. Phase diagram and orientational order in a biaxial lattice model. a monte carlo study. *Phys. Rev. Lett.*, 75:1803, 1995.

[28] C. Chiccoli, P. Pasini, I. Feruli, and C. Zannoni. Biaxial nematic droplets and their optical textures. a lattice model computer simulation study. *Mol. Cryst. Liq. Cryst.*, 441:319–328, 2005.

[29] Renate Onris-Crawford, Evan P. Boyko, Brian G. Wagner, John H. Erdmann, Slobodan Zumer, and J. William Doane. Microscope textures of nematic droplets in polymer dispersed liquid crystals. *J. Appl. Phys.*, 69(9):6380, 1991.

[30] P.A. Lebwohl and G. Lasher. Nematic-liquid-crystal ordera monte carlo calculation. *Phys. Rev. A*, 6:426, 1972.

[31] C. Chiccoli, P. Pasini, F. Semeria, and C. Zannoni. Monte carlo simulations of model nematic droplets. *Mol. Cryst. Liq. Cryst.*, 212:197–204, 1992.

[32] E. Berggren, C. Zannoni, C. Chiccoli, P. Pasini, and F. Semeria. Monte carlo study of the effect of an applied field on the molecular organization of polymer-dispersed liquid-crystal droplets. *Phys. Rev. E*, 49:614–622, 1994.

[33] A.P.J. Emerson and C. Zannoni. A monte carlo study of gay-berne liquid crystal droplets. *J. Chem. Soc. Faraday Trans.*, 91:3441–3447, 1995.

[34] C. Chiccoli, P. Pasini, G. Skacej, C. Zannoni, and S. Zumer. Nmr spectra from monte carlo simulations of polymer dispersed liquid crystals. *Phys. Rev. E*, 60:4219–4225, 1999.

[35] C. Chiccoli, P. Pasini, G. Skacej, C. Zannoni, and S. Zumer. Dynamical and field effects in polymer dispersed liquid crystals: Monte carlo simulations of nmr spectra of pdlc. *Phys. Rev. E*, 62:3766–3774, 2000.

[36] C. Chiccoli, Y. Lansac, P. Pasini, J. Stelzer, and C. Zannoni. Effect of surface orientation on director configurations in a nematic droplet. a monte carlo simulation. *Mol. Cryst. Liq. Cryst.*, 372:157–165, 2001.

[37] C. Chiccoli, P. Pasini, G. Skacej, C. Zannoni, and S. Zumer. Inhomogeneous translational diffusion in polymer dispersed liquid crystals: Monte carlo simulations of nmr spectra. *Mol. Cryst. Liq. Cryst.*, 367:2987–2997, 2001.

[38] L.V. Mirantsen and S. Romano. Molecular dynamics simulation of polymer dispersed liquid crystal droplets under competing boundary conditions. *Liquid Crystals*, 33(2):187194, 2006.

[39] C. Chiccoli, P. Pasini, F. Semeria, and C. Zannoni. A detailed monte carlo investigation of the tricritical region of a biaxial liquid crystal system. *Int. J. Mod. Phys. C*, 10:469–476, 1999.

[40] S. Romano. *Int. J. mod. Phys. B*, 12:2305, 1998.

[41] K. P. N. Murthy. *Monte Carlo methods in Satistical Physics*. Universities Press, 2003.

[42] T. Gruhn and S. Hess. *Z. Naturforsch.*, A51:1, 1996.

[43] G.R. Luckhurst and S. Romano. Computer simulation study of a nematogenic lattice model based on an elastic energy mapping of the pair potential. *Liq. Cryst.*, 26:871, 1999.

[44] P.J. Le Masurier, G.R. Luckhurst, , and G. Saielli. Monte carlo lattice simulations of the elastic behaviour of nematic liquid crystals. *Liq. Cryst.*, 28:769, 2001.

[45] N. Schopohl and T.J. Sluckin. *J. Physique*, 49:1097, 1988.

Chapter 7

Conclusions

Computer simulation methods are proving to be efficient tools to study complex molecular structures in interesting soft materials like confined liquid crystals under chosen boundary conditions. This thesis reports results of such investigations in a variety of such systems. A hybrid film of uniaxial molecules was studied using non - Boltzmann sampling methods. Thin films confined between substrates inducing competing boundary conditions were studied by varying the temperature, the anchoring strength of the substrates and the thickness of the liquid crystal film. These novel sampling methods provided relatively free estimates of different parameter as a function of finely controlled temperature. This study helped in characterizing this transition more reliably and accordingly, providing more readily observable physical variables to detect the onset of new phases. As a special case to hybrid films, a thin film of liquid crystals was confined between two cylindrical substrates inducing order in perpendicular directions. Due to the curvature present in the system the elastic energy (different at the two substrates due to differing curvatures) plays an important role. A biaxial phase in this system is observed when the anchoring strength of the two substrates is carefully tuned to induce balanced competing influences on the intermediate layers of the system. The biaxial phase observed in these hybrid films is due to the confinement effects on uniaxial liquid crystal molecules, and in classified as phase biaxiality.

In reality liquid crystal molecules are known to have finite molecular biaxiality. For simplicity, they are mostly modeled as uniaxial rod - like or disc - like molecules. Curiosity lies in understanding as to why a macroscopic biaxial order is not observed when

the liquid crystal molecules are themselves are microscopically not symmetric around their long axes. From the point of experiments, unambiguous acceptance of the realization of a biaxial phase is counting to be a challenging question to be resolved. In this context predictions based more general Hamiltonian models could be useful in understanding the molecular origin for observation of macroscopic biaxial symmetry. Accordingly, molecular modeling of a biaxial liquid crystal was attempted in order to lead to the possibility of determining microscopic criteria for realistic biaxial liquid crystal. A general model incorporating two parameters was used for this study (equation 1.5.4). Phase diagrams were computed with the variation of the two parameters (Γ, Λ). These predictions are new, and are interesting from the point of view of developing appropriate criteria at a molecular level for the observation of a biaxial phase.

Such studies on biaxial liquid crystals were extended was studied hybrid films, realized by applying competing boundary conditions creating restrictive constraints. It was observed that for such confined systems there are two biaxial phases possible at low temperature. The phase formed immediately below the isotropic phase is a biaxial phase exclusively due to the phase biaxiality, arising from the self - organization of the long axes of the molecules. The lower temperature biaxial phase is primarily due to the molecular biaxiality arising from the interacting biaxial components of the molecules. This system was further studied by varying the relative anchoring strengths of the substrates keeping. It is seen that there exists a threshold anchoring strength beyond which there is an abrupt change in the director structure, and consequently the associated physical parameters.

Finally a liquid crystal droplet confined in a polymer is revisited using canonical Monte Carlo studies. The Hamiltonian used for this study has the facility to include elastic constants as parameters that can be varied independently. The droplet considered has been subjected to radial anchoring at the polymer surface, so that one need to consider only splay distortion as the relevant condition in the Hamiltonian. With the variation in the anchoring strength sudden transition between two qualitatively different structures is observed. This system is further by varying the splay elastic constant and on finds that it affects both the

threshold anchoring strengths, as well as the size of the inner uniaxial core. The reliability of the computations and the applicability of the model were investigated by changing the spatial extent over which the director is defined. The anchoring transition reported in this study exhibits strong hysteresis, and seems to correspond to complete wetting.

This thesis thus makes of a humble attempt to demonstrate the novel features of confined liquid crystals comprising of molecules of different symmetries and reports new structures and phase transition among them, utilizing the power and convenience of Markov chain Monte Carlo techniques.